CHALMERS

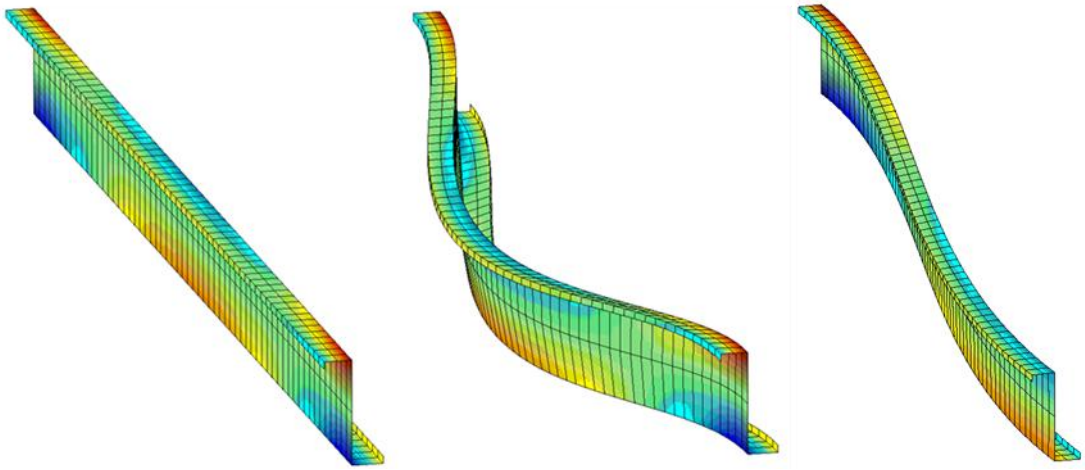

Application of first-order Generalised Beam Theory on open thin-walled members

Master of Science Thesis in the Master's Programme Structural Engineering and Building Technology

GUSTAF GELL
HENRIC THOMPSSON

Department of Civil and Environmental Engineering
Division of Structural Engineering
Steel and Timber Structures
CHALMERS UNIVERSITY OF TECHNOLOGY
Göteborg, Sweden 2013
Master's Thesis 2013:86

MASTER'S THESIS 2013:86

Application of first-order Generalised Beam Theory on open thin-walled members

Master of Science Thesis in the Master's Programme Structural Engineering and Building Technology

GUSTAF GELL

HENRIC THOMPSSON

Department of Civil and Environmental Engineering
Division of Structural Engineering
Steel and Timber Structures
CHALMERS UNIVERSITY OF TECHNOLOGY
Göteborg, Sweden 2013

Application of first-order Generalised Beam Theory on open thin-walled members

Master of Science Thesis in the Master's Programme Structural Engineering and Building Technology

GUSTAF GELL
HENRIC THOMPSSON

Examensarbete / Institutionen för bygg- och miljöteknik,
Chalmers tekniska högskola 2013:86

Department of Civil and Environmental Engineering
Division of Structural Engineering
Steel and Timber Structures
Chalmers University of Technology
SE-412 96 Göteborg
Sweden
Telephone: + 46 (0)31-772 1000

Cover:
Output from MATLAB implementation of GBT method. Shows the displacements and stresses for fixed-fixed and fixed-guided conditions.

Department of Civil and Environmental Engineering Göteborg, Sweden 2013

Application of first-order Generalised Beam Theory on open thin-walled members

Master of Science Thesis in the Master's Programme Structural Engineering and Building Technology

GUSTAF GELL
HENRIC THOMPSSON
Department of Civil and Environmental Engineering
Division of Structural Engineering
Steel and Timber Structures
Chalmers University of Technology

ABSTRACT

The aim of the project has been to study and apply the fundamental parts of first-order Generalized Beam Theory (GBT) for open thin-walled cross-sections. A literature survey has been performed to document the development of the theory until today. Based on the acquired knowledge, computational algorithms were established and implemented as MATLAB routines in order to verify GBT in comparison to ordinary finite shell-elements. The algorithms analysed one single structural member and enclosed information about internal displacements and stresses. Further, the results were verified and compared to conventional finite element software regarding accuracy, convergence, and computational effort. GBT provides accurate values compared to the reference shell-models. No singularities are occurring in the GBT solution and the extraction of results is easy compared to the finite elements. The GBT boundary conditions that were possible to mimic with shell-elements have been tested and verified. The computational efficiency was found to be higher for GBT than for the reference model, due to lower total number degrees of freedom. The commonly used assumption of an uncoupled GBT equation system was verified to be correct, since the coupling terms did not contribute noticeable. It was also found important to verify the discretization of the cross-section in order to capture the real behaviour of the member. If the analysis is performed correctly, GBT provides a fast, pedagogical and elegant approach to understand more of the underlying factors influencing the response of a beam subjected to a different set of applied loads.

Key words: amplitude functions, boundary conditions, cross-section analysis, deformation modes, displacements, discretization, finite element method, FEM, Generalized Beam Theory, GBT, MATLAB, member analysis, normal stress, shear stress, technical beam theory, warping function.

Tillämpning av första ordningens Generalised Beam Theory på öppna tunnväggiga strukturelement

Examensarbete inom Structural Engineering and Building Technology

GUSTAF GELL, HENRIC THOMPSSON
Institutionen för bygg- och miljöteknik
Avdelningen för Konstruktionsteknik
Stål och träbyggnad
Chalmers tekniska högskola

SAMMANFATTNING

Syftet med examensarbetet var att undersöka och tillämpa de grundläggande delarna inom första ordningens Generalized Beam Theory (GBT) för öppna tunnväggiga tvärsnitt. En litteraturstudie har genomförts där teorins utveckling fram till idag har dokumenterats. Genom den funna informationen har beräkningsgångar etablerats och implementerats i MATLAB för att kunna verifiera teorin och jämföra med vanliga finita skalelement. Implementeringen analyserade ett strukturelement och returnerade värden på förskjutningar och spänningar. Resultaten verifierades och jämfördes med resultat från ett kommersiellt finita elementprogram gällande exakthet och beräkningseffektivitet. Teorin stämde bra överens i jämförelse med de finita referensmodellerna. De randvillkor som var möjliga att efterlikna med skalelement har testats och verifierats. Beräkningseffektiviteten var högre för GBT än för referensmodellen beroende på det lägre antal frihetsgrader som krävs. Det allmänt vedertagna antagandet om ett okopplat ekvationssystem i GBT har verifierats som korrekt eftersom kopplingstermerna inte ger några nämnvärda bidrag. Under projektet uppmärksammades vikten av att verifiera diskretiseringen av tvärsnittet för att fånga balkens riktiga beteende. Om analysen genomförs på ett korrekt sätt så möjliggör GBT ett snabbt, pedagogiskt och elegant sätt för att förstå mer av de underliggande faktorerna som avgör hur en balk reagerar vid olika typer av belastning.

Nyckelord: amplitudfunktion, deformationsmod, diskretisering, FEM, finita element metod, förskjutning, GBT, Generalized Beam Theory, MATLAB, normalspänning, randvillkor, skjuvspänning, strukturanalys, teknisk balkteori, tvärsnittsanalys, välvfunktion.

Contents

Preface

When we started this project no one had a clue on how far we would reach. Thanks to the free nature of the process, free coffee and the good spirit among friends we succeeded beyond our own expectations. Unfortunately time has its way and we have to let the loose ends pass for now. Hopefully some daredevil will take up the process and continue exploring the fascinating subject of Generalized Beam Theory.

We would like to thank our supervisor Fredrik Larsson who understood things that we barley could explain and always gave us recognition for the good work. Also we would like to thank examiner Mohammad Al-Emrani, who gave us the idea to this topic and the freedom to explore it in a free and stimulating way. Last but not forgotten we would like to thank our beloved ones, who always stood by and supported our work.

Göteborg June 2013

Gustaf Gell and Henric Thompsson

Notations

The following variables and notations are used throughout the report.

Roman upper case letters

A	Area of the cross-section	[length^2]
$\boldsymbol{B}$	GBT basic matrix defined by the B_{ik}-term	[force / length^2]
B_{ik}	Stiffness term defining the GBT basic matrix $\boldsymbol{B}$	[force / length^2]
$\tilde{B}_1, \tilde{B}_2, \tilde{B}_3, \tilde{B}_4, \tilde{B}_{k>4}$	The diagonal terms in the diagonal transformed GBT basic matrix $\widetilde{\boldsymbol{B}}$ corresponding to deformation mode k	[force / length^4], [force / length^2], [force / length^2], [force], [force / length^2]
$\boldsymbol{C}$	GBT basic matrix defined by the C_{ik}^{I}- and C_{ik}^{II}-terms	[length^4]
$C_{ik}^{I}, C_{ik}^{II}, C_{ik}^{III}, C_{ik}^{IV}$	Stiffness terms defining the GBT basic matrix $\boldsymbol{C}$	[length^4]
$\tilde{C}_1, \tilde{C}_2, \tilde{C}_3, \tilde{C}_4, \tilde{C}_{k>4}$	The diagonal terms in the diagonal transformed GBT basic matrix $\widetilde{\boldsymbol{C}}$ corresponding to deformation mode k	[length^2], [length^4], [length^4], [length^6], [length^4]
C_M	Warping stiffness constant	[length^6]
C_1, C_2, C_3, C_4	Integration constants	[various]
$\boldsymbol{D}$	GBT basic matrix defined by the D_{ik}^{I}-, D_{ik}^{II}- and D_{ik}^{III}-terms	[length^2]
$D_{ik}^{I}, D_{ik}^{II}, D_{ik}^{III}, D_{ik}^{IV}$	Stiffness terms defining the GBT basic matrix $\boldsymbol{D}$	[length^2]
$\widetilde{D}_1, \widetilde{D}_2, \widetilde{D}_3, \widetilde{D}_4, \widetilde{D}_{k>4}$	The diagonal terms in the approximate diagonal transformed GBT basic matrix $\widetilde{\boldsymbol{D}}$ corresponding to deformation mode k	[-], [length^2], [length^2], [length^4], [length^2]
E	Young's modulus of elasticity	[force / length^2]
$\boldsymbol{F}_v$	$(u - v)$ relation matrix	[1 / length]

$\boldsymbol{F}_w$	$(u-w)$ relation matrix	[1 / length]
$\boldsymbol{F}_{w1}$	$(u-w_1)$ relation matrix	[1 / length]
$\boldsymbol{F}_{w2}$	$(u-w_2)$ relation matrix	[1 / length]
$\boldsymbol{F}_{\vartheta}$	$(u-\vartheta)$ relation matrix	[1 / length^2]
G	Shear modulus	[force / length^2]
I_D	Saint-Venant torsion stiffness constant	[length^4]
I_y, I_z	Second moment of inertia about y- and z-axis respectively	[length^4]
K, K_r	Plate stiffness, Plate element stiffness	[force · length]
K_{ik}	Terms involving nonlinear terms (used in second order analysis which is not used within this thesis)	[-]
$\boldsymbol{K}_{3x3}$	Matrix defined by the K_{ik}	[-]
$\boldsymbol{M}$	$(u-m_s)$ relation matrix	[force · length / length^2]
M_y, M_z	Bending moments about the principle axis y and z	[force · length]
N	Normal force	[force]
P_x, P_y, P_z	Point forces in x-, y- and z-direction respectively	[force]
$S_{k.r}$	Shear force in plate element r	[force]
U, V, W	Displacement components, defined in global (X, Y, Z)-coordinate system	[length]
$\overline{\boldsymbol{U}}$	Matrix containing the warping values according to unit displacements one degree of freedom at the time.	[length]
$\widetilde{\boldsymbol{U}}$	Cross-sectional modal matrix containing all deformation modes $\widetilde{\boldsymbol{u}}_k$.	[varies with k]
W	Bi-moment	[force · length^2]

$\widetilde{W}_1, \widetilde{W}_2, \widetilde{W}_3, \widetilde{W}_4, \widetilde{W}_{k>4}$	The GBT sectional force for mode k	[force], [force · length], [force · length], [force · length^2], [force · length]
(X, Y, Z)	Global coordinate system	[-]
$\bar{\boldsymbol{X}}$	Matrix containing unit displacement modes according to unit displacement one degree of freedom at the time	[length]
$\widetilde{\boldsymbol{X}}$	Eigenmatrix or transformation matrix containing all normalized eigenvectors $\widetilde{\boldsymbol{x}}_k$	[varies with k]

Roman lower case letters

$b, b_r, b_{r.i}$	Width, width of plate element r, width of sub-plate r_i	[length]
m_D	Distributed torsion moment	[force · length / length]
$m_{s.r}$	Transverse distributed nodal bending moments	[force · length / length]
$\bar{m}_{s.r}, \hat{m}_{s.r}$	Average transverse bending moments for plate element r (The bar notation do not denote unit bending moment in this case)	[force · length / length^2]
$q(x, s)$	General distributed surface load	[force / length^2]
q_i	Loading term containing s and z load components	[force / length]
$\tilde{q}_k$	The GBT load along the member associated with the s and z load components	[force / length]
q_x, q_s, q_z	Surface load components of $q(x, s)$ in x-, s- and z- direction respectively	[force / length^2]
q_x, q_y, q_z	Distributed loads in x-, y- and z-direction respectively	[force / length]
$q_{x,x.i}$	Loading term containing the x load component	[force / length]
$\tilde{q}_{x,x.k}$	The GBT load along the member associated with the x load component	[force / length]
t, t_r	Thickness, thickness of plate element r	[length]

u, v, w	Displacement components, defined in local (x, s, z)-coordinate system	[length]
$u(s), v(s), w(s)$	Mid-line displacement profiles	[-]
$u(s_r), \bar{u}_r$	Nodal unit warping at node r	[length]
u_i, v_i, w_i	Cross-sectional s-dependent deformation functions associated with virtual displacement mode i	[-]
u_k, v_k, w_k	Cross-sectional s-dependent deformation functions associated with deformation mode k	[-]
u_r	Warping value at node r	[length]
$\tilde{\boldsymbol{u}}_1, \tilde{\boldsymbol{u}}_2, \tilde{\boldsymbol{u}}_3, \tilde{\boldsymbol{u}}_4, \tilde{\boldsymbol{u}}_{k>4}$	Cross-sectional deformation modes	[-], [length], [length], [length^2], [length]
v_r	Local transverse and in-plane plate element displacement parallel to the mid-plane of plate element r	[length]
$w_{1.r}, w_{2.r}$	First and second end local displacement components perpendicular to the mid-plane of plate element r	[length]
w_r	Local transverse plate element displacement perpendicular to the mid-plane of plate element r	[length]
(x, s, z)	Local coordinate system	[-]
$\boldsymbol{x}$	Degrees of freedom vector	[length]
$\tilde{\boldsymbol{x}}_1, \tilde{\boldsymbol{x}}_2, \tilde{\boldsymbol{x}}_3, \tilde{\boldsymbol{x}}_4, \tilde{\boldsymbol{x}}_{k>4}$	Normalized eigenvectors	[1 / length], [-], [-], [length], [-]
$\tilde{\boldsymbol{x}}_k^I, \tilde{\boldsymbol{x}}_k^{II}, \tilde{\boldsymbol{x}}_k^{III}$	Eigenvectors obtained in the first, second and third eigenproblem in the diagonalization process before normalization.	[-]

Greek letters

α_r	Angle before deformation for plate element r	[rad, -]
δ_r	$(\theta_r - m_{s.r})$ relation term which defines the $\boldsymbol{\Delta}_{ik}$-matrix	[1 / force]
$\delta\varepsilon_{xx}, \delta\varepsilon_{ss}, \delta\gamma_{xs}$	Virtual strain components	[-]
$\delta\Pi$	Total variation in the virtual work due to external forces	[force · length]
δU	Total variation in the virtual work due to internal forces	[force · length]
$\delta U_{xx}, \delta U_{ss}, \delta U_{xs}$	Internal virtual work components in x-, s- and xs-direction respectively	[force · length]
δV	Total potential energy of a member	[force · length]
$\delta\phi_i(x)$	Virtual amplitude function component	[length]
$\boldsymbol{\Delta}_{ik}$	$(\Delta\vartheta_r - m_{s.r})$ relation matrix	[1 / force]
$\Delta\alpha_r$	Angle difference between plate element r and $r-1$ at node r	[rad, -]
$\Delta\boldsymbol{F}_{\vartheta}$	$(u - \Delta\vartheta)$ relation matrix	[1 / length^2]
$\Delta\vartheta_r$	Rotation at node r	[rad, -]
$\varepsilon_{xx}^B, \varepsilon_{ss}^B, \gamma_{xs}^B$	Bending strain components	[-]
$\varepsilon_{xx}^M, \varepsilon_{ss}^M, \gamma_{xs}^M$	Membrane strain components	[-]
η	Local plate element coordinate	[-]
ϑ	Cross-sectional rotation	[rad, -]
ϑ_r	Plate element rotation of plate element r	[rad, -]
θ_r	"Support rotation" at node r due to the nodal transverse bending moment $m_{s.r}$	[rad, -]
$\lambda_k^I, \lambda_k^{II}, \lambda_k^{III}$	Eigenvalues obtained in the diagonalization process	[various]
ν	Poisson's ratio	[-]
σ_{ss}	Normal stress along local s-direction	[force / length^2]

$\sigma_x, \sigma_{xx}, \sigma_{x.k}$	Normal stress along local x-direction, normal stress associated with deformation mode k	[force / length^2]
$\tau_{xs}, \tau_{xs.k}$	Shear stress in "xs-direction", shear stress associated with deformation mode k	[force / length^2]
$\phi_i(x)$	Amplitude function associated with virtual displacement mode i	[length]
$\phi_k(x)$	Amplitude function associated with deformation mode k	[length]
$\tilde{\phi}_1, \tilde{\phi}_2, \tilde{\phi}_3, \tilde{\phi}_4, \tilde{\phi}_{k>4}$	Amplitude functions corresponding to deformation mode k	[length^2], [length], [length], [-], [length]
$\psi_k(x)$	Amplitude function associated with deformation mode k	[-]
Ψ_{1-4}	Integration helping functions or shape functions	[-]
ω	Warping ordinate	[length^2]

Other notations

$(\cdot)_{,x}, (\cdot)_{,s}$	Partial derivative with respect to x, partial derivative with respect to s
$(\cdot)^M, (\cdot)^B$	M represents membrane components, B represents bending components
$(\cdot)_r$	Plate numbering or node numbering
$\overline{(\cdot)}$	Bar notation denotes that the variable correspond the unit displacement of a degree of freedom
$\widetilde{(\cdot)}$	Tilde notation denotes the transformed variable into the eigenvector coordinate system
$(\cdot)_{n\times m}$	This subscript denotes the submatrix containing the first n rows and the first m columns of the corresponding matrix.
$\boldsymbol{F}_v$	Bold notation for matrix and vector notations

1 Introduction

The usage of cold-formed steel profiles have gradually increased throughout the years. Some of the reasons for this are structural efficiency, manufacturing versatility and low production and erection costs. The structural efficiency is defined as a large strength-to-weight ratio, hence the possibility to produce thin-walled cross-sections. If structural elements consist of these kinds of profiles their behaviour when subjected to load is rather complex to analyze and predict. Especially for open cross-sections which are rather sensitive to torsion and non-uniform torsion, since their capacity for this sort of action is poor [1].

For structural members consisting of thin-walled profiles loaded in compression the ultimate strength is greatly influenced by the buckling capacity [2]. Three kinds of buckling can occur in the member; local, distortional and global [3]. In case of local or distortional buckling there exists a post-buckling reserve capacity, which allows extra load to be applied. If the member buckles globally there is no allowance for additional load and the member collapses [2]. Hence it's of great importance to understand and analyze the behaviour so that the real capacity of the member can be determined.

At present time the Euler-Bernoulli and Timoshenko beam theories are widely used in calculations due to their simplicity and accuracy in describing bending and deflection behaviour. The theories are based upon assumptions such as plane cross-sections remain plane, and in the case of Euler-Bernoulli theory, even perpendicular to the neutral axis.

Consequently, these theories are not applicable when local effects, such as local and distortional buckling, should be investigated. Therefore, there is a need for other theories to capture this kind of phenomena, primarily in thin-walled structural members. Today, finite plate elements are the most used method to model thin-walled structures. The drawback with this method is the large computational effort needed to carry out such stability analysis due to the large number of degrees of freedom and modal identifications are very ineffective in finite element methods (FEM) [4].

When calculating the load bearing capacity of thin-walled steel beams subjected to both bending and axial compression where the cross-section is not double-symmetric and the boundary conditions are not fork-like Eurocode 3 refers to FEM. The drawback of this is argued about above, further the FEM-programs are expensive. Therefore, a compliment to the FEM analysis is of interest. A modal based method was developed by Richard Schardt and is called Generalized Beam Theory (GBT). This beam theory includes local effects and is applicable on thin-walled structural elements. The subject of this Master's project will be to investigate the derivation of the theory and also apply it on some structural cases.

1.1 Aim

The aim of the Master's project was to study the applicability and benefits of GBT. This method was evaluated in terms of versatility, accuracy and computational effort with the objectives defined as:

- Application of first-order GBT on thin-walled steel members
- Verification and evaluation of the first-order theory

1.2 Method

In order to reach the goal, the project was divided into three major steps, namely a literature study, application and verification.

Firstly, the literature study was performed in order to collect important information as well as documenting the development of the theory from its start up until present date. Also important additions to the theory were highlighted and existing implementations were identified.

Later, the GBT formulas were derived for a thin-walled and open cross-sectioned member. Based on those formulas, computational algorithms were implemented as MATLAB routines. The acquired results were then compared to those of a commercial FE-software in order to verify the validity of the application, but also to verify the whole concept of GBT.

Finally, a parametric study was performed in order to evaluate the GBT method further. This step involved different loadings and boundary conditions but also different cross-sectional discretizations.

Based on the results from the verification and the evaluation of GBT, conclusions were drawn regarding the validity, versatility and computational effort.

1.3 Limitations

The field of GBT is rather broad; hence limitations were needed to narrow it down into this project. Introduced restrictions are presented below:

- First order theory (displacements and stresses)
- Static analysis
- One single member
- Open cross-sections
- Isotropic material conditions

Furthermore, the theory was applied on members where no cross-sectional restraints were considered, i.e. no restraints along the member.

1.4 Outline of the thesis

Chapter 2 encloses the development of the GBT, from its start until present time. Chapter 3 contains a short summary of prerequisite knowledge about classic beam theories. This is written to enhance the readers understanding of similarities between GBT and other beam theories. Chapter 4 presents all derivations in the context of GBT. This involves both the derivation of the fundamental equilibrium equation and the establishment of the cross-sectional deformation modes. In Chapter 5 the implementation of the theory is presented in terms of flow charts and calculation algorithms. Chapter 6 shows the application procedure of GBT on a Z-profile beam. This member is also analysed using the commercial FE-software ABAQUS. A comparison between the results is performed. Chapter 7 encloses a parametric study where some conditions of the solved member are changed. The response of the beam is then compared to ABAQUS values in order to verify GBT. Chapter 8 and 9 contains the final discussion and conclusions along with identified areas of further research.

2 The development of Generalised Beam Theory

In this chapter the historical development of the Generalised Beam Theory (GBT), until present time, will be presented.

2.1 Origin

GBT was first presented in the 1960:s by a German professor named Richard Schardt. The theory could be interpreted as a combination the folded plate theory and the Vlasov's theory for thin-walled beams [5]. Schardt and his associates at the Technical University of Darmstadt continued the development of the basic theory during almost three decades without any notable attention from the rest of the research world. The main reason for this was probably that most of the published results were written in German, and hence the English speaking researcher's didn´t intercept the theory. One of the most important references, concerning the basic GBT, is the book *Verallgemeinerte Technische Biegetheorie* [6] published by the mentioned professor Schardt. As suspected from the name, the book is written in German, and no known translation of the text exists [7].

The lack of recognition of the theory during this period had probably mostly linguistic and communicative reasons; if research databases had been around, the information could have reached its designated crowd faster. Perhaps also increasing use of FEM analysis made the theory a bit neglected, since acceptable results could be modelled in this fashion.

2.2 Development from the 1990:s until today

During the 1990:s the work carried out by the research team in Germany became available to the English speaking community through a series of publications by J. Michael Davies, at the time a researcher at the University of Salford in the United Kingdom. Not only did Davies and his colleagues translate the theory, but they also contributed with the extension of the theory to the buckling behaviour of cold-formed steel members. They also showed that GBT can be more efficient than Finite Element Analysis (FEA) or Finite Strip Analysis (FSA) [8].

After the publications of the groups at Salford and Dortmund, the rate of progress for the theoretical advances decreased. During the years 1995-2000, the numbers of articles published in the field were few. The reason for this is unknown to the authors, but throughout the research there's definitely a gap and no references to articles of great importance written during this period has been found. Since the early 2000:s the rate of articles increased again with contributions from researchers in USA, Hungary, Romania, Spain, France, Denmark and Portugal among others.

Throughout the last decade, a research group at the Technical University of Lisbon, Portugal, has by far published the largest number of scientific articles in the field of GBT. From this team Nuno Silvestré and Dinar Camotim are the most frequently occurring authors, together with various co-authors. They have explored and expanded the theory in a number of different areas, and are still publishing interesting articles at a fast rate. In the next section their research contribution, among others, are described.

2.3 Research fields

In this section, a review of the research of GBT in different fields of structural analysis is given. The intention is to give the reader an idea about how the theory has developed and been applied in a way that is easy to grasp. The authors refer to the given references for deeper knowledge.

2.3.1 First order theory

This theory is linear and generally based on the assumptions that Hooke's law is valid, there are no imperfections, and that the deformations are small. Hence the equilibrium systems are given for the undeformed structure [9]. Deformations, internal forces and stresses are calculated according to this theory.

The earliest publications by Schardt et al. concerned the first order structural analysis in the framework of GBT. By combining the predetermined modes of deformation with the solution of the pertinent linear differential equation for each mode, the deflections, rotations and internal forces could be determined. Throughout this analysis the assumption of isotropic material was used. Davies (mentioned in previous section) published an article [7] on first order GBT. This document is recommended by the authors to the reader who wants to know how the member analysis is performed, after that the cross-sectional deformations modes have been determined. It shows the theory on a level that is possible to follow by using hand calculations. It also shows the relations between the cross-sectional deformation modes and the cross-section constants.

In its infancy, GBT concerned thin-walled open-cross sections. The lack of possibility to analyse common profiles like I-beams and H-beam made, of course, the theory a bit restrained. The references [10] and [8] are the earliest found articles on the topic of how to expand the theory into analyses of arbitrarily shaped sections. Figure 2.1 below shows the categorization of the properties of cross-sections when discussing profiles in the analysis. To the left is a pair of open-sections, which were possible to analyse with the early theory. Next are pairs of branched, boxed and branched-boxed sections. With these developments the versatility of the GBT method increased, and now all the common thin-walled profiles are able to undergo GBT analysis.

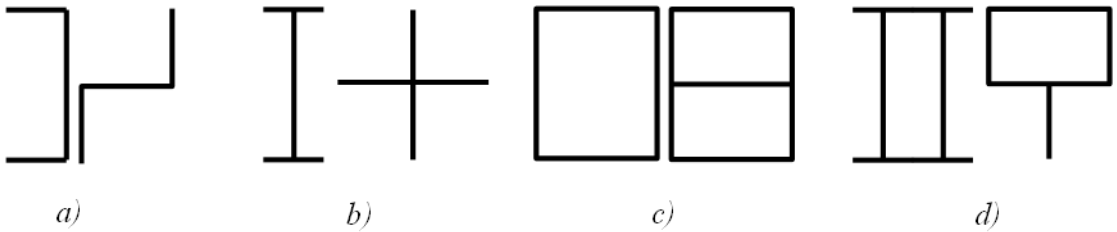

Figure 2.1: This figure illustrates a) open sections, b) branched sections, c) boxed sections and d) branched and boxed sections.

Orthotropic analysis for first-order GBT was introduced by Silvestre et al. and this enabled calculations on various types of composites and other profiles assembled having different material properties in different plates and directions. The same researchers also published an article [11] about the effects from shear, which had been

neglected earlier. By performing the typical GBT cross section modal analysis including the assumption of shear, an additional set of modes were identified. In the basic theory global, local and distortional modes are obtained; hence the extra set of modes represents the effects of shear. By using these modes in the analysis the effect of the phenomena are determined, and a better structural understanding is achieved. The Portuguese group has furthermore expanded the theory from single members into frames. Paper [1] is devoted to this topic, and paper [12] deals entirely with how to model the joints in the frame. Warping transmission in joints is the crucial part, and is discussed and modelled. This is performed to incorporate the phenomena in a representative manner.

Common for all the research carried out after year 2000 is that there's a main focus not on the first-order theory, but rather on the higher order theory. The calculation of e.g. critical buckling loads and the buckling shapes are of a greater interest to scientists than only the determination of internal forces, stresses and moments. A trend toward this had started earlier, and after the year of 2000 articles about first order GBT specifically are rare.

2.3.2 Higher order theory

As opposed to first order theory, higher order theories are by definition nonlinear and include terms that otherwise were neglected. These assumptions could be divided into physical and geometrical categories. Physical nonlinearity concerns the actual behaviour of the material used in the analysis, where there e.g. exists a yield limit and plastic deformation may occur. Geometrical nonlinearity mainly concerns stability issues for the analysed structure, where assumed initial imperfections can be included. The calculation result from higher order theory aims at achieving an economically efficient structure, with satisfactory structural capacity regarding critical buckling load and known buckling shapes [9].

The basic equation for GBT theory is expanded with additional terms when formulated for second order analysis. With the aid of these terms the stability eigenvalue problem can be formulated and solved to investigate the structural integrity of the construction. Already in the early 1990:s methods and examples on second order theory for GBT were published in [13] and [14]. The articles are written by Davies & Leach, which at the time worked in the UK.

As mentioned earlier, a lot of the research the last decade has been performed by the researchers at the Technical University of Lisbon, Portugal. Apart from improving the theory into e.g. arbitrarily shaped cross-sections, orthotropic material, several boundary conditions and loads, their main focus has been to investigate the buckling behaviour. At a fast rate, they have published articles dealing with nonlinear analysis of members showing elastic and elastic-plastic material properties, geometrically imperfections and having intermediate supports. References [2], [10], [15], [16] and [17] are some of the publications regarding second order theory. The authors specially recommend paper [10] as an adequate summary of their research progress up until the year of 2004.

Schardt, and colleagues, have extended the theory for the case of dynamic analysis, with isotropic linear elastic material conditions. Furthermore the research group in Lisbon has improved the formulation to include arbitrary orthotropic material

behaviour also for this kind of analysis. Note that also the latter formulation holds only for linear elastic material properties [10].

2.3.3 Interesting areas of application

For structural engineers the applicability of the theory into real structural situations is of great importance. Therefore the authors in this section are trying to give some indications on how the theory has been evolved to become more practical and multifaceted.

It is important to be able to model intermediate actions along the length of the beam, for example a purlin restraining the beam from warping freely or buckling at the connection. The original book [6] and the paper [18] are dealing with this issue, still on a very theoretical level. By using rigid supports, translational springs and rotational springs at specific points along the member they are showing a methodology how to model such situations. In this fashion, numerical results are obtained and results compared to shell models in ANSYS are promising. The earliest found reference on this topic is [19] where a calculation is performed for the case of a beam on several supports and restrained by a metal sheet roof.

Another interesting field of application of GBT is for non-prismatic beams. The usage of tapered (non-prismatic) beams is common in the steel-construction industry and therefore it is of importance that the theory of GBT applies to this kind of problems. Mihai Nedelcu has written articles in the field and in [20] he shows a theoretical procedure and some numerical examples on how to obtain results. If the slope of the tapering is uniform, and can be describe by a function along the member length, the effect can be taken into account during the derivation of equations. Note that this holds true if the thicknesses of the plate walls are constant. For arbitrary differences in the cross-section along the member he proposes a rougher numerical calculation. The basic idea in this procedure is to perform the calculation of the modes, as in ordinary GBT, for every coordinate along the member length. As a result the ordinary beam equation constants start to depend on the location along the axis and the response for a tapered beam can be determined.

During the calculation according to Nedelcu the cross-sectional analysis is performed for each point (read cross-section) along the member length, hence the variation of constants. In other words the stiffness along the beam will vary with the coordinate in the longitudinal direction of the beam. Since the calculation is performed for every part of the beam it's possible to calculate the response for a beam with varying wall thickness. The article is arguing for the theory by comparison of numerical examples to standard calculation procedures.

2.3.4 Calculation efficiency

In paper [21] a comparison of buckling analysis performed using GBT and an ordinary FEA using shell elements was performed, both for the linear and non-linear case. The examined structural member was a simply supported beam, modelled both with and without intermediate restraints. When the results were compared, the maximum difference was determined to approximately 3.4%. The number of degrees of freedom used in the GBT analysis was 108 and in the traditional FEA model 6750. By only using 1.6% of degrees of freedom and still perform this accurate, if handled properly, the power of GBT was exposed.

2.4 Existing implementations

The explicitly GBT based software applications are few, where CUFSM and GBTUL are the frequent examples [22]. Common for the calculations in the programs are that they are designed and intended to provide the cross-section modal information and also to describe the buckling behaviour of one single member. None of the different software's tested by the authors has provided any information about deflections, stresses or forces in the member. Hence they are intended to focus on higher order theory to provide buckling loads, buckling shapes and the modal participation into the result.

CUFSM is a MATLAB implementation of some GBT concepts into FSM theory. FSM theory is similar to FEM theory, but only discretizes the cross-section along the member length, not transversally. By constraining the FSM mesh to buckle in a specific, GBT based, mode the buckling load can be calculated. The modes are selected in an interface where, for the first time, the user is able to view and select global, local or distortional modes to include in the analysis. The creators of the application have made the MATLAB code open-source, which makes it possible for everyone to download, use and modify the behaviour. The name of the program originally originates from cFSM which is an acronym for the description *Constrained Finite Strip Method*.

GBTUL is developed as a separate windows application and also performs buckling analyses in the context of GBT. Also in this implementation the user is free to choose which modes to include in the analysis. However, the modal decomposition into global, local and distortional modes is not present, as for CUFSM [22].

3 Prerequisites

In the context of technical beam theory there are mainly four basic phenomena that are present, namely the axial extension, major and minor principle axis bending and torsion. The intention of this chapter is to give some short background to these theories.

3.1 The four technical beam theories

When evaluating the behaviour of a beam there are four main theories involved, namely the axial extension, major and minor axis bending and torsion. The theories of interest in the context of GBT are the rod-theory, Euler-Bernoulli beam theory and non-uniform torsion or Vlasov torsion theory, see Figure 3.1.

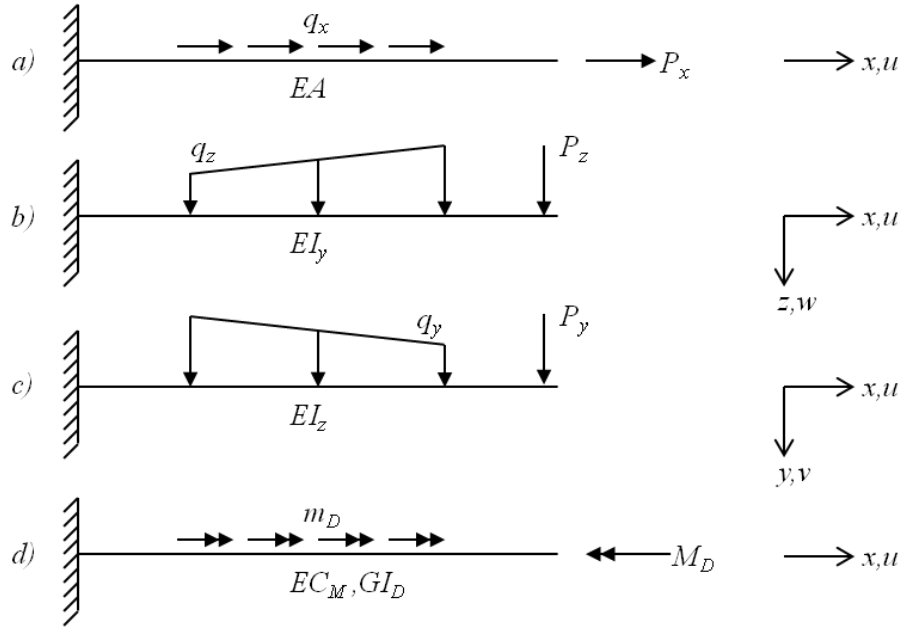

Figure 3.1: A description of and notations used in the four main beam theories where a) rod-action b) major axis bending c) minor axis bending and d) non-uniform torsion.

The fundamental differential equations in the four beam theories and the corresponding sectional forces are stated below and they are stated in the same order as in Figure 3.1:

$$\begin{aligned} &a) && EAu'' = -q_x && N = EAu' \\ &b) && EI_y w'''' = q_z && M_y = -EI_y w'' \\ &c) && EI_z v'''' = q_y && M_z = -EI_z v'' \\ &d) && EC_M \vartheta'''' - GI_D \vartheta'' = m_D && W = -EC_M \vartheta'' \end{aligned} \tag{3.1}$$

In general the stress state, distortions and deformations can be determined in each point (x, y, z) along the member from the solutions to the differential equations (3.1) and knowing its derivatives. Due to the orthogonality between the main coordinate axes the cross-sectional distribution and the longitudinal distributions are uncoupled and independent of each other. The stress and displacement distributions can therefore be seen to be expressed in to different functions, one that describes the cross-sectional distributions (in y- and z-direction) and one that prescribes the variation along the member in x-direction [6].

So, for instance looking on the longitudinal u-displacements for the four beam theories stated above the separation of variables might look like:

$$\begin{aligned} a) \quad & u(x,y,z) = u(x) \\ b) \quad & u(x,y,z) = -z \cdot w'(x) \\ c) \quad & u(x,y,z) = -y \cdot v'(x) \\ d) \quad & u(x,y,z) = \omega(y,z) \cdot \vartheta'(x) \end{aligned} \tag{3.2}$$

Where y and z are the coordinates defined from the centre of gravity of the cross-section and $\omega(x, y)$ is the warping ordinate. The variation in u-displacements over the cross-section is described in Figure 3.2 below.

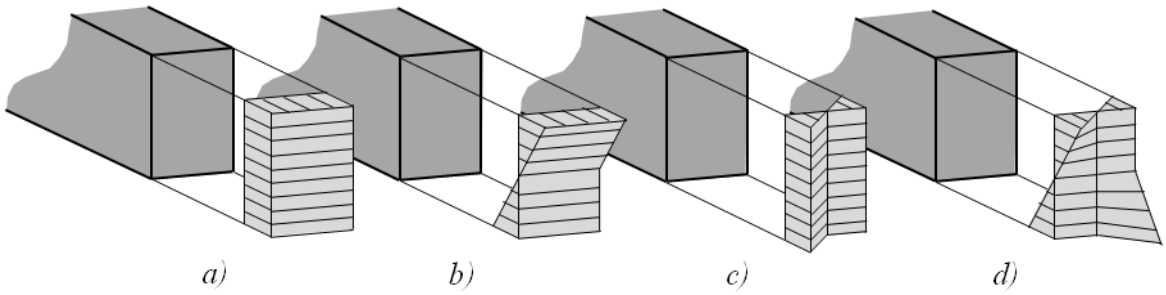

Figure 3.2: The variation in u-displacements for the four beam theories a) rod action b) major axis bending c) minor axis bending and d) non-uniform torsion.

3.1.1 Stresses

In the longitudinal direction or x-direction normal stresses will arise due to the u-deformations and are denoted with σ_x. The stresses for the different beam theories above and for linear elastic materials can be stated through the kinematic relations and Hook's law as:

$$\begin{aligned} a) \quad & \sigma_x(x,y,z) = E \cdot u'(x) \\ b) \quad & \sigma_x(x,y,z) = -E \cdot z \cdot w''(x) \\ c) \quad & \sigma_x(x,y,z) = -E \cdot y \cdot v''(x) \\ d) \quad & \sigma_x(x,y,z) = E \cdot \omega(x,y) \cdot \vartheta''(x) \end{aligned} \tag{3.3}$$

Since the beam theories are decoupled due to orthogonality the total stress in a member subjected to several loading types is obtained by summation of each contribution as:

$$\sigma_x(x,y,z) = \sum_k \sigma_{x.k}\,(x,y,z) \tag{3.4}$$

In addition the normal stresses, shear stresses will also arise and are denoted τ_{sx}. The expression for the shear stresses are derived from equilibrium conditions of an arbitrary infinitesimal cut-out from a wall element, see Figure 3.3.

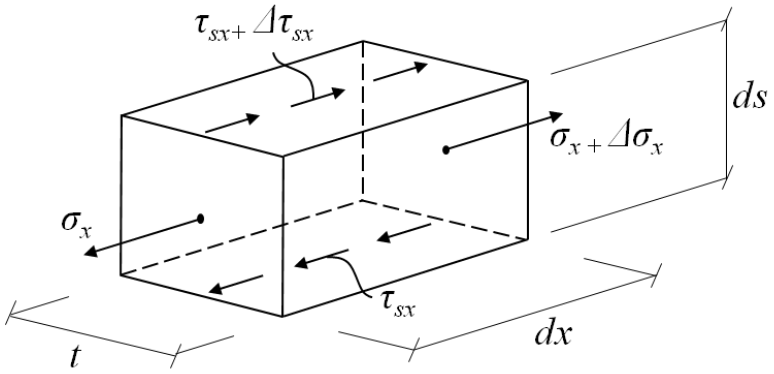

Figure 3.3: An infinitesimal cut out part from one plate element in the cross-section which has the thickness t, length dx and a height ds. The normal stresses σ_x acts in the longitudinal direction parallel to the x-axis and the shear stresses are denoted with τ_{sx}.

The infinitesimal part must be in equilibrium and the shear stresses can out of that condition be determined in terms of the longitudinal normal stresses as:

$$\rightarrow: \quad (\sigma_x + \Delta\sigma_x)tds - \sigma_x tds + (\tau_{xs} + \Delta\tau_{xs})tdx - \tau_{xs}tdx = 0$$

$$d\sigma_x \cdot tds + d\tau_{xs} \cdot tdx = 0$$

$$\frac{d\sigma_x}{dx} \cdot t + \frac{d\tau_{xs} \cdot t}{ds} = 0$$

$$\tau_{xs} = -\frac{1}{t(s)} \int_0^s t \cdot \sigma_x^{'} ds \tag{3.5}$$

Insert the expression for the normal stresses (3.3) into the derived expression for the shear stress (3.5) gives the following expressions for the four beam theories:

$$a) \quad \tau_{xs} = \frac{1}{t(s)} \int_0^s t \cdot E \cdot u^{''}(x) ds$$

$$b) \quad \tau_{xs} = \frac{1}{t(s)} \int_0^s t \cdot E \cdot z \cdot w^{'''}(x) ds \tag{3.6}$$

$$c) \quad \tau_{xs} = \frac{1}{t(s)} \int_0^s t \cdot E \cdot y \cdot v''' (x) ds$$

$$d) \quad \tau_{xs} = -\frac{1}{t(s)} \int_0^s t \cdot E \cdot \omega(x,y) \cdot \vartheta''' (x) ds$$

The total shear stress for a member subjected to several loading types is obtained in the same manner as the normal stresses, namely by simply adding them together as:

$$\tau_{xs}(x,y,z) = \sum_k \tau_{xs.k}(x,y,z) \tag{3.7}$$

3.1.2 Sectional forces and cross-sectional parameters

The sectional forces in the different beam theories are defined as an integral of the longitudinal stresses σ_x over the cross-sectional area A. When talking about rod action the sectional force is the normal force N, for major and minor axis bending are the corresponding bending moments M_y, M_z and for the non-uniform torsion the sectional force is the bimoment W. The integrals are defined as:

$$N = \int_A \sigma_x dA \qquad M_z = \int_A \sigma_x y dA \quad M_y = \int_A \sigma_x z dA \quad W = -\int_A \sigma_x \omega dA \tag{3.8}$$

Out of the expressions of cross-sectional forces the definition of the cross-sectional parameters can be obtained by simply insert the expressions for the normal stresses σ_x (3.3) into the expression for sectional forces (3.8), one gets:

$$A = \int_A 1 dA \qquad I_z = \int_A y^2 dA \qquad I_y = \int_A z^2 dA \quad C_M = -\int_A \omega^2 dA \tag{3.9}$$

If the sectional forces and the cross-sectional properties are known the normal stresses can be determined as:

$$\sigma_x(x,y,z) = \frac{N(x)}{A} \qquad \sigma_x(x,y,z) = \frac{M_z(x)}{I_z} y$$

$$\sigma_x(x,y,z) = \frac{M_y(x)}{I_y} z \qquad C_M = -\frac{W(x)}{C_M} \omega(y,z) \tag{3.10}$$

A summary of the four beam differential equations and the corresponding stresses, internal forces and cross-sectional parameters and also the analogies to GBT are tabulated in Appendix E.

4 Derivations within the context of GBT

This chapter contain all derivations within the context of first order GBT with linear elastic materials. The derivation involves the GBT fundamental equilibrium equation, cross-sectional discretization where the transverse displacements are expressed in terms of the longitudinal warping function, extension of the theory to include intermediate nodes, the transformation into an eigenvector coordinate system (diagonalization of the GBT-matrices) and also an application of finite element method to solve the GBT fundamental equation.

4.1 The GBT fundamental equilibrium equations

The following derivation is for a prismatic member consisting of an arbitrary open thin-walled cross-section which consists of rectangular plate element with constant thickness. In order to carry out this derivation some preliminary definitions must be set. The global coordinate system is a right-handed orthogonal system (X, Y, Z) where the X-coordinate is defined parallel to the member axis. The corresponding global displacements are denoted as (U, V, W) where U is defined in the X-direction, V in Y-direction and W in the Z-direction.

As a complement to the global system a local coordinate system is introduced. This is also an orthogonal system (x, s, z) where x-coordinate is defined parallel to the global X-coordinate, the s-coordinate is defined along the cross-sectional midline and the z-coordinate is defined perpendicular to the cross-sectional mid-plane. The local displacements (u, v, w) are defined in the local coordinate system where u is defined in x-direction, v in s-direction and w is defined in the z-coordinate direction, see Figure 4.1.

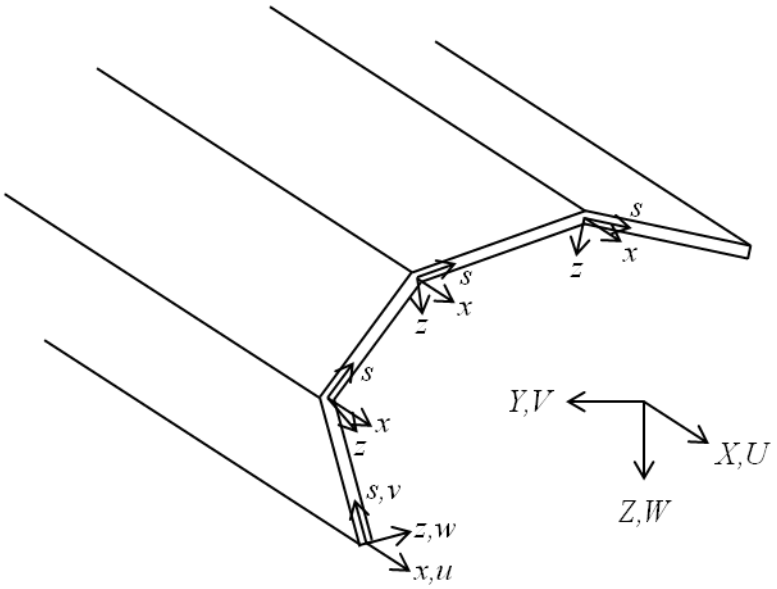

Figure 4.1: The definitions of the global coordinate system (X, Y, Z), the global displacements (U, V, W), the local coordinate system (x, s, z) and the local displacements (u, v, w) are here defined for a prismatic member with an arbitrary open thin-walled cross-section.

The cross-section is discretized into a number of plate elements defined by nodes. There are two types of nodes handled within this derivation, namely natural nodes and intermediate nodes. The natural nodes are defined at the intersection between two plate elements where the mutual angle difference is non-zero. The natural nodes also include the two end nodes, even though they differ from the definition. The intermediate nodes are nodes defined within a plate element between two natural nodes, see Figure 4.2.

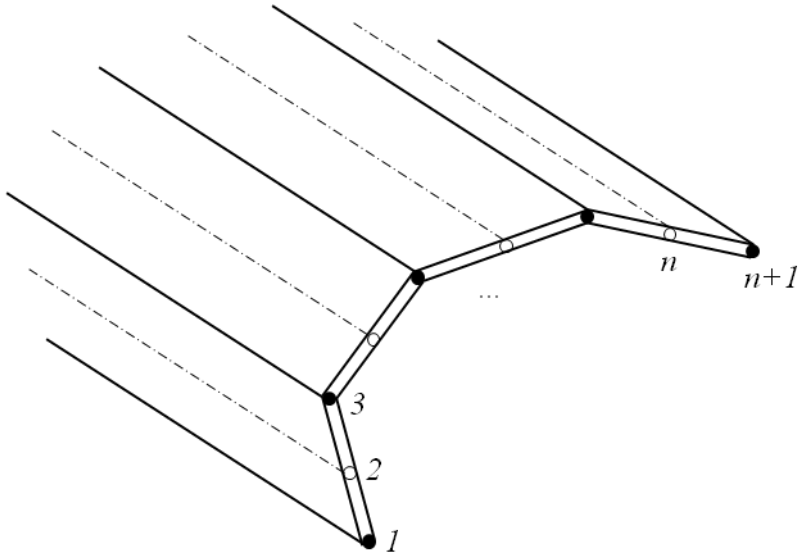

Figure 4.2: The cross-section is descetized in terms of natural nodes and intermediate nodes. Filled dotes are representing natural nodes (node 1, 3 and $n+1$) and rings are representing the intermediate nodes (node 2 and n). n do in this figure stand for the total number of sub-plates. The node numbering is defined such that the node number increases with the increasing s-coordinate.

4.1.1 Separation of variables procedure

The locally defined displacement components $u(x,s)$, $v(x,s)$ and $w(x,s)$ must be expressed as a product of two single-variable function in order to have an displacement representation compatible with the classical beam theories. This give:

$$u(x,s) = u(s) \cdot \psi_{k,x}(x) \quad v(x,s) = v(s) \cdot \psi_k(x) \quad w(x,s) = w(s) \cdot \psi_k(x) \qquad (4.1)$$

Where $u(s)$, $v(s)$ and $w(s)$ are mid-line displacement profiles and $\psi(x)$ is a dimensionless displacement amplitude function defined along the member. The comma subscript $(\cdot)_{,}$ stands for partial derivatives and the reason to the derivative on the u-displacements will be derived in Section 4.2 so within this section the first derivative is just stated and accepted as it is.

Assuming that $u(s)$ vary linearly[1] within each plate element, i.e. that $u(s)$ is completely defined by its nodal values. Thus the displacement $u(s)$ can be written as:

[1]This assumption is proofed in Section 4.2.2.

$$u(s) = u_k(s) \cdot u(s_r) \tag{4.2}$$

Where $u_k(s)$ is a linear function of s which has unit value at the corresponding node r and are zero at all other nodes and $u(s_r)$ is the *nodal warping value*[2] at node r, also referred as u_r. The summation convention applies to subscript k (number of modes) and the discretization of the deformed cross-section amounts to configure it into a number of deformation modes equal to the number of degrees of freedom. The number of degrees of freedom depends if intermediate nodes are included or not. If they are excluded the numbers of degrees of freedom is the same as the number of natural nodes (nodal warping values) but if they are included the number of degrees of freedom is the same as the total number of nodes plus two extra degrees of freedom associated with the two boundary nodes, see Section 4.3.1.

The displacement fields are then obtained by combining (4.1) and (4.2) and can be written as:

$$u(x,s) = u_k(s)\phi_{k,x}(x) \quad v(x,s) = v_k(s)\phi_k(x) \quad w(x,s) = w_k(s)\phi_k(x) \tag{4.3}$$

Where $u_k(s)$, $v_k(s)$ and $w_k(s)$ are cross-section deformation modes and $\phi_k(x)$ is the corresponding amplitude function defined as:

$$\phi_k(x) = u(s_r) \cdot \psi_k(x) \tag{4.4}$$

The behaviour of the member is obtained as a summation over the cross-sectional deformation modes k and the more modes included the more accurate results will be obtained. This is an advantage where the user can choose which modes that should be accounted for and also easily sees how large influence different deformation modes have on the total behaviour of the member.

$$\begin{aligned} u(x,s) &= \sum_k u_k(s)\phi_{k,x}(x) \\ v(x,s) &= \sum_k v_k(s)\phi_k(x) \\ w(x,s) &= \sum_k w_k(s)\phi_k(x) \end{aligned} \tag{4.5}$$

4.1.2 Assumptions

The formulation of the GBT is based on the following simplifying assumptions. Thin plate theory is adopted which means that the Kirchoff-Love hypothesis is valid for all plate elements forming the member. Thus, fibres normal to the mid-plane remains straight, normal and inextensional to the mid-plane after deformation. This more precisely expressed in strain components give:

[2] Warping is a commonly used expression in the context of GBT. This is somewhat disconcerting due to its immediate association with non-uniform torsion. Here warping is a representation for the axial deformation and not only associated with the torsion deformation mode (mode 4).

$$\varepsilon_{zz} = \gamma_{xz} = \gamma_{sz} = 0 \tag{A4.1}$$

The other assumption is that membrane transverse extensions and shear strains are neglected, thus the only retained membrane strains are the longitudinal strains. Expressed in strain components one have:

$$\varepsilon_{ss}^{M} = \gamma_{xs}^{M} = 0 \tag{A4.2}$$

4.1.3 Kinematic relations

The strains consist of two parts, namely the uniform axial membrane strains and the strains corresponding to bending of the plate elements. Following the Kirchoff-Love hypothesis stated above the strains can be determined according to Figure 4.3.

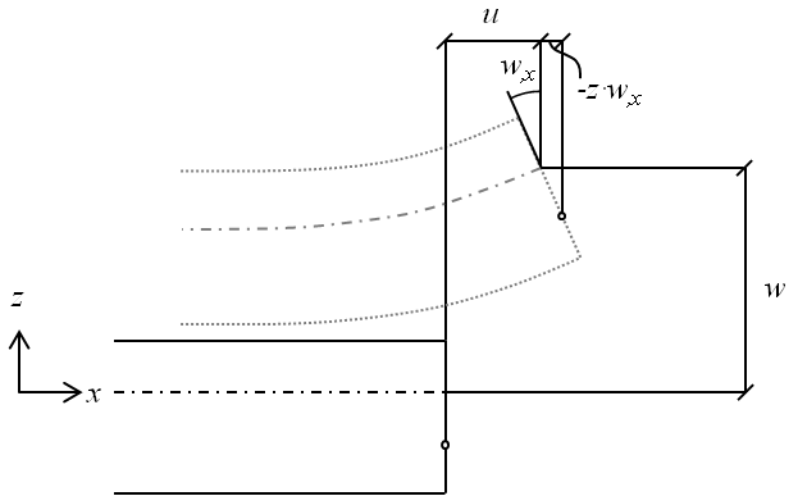

Figure 4.3: Kinematic relations for a plate element. Here the plate in x-direction is depicted but the same applies in s-direction.

The membrane strains are expressed and defined as the first derivative in x- and s-direction respectively, which give:

$$\varepsilon_{xx}^{M} = u_{,x} \qquad \varepsilon_{ss}^{M} = v_{,s} \qquad \gamma_{xs}^{M} = v_{,x} + u_{,s} \tag{4.6}$$

The strains corresponding to bending of the plate element are defined as:

$$\varepsilon_{xx}^{B} = -z \cdot w_{,xx} \qquad \varepsilon_{ss}^{B} = -z \cdot w_{,ss} \qquad \gamma_{xs}^{B} = -2z \cdot w_{,xs} \tag{4.7}$$

Note: The comma subscript $(\cdot)_{,}$ stands for partial derivatives, the superscripts $(\cdot)^{M}$ and $(\cdot)^{B}$ indicates membrane and bending terms respectively. Using the assumptions (A4.1) and (A4.2) together with the kinematic relations (4.6) and (4.7) the strain-displacement relations can be expressed in terms of the mid-plane displacement components as:

$$\varepsilon_{xx} = \varepsilon_{xx}^{M} + \varepsilon_{xx}^{B} = u_{,x} - z \cdot w_{,xx}$$

$$\varepsilon_{ss} = \varepsilon_{ss}^{M} + \varepsilon_{ss}^{B} = 0 - z \cdot w_{,ss} = -z \cdot w_{,ss} \tag{4.8}$$

$$\gamma_{xs} = \gamma_{xs}^{M} + \gamma_{xs}^{B} = -2z \cdot w_{,xs}$$

4.1.4 Constitutive relation

Linear elastic materials are to be used which means that the relation between stresses and strains are defined in terms of the Young's modulus E, the shear modulus G and the Poisson's ratio ν. The relation is defined as:

$$\sigma_{xx}^{B} = \frac{E}{1-\nu^2}(\varepsilon_{xx}^{B} + \nu\varepsilon_{ss}^{B}) \quad \sigma_{ss}^{B} = \frac{E}{1-\nu^2}(\varepsilon_{ss}^{B} + \nu\varepsilon_{xx}^{B}) \quad \tau_{xs}^{B} = G\gamma_{xs}^{B}$$

$$\sigma_{xx}^{M} = E\varepsilon_{xx}^{M} \tag{4.9}$$

Note: σ_{zz} is not written out here since, according to (A4.1), $\varepsilon_{zz} = 0$ and therefore it will not contribute to the virtual work.

Introduce the kinematic relations (4.8) into the constitutive relation (4.9) the stress components are given as:

$$\sigma_{xx} = E\varepsilon_{xx}^{M} + \frac{E}{1-\nu^2}(\varepsilon_{xx}^{B} + \nu\varepsilon_{ss}^{B}) = Eu_{,x} - z\frac{E}{1-\nu^2}\left(w_{,xx} + \nu w_{,ss}\right)$$

$$\sigma_{ss} = E\underbrace{\varepsilon_{ss}^{M}}_{=0} + \frac{E}{1-\nu^2}(\varepsilon_{ss}^{B} + \nu\varepsilon_{xx}^{B}) = -z\frac{E}{1-\nu^2}\left(w_{,ss} + \nu w_{,xx}\right) \tag{4.10}$$

$$\tau_{xs} = G\underbrace{\gamma_{xs}^{M}}_{=0} + G\gamma_{xs}^{B} = G\gamma_{xs}^{B} \quad = -2Gzw_{,xs}$$

Finally, insert the displacement field notation (4.3) into (4.10) the expression for the stress components are defined as:

$$\begin{aligned}\sigma_{xx} &= E\left(u_k\phi_{k,x}\right)_{,x} - z\frac{E}{1-\nu^2}\left[(w_k\phi_k)_{,xx} + \nu(w_k\phi_k)_{,ss}\right] \\ &= \left(Eu_k - z\frac{E}{1-\nu^2}w_k\right)\phi_{k,xx} - z\frac{\nu E}{1-\nu^2}w_{k,ss}\phi_k \\ \sigma_{ss} &= -z\frac{E}{1-\nu^2}\left[(w_k\phi_k)_{,ss} + \nu(w_k\phi_k)_{,xx}\right] \\ &= -z\frac{E}{1-\nu^2}w_{k,ss}\phi_k - z\frac{\nu E}{1-\nu^2}w_k\phi_{k,xx}\end{aligned} \tag{4.11}$$

$$\tau_{xs} = -2Gz(w_k\phi_k)_{,xs} = -2Gzw_{k,s}\phi_{k,x}$$

4.1.5 Formulation of the virtual work

The GBT fundamental equilibrium equations are derived by means of the principle of the virtual work. The total potential energy of the member is defined by the virtual work due to the internal forces and the external loads and the equilibrium condition is defined when the total potential energy is zero. This give:

$$\delta V = \delta U + \delta \Pi = 0 \tag{4.12}$$

Where δV is the total potential energy of the member, δU the virtual work of internal forces and $\delta \Pi$ is the virtual work related to the external loads.

4.1.5.1 Virtual work of internal forces

The variation in the virtual work due to internal forces is defined as stress times a virtual strain component denoted with a δ-sign. According to the simplifying approximations and assumptions the internal virtual work only involves terms related to normal longitudinal stresses σ_{xx}, normal transverse stresses σ_{ss} and the in-plane shear stresses σ_{xs}. The virtual work due to internal forces are defined as:

$$\delta U = \iiint_{L,b,t} [\sigma_{xx}\delta\varepsilon_{xx} + \sigma_{ss}\delta\varepsilon_{ss} + \tau_{xs}\delta\gamma_{xs}]dzdsdx = \delta U_{xx} + \delta U_{ss} + \delta U_{xs} \tag{4.13}$$

Insert the displacement components (4.3) into the kinematic relations (4.8) and differentiate with respect to x, then the virtual strain components are obtained as:

$$\begin{aligned}
\delta\varepsilon_{xx} &= \delta\varepsilon_{xx}^{M} + \delta\varepsilon_{xx}^{B} = \delta\left[u_{,x} - zw_{,xx}\right] = \delta\left[\left(u_i\phi_{i,x}\right)_{,x} - z(w_i\phi_i)_{,xx}\right] \\
&= [u_i - zw_i]\delta\phi_{i,xx} \\
\delta\varepsilon_{ss} &= \delta\varepsilon_{ss}^{M} + \delta\varepsilon_{ss}^{B} = \delta\left[-zw_{,ss}\right] = \delta\left[-z(w_i\phi_i)_{,ss}\right] = -zw_{i,ss}\delta\phi_i \\
\delta\gamma_{xs} &= \delta\gamma_{xs}^{M} + \delta\gamma_{xs}^{B} = \delta\left[-2zw_{,xs}\right] = \delta\left[-2zw_{i,s}\delta\phi_{i,x}\right] = -2zw_{i,s}\delta\phi_{i,x}
\end{aligned} \tag{4.14}$$

Insert the stresses (4.11) and virtual strain components (4.14) into the expression for internal virtual work (4.13) gives the total variation in internal strain energy. This will in the following be evaluated in one direction at the time, i.e. δU_{xx}, δU_{ss} and δU_{xs}.

Furthermore the Einstein's summation rule is applied in order to reduce the length of the expressions. The general expression is defined as:

$$a_i b_i \equiv \sum_i a_i b_i$$

Internal strain energy in x-direction

The contribution to the internal virtual work in x-direction is defined as:

$$\delta U_{xx} = \iiint_{L,b,t} \sigma_{xx}\delta\varepsilon_{xx}\,dzdsdx =$$

$$= \iiint_{L,b,t} \left[\left(Eu_k - z\frac{E}{1-\nu^2}w_k\right)\phi_{k,xx} - z\frac{\nu E}{1-\nu^2}w_{k,ss}\phi_k\right][u_i - zw_i]\delta\phi_{i,xx}\,dzdsdx =$$

$$= \iiint_{L,b,t} \left[\left(Eu_k u_i + z^2\frac{E}{1-\nu^2}w_k w_i - z\frac{E}{1-\nu^2}w_k u_i - zEu_k w_i\right)\phi_{k,xx} + \left(z^2\frac{\nu E}{1-\nu^2}w_{k,ss}w_i - z\frac{\nu E}{1-\nu^2}w_{k,ss}u_i\right)\phi_k\right]\delta\phi_{i,xx}\,dzdsdx$$

$$= \int_L \left[E(C_{ik}^I + C_{ik}^{II} - C_{ik}^{III} - C_{ik}^{IV})\phi_{k,xx} + G(D_{ik}^{II} - D_{ik}^{IV})\phi_k\right]\delta\phi_{i,xx}\,dx$$

Since the virtual displacement components $\delta\phi_{i,xx}$ and $\delta\phi_{i,x}$ are expressed in its derivatives, integration by parts is necessary to have them in the original state. Perform integration by parts for the two involved terms gives:

$$\int_L E(C_{ik}^I + C_{ik}^{II} - C_{ik}^{III} - C_{ik}^{IV})\phi_{k,xx}\delta\phi_{i,xx}\,dx =$$

$$= \left[E(C_{ik}^I + C_{ik}^{II} - C_{ik}^{III} - C_{ik}^{IV})\phi_{k,xx}\delta\phi_{i,x}\right]_0^L - \left[E(C_{ik}^I + C_{ik}^{II} - C_{ik}^{III} - C_{ik}^{IV})\phi_{k,xxx}\delta\phi_i\right]_0^L + \int_L E(C_{ik}^I + C_{ik}^{II} - C_{ik}^{III} - C_{ik}^{IV})\phi_{k,xxxx}\delta\phi_i\,dx$$

$$\int_L G(D_{ik}^{II} - D_{ik}^{IV})\phi_k \delta\phi_{i,xx}\, dx$$

$$= \left[G(D_{ik}^{II} - D_{ik}^{IV})\phi_k \delta\phi_{i,x}\right]_0^L - \int_L G(D_{ik}^{II} - D_{ik}^{IV})\phi_{k,x} \delta\phi_{i,x}\, dx$$

$$= \left[G(D_{ik}^{II} - D_{ik}^{IV})\phi_k \delta\phi_{i,x}\right]_0^L - \left[G(D_{ik}^{II} - D_{ik}^{IV})\phi_{k,x} \delta\phi_i\right]_0^L$$

$$+ \int_L G(D_{ik}^{II} - D_{ik}^{IV})\phi_{k,xx} \delta\phi_i\, dx$$

Put the expressions for the two terms together, the variation in internal work in the x-direction is finally obtained as:

$$\begin{aligned}\delta U_{xx} = \int_L \big[&E(C_{ik}^{I} + C_{ik}^{II} - C_{ik}^{III} - C_{ik}^{IV})\phi_{k,xxxx} \\ &+ G(D_{ik}^{II} - D_{ik}^{IV})\phi_{k,xx}\big]\delta\phi_i\, dx \\ &+ \big[\big(E(C_{ik}^{I} + C_{ik}^{II} - C_{ik}^{III} - C_{ik}^{IV})\phi_{k,xx} \\ &+ G(D_{ik}^{II} - D_{ik}^{IV})\phi_k\big)\delta\phi_{i,x}\big]_0^L \\ &- \big[\big(E(C_{ik}^{I} + C_{ik}^{II} - C_{ik}^{III} - C_{ik}^{IV})\phi_{k,xxx} \\ &+ G(D_{ik}^{II} - D_{ik}^{IV})\phi_{k,x}\big)\delta\phi_i\big]_0^L\end{aligned} \tag{4.15}$$

Internal strain energy in s-direction

The virtual displacement component $\delta\phi_i$ is already expressed in its original state. Therefore no integration by parts is needed, hence the contribution to the internal virtual work in s-direction is defined as:

$$\delta U_{ss} = \iiint_{L,b,t} \sigma_{ss}\delta\varepsilon_{ss}dzdsdx =$$

$$= \iiint_{L,b,t} \left[-z\frac{E}{1-\nu^2}w_{k,ss}\phi_k - z\frac{\nu E}{1-\nu^2}w_k\phi_{k,xx}\right]\left[-zw_{i,ss}\delta\phi_i\right]dzdsdx =$$

$$= \iiint_{L,b,t} \left[z^2\frac{\nu E}{1-\nu^2}w_k w_{i,ss}\phi_{k,xx} + z^2\frac{E}{1-\nu^2}w_{k,ss}w_{i,ss}\phi_k\right]\delta\phi_i dzdsdx$$

The internal work in s-direction can then be written as:

$$\delta U_{ss} = \int_L \left[GD_{ik}^{III}\phi_{k,xx} + B_{ik}\phi_k\right]\delta\phi_i dx \tag{4.16}$$

Internal strain energy xs-terms

The contribution to the internal work in "xs-direction" or due to the shear components are defined as:

$$\delta U_{xs} = \iiint_{L,b,t} \tau_{xs}\delta\gamma_{xs}dzdsdx$$

$$= \iiint_{L,b,t} \left[-2Gzw_{k,s}\phi_{k,x}\right]\left[-2zw_{i,s}\delta\phi_{i,x}\right]dzdsdx =$$

$$= \iiint_{L,b,t} \left[4Gz^2 w_{k,s}w_{i,s}\phi_{k,x}\right]\delta\phi_{i,x}dzdsdx$$

$$= \int_L GD_{ik}^{I}\phi_{k,x}\delta\phi_{i,x}dx$$

The virtual displacement component $\delta\phi_{i,x}$ is expressed in its first derivative, so integration by parts is necessary in order to have a representation in its original state.

$$\int_L GD_{ik}^I \phi_{k,x} \delta\phi_{i,x} dx = \left[GD_{ik}^I \phi_{k,x} \delta\phi_i\right]_0^L - \int_L GD_{ik}^I \phi_{k,xx} \delta\phi_i dx$$

The variation in internal virtual work in xs-direction is then finally obtained as:

$$\delta U_{xs} = -\int_L GD_{ik}^I \phi_{k,xx} \delta\phi_i dx + \left[GD_{ik}^I \phi_{k,x} \delta\phi_i\right]_0^L \tag{4.17}$$

Now all the terms in each direction have been determined in (4.15), (4.16) and (4.17) respectively. The total variation in internal virtual work is obtained as the sum of the three terms as:

$$\begin{aligned}
\delta U &= \delta U_{xx} + \delta U_{ss} + \delta U_{xs} \\
&= \int_L \left[E(C_{ik}^I + C_{ik}^{II} - C_{ik}^{III} - C_{ik}^{IV})\phi_{k,xxxx}\right. \\
&\quad \left. + G(D_{ik}^{II} - D_{ik}^{IV})\phi_{k,xx}\right]\delta\phi_i dx \\
&\quad + \left[\left(E(C_{ik}^I + C_{ik}^{II} - C_{ik}^{III} - C_{ik}^{IV})\phi_{k,xx}\right.\right. \\
&\quad \left.\left. + G(D_{ik}^{II} - D_{ik}^{IV})\phi_k\right)\delta\phi_{i,x}\right]_0^L \\
&\quad - \left[\left(E(C_{ik}^I + C_{ik}^{II} - C_{ik}^{III} - C_{ik}^{IV})\phi_{k,xxx}\right.\right. \\
&\quad \left.\left. + G(D_{ik}^{II} - D_{ik}^{IV})\phi_{k,x}\right)\delta\phi_i\right]_0^L \\
&\quad + \int_L \left[GD_{ik}^{III}\phi_{k,xx} + B_{ik}\phi_k\right]\delta\phi_i dx - \int_L GD_{ik}^I \phi_{k,xx}\delta\phi_i dx \\
&\quad + \left[GD_{ik}^I \phi_{k,x}\delta\phi_i\right]_0^L
\end{aligned} \tag{4.18}$$

In the derived expression for the internal strain energy (4.18) each B_{ik}-, C_{ik}- and D_{ik}-term can be evaluated further, i.e. integration over the thickness t. These terms are defined below and also the result after integration and introduction of the plate stiffness K is shown. See all steps in the integration process in Appendix A.

$$B_{ik} = \frac{E}{1-\upsilon^2}\iint_{b,t} z^2 w_{k,ss} w_{i,ss} dzds = K\int_b w_{k,ss} w_{i,ss} ds \tag{4.19}$$

$$C_{ik}^I = \iint_{b,t} u_k u_i dzds = t\int_b u_k u_i ds \tag{4.20}$$

$$C_{ik}^{II} = \frac{1}{1-\nu^2}\iint_{b,t} z^2 w_k w_i dz ds = \frac{K}{E}\int_b w_k w_i ds \tag{4.21}$$

$$C_{ik}^{III} = \frac{1}{1-\nu^2}\iint_{b,t} z w_k u_i dz ds = 0 \tag{4.22}$$

$$C_{ik}^{IV} = \iint_{b,t} z u_k w_i dz ds = 0 \tag{4.23}$$

$$D_{ik}^{I} = 4\iint_{b,t} z^2 w_{k,s} w_{i,s} dz ds = \frac{t^3}{3}\int_b w_{k,s} w_{i,s} ds \tag{4.24}$$

$$D_{ik}^{II} = \frac{1}{G}\frac{\nu E}{1-\nu^2}\iint_{b,t} z^2 w_{k,ss} w_i dz ds = \frac{\nu K}{G}\int_b w_{k,ss} w_i ds \tag{4.25}$$

$$D_{ik}^{III} = \frac{1}{G}\frac{\nu E}{1-\nu^2}\iint_{b,t} z^2 w_k w_{i,ss} dz ds = \frac{\nu K}{G}\int_b w_k w_{i,ss} ds \tag{4.26}$$

$$D_{ik}^{IV} = \frac{1}{G}\frac{\nu E}{1-\nu^2}\iint_{b,t} z w_{k,ss} u_i dz ds = 0 \tag{4.27}$$

Where the plate stiffness K is defined as:

$$K = \frac{E t^3}{12(1-\nu^2)} \tag{4.28}$$

4.1.5.2 The virtual work of external loads

A general applied external load $q(x,s)$ acting at the mid-surface of a plate element and the load consists of the three components q_x, q_s and q_z defined in the local coordinate system (x,s,z). The q_x and q_s components are distributed in-plane loads and the q_z-component is the out of plane load, see Figure 4.4.

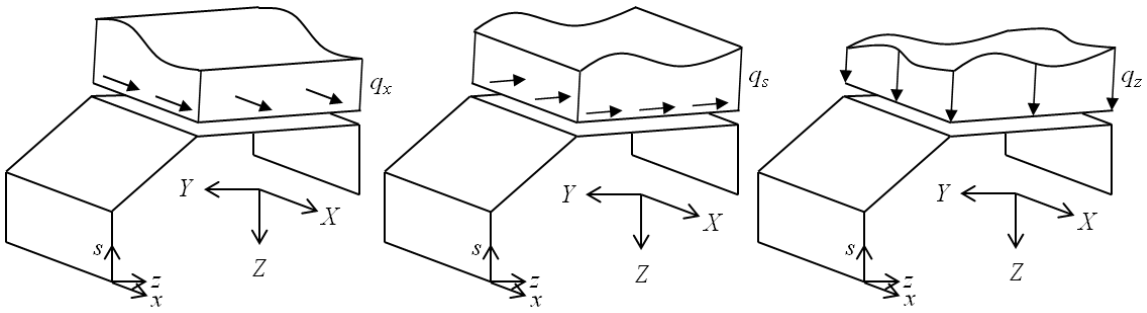

Figure 4.4: A general applied external load $q(x,s)$ consist of the three components $q_x(x)$, $q_s(s)$ and $q_z(x,s)$.

The general applied load is defined by its local components as:

$$q(x,s) = q_x(x) + q_s(s) + q_z(x,s) \tag{4.29}$$

The expression for the external virtual work is defined as the load component times the corresponding virtual displacement as:

$$\delta\Pi = -\iint_{L,b} (q_x \delta u + q_s \delta v + q_z \delta w)\, ds dx \tag{4.30}$$

Note that integration over the thickness t is already incorporated in the definition of $q(x,s)$. The virtual displacements are defined and obtained by inserting the displacement field notation (4.3) as:

$$\delta u = u_i \delta\phi_{i,x} \qquad \delta v = v_i \delta\phi_i \qquad \delta w = w_i \delta\phi_i \tag{4.31}$$

Insert the virtual displacements (4.31) into the expression for the external virtual work (4.30) gives:

$$\delta\Pi = -\iint_{L,b} \left(q_x u_i \delta\phi_{i,x} + q_s v_i \delta\phi_i + q_z w_i \delta\phi_i\right) ds dx \tag{4.32}$$

The virtual displacement on the load component q_x is expressed in the first order derivative, hence integration by parts is necessary to obtain its ordinary state:

$$\iint_{L,b} q_x u_i \delta\phi_{i,x} ds dx = \left[\int_b q_x u_i \delta\phi_i ds\right]_0^L - \iint_{L,b} q_{x,x} u_i \delta\phi_i ds dx \tag{4.33}$$

Insert q_x-terms (4.33) into (4.32) gives the total variation in external virtual work:

$$\begin{aligned} \delta\Pi &= -\iint_{L,b} \left(-q_{x,x} u_i + q_s v_i + q_z w_i\right)\delta\phi_i \, ds dx - \left[\int_b q_x u_i \delta\phi_i ds\right]_0^L \\ &= -\int_L q_i \, \delta\phi_i dx + \int_L q_{x,x.i} \, \delta\phi_i dx - \left[\int_b q_x u_i \delta\phi_i ds\right]_0^L \end{aligned} \tag{4.34}$$

Where:

$$q_i = \int_b (q_s v_i + q_z w_i) ds \qquad q_{x,x.i} = \int_b q_{x,x} u_i ds \tag{4.35}$$

4.1.5.3 Total potential energy of the member

The total potential energy of the member is obtained by putting the expressions for variation in internal virtual work (4.18) and the external virtual work (4.34) into the expression of the total potential energy (4.12). This give:

$$\begin{aligned}
\delta V = \int_L \left[E(C_{ik}^I + C_{ik}^{II})\phi_{k,xxxx} + GD_{ik}^{II}\phi_{k,xx}\right]\delta\phi_i dx \\
+ \left[\left(E(C_{ik}^I + C_{ik}^{II})\phi_{k,xx} + GD_{ik}^{II}\phi_k\right)\delta\phi_{i,x}\right]_0^L \\
- \left[\left(E(C_{ik}^I + C_{ik}^{II})\phi_{k,xxx} + GD_{ik}^{II}\phi_{k,x}\right)\delta\phi_i\right]_0^L \\
+ \int_L \left[GD_{ik}^{III}\phi_{k,xx} + B_{ik}\phi_k\right]\delta\phi_i dx - \int_L GD_{ik}^{I}\phi_{k,xx}\delta\phi_i dx \\
+ \left[GD_{ik}^{I}\phi_{k,x}\delta\phi_i\right]_0^L - \int_L q_i\,\delta\phi_i dx + \int_L q_{x,x.i}\,\delta\phi_i dx \\
- \left[\int_b q_x u_i \delta\phi_i ds\right]_0^L \\
= \int_L \left[E(C_{ik}^I + C_{ik}^{II})\phi_{k,xxxx} - G\left(D_{ik}^I - (D_{ik}^{II} + D_{ik}^{III})\right)\phi_{k,xx}\right. \\
\left. + B_{ik}\phi_k\right]\delta\phi_i dx - \int_L q_i\,\delta\phi_i dx + \int_L q_{x,x.i}\,\delta\phi_i dx \\
+ \left[\left(E(C_{ik}^I + C_{ik}^{II})\phi_{k,xx} + GD_{ik}^{II}\phi_k\right)\delta\phi_{i,x}\right]_0^L \\
+ \left[\left(-E(C_{ik}^I + C_{ik}^{II})\phi_{k,xxx} + G(D_{ik}^I - D_{ik}^{II})\phi_{k,x}\right)\delta\phi_i\right. \\
\left. - \int_b q_x u_i \delta\phi_i ds\right]_0^L = 0
\end{aligned}$$

4.1.6 The equilibrium equation and boundary conditions

Since $\delta\phi_i$ is an admissible and an arbitrary function and the expression within the integrals must hold any way, the system of equilibrium equations are then obtained as:

$$EC_{ik}\phi_{k,xxxx} - GD_{ik}\phi_{k,xx} + B_{ik}\phi_k = q_i - q_{x,x.i} \tag{4.36}$$

Where:

$$C_{ik} = C_{ik}^{I} + C_{ik}^{II} \tag{4.37}$$

$$D_{ik} = D_{ik}^{I} - (D_{ik}^{II} + D_{ik}^{III}) \tag{4.38}$$

The boundary conditions are just stated as they are obtained and will be treated more specific after the eigenvector transformation have been introduced, see Section 4.6.1. Hence, the boundary term is just stated as it is obtained here.

$$\begin{aligned} &\left[\left(-EC_{ik}\phi_{k,xxx} + G(D_{ik}^{I} - D_{ik}^{II})\phi_{k,x} - \int_{b} q_x u_i ds\right)\delta\phi_i\right] = 0 \\ &\left[\left(EC_{ik}\phi_{k,xx} + GD_{ik}^{II}\phi_k\right)\delta\phi_{i,x}\right]_0^L = 0 \end{aligned} \tag{4.39}$$

Note: Summation convention over i and k applies in order to have the total potential energy of the member.

4.2 Cross-sectional analysis – geometric relations

In Section4.1the derivation of the GBT fundamental equilibrium equation (4.36) is carried out with arbitrary displacement functions. In this section, those displacement functions are defined and the relation between them will also be determined.

The following derivation is carried out by only considering natural nodes, so within this chapter "nodes" referrers to natural nodes. The index k is in the following skipped since the relation between the u-, v- and w-displacements must hold for all deformation modes k.

4.2.1 Definition of coordinate systems and displacement notations

Figure 4.5 shows the notations used in the following derivations were rings denote node numbering and squares denote plate element numbering. The global coordinate system (X, Y, Z), the global displacements (U, V, W), the local coordinate system (x, s, z) and the local displacements are defined in Section 4.1. The global nodal displacements are denoted as U_r, V_r and W_r for the corresponding node r.

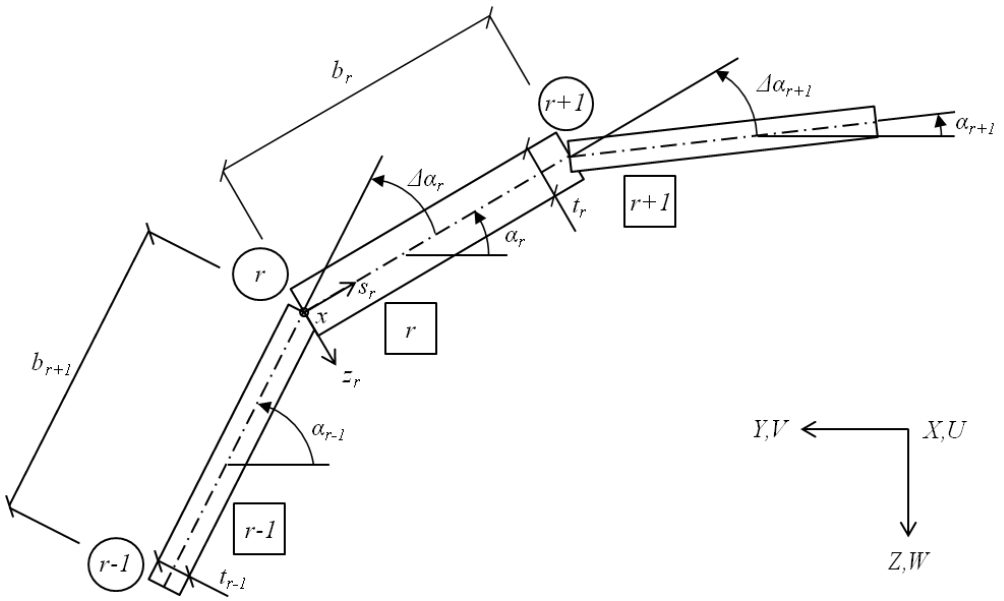

Figure 4.5: Definition of cross-section entities: For plate r the corresponding widths b_r, thickness t_r and angle α_r are defined. For the inner (natural) nodes $r = 2$ to $r = n$ the nodal angel difference $\Delta\alpha_r$ is defined as well.

As shortly mentioned in Section 4.1, a plate element is defined between non-zero angles differences, i.e. a flat plate only consist of one plate element. The cross-sections consists of n plate elements and $n + 1$ nodes and the cross-sectional dimensions for plate element r are the thickness t_r and the plate-width b_r. The angel that each plate element r forms with the Y-axis have the notation α_r and the difference compared to the previous plate element $r - 1$ is defined as $\Delta\alpha_r$.

4.2.1.1 Local displacements

The displacement parallel to the mid-plane and in the s-direction is denoted v_r and is defined from the mid-point $m$at the mid-plane and are according to assumption (A4.2) constant along the plate element. The displacements perpendicular to the mid-plane or parallel to z-axis are denoted as $w_{1.r}$ for the first node, $w_{2.r}$ for the end node and the element average displacement w_r is defined from the mid-point. The plate element rotation is defined as ϑ_r, see Figure 4.6.

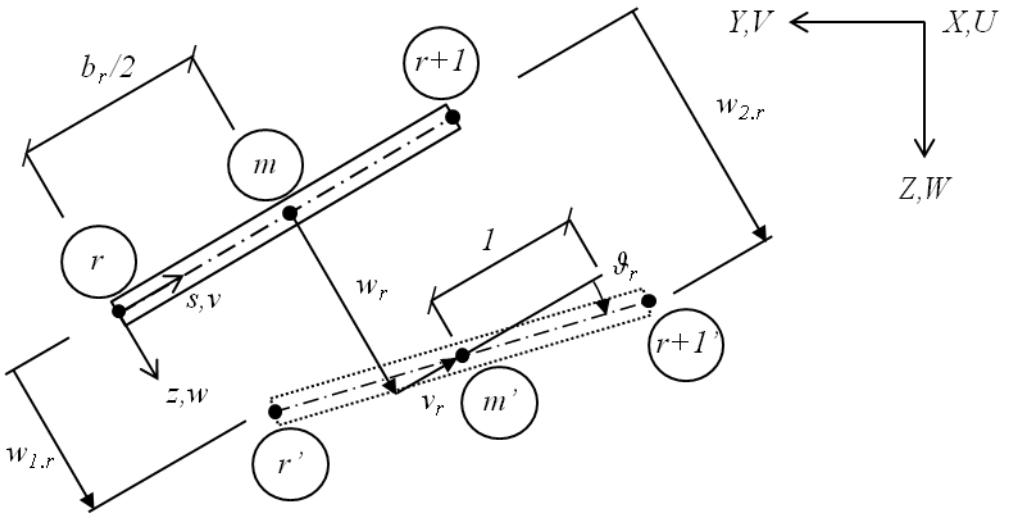

Figure 4.6: Designation of the cross-sectional displacements

From assumptions (A4.1) and (A4.2) one can read that the displacements no longer are independent of each other. The relation between the axial u-displacements and the v-displacements can be therefore be completely defined, wherefrom one can read that the u-displacements must vary linearly within each plate element. This makes it possible to express all displacement components v_r, w_r and ϑ_r in the longitudinal displacement u_r and they therefore form the degrees of freedom in the analysis. Since all of these functions are "discrete" in that meaning that the nodes can describe the behaviour and therefore a more compact matrix notation will be introduced.

4.2.2 In-plane displacements

From assumption (A4.2) and the kinematic relations (4.6) no deformations in s-direction will occur, i.e. $v_{,s} = 0$ and therefore v-displacements must be constant within each plate element. One can also read that the u-displacements must vary linearly within each plate and the u- and v-displacements can be determined according to Figure 4.7.

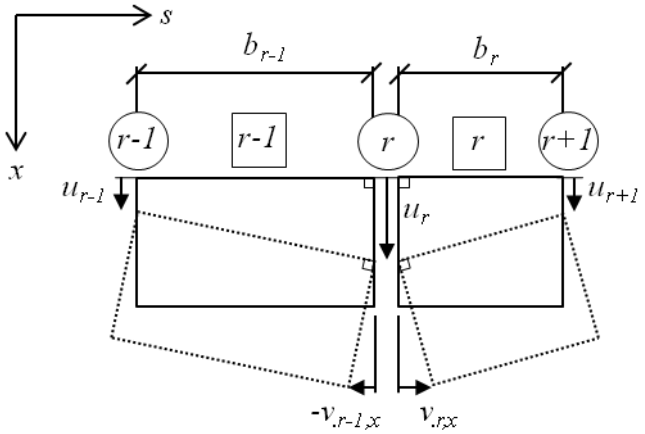

Figure 4.7: Geometric relations in longitudinal-transversal direction for an arbitrary flattened cross-section where the adjacent plate elements to node r is depicted.

The u- and v-displacement relation is defined as:

$$v_{r,x} = -u_{r,s} = -\frac{u_{r+1} - u_r}{b_r} = \frac{1}{b_r}u_r - \frac{1}{b_r}u_{r+1} \tag{4.40}$$

This also can be written in a more compact matrix form as:

$$\boldsymbol{v}_{,x} = \boldsymbol{F}_v \cdot \boldsymbol{u} \tag{4.41}$$

Where each matrix is of the sizes $\dim(\boldsymbol{v}_{,x}) = \{n \times 1\}$, $\dim(\boldsymbol{u}) = \{(n+1) \times 1\}$ and $\dim(\boldsymbol{F}_v) = \{n \times (n+1)\}$. A programming ready $\boldsymbol{F}_v$-matrix is defined in Appendix B and the other two vectors are on the form:

$$\begin{aligned} \boldsymbol{u} &= [u_1 \quad u_2 \quad \cdots \quad u_{n+1}]^T \\ \boldsymbol{v}_{,x} &= [v_{1,x} \quad v_{2,x} \quad \cdots \quad v_{n,x}]^T \end{aligned} \tag{4.42}$$

Note that (4.41) only describes the relation between u-displacements and first order derivative of v-displacements and also that the vector $\boldsymbol{v}_{,x}$ contains the element displacements while the $\boldsymbol{u}$-vector contains the nodal displacements.

4.2.3 Displacements perpendicular to the plate elements

Thew_r-displacements perpendicular to the mid-plane of plate element r is of interest to be expressed in the longitudinal displacement u_r. This relation is obtained by first relate the w-displacements to the v-displacements, see Figure 4.8. Since the $u - v$-relations (4.40) are known also the $u - w$-relation can be completely determined.

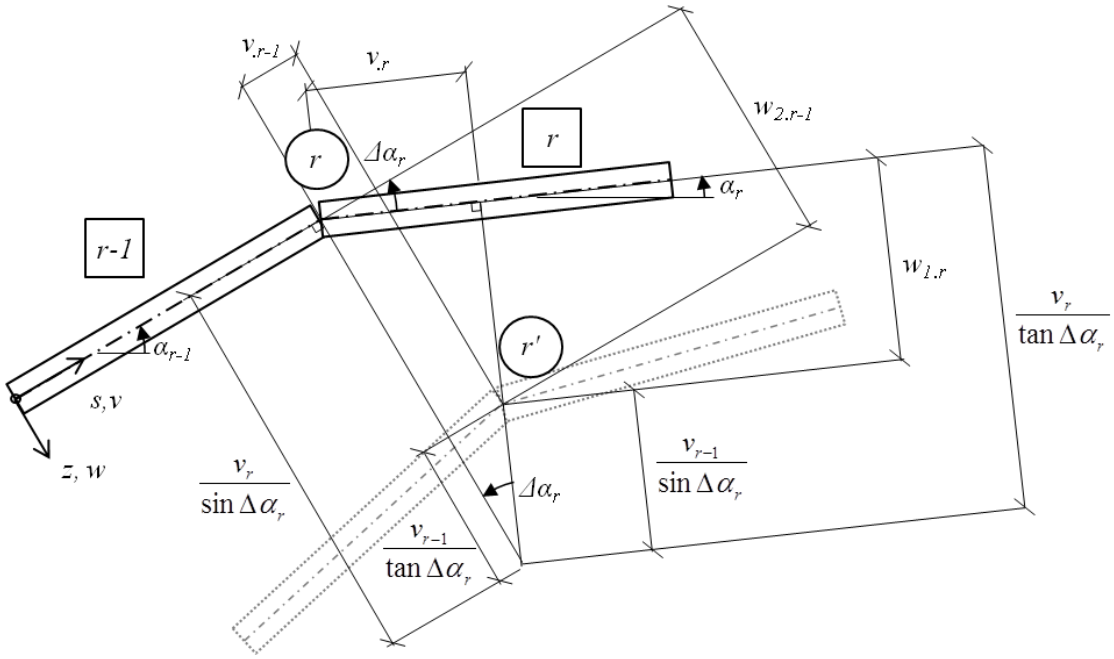

Figure 4.8: Geometric relations between the in-plane displacements v_r and the vertical displacements w_r are defined for node r(ring) and the adjacent plate elements $r-1$ and r (squares). The vertical element displacement w_r is defined by the nodal displacements at the plate ends denoted $w_{1.r}$ for the first end and $w_{2.r}$ for the second end of plate element r.

The relations can be expressed via trigonometric functions and the angel difference $\Delta\alpha_r$ at the node r defined as:

$$\Delta\alpha_r = \alpha_{r-1} - \alpha_r \tag{4.43}$$

According to this the end displacements at node r can be defined by the second end of plate element $r-1$ and the first end of plate element r. This give:

$$w_{2.r-1} = \frac{v_r}{\sin\Delta\alpha_r} - \frac{v_{r-1}}{\tan\Delta\alpha_r} \qquad w_{1.r} = \frac{v_r}{\tan\Delta\alpha_r} - \frac{v_{r-1}}{\sin\Delta\alpha_r} \tag{4.44}$$

In order to relate the nodal transverse displacements $w_{2.r-1}$ and $w_{1.r}$ to the u-displacements, derivate (4.44) with respect to x once and insert the $u-v$-reltation (4.40) the transverse nodal end displacements are obtained as:

$$\begin{aligned} w_{1.r,x} &= \frac{v_{r,x}}{\tan\Delta\alpha_r} - \frac{v_{r-1,x}}{\sin\Delta\alpha_r} \\ &= \frac{1}{b_r\tan\Delta\alpha_r}u_r - \frac{1}{b_r\tan\Delta\alpha_r}u_{r+1} - \frac{1}{b_{r-1}\sin\Delta\alpha_r}u_{r-1} \\ &\quad + \frac{1}{b_{r-1}\sin\Delta\alpha_r}u_r \\ &= -\frac{1}{b_{r-1}\sin\Delta\alpha_r}u_{r-1} + \left(\frac{1}{b_{r-1}\sin\Delta\alpha_r} + \frac{1}{b_r\tan\Delta\alpha_r}\right)u_r \\ &\quad - \frac{1}{b_r\tan\Delta\alpha_r}u_{r+1} \end{aligned} \tag{4.45}$$

$$\begin{aligned} w_{2.r,x} &= \frac{v_{r+1,x}}{\sin\Delta\alpha_r} - \frac{v_{r,x}}{\tan\Delta\alpha_r} \\ &= \frac{1}{b_{r+1}\sin\Delta\alpha_r}u_{r+1} - \frac{1}{b_{r+1}\sin\Delta\alpha_r}u_{r+2} - \frac{1}{b_r\tan\Delta\alpha_r}u_r \\ &\quad + \frac{1}{b_r\tan\Delta\alpha_r}u_{r+1} \\ &= -\frac{1}{b_r\tan\Delta\alpha_r}u_r + \left(\frac{1}{b_r\tan\Delta\alpha_r} + \frac{1}{b_{r+1}\sin\Delta\alpha_r}\right)u_{r+1} \\ &\quad - \frac{1}{b_{r+1}\sin\Delta\alpha_r}u_{r+2} \end{aligned} \tag{4.46}$$

In order to have the element displacement $w_{r,x}$ take the average of the nodal displacements $w_{1.r,x}$ and $w_{2.r,x}$. This can be written in a more compact matrix form as:

$$\boldsymbol{w}_{1,x} = \boldsymbol{F}_{w1}\cdot\boldsymbol{u} \tag{4.47}$$

$$\boldsymbol{w}_{2,x} = \boldsymbol{F}_{w2}\cdot\boldsymbol{u} \tag{4.48}$$

$$\boldsymbol{w}_{,x} = \frac{\boldsymbol{w}_{1,x} + \boldsymbol{w}_{2,x}}{2} = \frac{\boldsymbol{F}_{w1} + \boldsymbol{F}_{w2}}{2}\cdot\boldsymbol{u} = \boldsymbol{F}_w\cdot\boldsymbol{u} \tag{4.49}$$

Where the matrices are of the size $\dim(\boldsymbol{w}_{1,x}) = \dim(\boldsymbol{w}_{2,x}) = \{n \times 1\}$ and $\dim(\boldsymbol{F}_{w1}) = \dim(\boldsymbol{F}_{w2}) = \dim(\boldsymbol{F}_{w}) = \{n \times (n+1)\}$. The displacements of the inner nodes (node 2 to node n) can now be expressed by the known u-displacements. The outer displacements $w_{1.1,x}$ and $w_{2.n,x}$ are still unknown but can be solved by means of the force method and in particular the nodal transverse bending moments m_s, see Section 4.2.7. Programming ready $\boldsymbol{F}_{w1}$- and $\boldsymbol{F}_{w2}$-matrices can be found in Appendix B. The corresponding nodal transverse displacement vectors $\boldsymbol{w}_{1,x}$ and $\boldsymbol{w}_{2,x}$ will have the form:

$$\begin{aligned} \boldsymbol{w}_{1,x} &= [w_{1.1,x} \quad w_{1.2,x} \quad \cdots \quad w_{1.n,x}]^T \\ \boldsymbol{w}_{2,x} &= [w_{2.1,x} \quad w_{2.2,x} \quad \cdots \quad w_{2.n,x}]^T \end{aligned} \tag{4.50}$$

Note that the vectors still contain the first order derivatives of the end displacements.

4.2.4 The plate element rotations

The element rotations ϑ_r are necessary to be determined so that in the following the nodal rotations $\Delta\vartheta_r$ and the nodal moments $m_{s.r}$ can be determined and finally out of that the first and last plate element displacements can be defined. The element rotations are also used in the normalization of the deformation mode 4 corresponding to rigid body rotation mode, see Section 4.5. But first, the element rotations must be defined and are obtained from Figure 4.9.

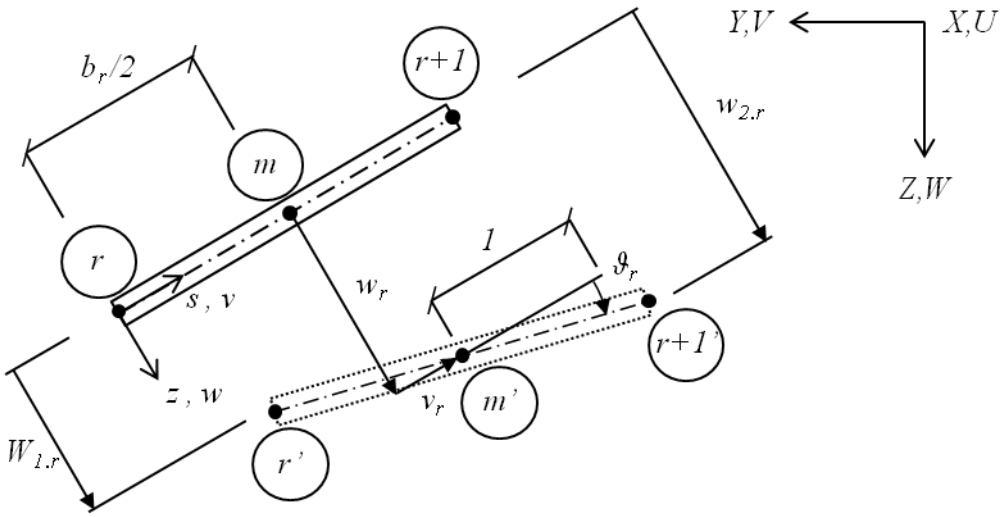

Figure 4.9: Designation of the local displacments in the in the cross-sectional plane

The relation between the element rotation ϑ_r and the vertical nodal transversal displacements $w_{1.r}$ and $w_{2.r}$ is obtained as:

$$\vartheta_r = \frac{w_{2.r} - w_{1.r}}{b_r} \tag{4.51}$$

Since the nodal displacements $w_{1.r,x}$ and $w_{2.r,x}$ are expressed in the first ordered derivative the element rotation will also be expressed in the first ordered derivative as:

$$\vartheta_{r,x} = \frac{w_{2.r,x} - w_{1.r,x}}{b_r} \tag{4.52}$$

This can be written in a more compact matrix form by simply using the nodal transversal displacements defined in (4.50) as:

$$\boldsymbol{\vartheta}_{,x} = (\boldsymbol{F}_{\vartheta 2} - \boldsymbol{F}_{\vartheta 1}) \cdot \boldsymbol{u} = \boldsymbol{F}_{\vartheta} \cdot \boldsymbol{u} \tag{4.53}$$

$\boldsymbol{F}_{\vartheta 1}$ and $\boldsymbol{F}_{\vartheta 2}$ can be obtained by simple divide row r in $\boldsymbol{F}_{w1}$(4.47) (4.47) and $\boldsymbol{F}_{w2}$ (4.48) by the corresponding plate element width b_r.

In order to calculate the transverse bending moments m_s out of the longitudinal displacement u the change of the mutual angle must be used which only can be defined for the inner nodes (node 3 to node $n-1$). Using the definition in (4.51) one gets the angle difference as:

$$\Delta\vartheta_r = \vartheta_r - \vartheta_{r-1} = \frac{w_{2.r,x} - w_{1.r,x}}{b_r} - \frac{w_{2.r-1,x} - w_{1.r-1,x}}{b_{r-1}} \tag{4.54}$$

This could be expressed on more compact matrix form by combining the $\boldsymbol{F}_{\vartheta 1}$- and $\boldsymbol{F}_{\vartheta 2}$-matrices defined in (4.53).

$$\boldsymbol{\Delta\vartheta}_{,x} = \Delta\boldsymbol{F}_{\vartheta} \cdot \boldsymbol{u} \tag{4.55}$$

4.2.5 The separation of variables approach

The preceding Sections 4.2.2, 4.2.3 and 4.2.4 have shown that is it possible to express the displacement components v, w and ϑ by geometric relations through the longitudinal displacement u. Therefore forms the warping values the basis of the displacements, stresses and the resultant force sizes. Introduce the unit warping function $\bar{u}_r(s)$. It is defined as a linear function within a plate element which has unit value for node r and zero for all other nodes, see Figure 4.10. Note: this function is denoted with a bar to distinguish that it corresponds to unit displacements.

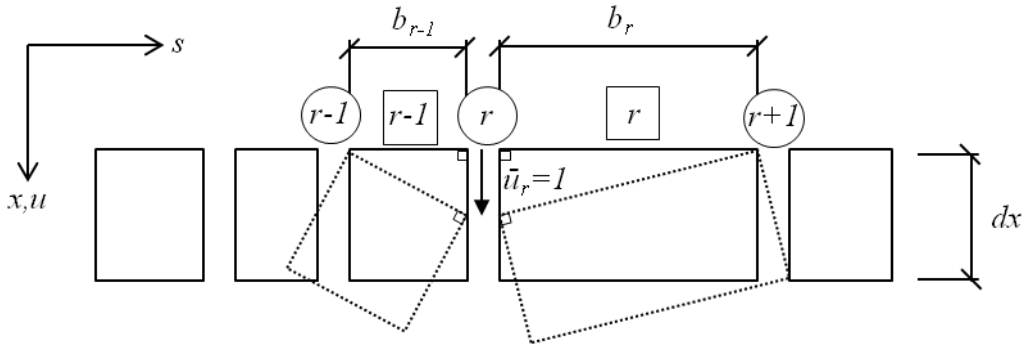

Figure 4.10: Basic warping function defined on an unfolded cross-section

In order to have a satisfactory presentation of the beam theories, all displacement variables are expressed by the separation of variables approach. The cross-sectional local coordinates s and z are separated from the longitudinal x coordinate which is

described by the longitudinal amplitude function $\phi(x)$ with its derivatives $\phi_{,x}(x)$, $\phi_{,xx}(x)$ etc. An arbitrary warping function $u(s,x)$ can then be expressed by the linear combination:

$$u(s,x) = \sum_{r=1}^{n+1} \bar{u}_r(s) \cdot \bar{\phi}_{r,x}(x) \tag{4.56}$$

The amplitude function $\bar{\phi}_r(x)$ is denoted with a bar to express that it is related to the unit warping function $\bar{u}_r(s)$. For one term in the summation above one has:

$$u(x) = \bar{u}_r \cdot \bar{\phi}_{r,x}(x) \tag{4.57}$$

This can be written on a more compact matrix form as:

$$\boldsymbol{u}(x) = \bar{\boldsymbol{U}} \cdot \bar{\boldsymbol{\phi}}_{,x}(x) \tag{4.58}$$

Where the involved terms are defined as:

$$\boldsymbol{u}(x) = [u_1(x) \quad u_2(x) \quad \cdots \quad u_{n+1}(x)]^T \tag{4.59}$$

$$\bar{\boldsymbol{u}}_r = \begin{bmatrix} 0 & \cdots & 0 & \underbrace{1}_{position\ r} & 0 & \cdots & 0 \end{bmatrix}^T \tag{4.60}$$

$$\bar{\boldsymbol{U}} = [\bar{\boldsymbol{u}}_1 \quad \bar{\boldsymbol{u}}_2 \quad \cdots \quad \bar{\boldsymbol{u}}_{n+1}]^T \tag{4.61}$$

$$\bar{\boldsymbol{\phi}}(x) = [\bar{\phi}_1(x) \quad \bar{\phi}_2(x) \quad \cdots \quad \bar{\phi}_{n+1}(x)]^T \tag{4.62}$$

Using the notation in (4.58), the cross-sectional displacements (4.41), (4.49) and (4.55) can be obtained as:

$$\boldsymbol{v}_{,x}(x) = \boldsymbol{F}_v \cdot \bar{\boldsymbol{U}} \cdot \bar{\boldsymbol{\phi}}_{,x}(x) = \bar{\boldsymbol{F}}_v \cdot \bar{\boldsymbol{\phi}}_{,x}(x) \tag{4.63}$$

$$\boldsymbol{w}_{,x}(x) = \boldsymbol{F}_w \cdot \bar{\boldsymbol{U}} \cdot \bar{\boldsymbol{\phi}}_{,x}(x) = \bar{\boldsymbol{F}}_w \cdot \bar{\boldsymbol{\phi}}_{,x}(x) \tag{4.64}$$

$$\boldsymbol{\vartheta}_{,x}(x) = \boldsymbol{F}_\vartheta \cdot \bar{\boldsymbol{U}} \cdot \bar{\boldsymbol{\phi}}_{,x}(x) = \bar{\boldsymbol{F}}_\vartheta \cdot \bar{\boldsymbol{\phi}}_{,x}(x) \tag{4.65}$$

$$\boldsymbol{\Delta\vartheta}_{,x}(x) = \Delta\boldsymbol{F}_\vartheta \cdot \bar{\boldsymbol{U}} \cdot \bar{\boldsymbol{\phi}}_{,x}(x) = \Delta\bar{\boldsymbol{F}}_\vartheta \cdot \bar{\boldsymbol{\phi}}_{,x}(x) \tag{4.66}$$

Since $\bar{\boldsymbol{U}}$ is a unit matrix $\boldsymbol{F}_v$ will remain identical to $\bar{\boldsymbol{F}}_v$. The same holds for the other matrices $\bar{\boldsymbol{F}}_w$, $\bar{\boldsymbol{F}}_\vartheta$ and $\boldsymbol{\Delta}\bar{\boldsymbol{F}}_\vartheta$. Both left and right hand side in equation (4.63), (4.64), (4.65) and (4.66) are expressed in the same number of derivatives. Since $\bar{\boldsymbol{F}}_v$, $\bar{\boldsymbol{F}}_w$, $\bar{\boldsymbol{F}}_\vartheta$ and $\boldsymbol{\Delta}\bar{\boldsymbol{F}}_\vartheta$ are constant and independent of the x-coordinate they will not be affected by the integration. There will nether be an integration constant since if $\bar{\phi}(x)$ would be constant there will not be any warping. Integration with respect to x on both sides is then lead to:

$$\boldsymbol{v}(x) = \bar{\boldsymbol{F}}_v \cdot \bar{\boldsymbol{\phi}}(x) \tag{4.67}$$

$$\boldsymbol{w}(x) = \bar{\boldsymbol{F}}_w \cdot \bar{\boldsymbol{\phi}}(x) \tag{4.68}$$

$$\boldsymbol{\vartheta}(x) = \bar{\boldsymbol{F}}_\vartheta \cdot \bar{\boldsymbol{\phi}}(x) \tag{4.69}$$

$$\boldsymbol{\Delta\vartheta}(x) = \Delta\overline{\boldsymbol{F}}_{\vartheta} \cdot \overline{\boldsymbol{\phi}}(x) \tag{4.70}$$

4.2.6 The unit transverse bending moments

The nodal unit rotations $\Delta\bar{\vartheta}_r$ for the inner nodes $r = 3$ to $r = n - 1$ are known and therefore the corresponding nodal unit bending moments can be determined by means of the force method. Introduce rollers at each fold lines (inner natural nodes), see Figure 4.11. The outer plate elements $r = 1$ and $r = n$ are treated as cantilevers.

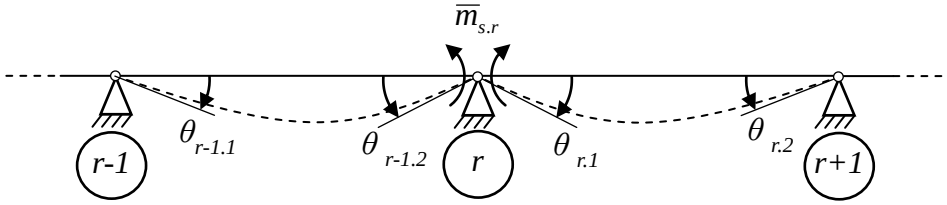

Figure 4.11: The cross-section is here flattened out and rollers are introduced at each inner natural node. The transverse unit nodal bending moment $\overline{m}_{s.r}$ can then be determined by the means of the force method.

By solving the plate differential equation $Kw_{,ssss}(s) = 0$ subjected to a "support moment" $\overline{m}_{s.r}$ (still unknown) the "support rotations" θ_{r-1}, θ_r and θ_{r+1} can be determined and expressed in terms of the moment as:

$$\theta_{r-1.1} = \frac{b_{r-1}}{6K_{r-1}}\overline{m}_{s.r} = \delta_{r-1} \cdot \overline{m}_{s.r} \tag{4.71}$$

$$\theta_{r-1.2} + \theta_{r.1} = \frac{1}{3}\left(\frac{b_{r-1}}{K_{r-1}} + \frac{b_r}{K_r}\right)\overline{m}_{s.r} = \delta_r \cdot \overline{m}_{s.r} \tag{4.72}$$

$$\theta_{r.2} = \frac{b_r}{6K_r}\overline{m}_{s.r} = \delta_{r+1} \cdot \overline{m}_{s.r} \tag{4.73}$$

Where K_r is the plate stiffness of plate element r defined as:

$$K_r = \frac{Et_r^3}{12(1-\nu^2)} \tag{4.74}$$

The unit nodal rotation $\Delta\bar{\vartheta}_r$ obtained in (4.70) must coincide with the "support rotations" θ_r. Since the unit nodal rotations only are defined for the inner nodes (node 3 to node $n - 1$) the corresponding unit nodal moments $\overline{m}_{s.r}$ only can be determined for those inner nodes. This can be written in matrix form as:

$$\boldsymbol{\Delta}_{ik} \cdot \overline{\boldsymbol{m}}_s = -\Delta\overline{\boldsymbol{F}}_{\vartheta} \cdot \overline{\boldsymbol{\phi}} \tag{4.75}$$

Where the $\boldsymbol{\Delta}_{ik}$-matrix involves the δ-terms defined in (4.71), (4.72) and (4.73). The nodal unit bending moments $\overline{\boldsymbol{m}}_s$ is then obtained by left-multiplication by the inverse of the $\boldsymbol{\Delta}_{ik}$-matrix which gives:

$$\overline{\boldsymbol{m}}_s = -\boldsymbol{\Delta}_{ik}^{-1} \cdot \Delta\overline{\boldsymbol{F}}_{\vartheta} \cdot \overline{\boldsymbol{\phi}} = \overline{\boldsymbol{M}} \cdot \overline{\boldsymbol{\phi}} \tag{4.76}$$

Where:

$$\bar{\boldsymbol{m}}_s = [\bar{m}_{s.1} \quad \bar{m}_{s.2} \quad \cdots \quad \bar{m}_{s.n+1}]^T \qquad \bar{\boldsymbol{M}} = -\boldsymbol{\Delta}_{ik}^{-1} \cdot \Delta\bar{\boldsymbol{F}}_{\vartheta} \tag{4.77}$$

A programming ready $\boldsymbol{\Delta}_{ik}$-matrix is defined in Appendix B.

4.2.7 The displacements of the outer plate elements

The transverse nodal displacements and the element rotations for the outer plate elements cannot be defined in the same way as for the inner plate elements, hence another approach must be used for those two plate elements. Since the nodal unit bending moments $\bar{m}_{s.3}$ and $\bar{m}_{s.n-1}$ are defined at node 3 and node $n-1$ the plate rotations of the outer plate elements can be determined, see Figure 4.12.

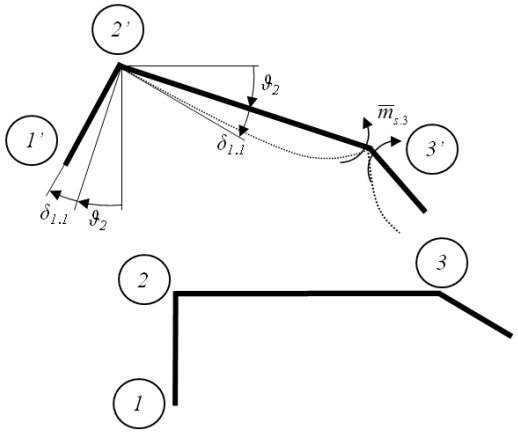

Figure 4.12: The element rotations of the outer two plate element can be determined from the unit bending moment $\bar{m}_{s.3}$ at node $r = 3$ and $r = n-1$ respectively.

The element rotation consist of two parts, namely the rotation of the adjacent plate element $r = 2$ or $r = n-1$ and the "support rotation" corresponding to the transverse nodal bending moment at node $r = 3$ or $r = n-1$. The plate element rotations are then obtained as:

$$\bar{\vartheta}_1 = \bar{\vartheta}_2 + \delta_{1.1} = \bar{\vartheta}_2 + \frac{b_2}{6K_2}\bar{m}_{s.3} \qquad \bar{\vartheta}_n = \bar{\vartheta}_{n-1} - \delta_{n.2} = \bar{\vartheta}_2 - \frac{b_{n-1}}{6K_{n-1}}\bar{m}_{s.n-1} \tag{4.78}$$

When the element rotations are known the w-displacements of node $r = 1$ and $r = n+1$ can then be determined from (4.51) as:

$$\bar{w}_{1.1} = -\bar{\vartheta}_1 \cdot b_1 + \bar{w}_{2.1} \qquad\qquad \bar{w}_{2.n} = \bar{\vartheta}_n \cdot b_n + \bar{w}_{1.n} \tag{4.79}$$

4.2.8 Global displacements

Once the local cross-sectional unit deformations $(\bar{v}_r, \bar{w}_r, \bar{\vartheta}_r)$ of each plate element r are known and the unit warping $\bar{u}_r$ for each node r is known, it can be translated to the global coordinate system (X, Y, Z) and the global nodal unit displacements $(\bar{U}, \bar{V}, \bar{W})$. The geometric relations are illustrated in Figure 4.13.

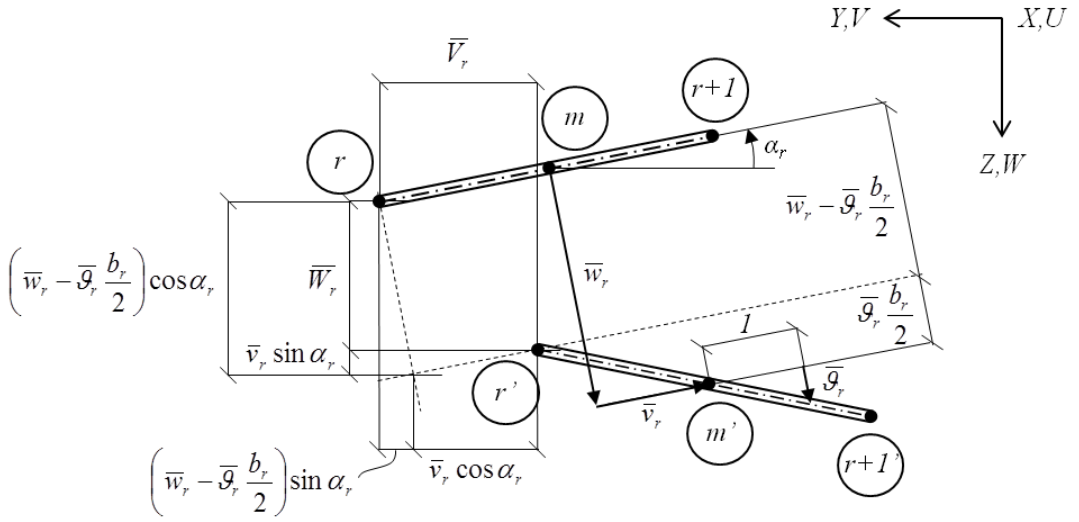

Figure 4.13: This figure illustrates the transformation from local element unit displacements $\bar{v}_r$, $\bar{w}_r$ and $\bar{\vartheta}_r$ to global nodal unit displacement $\bar{V}_r$ and $\bar{W}_r$.

The geometric relations between the local and global displacements are given as:

$$\bar{U}_r = \bar{u}_r \tag{4.80}$$

$$\bar{V}_r = -\bar{v}_r \cdot \cos\alpha_r - \left(\bar{w}_r - \bar{\vartheta}_r \cdot \frac{b_r}{2}\right) \cdot \sin\alpha_r \tag{4.81}$$

$$\bar{W}_r = -\bar{v}_r \cdot \sin\alpha_r + \left(\bar{w}_r - \bar{\vartheta}_r \cdot \frac{b_r}{2}\right) \cdot \cos\alpha_r \tag{4.82}$$

The geometric relations for the last node $r = n + 1$are given as:

$$\bar{U}_{n+1} = \bar{u}_{n+1} \tag{4.83}$$

$$\bar{V}_{n+1} = -\bar{v}_n \cdot \cos\alpha_n - \left(\bar{w}_n + \bar{\vartheta}_n \cdot \frac{b_n}{2}\right) \cdot \sin\alpha_n \tag{4.84}$$

$$\bar{W}_{n+1} = -\bar{v}_n \cdot \sin\alpha_n + \left(\bar{w}_n + \bar{\vartheta}_n \cdot \frac{b_n}{2}\right) \cdot \cos\alpha_n \tag{4.85}$$

4.3 Intermediate nodes

In the previous Section 4.2 only the natural nodes was considered in the derivation and the maximum number of deformation modes was then equal to the number of natural nodes $(n + 1)$. A drawback is the lack of accuracy in the behaviour within the plate elements and since the load only can be applied at the natural nodes the loading procedure will be approximate. A way to overcome this is to introduce intermediate nodes and as a consequence a larger number of degrees of freedom and also a larger number of deformation modes will be obtained since also local deformation modes are added to the existing distortional modes.

The definition of an intermediate node tells that the mutual angle difference $\Delta\alpha_r$ at the corresponding node r is zero, hence another approach must be used compared to the

use of only natural nodes derived in Section 4.2. In this chapter an extension of the previous derivation will be presented due to the imposition of intermediate nodes and only the affected matrices and terms will be mentioned and presented.

4.3.1 The degrees of freedom

The use of intermediate nodes will contribute to a larger number of degrees of freedom. According to the assumption (A4.2) and that the nodal angle difference is zero the warping deformation mode $u_k(s)$ must vary linear within the plate element. The warping values at the intermediate nodes can therefore be completely defined by interpolation of the warping values at the natural nodes and hence not contribute to the degrees of freedom. There is no restriction on the transverse displacements at the intermediate nodes though and they will therefore contribute to the number of degrees of freedom. The end nodes can also be treated in this way by introducing an extra transverse degree of freedom which therefore will contain one warping and one transverse degree of freedom each. The total number of degrees of freedom for a cross-section consists of:

- The number of natural nodes (the warping degrees of freedom, u)
- The number of intermediate nodes (the transverse degrees of freedom, w)
- Two end nodes (two transverse degrees of freedom, w)

When introducing intermediate nodes there is a need to distinguish between plate elements and sub-plate elements. In the following plate elements represents the whole plates between natural nodes and are associated with subscript r. The sub-plates are the elements obtained by implementation of intermediate nodes and is listening to subscript ri where i denotes sub-plate i of plate element r. If one plate element not contains any intermediate nodes it will in the following listen to one sub-plate. The total number of sub-plates are denoted n_{sub} and the total number of nodes (natural and intermediate together) are then $n_{sub} + 1$, see Figure 4.14.

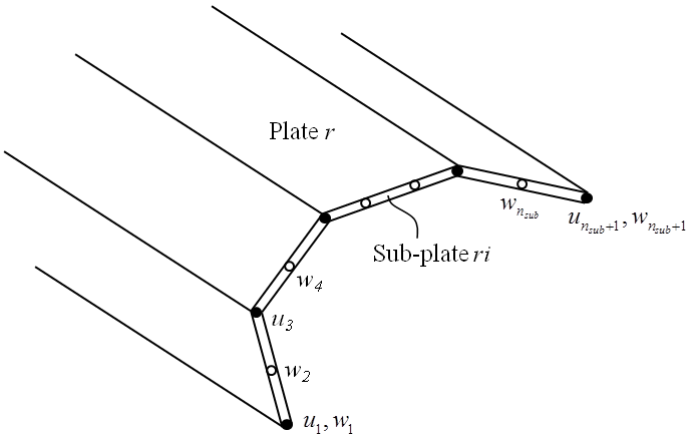

Figure 4.14: The imposition of intermediate nodes will contribute to extra degrees of freedom. The u-degrees of freedoms are the nodal warping values associated with the natural nodes and the w-degrees of freedom are associated with the intermediate nodes and end nodes.

The degrees of freedom are presented in the newly defined vector $\boldsymbol{x}$. The warping values associated with the natural nodes are lined up first and after them the degrees

of freedom associated with the end nodes and intermediate nodes. The $\boldsymbol{x}$-vector is defined below where the subscripts refer to the node numbering:

$$\boldsymbol{x} = [u_1 \quad \cdots \quad u_{n_{sub}+1} \quad w_1 \quad \cdots \quad w_{n_{sub}+1}]^T \tag{4.86}$$

The $\boldsymbol{x}$-vector contain both warping and transverse degrees of freedom which is the main difference compared with the derivation in Section 4.2, see equation (4.42). By applying unit displacements one degree of freedom at the time and all $\boldsymbol{x}$-vectors collected in a matrix $\bar{\boldsymbol{X}}$ give:

$$\bar{\boldsymbol{X}} = [\boldsymbol{x}_1 \quad \boldsymbol{x}_2 \quad \cdots \quad \boldsymbol{x}_{n_{sub}+1}]^T \tag{4.87}$$

This will give that the $\bar{\boldsymbol{X}}$-matrix not will be a unit matrix but will contain coupling terms since unit warping will give contribution at the intermediate nodes. In order to describe the appearance an example will be used, see Figure 4.15.

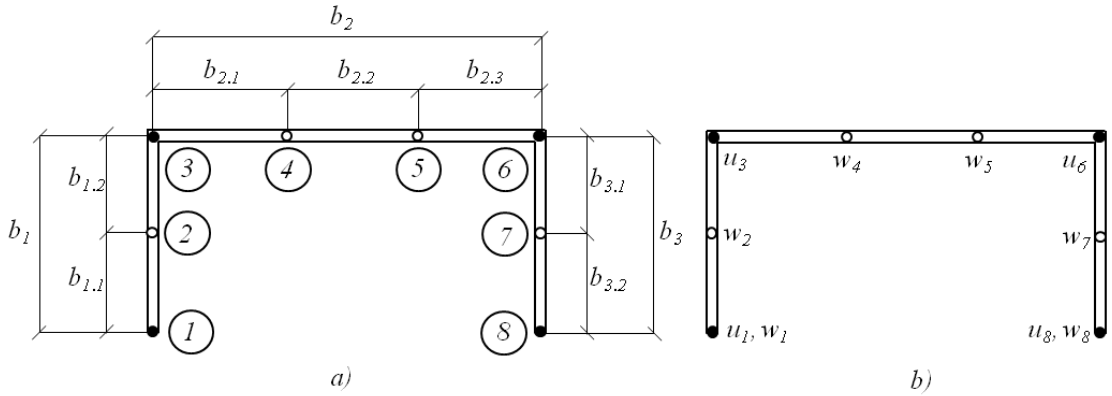

Figure 4.15: This figure illustrates the discretization of a U-section where the natural nodes (filled dots) and intermediate nodes (empty dots) define the cross-section. a) The widths of the plate elements b_r and widths of sub-plate elements $b_{r.i}$ are defined together with the node numbering (large rings). b) The degrees of freedom at each node are defined where the subscript is associated with the corresponding node numbering.

The warping values u_r at the intermediate nodes are obtained by interpolation of the warping values at the natural nodes which for the example above will give:

$$\begin{aligned}
u_2 &= u_1 + \frac{b_{1.1}}{b_1}(u_3 - u_1) = \left(1 - \frac{b_{1.1}}{b_1}\right)\cdot u_1 + \frac{b_{1.1}}{b_1}\cdot u_3 \\
u_4 &= u_3 + \frac{b_{2.1}}{b_2}(u_6 - u_3) = \left(1 - \frac{b_{2.1}}{b_2}\right)\cdot u_3 + \frac{b_{2.1}}{b_2}\cdot u_6 \\
u_5 &= u_3 + \frac{b_{2.1} + b_{2.2}}{b_2}(u_6 - u_3) \\
&= \left(1 - \frac{b_{2.1} + b_{2.2}}{b_2}\right)\cdot u_3 + \frac{b_{2.1} + b_{2.2}}{b_2}\cdot u_6 \\
u_7 &= u_6 + \frac{b_{3.1}}{b_3}(u_8 - u_6) = \left(1 - \frac{b_{3.1}}{b_3}\right)\cdot u_6 + \frac{b_{3.1}}{b_3}\cdot u_8
\end{aligned} \tag{4.88}$$

This can be written on a more compact matrix form as:

$$\boldsymbol{u} = \bar{\boldsymbol{U}} \cdot \boldsymbol{x} \tag{4.89}$$

Where:

$$\boldsymbol{u} = [u_1 \quad u_2 \quad u_3 \quad u_4 \quad u_5 \quad u_6 \quad u_7 \quad u_8]^T \tag{4.90}$$

$$\boldsymbol{x} = [u_1 \quad u_3 \quad u_6 \quad u_8 \quad w_1 \quad w_2 \quad w_4 \quad w_5 \quad w_7 \quad w_8]^T \tag{4.91}$$

$$\bar{\boldsymbol{U}} = \begin{bmatrix} 1 & 0 & 0 & 0 & 0 & 0 & 0 & 0 & 0 & 0 \\ \left(1 - \frac{b_{1.1}}{b_1}\right) & \frac{b_{1.1}}{b_1} & 0 & 0 & 0 & 0 & 0 & 0 & 0 & 0 \\ 0 & 1 & 0 & 0 & 0 & 0 & 0 & 0 & 0 & 0 \\ 0 & \left(1 - \frac{b_{2.1}}{b_2}\right) & \frac{b_{2.1}}{b_2} & 0 & 0 & 0 & 0 & 0 & 0 & 0 \\ 0 & \left(1 - \frac{b_{2.1} + b_{2.2}}{b_2}\right) & \frac{b_{2.1} + b_{2.2}}{b_2} & 0 & 0 & 0 & 0 & 0 & 0 & 0 \\ 0 & 0 & 1 & 0 & 0 & 0 & 0 & 0 & 0 & 0 \\ 0 & 0 & \left(1 - \frac{b_{3.1}}{b_3}\right) & \frac{b_{3.1}}{b_3} & 0 & 0 & 0 & 0 & 0 & 0 \\ 0 & 0 & 0 & 0 & 1 & 0 & 0 & 0 & 0 & 0 \end{bmatrix} \tag{4.92}$$

Note: The $\bar{\boldsymbol{U}}$-matrix is not a unit matrix as in (4.58).

Another consequence of that two types of degrees of freedom are used is that the cross-sectional displacements $\boldsymbol{v}$ and $\boldsymbol{w}$ not only can be determined by the warping vector $\boldsymbol{u}$ any more but must be expressed in terms of the degrees of freedom vector $\boldsymbol{x}$, hence the $\boldsymbol{F}_v$, $\boldsymbol{F}_{w1}$ and $\boldsymbol{F}_{w2}$ matrices must be rebuilt to be suitable to the new form:

$$\boldsymbol{v} = \boldsymbol{F}_{\boldsymbol{v}} \cdot \boldsymbol{x} \qquad \boldsymbol{w}_1 = \boldsymbol{F}_{w1} \cdot \boldsymbol{x} \qquad \boldsymbol{w}_2 = \boldsymbol{F}_{w2} \cdot \boldsymbol{x} \tag{4.93}$$

The matrices are built in the same way, i.e. by applying unit displacements one degree of freedom at the time. Since the warping deformation mode varies linear between the natural nodes the same $\boldsymbol{F}_v$, $\boldsymbol{F}_{w1}$ and $\boldsymbol{F}_{w2}$ matrices can be used as for natural nodes but must be modified. The v-displacements are still constant within the plate elements which give the same v-displacements for the intermediate nodes as for the natural nodes. As in the case of only natural nodes the rows are related to plate elements and the columns are related to the degrees of freedom but when having intermediate nodes the rows correspond to sub-plates and the columns are related to all degrees of freedom defined in $\boldsymbol{x}$. The $\bar{\boldsymbol{F}}_v$-matrix is then obtained for the example defined in Figure 4.15 above as:

$$\bar{\boldsymbol{F}}_v = \begin{bmatrix} \frac{1}{b_1} & -\frac{1}{b_1} & 0 & 0 & 0 & 0 & 0 & 0 & 0 & 0 \\ \frac{1}{b_1} & -\frac{1}{b_1} & 0 & 0 & 0 & 0 & 0 & 0 & 0 & 0 \\ 0 & \frac{1}{b_2} & -\frac{1}{b_2} & 0 & 0 & 0 & 0 & 0 & 0 & 0 \\ 0 & \frac{1}{b_2} & -\frac{1}{b_2} & 0 & 0 & 0 & 0 & 0 & 0 & 0 \\ 0 & \frac{1}{b_2} & -\frac{1}{b_2} & 0 & 0 & 0 & 0 & 0 & 0 & 0 \\ 0 & 0 & \frac{1}{b_3} & -\frac{1}{b_3} & 0 & 0 & 0 & 0 & 0 & 0 \\ 0 & 0 & \frac{1}{b_3} & -\frac{1}{b_3} & 0 & 0 & 0 & 0 & 0 & 0 \end{bmatrix} \tag{4.94}$$

The row and column related to the transverse degrees of freedom in the $\overline{\boldsymbol{F}}_{w1}$ and $\overline{\boldsymbol{F}}_{w2}$ matrices will contain unit values at the corresponding position and zeros at all other positions. The first and last row will therefore be completed without the knowledge of the nodal moments which is the case when only considering natural nodes. Recall the example defined in Figure 4.15 and the corresponding matrices are obtained as:

$$\overline{\boldsymbol{F}}_{w1} = \begin{bmatrix} 0 & 0 & 0 & 0 & 1 & 0 & 0 & 0 & 0 & 0 \\ 0 & 0 & 0 & 0 & 0 & 1 & 0 & 0 & 0 & 0 \\ -\frac{1}{b_1 \sin\Delta\alpha_3} & \left(\frac{1}{b_1 \sin\Delta\alpha_3}+\frac{1}{b_2 \tan\Delta\alpha_3}\right) & -\frac{1}{b_2 \tan\Delta\alpha_3} & 0 & 0 & 0 & 0 & 0 & 0 & 0 \\ 0 & 0 & 0 & 0 & 0 & 0 & 1 & 0 & 0 & 0 \\ 0 & 0 & 0 & 0 & 0 & 0 & 0 & 1 & 0 & 0 \\ 0 & -\frac{1}{b_2 \sin\Delta\alpha_6} & \left(\frac{1}{b_2 \sin\Delta\alpha_6}+\frac{1}{b_3 \tan\Delta\alpha_6}\right) & -\frac{1}{b_3 \tan\Delta\alpha_6} & 0 & 0 & 0 & 0 & 0 & 0 \\ 0 & 0 & 0 & 0 & 0 & 0 & 0 & 0 & 1 & 0 \end{bmatrix} \tag{4.95}$$

$$\overline{\boldsymbol{F}}_{w2} = \begin{bmatrix} 0 & 0 & 0 & 0 & 0 & 1 & 0 & 0 & 0 & 0 \\ -\frac{1}{b_1 \tan\Delta\alpha_3} & \left(\frac{1}{b_1 \tan\Delta\alpha_3}+\frac{1}{b_2 \sin\Delta\alpha_3}\right) & -\frac{1}{b_2 \sin\Delta\alpha_3} & 0 & 0 & 0 & 0 & 0 & 0 & 0 \\ 0 & 0 & 0 & 0 & 0 & 0 & 1 & 0 & 0 & 0 \\ 0 & 0 & 0 & 0 & 0 & 0 & 0 & 1 & 0 & 0 \\ 0 & -\frac{1}{b_2 \tan\Delta\alpha_6} & \left(\frac{1}{b_2 \tan\Delta\alpha_6}+\frac{1}{b_3 \sin\Delta\alpha_6}\right) & -\frac{1}{b_3 \sin\Delta\alpha_6} & 0 & 0 & 0 & 0 & 0 & 0 \\ 0 & 0 & 0 & 0 & 0 & 0 & 0 & 0 & 1 & 0 \\ 0 & 0 & 0 & 0 & 0 & 0 & 0 & 0 & 0 & 1 \end{bmatrix} \tag{4.96}$$

Note that the $\overline{\boldsymbol{F}}_{v}$, $\overline{\boldsymbol{F}}_{w1}$ and $\overline{\boldsymbol{F}}_{w2}$ matrices are denoted with a bar to distinguish that they correspond to unit displacements of each degree of freedom, in the same way as for the case of only natural nodes but here unit displacements also apply on the transverse degrees of freedom at the ends and intermediate nodes.

Out of the $\overline{\boldsymbol{F}}_{v}$, $\overline{\boldsymbol{F}}_{w1}$ and $\overline{\boldsymbol{F}}_{w2}$ matrices defined in (4.94), (4.95) and (4.96) above the other matrices corresponding to the plate rotations $\overline{\boldsymbol{F}}_{\vartheta}$ and $\boldsymbol{\Delta}\overline{\boldsymbol{F}}_{\vartheta}$ can completely be defined in the same way as in equation (4.52) and (4.54) but with the only difference is that the sub-plate widths $b_{r.i}$ are used instead of the plate element widths b_r. Another difference is that the second and the second last node rotations are completely defined (since the first and last row in $\overline{\boldsymbol{F}}_{w1}$ and $\overline{\boldsymbol{F}}_{w2}$ will be non-zero). A consequence of this is that the $\boldsymbol{\Delta}_{ik}$-matrix defined in (4.75) could be filled one row earlier and one row later, i.e. the second and the second last row will be non-zero. In the expression for $\boldsymbol{\Delta}_{ik}$ the sub-plate widths $b_{r.i}$ should be used instead of the plate element widths b_r. According to this, the second and the second last nodal moments $m_{s.r}$ will now be non-zero and there is therefore no need to modify the $\overline{\boldsymbol{F}}_{w1}$ and $\overline{\boldsymbol{F}}_{w2}$ any more as in the case of only considering natural nodes.

4.4 Determination of the GBT matrices

In the discretization process in Section 4.1 the C_{ik}, D_{ik} and B_{ik} terms in the GBT fundamental equilibrium equation (4.36) will then be expanded into $\boldsymbol{C}$, $\boldsymbol{D}$ and $\boldsymbol{B}$matrices instead. Those terms are defined by the deformation mode functions $u_k(s)$ and $w_k(s)$, see equation (4.19), (4.23) and (4.26). The deformation mode function $u_k(s)$ is defined in (4.2) and will vary linearly within each plate element, i.e. between two natural nodes. The $w(s)$ will not vary linear since the nodal transverse bending

moments $m_{s.r}$ will affect the variation within each plate element. In order to capture the variation four helping functions or shape functions Ψ_{1-4} are introduced.

4.4.1 The deformation mode function *w*(*s*)

The cross-sectional deformation mode $w_k(s)$ will be affected by the average element deflection w_r, the element rotation ϑ_r and the nodal transverse bending moments $m_{s.r}$ and $m_{s.r+1}$. The average element deflection w_r is constant within each element r, hence the corresponding shape function Ψ_1 will be a constant. The element rotation ϑ_r will contribute to a linear variation within each element, hence Ψ_2 is a linear function. In order to describe the variation due to the nodal moments two shape functions are used, namely Ψ_3 and Ψ_4, see Figure 4.16.

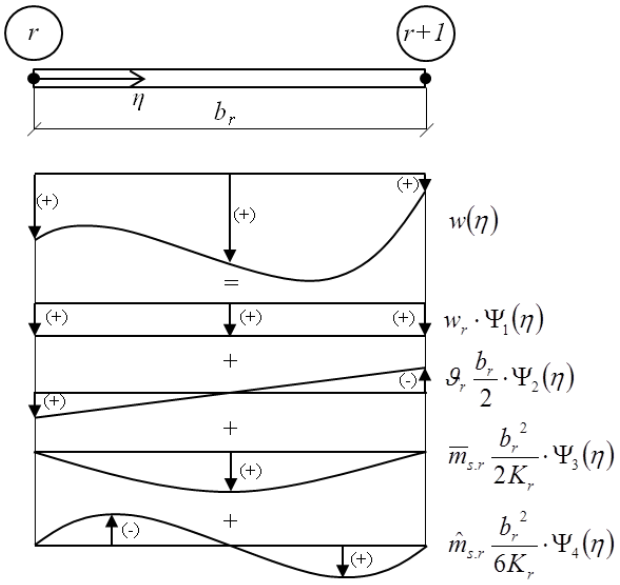

Figure 4.16: The variation of the deflection $w_k(s)$ between the nodes are affected by both the average element deflection w_r, the element rotation ϑ_r and the nodal transverse bending moments $m_{s.r}$ and $m_{s.r+1}$. This figure also shows how the shape functions Ψ_{1-4} varies and are defined.

The cross-sectional deformation mode $w_k(s)$ can now be determined using the shape functions Ψ_{1-4} and the local plate coordinate η, defined as:

$$\eta(s) = \frac{s}{b_r}, \quad \eta \in \{0,1\} \tag{4.97}$$

The deformation mode $w_k(s)$ is now defined as:

$$w_k(s) = \sum_{r=1}^{n} \left[w_r \cdot \Psi_1(\eta) + \vartheta_r \frac{b_r}{2} \cdot \Psi_2(\eta) + \overline{m}_{s.r} \frac{b_r^2}{2K_r} \cdot \Psi_3(\eta) - \hat{m}_{s.r} \frac{b_r^2}{6K_r} \cdot \Psi_4(\eta) \right] \tag{4.98}$$

Where the shape functions are defined as:

$$\Psi_1(\eta) = 1 \qquad \Psi_2(\eta) = 2\eta - 1$$
$$\Psi_3(\eta) = \eta(1-\eta) \qquad \Psi_4(\eta) = \eta\big(1-\eta(3-2\eta)\big) \tag{4.99}$$

And the "average" element moments used in (4.98) are defined as:

$$\bar{m}_{s.r} = \frac{m_{s.r+1} + m_{s.r}}{2} \qquad \hat{m}_{s.r} = \frac{m_{s.r+1} - m_{s.r}}{2} \tag{4.100}$$

Note: Do not mix up the average element moment $\bar{m}_{s.r}$ with the unit nodal moments $\bar{m}_{s.r}$.

4.4.1.1 Determination of Ψ_1 and Ψ_2

The average element deflection w_r, see (4.49), is constant within each plate element r and therefore the corresponding shape function $\Psi_1(\eta)$ must be constant. This gives the shape function:

$$\Psi_1(\eta) = 1 \tag{4.101}$$

The element rotation ϑ_r, defined in equation (4.51), will contribute to a linear variation of the deformation mode $w_k(s)$ within each plate element r. This gives the shape function:

$$\Psi_2(\eta) = 2\eta - 1 \tag{4.102}$$

4.4.1.2 Determination of Ψ_3 and Ψ_4

To capture the variation of the deformation mode $w_k(s)$ due to nodal bending moments use the differential equation for a plate r with the width b_r, the plate stiffness K_r (4.74) and simply supported at the edges, e.g. at the natural nodes r and $r+1$. The differential equation is defined as:

$$-K_r w_{,ssss}(s) = 0 \tag{4.103}$$

The solution to (4.103) is then obtained by integration four times. This give:

$$-Kw(s) = C_1\frac{s^3}{6} + C_2\frac{s^2}{2} + C_3 s + C_4 \tag{4.104}$$

In order to find the solution four boundary conditions are needed which for a simply supported plate is defined as:

$$w(0) = 0 \qquad w(b_r) = 0$$
$$m(0) = -K_r w_{,ss}(0) = m_{s.r} \qquad m(b_r) = -K_r w_{,ss}(b_r) = m_{s.r+1} \tag{4.105}$$

By introducing the four boundary conditions (4.105) into (4.104) the four unknown constants can be determined as:

$$C_1 = \frac{m_{s.r+1} - m_{s.r}}{b_r} \qquad C_2 = m_{s.r}$$
$$C_3 = -\frac{b_r}{3} m_{s.r} - \frac{b_r}{6} m_{s.r+1} \qquad C_4 = 0 \tag{4.106}$$

The deflection $w(s)$ within plate r is now defined as a function of the coordinate s as:

$$w(s) = -\frac{1}{K}\left[\frac{m_{s.r+1} - m_{s.r}}{6b_r} s^3 + \frac{m_{s.r}}{2} s^2 - \left(\frac{b_r}{3} m_{s.r} + \frac{b_r}{6} m_{s.r+1}\right) s\right] \tag{4.107}$$

In order to distinguish two shape functions Ψ_3 and Ψ_4 some rewriting of (4.107) is needed. The deflection can be written in the local coordinate $\eta(s)$ defined in (4.97). This give:

$$\begin{aligned} w(\eta) = {} & \frac{m_{s.r+1} + m_{s.r}}{2} \cdot \frac{b_r^2}{2K_r} \cdot \eta(1-\eta) - \frac{m_{s.r+1} - m_{s.r}}{2} \cdot \frac{b_r^2}{6K_r} \\ & \cdot \eta\big(1 - \eta(3 - 2\eta)\big) \\ & = \bar{m}_{s.r} \cdot \frac{b_r^2}{2K_r} \cdot \Psi_3(\eta) - \hat{m}_{s.r} \cdot \frac{b_r^2}{6K_r} \cdot \Psi_4(\eta) \end{aligned} \tag{4.108}$$

4.4.1.3 First and second order derivative of the deformation mode

In the expressions for the matrices $\boldsymbol{C}$, $\boldsymbol{D}$ and $\boldsymbol{B}$ the derivatives of the deformation mode $w_k(s)$ are used. In order to save some writing later the derivatives of (4.98) are defined and computed here. The derivatives are given as:

$$\begin{aligned} w_{k,s}(s) = {} & \sum_{r=1}^{n} \Bigg[w_r \cdot \Psi_{1,\eta} \eta_{,s} + \vartheta_r \frac{b_r}{2} \cdot \Psi_{2,\eta} \eta_{,s} + \bar{m}_{s.r} \frac{b_r^2}{2K_r} \cdot \Psi_{3,\eta} \eta_{,s} \\ & - \hat{m}_{s.r} \frac{b_r^2}{6K_r} \cdot \Psi_{4,\eta} \eta_{,s} \Bigg] \\ = {} & \sum_{r=1}^{n} \Bigg[w_r \frac{1}{b_r} \cdot \Psi_{1,\eta} + \vartheta_r \frac{1}{2} \cdot \Psi_{2,\eta} + \bar{m}_{s.r} \frac{b_r}{2K_r} \cdot \Psi_{3,\eta} \\ & - \hat{m}_{s.r} \frac{b_r}{6K_r} \cdot \Psi_{4,\eta} \Bigg] \end{aligned} \tag{4.109}$$

$$
\begin{aligned}
w_{k,ss}(s) = \sum_{r=1}^{n} \Bigg[& w_r \cdot \Psi_{1,\eta\eta} \cdot \eta_{,s}^2 + \vartheta_r \frac{b_r}{2} \cdot \Psi_{2,\eta\eta} \cdot \eta_{,s}^2 + \bar{m}_{s.r} \frac{b_r^2}{2K_r} \cdot \Psi_{3,\eta\eta} \cdot \eta_{,s}^2 \\
& - \hat{m}_{s.r} \frac{b_r^2}{6K_r} \cdot \Psi_{4,\eta\eta} \cdot \eta_{,s}^2 \Bigg] \\
= \sum_{r=1}^{n} \Bigg[& w_r \frac{1}{b_r^2} \cdot \Psi_{1,\eta\eta} + \vartheta_r \frac{1}{2b_r} \cdot \Psi_{2,\eta\eta} + \bar{m}_{s.r} \frac{1}{2K_r} \cdot \Psi_{3,\eta\eta} \\
& - \hat{m}_{s.r} \frac{1}{6K_r} \cdot \Psi_{4,\eta\eta} \Bigg]
\end{aligned}
\tag{4.110}
$$

In (4.109) and (4.110) the first respectively the second derivative of the shape functions Ψ_{1-4} with respect to η are obtained. Those are obtained as:

$$
\begin{aligned}
&\Psi_{1,\eta}(\eta) = 0 && \Psi_{1,\eta\eta}(\eta) = 0 \\
&\Psi_{2,\eta}(\eta) = 2 && \Psi_{2,\eta\eta}(\eta) = 0 \\
&\Psi_{3,\eta}(\eta) = 1 - 2\eta && \Psi_{3,\eta\eta}(\eta) = -2 \\
&\Psi_{4,\eta}(\eta) = 6\eta^2 - 6\eta + 1 && \Psi_{4,\eta\eta}(\eta) = 12\eta - 6
\end{aligned}
\tag{4.111}
$$

4.4.2 The *B*-matrix

The positions i and k in the $\boldsymbol{B}$-matrix is defined by the B_{ik}-terms defined in (4.19). Insert the expression for the second derivative (4.110) into (4.19) one gets:

$$
\begin{aligned}
B_{ik} = K \int_b & w_{k,ss} w_{i,ss} ds \\
= \sum_{r=1}^{n} K_r \int_0^1 \Bigg[& w_{r.k} \frac{1}{b_r^2} \cdot \underbrace{\Psi_{1,\eta\eta}}_{=0} + \vartheta_{r.k} \frac{1}{2b_r} \cdot \underbrace{\Psi_{2,\eta\eta}}_{=0} \\
& + \bar{m}_{s.r.k} \frac{1}{2K_r} \cdot \Psi_{3,\eta\eta} - \hat{m}_{s.r.k} \frac{1}{6K_r} \cdot \Psi_{4,\eta\eta} \Bigg] \\
& \cdot \Bigg[w_{r.i} \frac{1}{b_r^2} \cdot \underbrace{\Psi_{1,\eta\eta}}_{=0} + \vartheta_{r.i} \frac{1}{2b_r} \cdot \underbrace{\Psi_{2,\eta\eta}}_{=0} + \bar{m}_{s.r.i} \frac{1}{2K_r} \cdot \Psi_{3,\eta\eta} \\
& - \hat{m}_{s.r.i} \frac{1}{6K_r} \cdot \Psi_{4,\eta\eta} \Bigg] b_r \, d\eta \\
= \sum_{r=1}^{n} K_r b_r \int_0^1 \Bigg[& \bar{m}_{s.r.k} \bar{m}_{s.r.i} \frac{1}{2K_r} \frac{1}{2K_r} \cdot \Psi_{3,\eta\eta} \Psi_{3,\eta\eta} \\
& - \hat{m}_{s.r.k} \bar{m}_{s.r.i} \frac{1}{6K_r} \frac{1}{2K_r} \cdot \Psi_{4,\eta\eta} \Psi_{3,\eta\eta} - \bar{m}_{s.r.k} \hat{m}_{s.r.i} \frac{1}{2K_r} \frac{1}{6K_r} \\
& \cdot \Psi_{3,\eta\eta} \Psi_{4,\eta\eta} + \hat{m}_{s.r.k} \hat{m}_{s.r.i} \frac{1}{6K_r} \frac{1}{6K_r} \cdot \Psi_{4,\eta\eta} \Psi_{4,\eta\eta} \Bigg] d\eta
\end{aligned}
\tag{4.112}
$$

The integration of shape function products is performed and the results are tabulated in Table 4.1.

Table 4.1: This table contains the integration of shape function products defined as $\int_0^1 \Psi_{,\eta\eta}\,\Psi_{,\eta\eta}\,d\eta$.

	$\Psi_{3,\eta\eta}$	$\Psi_{4,\eta\eta}$
$\Psi_{3,\eta\eta}$	4	0
$\Psi_{4,\eta\eta}$	0	12

Insert the values from Table 4.1 into (4.112) the B_{ik}-term is given as:

$$\begin{aligned} B_{ik} = \sum_{r=1}^{n} K_r b_r \Big[& \bar{m}_{s.r.k}\bar{m}_{s.r.i}\frac{1}{2K_r}\frac{1}{2K_r}\cdot 4 - \hat{m}_{s.r.k}\bar{m}_{s.r.i}\frac{1}{6K_r}\frac{1}{2K_r}\cdot 0 \\ & - \bar{m}_{s.r.k}\hat{m}_{s.r.i}\frac{1}{2K_r}\frac{1}{6K_r}\cdot 0 + \hat{m}_{s.r.k}\hat{m}_{s.r.i}\frac{1}{6K_r}\frac{1}{6K_r}\cdot 12\Big] b_r \\ = \sum_{r=1}^{n} & \frac{b_r}{K_r}\left[\bar{m}_{s.r.k}\bar{m}_{s.r.i} + \frac{1}{3}\hat{m}_{s.r.k}\hat{m}_{s.r.i}\right] \end{aligned} \tag{4.113}$$

The B_{ik}-term can now be obtained as:

$$B_{ik} = \sum_{r=1}^{n} \frac{b_r}{K_r}\left[\bar{m}_{s.r.k}\bar{m}_{s.r.i} + \frac{1}{3}\hat{m}_{s.r.k}\hat{m}_{s.r.i}\right] \tag{4.114}$$

Now the $\boldsymbol{B}$-matrix is determined and it will be a symmetric and full matrix. Another way to compute the $\boldsymbol{B}$-matrix is $\boldsymbol{B} = -\boldsymbol{\Delta\bar{F}}_{\vartheta} \cdot \boldsymbol{\bar{M}}$ where $\boldsymbol{\Delta\bar{F}}_{\vartheta}$ is defined in (4.55) and $\boldsymbol{\bar{M}}$ is defined in (4.77) [6].

4.4.3 The $\boldsymbol{C}$-matrix

The $\boldsymbol{C}$matrix consist of two sub-matrices, $\boldsymbol{C}_1$ and $\boldsymbol{C}_2$. The position (i,k) in the $\boldsymbol{C}_1$-matrix and the $\boldsymbol{C}_2$-matrix is defined by C_{ik}^{I}-term and the C_{ik}^{II}-term which are determined in (4.23). The definition explicitly defined as:

$$\boldsymbol{C} = \boldsymbol{C}_1 + \boldsymbol{C}_2 \tag{4.115}$$

4.4.3.1 The C_1-matrix

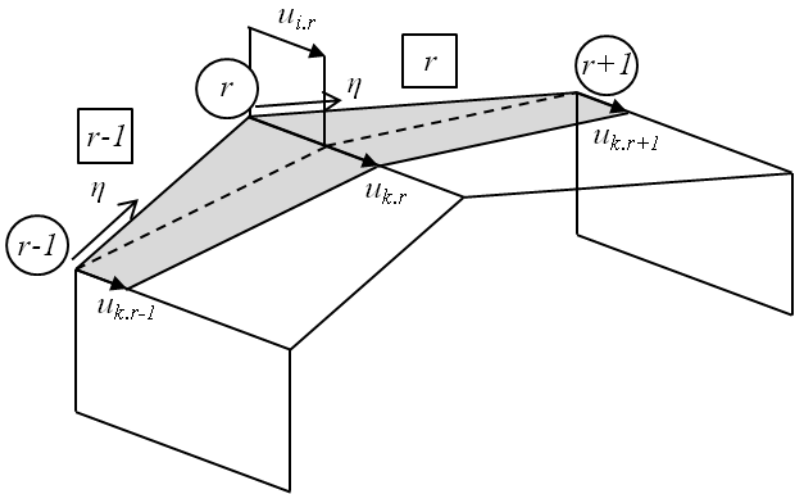

Figure 4.17: This figure illustrates the linear variation of the cross-section deformation mode $u_k(s)$ (solid line) and the linear variation of the virtual displacement $u_i(s)$ (broken line). Rings denote natural nodes and squares denotes plate numbering.

The longitudinal displacement mode $u_k(s)$ varies linear between the natural nodes and the virtual unit displacement $u_{r.i} = \overline{1}$ at node r and zero at all other nodes and linear variation between the nodes. For a unit displacement at node r the two adjacent elements $r-1$ and r will be affected which must be accounted for, see Figure 4.17. The $u_k(s)$-displacement and $u_i(s)$-displacement can then be described in the same local coordinate η defined in (4.97). This give:

$$u_k(s) = u_k(\eta) = \begin{cases} (1-\eta)\cdot u_{k.r-1} + \eta \cdot u_{k.r}, & \eta = \dfrac{s}{b_{r-1}}, \quad \eta \in \{0,1\} \\ (1-\eta)\cdot u_{k.r} + \eta \cdot u_{k.r+1}, & \eta = \dfrac{s}{b_r}, \quad \eta \in \{0,1\} \end{cases} \tag{4.116}$$

$$u_i(s) = u_i(\eta) = \begin{cases} \eta \cdot u_{i.r}, & \eta = \dfrac{s}{b_{r-1}}, \quad \eta \in \{0,1\} \\ (1-\eta)\cdot u_{i.r}, & \eta = \dfrac{s}{b_r}, \quad \eta \in \{0,1\} \end{cases} \tag{4.117}$$

The C_{ik}^l-term can now be determined by inserting (4.116) and (4.117) into (4.20) and compute the integral. The variable substitution $s \Rightarrow \eta$ gives that $ds = b_r d\eta$ which must be accounted for.

$$
\begin{aligned}
C_{ik}^{I} = t \int_{b} u_k u_i ds = \\
&= t_{r-1} \int_{0}^{1} [(1-\eta)\cdot u_{k.r-1} + \eta \cdot u_{k.r}]\eta \cdot u_{i.r} b_{r-1} d\eta \\
&+ t_r \int_{0}^{1} [(1-\eta)\cdot u_{k.r} + \eta \cdot u_{k.r+1}](1-\eta)\cdot u_{i.r} b_r d\eta \\
&= t_{r-1} b_{r-1} \left[\left(\frac{\eta^2}{2} - \frac{\eta^3}{3}\right) u_{k.r-1} + \frac{\eta^3}{3} u_{k.r}\right]_0^1 \cdot \bar{1} \\
&+ t_r b_r \left[\left(\eta - \eta^2 + \frac{\eta^3}{3}\right) u_{k.r} + \left(\frac{\eta^2}{2} - \frac{\eta^3}{3}\right) u_{k.r+1}\right]_0^1 \cdot \bar{1} \\
&= t_{r-1} b_{r-1} \left[\frac{1}{6} u_{k.r-1} + \frac{1}{3} u_{k.r}\right] + t_r b_r \left[\frac{1}{3} u_{k.r} + \frac{1}{6} u_{k.r+1}\right] \\
&= \frac{1}{6} [b_{r-1} t_{r-1} u_{k.r-1} + 2(b_{r-1} t_{r-1} + b_r t_r) u_{k.r} \\
&+ b_{r+1} t_{r+1} u_{k.r+1}]
\end{aligned}
\tag{4.118}
$$

The C_{ik}^{I}-term can now be obtained as:

$$
C_{ik}^{I} = \frac{1}{6} [b_{r-1} t_{r-1} u_{k.r-1} + 2(b_{r-1} t_{r-1} + b_r t_r) u_{k.r} + b_{r+1} t_{r+1} u_{k.r+1}] \tag{4.119}
$$

Since C_{ik}^{I} is expressed in the nodal u-displacements it can easily be written in matrix form. The matrix $\boldsymbol{C}_1$ will be symmetric and have three diagonal non-zero bands. A programming ready matrix is defined in Appendix B.

4.4.3.2 The $\boldsymbol{C_2}$-matrix

The $\boldsymbol{C}_2$-matrix is defined by the C_{ik}^{II}-term. Here the integral is computed using the shape functions Ψ_{1-4} defined in (4.99) and the cross-sectional deformation mode w_k defined in (4.98).

$$
\begin{aligned}
C_{ik}^{II} = \frac{K}{E}\int_b w_k w_i ds = \\
&= \frac{1}{E}\sum_{r=1}^{n} K_r \int_0^1 \Bigg[w_{r.k}\cdot\Psi_1 + \vartheta_{r.k}\frac{b_r}{2}\cdot\Psi_2 + \bar{m}_{s.r.k}\frac{b_r^2}{2K_r}\cdot\Psi_3 \\
&- \hat{m}_{s.r.k}\frac{b_r^2}{6K_r}\cdot\Psi_4\Bigg] \\
&\cdot\Bigg[w_{r.i}\cdot\Psi_1 + \vartheta_{r.i}\frac{b_r}{2}\cdot\Psi_2 + \bar{m}_{s.r.i}\frac{b_r^2}{2K_r}\cdot\Psi_3 - \hat{m}_{s.r.i}\frac{b_r^2}{6K_r} \\
&\cdot\Psi_4\Bigg] b_r d\eta \\
&= \frac{1}{E}\sum_{r=1}^{n} K_r b_r \int_0^1 \Bigg[w_{r.k}w_{r.i}\cdot\Psi_1\Psi_1 + \vartheta_{r.k}w_{r.i}\frac{b_r}{2}\cdot\Psi_2\Psi_1 \\
&+ \bar{m}_{s.r.k}w_{r.i}\frac{b_r^2}{2K_r}\cdot\Psi_3\Psi_1 - \hat{m}_{s.r.k}w_{r.i}\frac{b_r^2}{6K_r}\cdot\Psi_4\Psi_1 \\
&+ w_{r.k}\vartheta_{r.i}\frac{b_r}{2}\cdot\Psi_1\Psi_2 + \vartheta_{r.k}\vartheta_{r.i}\frac{b_r}{2}\frac{b_r}{2}\cdot\Psi_2\Psi_2 \\
&+ \bar{m}_{s.r.k}\vartheta_{r.i}\frac{b_r^2}{2K_r}\frac{b_r}{2}\cdot\Psi_3\Psi_2 - \hat{m}_{s.r.k}\vartheta_{r.i}\frac{b_r^2}{6K_r}\frac{b_r}{2}\cdot\Psi_4\Psi_2 \\
&+ w_{r.k}\bar{m}_{s.r.i}\frac{b_r^2}{2K_r}\cdot\Psi_1\Psi_3 + \vartheta_{r.k}\bar{m}_{s.r.i}\frac{b_r}{2}\frac{b_r^2}{2K_r}\cdot\Psi_2\Psi_3 \\
&+ \bar{m}_{s.r.k}\bar{m}_{s.r.i}\frac{b_r^2}{2K_r}\frac{b_r^2}{2K_r}\cdot\Psi_3\Psi_3 - \hat{m}_{s.r.k}\bar{m}_{s.r.i}\frac{b_r^2}{6K_r}\frac{b_r^2}{2K_r} \\
&\cdot\Psi_4\Psi_3 - w_{r.k}\hat{m}_{s.r.i}\frac{b_r^2}{6K_r}\cdot\Psi_1\Psi_4 - \vartheta_{r.k}\hat{m}_{s.r.i}\frac{b_r}{2}\frac{b_r^2}{6K_r}\cdot\Psi_2\Psi_4 \\
&- \bar{m}_{s.r.k}\hat{m}_{s.r.i}\frac{b_r^2}{2K_r}\frac{b_r^2}{6K_r}\cdot\Psi_3\Psi_4 + \hat{m}_{s.r.k}\hat{m}_{s.r.i}\frac{b_r^2}{6K_r}\frac{b_r^2}{6K_r} \\
&\cdot\Psi_4\Psi_4\Bigg] d\eta
\end{aligned}
\tag{4.120}
$$

The only η-dependent terms are the shape functions Ψ_{1-4}. The integration of the shape function products are computed and tabulated defined in Table 4.2.

Table 4.2: This table contains the integration of shape function products defined as $\int_0^1 \Psi_i \Psi_j \, d\eta$.

	Ψ_1	Ψ_2	Ψ_3	Ψ_4
Ψ_1	1	0	$\frac{1}{6}$	0
Ψ_2	0	$\frac{1}{3}$	0	$-\frac{1}{30}$
Ψ_3	$\frac{1}{6}$	0	$\frac{1}{30}$	0
Ψ_4	0	$-\frac{1}{30}$	0	$\frac{1}{210}$

Insert the values from Table 4.2 into (4.120) gives:

$$
\begin{aligned}
C_{ik}^{II} = \frac{1}{E}\sum_{r=1}^{n} K_r b_r \Bigg[& w_{r.k} w_{r.i} \cdot 1 + \vartheta_{r.k} w_{r.i} \frac{b_r}{2} \cdot 0 + \bar{m}_{s.r.k} w_{r.i} \frac{b_r^2}{2K_r} \cdot \frac{1}{6} \\
& - \hat{m}_{s.r.k} w_{r.i} \frac{b_r^2}{6K_r} \cdot 0 + w_{r.k} \vartheta_{r.i} \frac{b_r}{2} \cdot 0 + \vartheta_{r.k} \vartheta_{r.i} \frac{b_r}{2} \frac{b_r}{2} \cdot \frac{1}{3} \\
& + \bar{m}_{s.r.k} \vartheta_{r.i} \frac{b_r^2}{2K_r} \frac{b_r}{2} \cdot 0 - \hat{m}_{s.r.k} \vartheta_{r.i} \frac{b_r^2}{6K_r} \frac{b_r}{2} \cdot \left(-\frac{1}{30}\right) \\
& + w_{r.k} \bar{m}_{s.r.i} \frac{b_r^2}{2K_r} \cdot \frac{1}{6} + \vartheta_{r.k} \bar{m}_{s.r.i} \frac{b_r}{2} \frac{b_r^2}{2K_r} \cdot 0 \\
& + \bar{m}_{s.r.k} \bar{m}_{s.r.i} \frac{b_r^2}{2K_r} \frac{b_r^2}{2K_r} \cdot \frac{1}{30} - \hat{m}_{s.r.k} \bar{m}_{s.r.i} \frac{b_r^2}{6K_r} \frac{b_r^2}{2K_r} \cdot 0 \\
& - w_{r.k} \hat{m}_{s.r.i} \frac{b_r^2}{6K_r} \cdot 0 - \vartheta_{r.k} \hat{m}_{s.r.i} \frac{b_r}{2} \frac{b_r^2}{6K_r} \cdot \left(-\frac{1}{30}\right) \\
& - \bar{m}_{s.r.k} \hat{m}_{s.r.i} \frac{b_r^2}{2K_r} \frac{b_r^2}{6K_r} \cdot 0 + \hat{m}_{s.r.k} \hat{m}_{s.r.i} \frac{b_r^2}{6K_r} \frac{b_r^2}{6K_r} \cdot \frac{1}{210} \Bigg] \\
= \frac{1}{E}\sum_{r=1}^{n} K_r b_r \Bigg[& w_{r.k} w_{r.i} + \bar{m}_{s.r.k} w_{r.i} \frac{b_r^2}{12K_r} + \vartheta_{r.k} \vartheta_{r.i} \frac{b_r^2}{12} \\
& + \hat{m}_{s.r.k} \vartheta_{r.i} \frac{b_r^3}{360K_r} + w_{r.k} \bar{m}_{s.r.i} \frac{b_r^2}{12K_r} \\
& + \bar{m}_{s.r.k} \bar{m}_{s.r.i} \frac{b_r^4}{120K_r^2} + \vartheta_{r.k} \hat{m}_{s.r.i} \frac{b_r^3}{360K_r} \\
& + \hat{m}_{s.r.k} \hat{m}_{s.r.i} \frac{b_r^4}{7560K_r^2} \Bigg] =
\end{aligned}
$$

$$
\begin{aligned}
&= \frac{1}{E}\sum_{r=1}^{n} K_r b_r \left[w_{r.k} w_{r.i} + \vartheta_{r.k}\vartheta_{r.i}\frac{b_r^2}{12} \right. \\
&+ (w_{r.k}\bar{m}_{s.r.i} + \bar{m}_{s.r.k} w_{r.i})\frac{b_r^2}{12K_r} \\
&+ (\hat{m}_{s.r.k}\vartheta_{r.i} + \vartheta_{r.k}\hat{m}_{s.r.i})\frac{b_r^3}{360K_r} \\
&\left. + \left(\bar{m}_{s.r.k}\bar{m}_{s.r.i} + \frac{1}{63}\hat{m}_{s.r.k}\hat{m}_{s.r.i}\right)\frac{b_r^4}{120K_r^2} \right]
\end{aligned}
\tag{4.121}
$$

The C_{ik}^{II}-term can now be obtained as:

$$
\begin{aligned}
C_{ik}^{II} = \frac{1}{E}\sum_{r=1}^{n} K_r b_r \left[w_{r.k} w_{r.i} + \vartheta_{r.k}\vartheta_{r.i}\frac{b_r^2}{12} + (w_{r.k}\bar{m}_{s.r.i} + \bar{m}_{s.r.k} w_{r.i})\frac{b_r^2}{12K_r} \right. \\
+ (\hat{m}_{s.r.k}\vartheta_{r.i} + \vartheta_{r.k}\hat{m}_{s.r.i})\frac{b_r^3}{360K_r} \\
\left. + \left(\bar{m}_{s.r.k}\bar{m}_{s.r.i} + \frac{1}{63}\hat{m}_{s.r.k}\hat{m}_{s.r.i}\right)\frac{b_r^4}{120K_r^2} \right]
\end{aligned}
\tag{4.122}
$$

The $\boldsymbol{C}_2$-matrix is now fully determined and will be symmetric and all positions will be non-zero.

4.4.4 The $\boldsymbol{D}$-matrix

The $\boldsymbol{D}$-matrix is defined by the three sub-matrices $\boldsymbol{D}_1$, $\boldsymbol{D}_2$ and $\boldsymbol{D}_3$. Each sub-matrix is defined by the D_{ik}^{I}-, D_{ik}^{II}- and D_{ik}^{III}-terms respectively which are defined in (4.26). The $\boldsymbol{D}$-matrix is defined as:

$$
\boldsymbol{D} = \boldsymbol{D}_1 - (\boldsymbol{D}_2 + \boldsymbol{D}_3) \tag{4.123}
$$

4.4.4.1 The $\boldsymbol{D}_1$-matrix

The $\boldsymbol{D}_1$-matrix is defined by the D_{ik}^{I}-term. Here first order derivatives of the cross-sectional deformation mode $w_k(s)$ and $w_i(s)$ should be used and are defined in (4.109). Then one have:

$$
\begin{aligned}
D_{ik}^{I} &= \frac{t^3}{3}\int_b w_{k,s} w_{i,s}\, ds = \\
&= \sum_{r=1}^{n} \frac{t_r^3}{3} \int_0^1 \Bigg[w_{r.k} \frac{1}{b_r} \cdot \underbrace{\Psi_{1,\eta}}_{=0} + \vartheta_{r.k} \frac{1}{2} \cdot \Psi_{2,\eta} + \bar{m}_{s.r.k} \frac{b_r}{2K_r} \\
&\cdot \Psi_{3,\eta} - \hat{m}_{s.r.k} \frac{b_r}{6K_r} \cdot \Psi_{4,\eta} \Bigg] \\
&\cdot \Bigg[w_{r.i} \frac{1}{b_r} \cdot \underbrace{\Psi_{1,\eta}}_{=0} + \vartheta_{r.i} \frac{1}{2} \cdot \Psi_{2,\eta} + \bar{m}_{s.r.i} \frac{b_r}{2K_r} \cdot \Psi_{3,\eta} \\
&- \hat{m}_{s.r.i} \frac{b_r}{6K_r} \cdot \Psi_{4,\eta} \Bigg] b_r\, d\eta \\
&= \sum_{r=1}^{n} \frac{b_r t_r^3}{3} \int_0^1 \Bigg[\vartheta_{r.k} \vartheta_{r.i} \frac{1}{2}\frac{1}{2} \cdot \Psi_{2,\eta}\Psi_{2,\eta} + \bar{m}_{s.r.k} \vartheta_{r.i} \frac{b_r}{2K_r}\frac{1}{2} \\
&\cdot \Psi_{3,\eta}\Psi_{2,\eta} - \hat{m}_{s.r.k} \vartheta_{r.i} \frac{b_r}{6K_r}\frac{1}{2} \cdot \Psi_{4,\eta}\Psi_{2,\eta} + \vartheta_{r.k} \bar{m}_{s.r.i} \frac{1}{2}\frac{b_r}{2K_r} \\
&\cdot \Psi_{2,\eta}\Psi_{3,\eta} + \bar{m}_{s.r.k} \bar{m}_{s.r.i} \frac{b_r}{2K_r}\frac{b_r}{2K_r} \cdot \Psi_{3,\eta}\Psi_{3,\eta} \\
&- \hat{m}_{s.r.k} \bar{m}_{s.r.i} \frac{b_r}{6K_r}\frac{b_r}{2K_r} \cdot \Psi_{4,\eta}\Psi_{3,\eta} - \vartheta_{r.k} \hat{m}_{s.r.i} \frac{1}{2}\frac{b_r}{6K_r} \\
&\cdot \Psi_{2,\eta}\Psi_{4,\eta} - \bar{m}_{s.r.k} \hat{m}_{s.r.i} \frac{b_r}{2K_r}\frac{b_r}{6K_r} \cdot \Psi_{3,\eta}\Psi_{4,\eta} \\
&+ \hat{m}_{s.r.k} \hat{m}_{s.r.i} \frac{b_r}{6K_r}\frac{b_r}{6K_r} \cdot \Psi_{4,\eta}\Psi_{4,\eta} \Bigg] d\eta
\end{aligned}
\tag{4.124}
$$

The only η-dependent terms are the shape functions $\Psi_{1-4,\eta}$. The integration of the shape function products are computed and tabulated defined in Table 4.3.

Table 4.3: This table contains the integration of shape function products defined as $\int_0^1 \Psi_{,\eta}\Psi_{,\eta}\,d\eta$.

	$\Psi_{2,\eta}$	$\Psi_{3,\eta}$	$\Psi_{4,\eta}$
$\Psi_{2,\eta}$	4	0	0
$\Psi_{3,\eta}$	0	$\frac{1}{3}$	0
$\Psi_{4,\eta}$	0	0	$\frac{1}{5}$

Inserting the values in Table 4.3 into (4.124) gives:

$$\begin{aligned} D_{ik}^{I} = \sum_{r=1}^{n} \frac{b_r t_r^3}{3}\Bigg[& \vartheta_{r.k}\vartheta_{r.i}\frac{1}{2}\frac{1}{2}\cdot 4 + \overline{m}_{s.r.k}\vartheta_{r.i}\frac{b_r}{2K_r}\frac{1}{2}\cdot 0 - \widehat{m}_{s.r.k}\vartheta_{r.i}\frac{b_r}{6K_r}\frac{1}{2}\cdot 0 \\ & + \vartheta_{r.k}\overline{m}_{s.r.i}\frac{1}{2}\frac{b_r}{2K_r}\cdot 0 + \overline{m}_{s.r.k}\overline{m}_{s.r.i}\frac{b_r}{2K_r}\frac{b_r}{2K_r}\cdot\frac{1}{3} \\ & - \widehat{m}_{s.r.k}\overline{m}_{s.r.i}\frac{b_r}{6K_r}\frac{b_r}{2K_r}\cdot 0 - \vartheta_{r.k}\widehat{m}_{s.r.i}\frac{1}{2}\frac{b_r}{6K_r}\cdot 0 \\ & - \overline{m}_{s.r.k}\widehat{m}_{s.r.i}\frac{b_r}{2K_r}\frac{b_r}{6K_r}\cdot 0 + \widehat{m}_{s.r.k}\widehat{m}_{s.r.i}\frac{b_r}{6K_r}\frac{b_r}{6K_r}\cdot\frac{1}{5}\Bigg] = \\ = \sum_{r=1}^{n} \frac{b_r t_r^3}{3}\Bigg[& \vartheta_{r.k}\vartheta_{r.i} + \overline{m}_{s.r.k}\overline{m}_{s.r.i}\frac{b_r^2}{12K_r^2} \\ & + \widehat{m}_{s.r.k}\widehat{m}_{s.r.i}\frac{b_r^2}{180K_r^2}\Bigg] \\ = \sum_{r=1}^{n} \frac{b_r t_r^3}{3}\Bigg[& \vartheta_{r.k}\vartheta_{r.i} \\ & + \left(\overline{m}_{s.r.k}\overline{m}_{s.r.i} + \frac{1}{15}\widehat{m}_{s.r.k}\widehat{m}_{s.r.i}\right)\frac{b_r^2}{12K_r^2}\Bigg] \end{aligned} \tag{4.125}$$

The D_{ik}^{I}-term is then obtained as:

$$D_{ik}^{I} = \sum_{r=1}^{n} \frac{b_r t_r^3}{3}\left[\vartheta_{r.k}\vartheta_{r.i} + \left(\overline{m}_{s.r.k}\overline{m}_{s.r.i} + \frac{1}{15}\widehat{m}_{s.r.k}\widehat{m}_{s.r.i}\right)\frac{b_r^2}{12K_r^2}\right] \tag{4.126}$$

The $\boldsymbol{D}_1$-matrix is now fully determined and will be symmetric and all positions will in general be non-zero.

4.4.4.2 The $\boldsymbol{D}_2$-matrix

The $\boldsymbol{D}_2$-matrix is defined by the D_{ik}^{II}-term. Here the second order derivatives of the deformation modes $w_k(s)$ is used which is defined in (4.110).

$$
\begin{aligned}
D_{ik}^{II} = \frac{\nu K}{G}\int_b w_{k,ss} w_i \, ds = \\
&= \frac{\nu}{G}\sum_{r=1}^{n} K_r \int_0^1 \Bigg[w_{r.k}\frac{1}{b_r^2}\cdot \underbrace{\Psi_{1,\eta\eta}}_{=0} + \vartheta_{r.k}\frac{1}{2b_r}\cdot \underbrace{\Psi_{2,\eta\eta}}_{=0} \\
&+ \bar{m}_{s.r.k}\frac{1}{2K_r}\cdot\Psi_{3,\eta\eta} - \hat{m}_{s.r.k}\frac{1}{6K_r}\cdot\Psi_{4,\eta\eta}\Bigg] \\
&\cdot \Bigg[w_{r.i}\cdot\Psi_1 + \vartheta_{r.i}\frac{b_r}{2}\cdot\Psi_2 + \bar{m}_{s.r.i}\frac{b_r^2}{2K_r}\cdot\Psi_3 - \hat{m}_{s.r.i}\frac{b_r^2}{6K_r} \\
&\cdot \Psi_4\Bigg] b_r \, d\eta \\
&= \frac{\nu}{G}\sum_{r=1}^{n} K_r b_r \int_0^1 \Bigg[\bar{m}_{s.r.k} w_{r.i}\frac{1}{2K_r}\cdot\Psi_{3,\eta\eta}\Psi_1 - \hat{m}_{s.r.k} w_{r.i}\frac{1}{6K_r} \\
&\cdot \Psi_{4,\eta\eta}\Psi_1 + \bar{m}_{s.r.k}\vartheta_{r.i}\frac{1}{2K_r}\frac{b_r}{2}\cdot\Psi_{3,\eta\eta}\Psi_2 - \hat{m}_{s.r.k}\vartheta_{r.i}\frac{1}{6K_r}\frac{b_r}{2} \\
&\cdot \Psi_{4,\eta\eta}\Psi_2 + \bar{m}_{s.r.k}\bar{m}_{s.r.i}\frac{1}{2K_r}\frac{b_r^2}{2K_r}\cdot\Psi_{3,\eta\eta}\Psi_3 \\
&- \hat{m}_{s.r.k}\bar{m}_{s.r.i}\frac{1}{6K_r}\frac{b_r^2}{2K_r}\cdot\Psi_{4,\eta\eta}\Psi_3 - \bar{m}_{s.r.k}\hat{m}_{s.r.i}\frac{1}{2K_r}\frac{b_r^2}{6K_r} \\
&\cdot \Psi_{3,\eta\eta}\Psi_4 + \hat{m}_{s.r.k}\hat{m}_{s.r.i}\frac{1}{6K_r}\frac{b_r^2}{6K_r}\cdot\Psi_{4,\eta\eta}\Psi_4\Bigg] d\eta
\end{aligned}
\tag{4.127}
$$

The only η-dependent terms are the shape functions Ψ_{1-4} and $\Psi_{1-4,\eta\eta}$. The integration of the shape function products are computed and tabulated defined in Table 4.4.

Table 4.4: This table contains the integration of shape function products defined as $\int_0^1 \Psi_{,\eta\eta}\Psi \, d\eta$.

	Ψ_1	Ψ_2	Ψ_3	Ψ_4
$\Psi_{3,\eta\eta}$	-2	0	$-\frac{1}{3}$	0
$\Psi_{4,\eta\eta}$	0	2	0	$-\frac{1}{5}$

Insert the values from Table 4.4 into (4.127) gives:

$$
\begin{aligned}
D_{ik}^{II} = \frac{\nu}{G}\sum_{r=1}^{n} K_r b_r \Bigg[& \overline{m}_{s.r.k} w_{r.i} \frac{1}{2K_r} \cdot (-2) - \widehat{m}_{s.r.k} w_{r.i} \frac{1}{6K_r} \cdot 0 \\
& + \overline{m}_{s.r.k} \vartheta_{r.i} \frac{1}{2K_r} \frac{b_r}{2} \cdot 0 - \widehat{m}_{s.r.k} \vartheta_{r.i} \frac{1}{6K_r} \frac{b_r}{2} \cdot 2 \\
& + \overline{m}_{s.r.k} \overline{m}_{s.r.i} \frac{1}{2K_r} \frac{b_r^2}{2K_r} \cdot \left(-\frac{1}{3}\right) - \widehat{m}_{s.r.k} \overline{m}_{s.r.i} \frac{1}{6K_r} \frac{b_r^2}{2K_r} \cdot 0 \\
& - \overline{m}_{s.r.k} \widehat{m}_{s.r.i} \frac{1}{2K_r} \frac{b_r^2}{6K_r} \cdot 0 + \widehat{m}_{s.r.k} \widehat{m}_{s.r.i} \frac{1}{6K_r} \frac{b_r^2}{6K_r} \cdot \left(-\frac{1}{5}\right) \Bigg] \\
= \frac{\nu}{G}\sum_{r=1}^{n} K_r b_r \Bigg[& -\overline{m}_{s.r.k} w_{r.i} \frac{1}{K_r} - \widehat{m}_{s.r.k} \vartheta_{r.i} \frac{b_r}{6K_r} \\
& - \overline{m}_{s.r.k} \overline{m}_{s.r.i} \frac{b_r^2}{12K_r^2} - \widehat{m}_{s.r.k} \widehat{m}_{s.r.i} \frac{b_r^2}{180K_r^2} \Bigg] \\
= \frac{\nu}{G}\sum_{r=1}^{n} b_r \Bigg[& -\overline{m}_{s.r.k} w_{r.i} - \widehat{m}_{s.r.k} \vartheta_{r.i} \frac{b_r}{6} \\
& - \left(\overline{m}_{s.r.k} \overline{m}_{s.r.i} + \frac{1}{15} \widehat{m}_{s.r.k} \widehat{m}_{s.r.i}\right) \frac{b_r^2}{12K_r} \Bigg]
\end{aligned}
\tag{4.128}
$$

The D_{ik}^{II}-term is then obtained as:

$$
\begin{aligned}
D_{ik}^{II} = \frac{\nu}{G}\sum_{r=1}^{n} b_r \Bigg[& -\overline{m}_{s.r.k} w_{r.i} - \widehat{m}_{s.r.k} \vartheta_{r.i} \frac{b_r}{6} \\
& - \left(\overline{m}_{s.r.k} \overline{m}_{s.r.i} + \frac{1}{15} \widehat{m}_{s.r.k} \widehat{m}_{s.r.i}\right) \frac{b_r^2}{12K_r} \Bigg]
\end{aligned}
\tag{4.129}
$$

The $\boldsymbol{D}_2$-matrix is now fully determined and all positions will be non-zero. In comparison to the other matrices the $\boldsymbol{D}_2$-matrix will not be symmetric.

4.4.4.3 The $\boldsymbol{D}_3$-matrix

The $\boldsymbol{D}_3$-matrix is defined in by the D_{ik}^{III}-term. The only difference to the $\boldsymbol{D}_2$-matrix is that the indices i and k have changed position, i.e. index i have become index k in (4.129). The D_{ik}^{III}-term are then defined as:

$$
\begin{aligned}
D_{ik}^{III} = \frac{\nu}{G}\sum_{r=1}^{n} b_r \Bigg[& -\overline{m}_{s.r.i} w_{r.k} - \widehat{m}_{s.r.i} \vartheta_{r.k} \frac{b_r}{6} \\
& - \left(\overline{m}_{s.r.i} \overline{m}_{s.r.k} + \frac{1}{15} \widehat{m}_{s.r.i} \widehat{m}_{s.r.k}\right) \frac{b_r^2}{12K_r} \Bigg]
\end{aligned}
\tag{4.130}
$$

4.5 The diagonalization of the GBT fundamental equilibrium equation

The GBT fundamental equilibrium equation derived (4.36) and the corresponding components B_{ik}, C_{ik} and D_{ik} are derived in Section 4.4. Express the stiffness terms in the unit deformation modes $\bar{u}$, $\bar{v}$, $\bar{w}$ and $\bar{\vartheta}$ the GBT fundamental equilibrium equation is obtained in matrix form as:

$$E\overline{\boldsymbol{C}}\overline{\boldsymbol{\phi}}_{,xxxx} - G\overline{\boldsymbol{D}}\overline{\boldsymbol{\phi}}_{,xx} + \overline{\boldsymbol{B}}\overline{\boldsymbol{\phi}} = \overline{\boldsymbol{q}} - \overline{\boldsymbol{q}}_{,\boldsymbol{x}} \tag{4.131}$$

The bar denotes that they are expressed by the unit deformations. Since all position in the $\overline{\boldsymbol{B}}$, $\overline{\boldsymbol{C}}$ and $\overline{\boldsymbol{D}}$ matrices generally are non-zero, the differential equation (4.131) is highly coupled which complicates the solution process. In order to have an easier and more practical treatment of the differential equation above, a transformation into an eigenvector coordinate system is carried out in order to have diagonal matrices and with that uncoupled equations. Since the differential equation involves three matrices, the transformation will not succeed to completely diagonalize all of them. The transformation intends therefore to diagonalize the matrices to the largest extent possible.

4.5.1 Simultaneous diagonalization of the $\overline{\boldsymbol{C}}$- and $\overline{\boldsymbol{B}}$-matrix

The simultaneous diagonalization involves three main steps. Here they follow for cross-sections that are not restrained, i.e. no locked cross-sectional nodes:

1. Solve the generalized eigenvalue problem $(\overline{\boldsymbol{B}} - \lambda_k \cdot E\overline{\boldsymbol{C}})\widetilde{\boldsymbol{x}}_k^I = \boldsymbol{0}$.
2. Identify the torsion deformation mode corresponding to eigenvector $\widetilde{\boldsymbol{x}}_4$ by solving the second eigenvalue problem $\left(G\widetilde{\boldsymbol{D}}_{4\times4} - \lambda_k^{II} \cdot E\widetilde{\boldsymbol{C}}_{4\times4}\right)\widetilde{\boldsymbol{x}}_{k.4\times1}^{II} = \boldsymbol{0}$.
3. Identify the extension and bending modes corresponding to eigenvectors $\widetilde{\boldsymbol{x}}_{1-3}$ by solving the third eigenvalue problem $\left(\boldsymbol{K}_{3\times3} - \lambda_k^{III} \cdot E\widetilde{\boldsymbol{C}}_{3\times3}\right)\widetilde{\boldsymbol{x}}_{k.3\times1}^{III} = \boldsymbol{0}$.

4.5.1.1 The generalized eigenvalue $\left(\overline{\boldsymbol{B}} - \boldsymbol{\lambda_i^I} \cdot \boldsymbol{E\overline{C}}\right)\widetilde{\boldsymbol{x}}_{\boldsymbol{i}}^{\boldsymbol{I}} = \boldsymbol{0}$

The first step in the diagonalization procedure is to solve the generalized eigenvalue problem in order to establish the deformation modes. The eigenvalue problem is defined as:

$$(\overline{\boldsymbol{B}} - \lambda_k^I \cdot E\overline{\boldsymbol{C}})\widetilde{\boldsymbol{x}}_k^I = \boldsymbol{0} \tag{4.132}$$

The superscript $(\cdot)^I$ referrers to the first of eigenvalue problem in the diagonalization process. A necessary condition in order to have a simultaneous diagonalization is that the eigenvectors are orthogonal to each other, and the following condition is therefore fundamental:

$$\widetilde{\boldsymbol{x}}_i^I \cdot \overline{\boldsymbol{C}} \cdot \widetilde{\boldsymbol{x}}_k^I = \begin{cases} 0 & for\, i \neq k \\ \tilde{C}_{kk}\, for\, k = k \end{cases} \qquad \widetilde{\boldsymbol{x}}_i^I \cdot \overline{\boldsymbol{B}} \cdot \widetilde{\boldsymbol{x}}_k^I = \begin{cases} 0 & for\, i \neq k \\ \tilde{B}_{kk}\, for\, k = k \end{cases} \tag{4.133}$$

When solving the eigenvalue problem the same number of eigenvalues and eigenvectors are obtained as the total number of degrees of freedom ($ndof$) in the

cross-section. Sort the eigenvalues and the corresponding eigenvectors in numerical order $\lambda_1^I < \lambda_2^I \ldots < \lambda_{ndof}^I$ and normalize the eigenvectors such that the maximum value becomes unit value, i.e. $|\tilde{x}_k| = 1$. Collecting all the eigenvectors into theeigenmatrix $\widetilde{\boldsymbol{X}}$ gives:

$$\widetilde{\boldsymbol{X}} = \widetilde{\boldsymbol{X}}^I = \begin{bmatrix} \widetilde{\boldsymbol{x}}_1^I & \widetilde{\boldsymbol{x}}_2^I & \cdots & \widetilde{\boldsymbol{x}}_{ndof}^I \end{bmatrix} \tag{4.134}$$

The four first eigenvalues will be zero $\lambda_{1-4}^I = 0$and correspond to the four rigid body modes (extension, major and minor axis bending and torsion). Thus, the set of eigenvectors consist of $ndof - 4$ distinct orthogonal eigevectors ($k = 5, \ldots, ndof$) which are associated with the transverse bending or distortion modes and a four-dimensional eigenspace associated to the four rigid body deformation modes. The transformation to an arbitrary eigenvector coordinate system is obtained as:

$$\widetilde{\boldsymbol{B}}^I = \left(\widetilde{\boldsymbol{X}}^I\right)^T \cdot \overline{\boldsymbol{B}} \cdot \widetilde{\boldsymbol{X}}^I \qquad \widetilde{\boldsymbol{C}}^I = \left(\widetilde{\boldsymbol{X}}^I\right)^T \cdot \overline{\boldsymbol{C}} \cdot \widetilde{\boldsymbol{X}}^I \qquad \widetilde{\boldsymbol{D}}^I = \left(\widetilde{\boldsymbol{X}}^I\right)^T \cdot \overline{\boldsymbol{D}} \cdot \widetilde{\boldsymbol{X}}^I \tag{4.135}$$

Since the first vectors span a four-dimensional eigenspace there could be many eigenvectors that are orthogonal to the other ($k = 5, \ldots, ndof$) modes, the first four vectors needs therefore further treatment.

4.5.1.2 Determination of the fourth eigenvector $\tilde{x}_4$

The identification of the eigenvector $\tilde{\boldsymbol{x}}_4$ can be determined by taking the advantage of the fact that the $\widetilde{\boldsymbol{D}}$ matrix is diagonal and the first three diagonal elements is zero, i.e. $\widetilde{D}_{11} = \widetilde{D}_{22} = \widetilde{D}_{33} = 0$. Take the sub-matrices $\widetilde{\boldsymbol{C}}_{4\times4}$ and $\widetilde{\boldsymbol{D}}_{4\times4}$ associated to the four rigid body modes from the matrices defined in (4.135) and transform to a less arbitrary eigenvector coordinate system. Thus, another eigenproblem is defined as:

$$\left(G\widetilde{\boldsymbol{D}}_{4\times4} - \lambda_k^{II} \cdot E\widetilde{\boldsymbol{C}}_{4\times4}\right)\widetilde{\boldsymbol{x}}_{k.4\times1}^{II} = \boldsymbol{0} \tag{4.136}$$

The solution to the eigenproblem gives four eigenvalues and eigenvectors and sorted in numerical order gives that the three first eigenvalues are zero $\lambda_{1-3}^{II} = 0$ which now correspond to three rigid body modes left, i.e. extension, major and minor axis bending. The transformation is defined as:

$$\begin{aligned} \widetilde{\boldsymbol{X}}^{II} &= [\widetilde{\boldsymbol{x}}_1^{II} \quad \widetilde{\boldsymbol{x}}_2^{II} \quad \widetilde{\boldsymbol{x}}_3^{II} \quad \widetilde{\boldsymbol{x}}_4^{II}] = \\ &= \underbrace{[\widetilde{\boldsymbol{x}}_1^I \quad \widetilde{\boldsymbol{x}}_2^I \quad \widetilde{\boldsymbol{x}}_3^I \quad \widetilde{\boldsymbol{x}}_4^I]}_{(ndof)\times4} \cdot \underbrace{[\widetilde{\boldsymbol{x}}_{1.4\times1}^{II} \quad \widetilde{\boldsymbol{x}}_{2.4\times1}^{II} \quad \widetilde{\boldsymbol{x}}_{3.4\times1}^{II} \quad \widetilde{\boldsymbol{x}}_{4.4\times1}^{II}]}_{4\times4} \end{aligned} \tag{4.137}$$

The fourth eigenvalue is non-zero and the eigenvector corresponds to the torsion deformation mode and the eigenvector should be normalized such that unit rotation is obtained, i.e. all plate elements rotation have unit value $\tilde{\vartheta}_r = 1$. Replace the first four eigenvectorsin (4.134) with the transformed modes defined in (4.137) and the eigenmatrix $\widetilde{\boldsymbol{X}}$ is then defined as:

$$\widetilde{\boldsymbol{X}} = \begin{bmatrix} \widetilde{\boldsymbol{x}}_1^{II} & \widetilde{\boldsymbol{x}}_2^{II} & \widetilde{\boldsymbol{x}}_3^{II} & \widetilde{\boldsymbol{x}}_4^{II} & \widetilde{\boldsymbol{x}}_5^I & \cdots & \widetilde{\boldsymbol{x}}_{ndof}^I \end{bmatrix} \tag{4.138}$$

Perform the matrix multiplication and the diagonalization of the $\widetilde{\boldsymbol{B}}$, $\widetilde{\boldsymbol{C}}$ and $\widetilde{\boldsymbol{D}}$ matrices are defined as:

$$\widetilde{\boldsymbol{B}}^{II} = \left(\widetilde{\boldsymbol{X}}^{II}\right)^T \cdot \widetilde{\boldsymbol{B}}^{I} \cdot \widetilde{\boldsymbol{X}}^{II} \quad \widetilde{\boldsymbol{C}}^{II} = \left(\widetilde{\boldsymbol{X}}^{II}\right)^T \cdot \widetilde{\boldsymbol{C}}^{I} \cdot \widetilde{\boldsymbol{X}}^{II} \quad \widetilde{\boldsymbol{D}}^{II} = \left(\widetilde{\boldsymbol{X}}^{II}\right)^T \cdot \widetilde{\boldsymbol{D}}^{I} \cdot \widetilde{\boldsymbol{X}}^{II} \quad (4.139)$$

Where $\widetilde{\boldsymbol{X}}^{II}$ is defined in (4.137) and the matrices are defined in (4.135). The $\tilde{C}_{44}$-value will then coincide with the warping constant and the $\widetilde{D}_{44}$-value coincide with the torsion stiffness in Vlasov torsion theory or non-uniform torsion theory. The three first eigenvectors is still not explicitly defined and needs further treatment in order to capture the extension, major and minor axis bending modes.

4.5.1.3 The three first eigenvectors $\widetilde{\boldsymbol{x}}_{1-3}$

In order to identify the three remaining eigenvectors corresponding to the extension, and bending rigid-body modes a new geometrical matrix $\boldsymbol{K}$ must be used. This matrix is obtained and used in second-order analysis and this matrix corresponds to the non-linear terms. Here the matrix is only defined. For further reading and deeper understanding, the reader is referred to [6], [23] and [24]. The sub-matrix $\boldsymbol{K}_{3\times3}$ corresponding to the three remaining undefined eigenvectors is defined by:

$$K_{ik} = -\frac{1}{A}\sum_{r=1}^{n}(\tilde{v}_{i.r}\tilde{v}_{k.r} + \widetilde{w}_{i.r}\widetilde{w}_{k.r})b_r t_r \quad (4.140)$$

Where A is the total cross-sectional area, b_r and t_r are the plate element r's width and thickness respectively and the summation applies to the total number of plate elements n. The displacement components $\tilde{v}_k$ and $\widetilde{w}_k$ are obtained from the second eigenvector transformation, i.e. the $\tilde{v}_k$-and $\widetilde{w}_k$- terms are the position k in the $\widetilde{\boldsymbol{v}}$- and $\widetilde{\boldsymbol{w}}$-vector respectively. These vectors are defined as:

$$\widetilde{\boldsymbol{v}} = \overline{\boldsymbol{F}}_v \cdot \widetilde{\boldsymbol{X}}^{II}_{ndof\times3} \quad (4.141)$$

$$\widetilde{\boldsymbol{w}} = \overline{\boldsymbol{F}}_w \cdot \widetilde{\boldsymbol{X}}^{II}_{ndof\times3} \quad (4.142)$$

Where $\widetilde{\boldsymbol{X}}^{II}_{ndof\times3}$ is the sub-matrix containing the three first eigenvectors of $\widetilde{\boldsymbol{X}}^{II}$ defined as:

$$\widetilde{\boldsymbol{X}}^{II}_{ndof\times3} = [\widetilde{\boldsymbol{x}}^{II}_1 \quad \widetilde{\boldsymbol{x}}^{II}_2 \quad \widetilde{\boldsymbol{x}}^{II}_3] \quad (4.143)$$

Take the sub-matrix $\widetilde{\boldsymbol{C}}_{3\times3}$ from the $\widetilde{\boldsymbol{C}}^{II}$-matrix defined in (4.139). The third eigenproblem is then established as:

$$\left(\boldsymbol{K}_{3\times3} - \lambda^{III}_k \cdot E\widetilde{\boldsymbol{C}}_{3\times3}\right)\widetilde{\boldsymbol{x}}^{III}_{k.3\times1} = \boldsymbol{0} \quad (4.144)$$

The solution to the eigenproblem gives three eigenvalues and eigenvectors and when sorted in numerical order $\lambda^{III}_1 < \lambda^{III}_2 < \lambda^{III}_3$ gives that only the first eigenvalue is zero $\lambda^{III}_1 = 0$. The transformation is defined as:

$$\widetilde{\boldsymbol{X}}^{III} = [\widetilde{\boldsymbol{x}}_1^{III} \quad \widetilde{\boldsymbol{x}}_2^{III} \quad \widetilde{\boldsymbol{x}}_3^{III}] = \underbrace{[\widetilde{\boldsymbol{x}}_1^{II} \quad \widetilde{\boldsymbol{x}}_2^{II} \quad \widetilde{\boldsymbol{x}}_3^{II}]}_{(ndof)\times 3} \cdot \underbrace{[\widetilde{\boldsymbol{x}}_{1.3\times1}^{III} \quad \widetilde{\boldsymbol{x}}_{2.3\times1}^{III} \quad \widetilde{\boldsymbol{x}}_{3.3\times1}^{III}]}_{3\times 3} \tag{4.145}$$

Normalize the first eigenvector $\widetilde{\boldsymbol{x}}_1^{III}$ such that all nodal warping values of deformation mode 1 have negative unit value, i.e. $\tilde{u}_{1.r} = -1$. The minus sign is to make the longitudinal normal stresses $\sigma_{x.1}$ for the first deformation mode compatible with the other deformation modes $k \geq 2$. Normalize $\widetilde{\boldsymbol{x}}_2^{III}$ and $\widetilde{\boldsymbol{x}}_3^{III}$ such that the diagonal elements in $\widetilde{K}_{22} = \widetilde{K}_{33} = -1$ in the $\widetilde{\boldsymbol{K}}_{3\times3}$-matrix defined as:

$$\widetilde{\boldsymbol{K}}_{3\times3} = \left(\widetilde{\boldsymbol{X}}^{III}\right)^T \cdot \boldsymbol{K}_{3\times3} \cdot \widetilde{\boldsymbol{X}}^{III} \tag{4.146}$$

Replace the first three eigenvectors in the eigenmatrix $\widetilde{\boldsymbol{X}}$ defined in (4.138) with the three normalized eigenvectors calculated in (4.145) gives the final appearance of the eigenmatrix or transformation matrix $\widetilde{\boldsymbol{X}}$ as:

$$\widetilde{\boldsymbol{X}} = [\widetilde{\boldsymbol{x}}_1 \quad \cdots \quad \widetilde{\boldsymbol{x}}_{ndof}] = \left[\widetilde{\boldsymbol{x}}_1^{III} \quad \widetilde{\boldsymbol{x}}_2^{III} \quad \widetilde{\boldsymbol{x}}_3^{III} \quad \widetilde{\boldsymbol{x}}_4^{II} \quad \widetilde{\boldsymbol{x}}_5^{I} \quad \cdots \quad \widetilde{\boldsymbol{x}}_{ndof}^{I}\right] \tag{4.147}$$

Finally, the diagonalization procedure of the $\overline{\boldsymbol{B}}$ and $\overline{\boldsymbol{C}}$ is totally defined by the transformation into the eigenvector coordinate system. The transformed matrices are denoted with a tilde as:

$$\widetilde{\boldsymbol{B}} = \widetilde{\boldsymbol{X}}^T \cdot \overline{\boldsymbol{B}} \cdot \widetilde{\boldsymbol{X}} \qquad \widetilde{\boldsymbol{C}} = \widetilde{\boldsymbol{X}}^T \cdot \overline{\boldsymbol{C}} \cdot \widetilde{\boldsymbol{X}} \qquad \widetilde{\boldsymbol{D}} = \widetilde{\boldsymbol{X}}^T \cdot \overline{\boldsymbol{D}} \cdot \widetilde{\boldsymbol{X}} \tag{4.148}$$

The $\widetilde{\boldsymbol{B}}$ and $\widetilde{\boldsymbol{C}}$ matrix will be completely diagonalized but the $\widetilde{\boldsymbol{D}}$ matrix will still have some off-diagonal terms which are non-zero, hence it is not possible to have a complete uncoupled GBT equation. The transformed and coupled GBT fundamental equation will then be defined as:

$$E\widetilde{\boldsymbol{C}}\widetilde{\boldsymbol{\phi}}_{,xxxx} - G\widetilde{\boldsymbol{D}}\widetilde{\boldsymbol{\phi}}_{,xx} + \widetilde{\boldsymbol{B}}\widetilde{\boldsymbol{\phi}} = \widetilde{\boldsymbol{q}} - \widetilde{\boldsymbol{q}}_{x,x} \tag{4.149}$$

4.5.2 Diagonalization of the $\widetilde{\boldsymbol{D}}$-matrix

In simultaneous diagonalization process above there is only possible to diagonalize two matrices at the time ($\overline{\boldsymbol{B}}$ and $\overline{\boldsymbol{C}}$), hence the third $\overline{\boldsymbol{D}}$-matrix will not be completely diagonalized. It appears thought that the off-diagonal terms in general are small in comparison with the diagonal terms and can be neglected, i.e. the off-diagonal terms in the $\widetilde{\boldsymbol{D}}$-matrix obtained in (4.148) can be neglected if

$$\frac{\left(\widetilde{D}_{ik}\right)^2}{\widetilde{D}_{ii} \cdot \widetilde{D}_{kk}} \ll 1. \tag{4.150}$$

This is however only true for thin-walled open cross-sections. The influence of these coupling terms depends on the actual cross-section. For closed section this coupling terms cannot be neglected [6].

4.6 Transformed GBT fundamental equilibrium equation

The transformation into the eigenvector coordinate system leads to diagonal $\widetilde{\boldsymbol{C}}$ and $\widetilde{\boldsymbol{B}}$ matrices and the approximate diagonalization of the $\widetilde{\boldsymbol{D}}$ matrix makes it possible to handle the coupled GBT fundamental differential equation derived in (4.36) in an uncoupled way. Equation (4.36) can then be written as:

$$E\tilde{C}_k\tilde{\phi}_{k,xxxx} - G\tilde{D}_k\tilde{\phi}_{k,xx} + \tilde{B}_k\tilde{\phi}_k = \tilde{q}_k - \tilde{q}_{x.k,x} \tag{4.151}$$

The subscript $(\cdot)_k$ on the $\tilde{B}_k$, $\tilde{C}_k$ and $\tilde{D}_k$ terms stands for the diagonal position k in the corresponding matrix and the amplitude function $\tilde{\phi}_k$ is obtained as the solution to the transformed differential equation (4.151). The amplitude function $\tilde{\phi}_k$ is coupled to the corresponding deformation mode $\widetilde{\boldsymbol{u}}_k$ defined as the columns in the modal matrix $\widetilde{\boldsymbol{U}}$ defined as:

$$\widetilde{\boldsymbol{U}} = \overline{\boldsymbol{U}} \cdot \widetilde{\boldsymbol{X}} \tag{4.152}$$

The other displacement components are obtained in a similar way, namely:

$$\widetilde{\boldsymbol{F}}_v = \boldsymbol{F}_v \cdot \widetilde{\boldsymbol{U}} = \overline{\boldsymbol{F}}_v \cdot \widetilde{\boldsymbol{X}} \tag{4.153}$$

$$\widetilde{\boldsymbol{F}}_w = \boldsymbol{F}_w \cdot \widetilde{\boldsymbol{U}} = \overline{\boldsymbol{F}}_w \cdot \widetilde{\boldsymbol{X}} \tag{4.154}$$

$$\widetilde{\boldsymbol{F}}_\vartheta = \boldsymbol{F}_\vartheta \cdot \widetilde{\boldsymbol{U}} = \overline{\boldsymbol{F}}_\vartheta \cdot \widetilde{\boldsymbol{X}} \tag{4.155}$$

$$\Delta\widetilde{\boldsymbol{F}}_\vartheta = \Delta\boldsymbol{F}_\vartheta \cdot \widetilde{\boldsymbol{U}} = \Delta\overline{\boldsymbol{F}}_\vartheta \cdot \widetilde{\boldsymbol{X}} \tag{4.156}$$

$$\widetilde{\boldsymbol{M}} = \boldsymbol{M} \cdot \widetilde{\boldsymbol{U}} = \overline{\boldsymbol{M}} \cdot \widetilde{\boldsymbol{X}} \tag{4.157}$$

The local displacement components are then simply obtained as the value at the position corresponding to row r and column k in the corresponding matrices as:

$$\tilde{u}_{r.k} = \widetilde{\boldsymbol{U}}(r,k) \tag{4.158}$$

$$\tilde{v}_{r.k} = \widetilde{\boldsymbol{F}}_v(r,k) \tag{4.159}$$

$$\tilde{w}_{r.k} = \widetilde{\boldsymbol{F}}_w(r,k) \tag{4.160}$$

$$\tilde{\vartheta}_{r.k} = \widetilde{\boldsymbol{F}}_\vartheta(r,k) \tag{4.161}$$

$$\tilde{m}_{r.k} = \widetilde{\boldsymbol{M}}(r,k) \tag{4.162}$$

In order to have the transformed global nodal displacement components the following relation holds:

$$\widetilde{U}_{r.k} = \tilde{u}_{r.k} \tag{4.163}$$

$$\widetilde{V}_{r.k} = -\tilde{v}_{r.k} \cdot \cos\alpha_r - \left(\tilde{w}_{r.k} - \tilde{\vartheta}_{r.k} \cdot \frac{b_r}{2}\right) \cdot \sin\alpha_r \tag{4.164}$$

$$\widetilde{W}_{r.k} = -\tilde{v}_{r.k} \cdot \sin\alpha_r + \left(\tilde{w}_{r.k} - \tilde{\vartheta}_{r.k} \cdot \frac{b_r}{2}\right) \cdot \cos\alpha_r \tag{4.165}$$

And for the last node $r = n + 1$:

$$\widetilde{U}_{n+1} = \tilde{u}_{n+1} \tag{4.166}$$

$$\tilde{V}_{n+1} = -\tilde{v}_n \cdot \cos\alpha_n - \left(\tilde{w}_n + \tilde{\vartheta}_n \cdot \frac{b_n}{2}\right) \cdot \sin\alpha_n \tag{4.167}$$

$$\widetilde{W}_{n+1} = -\tilde{v}_n \cdot \sin\alpha_n + \left(\tilde{w}_n + \tilde{\vartheta}_n \cdot \frac{b_n}{2}\right) \cdot \cos\alpha_n \tag{4.168}$$

The global nodal displacements components $\widetilde{U}_{r.k}$, $\tilde{V}_{r.k}$ and $\widetilde{W}_{r.k}$ stored in vectors will then for deformation mode k have the following notations:

$$\widetilde{\boldsymbol{U}}_k, \widetilde{\boldsymbol{V}}_k, \widetilde{\boldsymbol{W}}_k \tag{4.169}$$

Note: Unfortunately, there is a lack of indices so do not mistake $\widetilde{\boldsymbol{W}}_k$ with the sectional force $\widetilde{W}_k(x)$.

4.6.1 GBT boundary conditions

The boundary condition terms defined in (4.39) are not defined in a representative way. The orthogonalization process must be integrated into the boundary condition terms as well and the terms must be associated with known boundary conditions of the member. Hence, introduce the GBT sectional forces defined in (4.187) and the transformed matrices. Since the $\widetilde{\boldsymbol{D}}_1$ and $\widetilde{\boldsymbol{D}}_2$ not are not completely diagonal, a summation over all off-diagonal terms listening to subscript i is introduced. This give for deformation mode k:

$$\left[\left(\widetilde{W}_{k,x} + G\sum_{i=1}^{ndof}\left(\widetilde{D}_{1.ki} - \widetilde{D}_{2.ki}\right)\tilde{\phi}_{k,x} - \int_b q_x \tilde{u}_k ds\right)\delta\tilde{\phi}_i\right]_0^L = 0 \tag{4.170}$$

$$\left[\left(\widetilde{W}_k - G\sum_{i=1}^{ndof}\widetilde{D}_{2.ki}\,\tilde{\phi}_k\right)\delta\tilde{\phi}_{i,x}\right]_0^L = 0 \tag{4.171}$$

The first boundary condition (4.170) can be fulfilled in two ways. Either are the amplitude function $\tilde{\phi}_k(0)$ and/or $\tilde{\phi}_k(L)$ prescribed, i.e. v- and w-displacements are prescribed and no virtual displacement can take place leading to $\delta\tilde{\phi}_i(0) = 0$ and/or $\delta\tilde{\phi}_i(L) = 0$. The other way of fulfilling the condition is that the expression within the parentheses is zero:

$$\left[\widetilde{W}_{k,x} + G\sum_{i=1}^{ndof}\left(\widetilde{D}_{1.ki} - \widetilde{D}_{2.ki}\right)\tilde{\phi}_{k,x} - \int_b q_x \tilde{u}_i ds\right]_0^L = 0 \tag{4.172}$$

The second boundary condition (4.171) is fulfilled in the same way, namely either are the warping prescribed leading to that no virtual displacement can occur, i.e.

$\delta\tilde{\phi}_{i,x}(0) = 0$ and/or $\delta\tilde{\phi}_{i,x}(L) = 0$ or the other alternative is that the expression within the parentheses is zero, namely:

$$\left[\widetilde{W}_k - G\sum_{i=1}^{ndof}\widetilde{D}_{2.ki}\,\tilde{\phi}_k\right]_0^L = 0 \tag{4.173}$$

There are four main type of boundary condition in ordinary beam theory, namely fixed, pinned, guided and free end, see Figure 4.18.

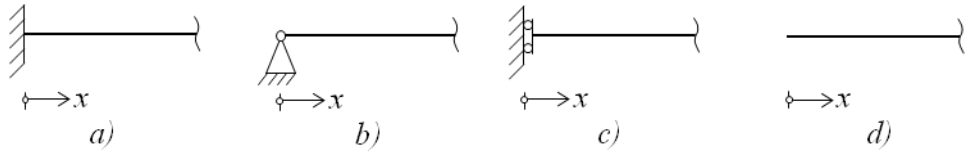

Figure 4.18: There are four main type of boundary conditions in ordinary beam theory, namely a) fixed, b) pinned, c) guided and d) free end.

The GBT boundary conditions must therefore be translated such that the boundary conditions in Figure 4.18 are fulfilled. Since the fundamental GBT equation involves forth ordered derivatives four boundary conditions is needed, two at each end. Here follows the corresponding conditions associated with the end conditions in Figure 4.18:

a) $\tilde{\phi}_k(0) = 0$
$\tilde{\phi}_{k,x}(0) = 0$

b) $\tilde{\phi}_{k,x}(0) = 0$
$\widetilde{W}_k(0) = 0$

c) $\tilde{\phi}_{k,x}(0) = 0$
$\widetilde{W}_{k,x}(0) = 0$

d) $\widetilde{W}_{k,x}(0) + G\sum_{i=1}^{ndof}\left(\widetilde{D}_{1.ki} - \widetilde{D}_{2.ki}\right)\tilde{\phi}_{k,x}(0) - \int_b q_x\tilde{u}_i\,ds = 0$
$\widetilde{W}_k(0) - G\sum_{i=1}^{ndof}\widetilde{D}_{2.ki}\,\tilde{\phi}_k(0) = 0$ (4.174)

However, even though the $\widetilde{\boldsymbol{D}}_3$-matrix is not involved in the boundary term for the free end above an approximation can be utilized, namely use the $\widetilde{\boldsymbol{D}}$-matrix defined in (4.148). The second boundary term can also be simplified. If the normal stresses σ_x is not of interest or not critical, the $\widetilde{\boldsymbol{D}}_2$-matrix can be excluded since the matrix contains

the transverse stress contribution σ_s which depends on Poisson's ratio ν [6]. These simplifications lead to:

$$\begin{aligned} &d) \quad \widetilde{W}_{k,x}(0) + G\widetilde{D}_k\tilde{\phi}_{k,x}(0) - \int_b q_x(0)\tilde{u}_k ds = 0 \\ &\qquad \widetilde{W}_k(0) = 0 \end{aligned} \tag{4.175}$$

A great feature of GBT is that each mode k has its own corresponding boundary conditions and since the total behaviour of the member is obtained as a summation over the mode contributions, there is a possibility to choose different boundary conditions for different modes in order to obtain a more realistic behaviour. In Figure 4.19 below there are three common boundary conditions illustrated which have quite different influences on the global behaviour of the member.

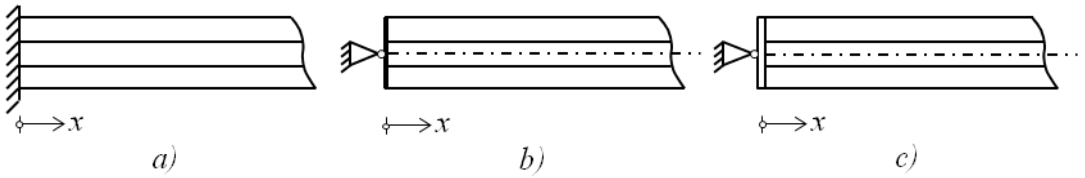

Figure 4.19: Three illustrative examples of how different boundary conditions for different modes can be utilized in order to have a more realistic behaviour of the member. a) fixed end b) pinned end with stiffener corresponding to $EA = \infty$ and $EI = 0$ and c) pinned with a stiffer stiffener corresponding to $EA = \infty$ and $EI = \infty$.

The main difference between the members in Figure 4.19 is the warping resistance. In member a) it is obvious that there cannot be any warping or transverse displacements. In member b) the transverse displacements are prevented but warping is allowed and in the third member no warping is allowed but the rotation at the support is still allowed. These conditions can be expressed in the cross-sectional forces and the amplitude function as:

$$\begin{aligned} &a) \quad \left.\begin{matrix} \tilde{\phi}_k(0) = 0 \\ \tilde{\phi}_{k,x}(0) = 0 \end{matrix}\right\} \text{ for } k = 2, \dots, ndof \\ &b) \quad \left.\begin{matrix} \tilde{\phi}_k(0) = 0 \\ \widetilde{W}_k(0) = 0 \end{matrix}\right\} \text{ for } k = 2, \dots, ndof \\ &c) \quad \left.\begin{matrix} \tilde{\phi}_k(0) = 0 \\ \widetilde{W}_k(0) = 0 \end{matrix}\right\} \text{ for } k = 2,3 \qquad \left.\begin{matrix} \tilde{\phi}_k(0) = 0 \\ \tilde{\phi}_{k,x}(0) = 0 \end{matrix}\right\} \text{ for } k = 4, \dots, ndof \end{aligned} \tag{4.176}$$

The first deformation mode is a bit special since the forth ordered GBT differential equation prescribes a second ordered rod-equation. However, the three examples above will have the same boundary condition for the first mode, namely $\tilde{\phi}_{1,x}(0) = 0$ since the u-displacements are prevented. The first deformation mode and its corresponding boundary conditions are treated further in Appendix C.

4.6.2 GBT modal loading terms

The GBT can handle different kind of loads, namely body, surface, line and point loads. All these type of forces must be translated into equivalent line-loads applied on the nodes.

4.6.2.1 Body loads and surface loads

The loads can either be defined in the local (x, s, z)-coordinate system or in the global (X, Y, Z)-coordinate system. In the local defined case a general applied distributed surface load p and a body load g are expressed in its local components (p_x, p_s, p_z) and (g_x, g_s, g_z), see Figure 4.20.

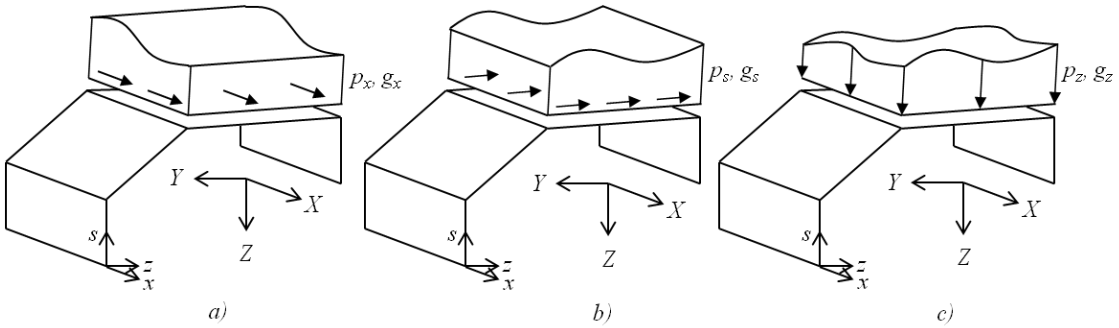

Figure 4.20:A general applied surface load p and body load g expressed in the local (x, s, z)-coordinate system and in the load components a) in x-direction as p_x, g_x, b) in s-direction as p_s, g_s and c) in z-direction p_z, g_z.

The applied loads can also be defined in the global (X, Y, Z)-coordinate system which expressed in the global components are given as (p_X, p_Y, p_Z) and (g_X, g_Y, g_Z), see Figure 4.21.

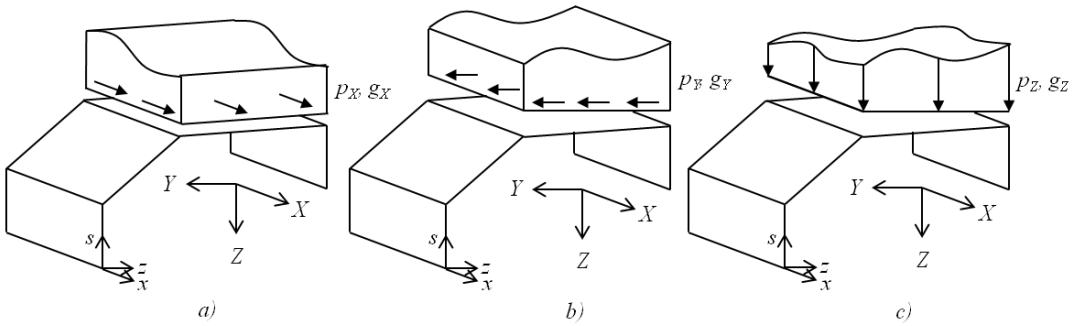

Figure 4.21: A general applied surface load p and body load g expressed in the global (X, Y, Z)-coordinate system and in the load components a) in X-direction as p_X, g_X, b) in Y-direction as p_Y, g_Y and c) in Z-direction p_Z, g_Z.

The discretization of the applied loads amounts to convert them into equivalent nodal loads which then are distributed along the member. If only natural nodes are considered, the first and the last node cannot be loaded since it is treated as cantilevers so if the first and last plate element are loaded the second and the second last node will carry all loads from the outer plate elements. If intermediate nodes are imposed in the analysis the first and last node also can be loaded as well.

The equivalent nodal loads are for the inner nodes calculated according to Figure 4.22. Rollers are introduced at each node such that each plate element are simply supported and the equivalent nodal load $q_{x.r}$, $q_{s.r}$ and $q_{z.r}$ is then obtained as the "reaction forces" at the corresponding roller due to the applied element loads.

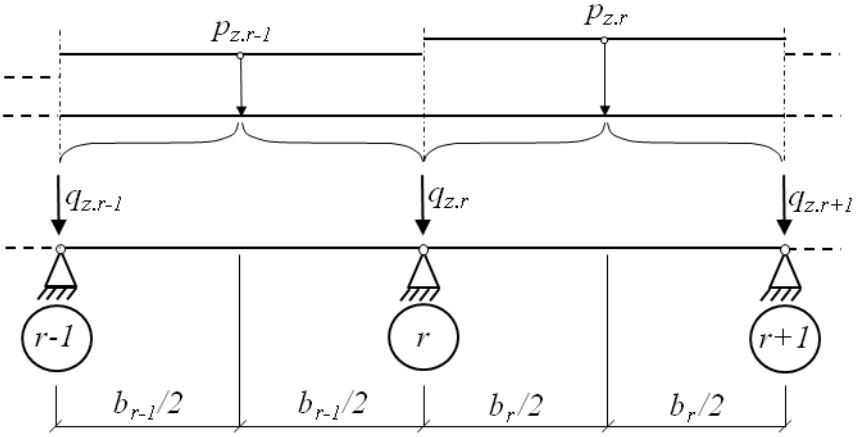

Figure 4.22: The load discretization of uniformly distributed surface plate elements loads $p_{z.r-1}$ and $p_{z.r}$ by imposition of rollers at the nodes and the equivalent nodal loads are then the corresponding "reaction forces". The equivalent nodal loads are denoted $q_{z.r-1}$, $q_{z.r}$, $q_{z.r+1}$ etc. A treatment of uniformly distributed p_x- and p_s-loads are completely analogue to the example defined in this figure.

For uniformly distributed surface loads $p_{z.r-1}$ and $p_{z.r}$ [force / length^2] on the two adjacent plate elements$r-1$ and r respectively the equivalent nodal load $q_{z.r}$ [force / length] is obtained as:

$$q_{z.r} = \frac{b_{r-1}}{2} \cdot p_{z.r-1} + \frac{b_r}{2} \cdot p_{z.r} \tag{4.177}$$

For a uniformly distributed body loads $g_{z.r-1}$ and $g_{z.r}$ [force / length^3] the equivalent nodal load $q_{z.r}$ [force / length] for node r is obtained as:

$$q_{z.r} = \frac{b_{r-1}t_{r-1}}{2} \cdot g_{z.r-1} + \frac{b_r t_r}{2} \cdot g_{z.r} \tag{4.178}$$

The treatment of distributed surface and body loads in the other directions are completely analogous as for equation (4.177) and (4.178). The loads defined in the global coordinate system.

4.6.2.2 Line loads and point loads

There is no need to discretize the line loads further if they are applied at the nodes otherwise the same approach is valid as for body loads and surface loads, namely that the equivalent nodal loads are obtained as the "reaction forces" at the rollers, see Figure 4.22.

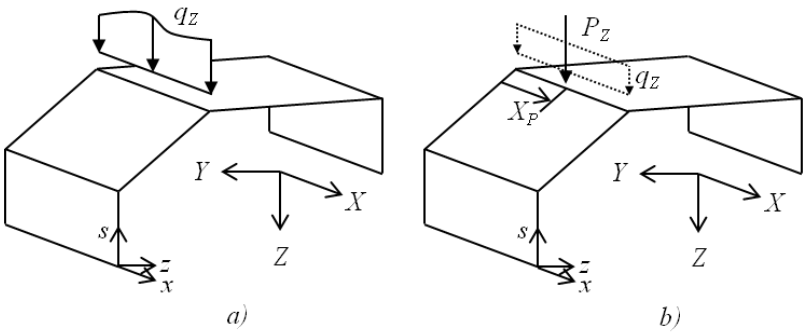

Figure 4.23: a) A line load q_Z and b) a point load P_Z are here defined in the global (X, Y, Z)-coordinate system. The point-force P is treated as an equivalent line load q_Z via Dirac's delta function (dotted line load).

In case of point loads so must they be treated as distributed line loads and this is carried out via Dirac's delta function, see Figure 4.23. The Dirac's delta function is defined as:

$$\delta(X - X_P) = \begin{cases} \infty, & X = X_P \\ 0, & \text{otherwise} \end{cases}$$

$$\int_{-\infty}^{\infty} \delta(X - X_P)\, dX = \int_{x_p^-}^{x_p^+} \delta(X - X_P)\, dX = 1 \tag{4.179}$$

Where X_P is the fixed point at which the point load P is acting. The equivalent line load which the point load is converted to is then defined as:

$$q_Z = P_Z \cdot \delta(X - X_P) \tag{4.180}$$

This applies for point loads defined in the other directions as well.

4.6.2.3 The GBT modal loads

The GBT loading terms are defined in (4.35) and after the transformation into eigenvector coordinate system together with the load discretization to equivalent nodal loads q_r the GBT modal loads $\tilde{q}_k$ and $\tilde{q}_{x.k,x}$ are obtained as:

$$\tilde{q}_k = \sum_{r=1}^{n+1} (q_{s.r}\tilde{v}_{r.k} + q_{z.r}\tilde{w}_{r.k}) \qquad \tilde{q}_{x.k,x} = \sum_{r=1}^{n+1} q_{x.r,x}\tilde{u}_{r.k} \tag{4.181}$$

The summation applies to all nodal load contributions $q_{x.r,x}$, $q_{s.r}$ and $q_{z.r}$ defined in the local (x, s, z)-coordinate system. $\tilde{u}_{r.k}$, $\tilde{v}_{r.k}$ and $\tilde{w}_{r.k}$ are the local displacement components defined in equation (4.158), (4.159) and (4.160).

The GBT modal loads can also be defined using the global load and displacement components in the same fashion as for the local defined loads. The following expressions hold therefore as:

$$\tilde{q}_k = \sum_{r=1}^{n+1} \left(q_{Y.r} \tilde{V}_{r.k} + q_{Z.r} \widetilde{W}_{r.k} \right) \qquad \tilde{q}_{x.k,x} = \sum_{r=1}^{n+1} q_{X.r,X} \widetilde{U}_{r.k} \tag{4.182}$$

The summation applies to all nodal load contributions $q_{X.r,X}$, $q_{Y.r}$ and $q_{Z.r}$ defined in the global (X, Y, Z)-coordinate system. $\widetilde{U}_{r.k}$, $\tilde{V}_{r.k}$ and $\widetilde{W}_{r.k}$ are the global displacement components defined in equation (4.163), (4.164) and (4.165).

4.6.3 The amplitude function

The solution to the differential equation (4.151) can be obtained in many ways. Basically there are two different methods, namely analytical and approximate. The analytical solution has some advantages compared to the use of approximate methods. The main advantage is that it is an exact solution in the meaning that no convergence study is needed. Another advantage is that the computational effort is less compared with the use of finite elements due to its imposed number of degrees of freedom. A drawback though is that the analytical solution requires uncoupled set of differential equations and it must be solved for each pair of boundary conditions and support conditions and therefore must be predefined when used in programming of the GBT.

The use of FEM, which is an approximate method, has some advantages compared to analytical solutions. This concerns especially the handling of boundary and support conditions. By locking[3] degrees of freedoms there is a greater versatility using this method, rather than having to deriving analytical expressions for each possible load and boundary situation. Another key benefit when using FEM is that there is no need of having uncoupled equations, i.e. the coupled GBT fundamental equation (4.149) can be utilized directly. Some of the negative aspects concern the induced number of degrees of freedoms and the extra computational effort, also a convergence study is needed in order to be sure that the FEM-approximation is satisfactory.

4.6.4 The displacement components

Once the amplitude functions $\tilde{\phi}_k$ and $\tilde{\phi}_{k,x}$ are determined, the nodal displacements U_r, V_r and W_r can be determined for each node r in the cross-section as the summation over each modal contribution k. For node r one gets the total global displacements as:

$$U_r(x) = \sum_{k=1}^{nmo} \widetilde{U}_{r.k} \tilde{\phi}_{k,x}(x)$$

$$V_r(x) = \sum_{k=1}^{nmo} \tilde{V}_{r.k} \tilde{\phi}_k(x) \tag{4.183}$$

$$W_r(x) = \sum_{k=1}^{nmo} \widetilde{W}_{r.k} \tilde{\phi}_k(x)$$

[3]With locking degrees of freedom, the authors refers to assign a value to that corresponding degree of freedom, e.g. at a support the transverse vertical displacement is prevented $W(x = 0) = 0$.

Wherenmo is the total number of obtained deformation modes and the displacement components $\widetilde{U}_{r.k}$, $\widetilde{V}_{r.k}$ and $\widetilde{W}_{r.k}$ are determined according to equation (4.163), (4.164) and (4.165) respectively.

4.6.5 Normal stresses and sectional forces

Recall the expressions for the stresses in the four fundamental beam theories defined in (3.3). There it was a possibility to describe the distribution within the cross-section in one function and the variation along the member in another function. This is fundamental in the derived transformed GBT equations. The first four deformation modes $\tilde{u}_{1-4}$ do correspond to the cross-sectional distribution and the amplitude function $\tilde{\phi}_{1-4}$ correspond to the variation along the member, see Figure 4.24 and compare with Figure 3.2.

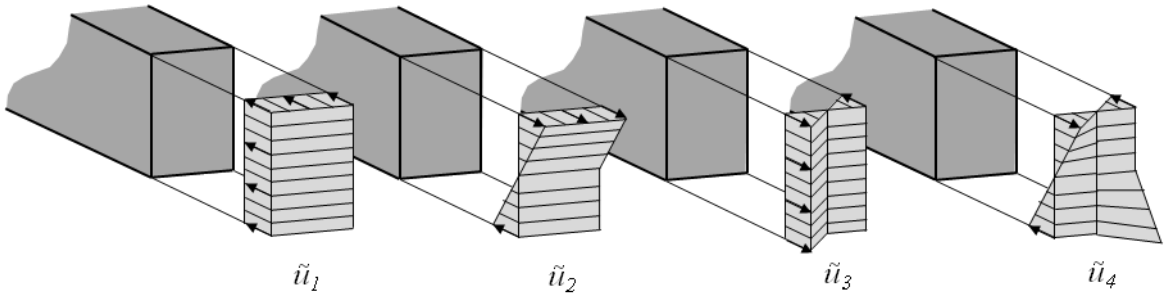

Figure 4.24: This figure illustrates the four first deformation modes $\tilde{u}_{1-4}$ and the analogy between the four fundamental beam theories defined in Chapter 3.1.

The analogy between stresses in the four fundamental beam theories, see (3.1) to (3.2), and the four first GBT deformation modes is here defined by introducing the separation of variables approach:

$$\begin{aligned}
\sigma_x(x,y,z) &= E \cdot u_{,x}(x) = E \cdot \tilde{u}_1(y,z) \cdot \tilde{\phi}_{1,xx}(x) \\
\sigma_x(x,y,z) &= -E \cdot z \cdot w_{,xx}(x) = -E \cdot \tilde{u}_2(y,z) \cdot \tilde{\phi}_{2,xx}(x) \\
\sigma_x(x,y,z) &= -E \cdot y \cdot v_{,xx}(x) = -E \cdot \tilde{u}_3(y,z) \cdot \tilde{\phi}_{3,xx}(x) \\
\sigma_x(x,y,z) &= E \cdot \omega(x,y) \cdot \vartheta_{,xx}(x) = E \cdot \tilde{u}_4(y,z) \cdot \tilde{\phi}_{4,xx}(x)
\end{aligned} \tag{4.184}$$

The common character of the stresses for the different modes can then be written in a more general way as:

$$\sigma_{x.k}(x,y,z) = E \cdot \tilde{u}_k \cdot \tilde{\phi}_{k,xx} \tag{4.185}$$

Above only the stresses corresponding to the four rigid-body modes are presented, but the same applies for all deformation modes k, not only the rigid-body modes.

The sectional forces are defined as the integral over the cross-section and the longitudinal stresses. The definitions for the sectional forces in the four first modes are defined in (3.8). Here follows the translation into the general GBT notation as:

$$N(x) = \int_A \sigma_x dA = \int_A \sigma_x \tilde{u}_1 dA = E \int_A \tilde{u}_1 \tilde{u}_1 dA \cdot \tilde{\phi}_{1,xx}(x)$$

$$M_y(x) = \int_A \sigma_x z dA = \int_A \sigma_x \tilde{u}_2 dA = -E \int_A \tilde{u}_2 \tilde{u}_2 dA \cdot \tilde{\phi}_{2,xx}(x)$$

$$M_z(x) = \int_A \sigma_x y dA = \int_A \sigma_x \tilde{u}_3 dA = -E \int_A \tilde{u}_3 \tilde{u}_3 dA \cdot \tilde{\phi}_{3,xx}(x) \tag{4.186}$$

$$W(x) = -\int_A \sigma_x \omega dA = -\int_A \sigma_x \tilde{u}_4 dA = -E \int_A \tilde{u}_4 \tilde{u}_4 dA \cdot \tilde{\phi}_{4,xx}(x)$$

These expressions can also be expressed in a more general way which also applies for all deformation modes, not only for the rigid-body modes. The general expression for sectional forces is defined as:

$$\widetilde{W}_k(x) = -\int_A \sigma_x \tilde{u}_k dA = -E \tilde{C}_k \tilde{\phi}_{k,xx}(x) \tag{4.187}$$

Note that the mismatch in the sing convention is handled during the normalization process of the first deformation mode, see Section 4.5. The introduced cross-sectional parameter $\tilde{C}_k$ above is defined as:

$$\tilde{C}_k = \int_A \tilde{u}_k \tilde{u}_k dA \tag{4.188}$$

For the first four rigid-body modes the corresponding cross-sectional parameters will corresponds to the area, major and minor second moment of inertia and the warping constant as:

$$\tilde{C}_1 = A \qquad \tilde{C}_2 = I_y \qquad \tilde{C}_3 = I_z \qquad \tilde{C}_4 = C_M \tag{4.189}$$

Note that the y- and z-supscript denotes the principle axes which not necessary have to be aligned with the global coordinate axes. The longitudinal stresses can now be determined out of the sectional forces. Compare the expression for the longitudinal stresses (4.185) with the expression for sectional forces (4.187) the stresses can be determined as:

$$\sigma_{x.k} = E \tilde{u}_k \tilde{\phi}_{k,xx} = -\frac{\widetilde{W}_k(x) \tilde{u}_k}{\tilde{C}_k} \tag{4.190}$$

Since all modes are decoupled due to the orthogonality condition the total normal stress σ_x in the member is obtained as a summation over each modal stress contribution $\sigma_{x.k}$ as:

$$\sigma_x(x,y,z) = \sum_k \sigma_{x.k}\,(x,y,z) \tag{4.191}$$

4.6.6 Shear stresses and shear force

An expression for the shear stress τ_{xs} is derived in Section 3.1.1. If one translates them into GBT notations the shear stress is obtained as:

$$\tau_{xs.k} = -\frac{1}{t(s)}\int_0^s \sigma_{x.k,x}\,t\,ds = \frac{\widetilde{W}_{k,x}(x)}{\tilde{C}_k\,t(s)}\int_0^s \tilde{u}_k\,t\,ds \tag{4.192}$$

To have the total shear stress τ_{xs} in the member the same applies as for the normal stresses, namely a summation over each modal contribution $\tau_{xs.k}$ which then is given as:

$$\tau_{xs}(x,y,z) = \sum_k \tau_{xs.k}\,(x,y,z) \tag{4.193}$$

The shear force within plate element r is defined as the integral over the element width b_r and over the shear flow as:

$$S_{k.r} = \int_{b_r} \tau_{xs.k}\cdot t\,ds \tag{4.194}$$

4.6.6.1 Programming ready expression for shear flow and shear stress

Use the definition for the warping function defined in (4.116) with the variable substitution $s \Rightarrow \eta$ and the discretization into elements and nodes the expression for the nodal shear flow $(\tau_{xs.k}t)_r$ at node r is obtained as:

$$\begin{aligned}(\tau_{xs.k}t)_r &= \frac{\widetilde{W}_{k,x}(x)}{\tilde{C}_k}\sum_{i=1}^{r-1}\int_0^1 \big((1-\eta)\cdot u_{k.i} + \eta\cdot u_{k.i+1}\big)t_i\cdot b_i\,d\eta = \\ &= \frac{\widetilde{W}_{k,x}(x)}{\tilde{C}_k}\sum_{i=1}^{r-1}\left[\left(\eta-\frac{\eta^2}{2}\right)\cdot u_{k.i} + \frac{\eta^2}{2}\cdot u_{k.i+1}\right]_0^1 t_i\cdot b_i \\ &= \frac{\widetilde{W}_{k,x}(x)}{\tilde{C}_k}\sum_{i=1}^{r-1}\frac{t_i b_i}{2}\cdot(u_{k.i}+u_{k.i+1})\end{aligned} \tag{4.195}$$

The shear stress in the corresponding node r is then simply obtained by divide both sides with the plate thickness t_r as:

$$\tau_{xs.k.r} = \frac{\widetilde{W}_{k,x}(x)}{\tilde{C}_k t_r}\sum_{i=1}^{r-1}\int_0^1 \big((1-\eta)\cdot u_{k.i} + \eta \cdot u_{k.i+1}\big)t_i \cdot b_i d\eta =$$
$$= \frac{\widetilde{W}_{k,x}(x)}{\tilde{C}_k}\sum_{i=1}^{r-1}\left[\left(\eta - \frac{\eta^2}{2}\right)\cdot u_{k.i} + \frac{\eta^2}{2}\cdot u_{k.i+1}\right]_0^1 t_i \cdot b_i \qquad (4.196)$$
$$= \frac{\widetilde{W}_{k,x}(x)}{\tilde{C}_k}\sum_{i=1}^{r-1}\frac{t_i b_i}{2}\cdot(u_{k.i} + u_{k.i+1})$$

Note: If the thickness t_r varies for the two adjacent plate elements to node r, the shear stress will have two nodal values but the shear flow will be continues over all nodes.

4.6.6.2 Programming ready expression for shear force

Due to the integration over the warping function the shear flow $(\tau_{xs.k}t)$ will not vary linearly between the nodes, see Figure 4.25. This must be accounted for in the shear force calculations.

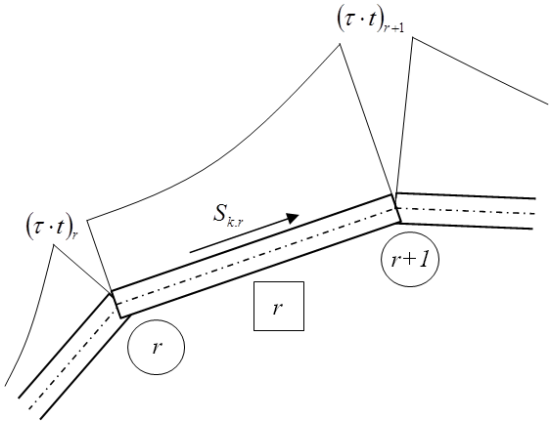

Figure 4.25: The shear flow $(\tau_{xs.k}t)_r$ will have a parabolic distribution within the corresponding plate element r. Nodes are denoted with rings and plate numbering in squares. In order to have the shear force $S_{k.r}$ integration over the corresponding plate element is needed.

Use the same warping function and variable substitution as above, and also utilize the accumulation feature of the shear flow, the shear force for plate element r is obtained as:

$$
\begin{aligned}
S_{k.r} &= \int_0^1 \left(\tau_{xs.k}(\eta)\cdot t(\eta)\right)_r \cdot b_r d\eta \\
&= \int_0^1 \Bigg((\tau_{xs.k}\cdot t)_r \\
&+ \frac{\widetilde{W}_{k,x}(x)}{\tilde{C}_k}\int_0^{\eta}\left((1-\eta)\cdot\tilde{u}_{k.r}+\eta\cdot\tilde{u}_{k.r+1}\right)t_r\cdot b_r d\eta\Bigg)\cdot b_r d\eta \\
&= \int_0^1 \Bigg((\tau_{xs.k}\cdot t)_r \\
&+ \frac{\widetilde{W}_{k,x}(x)}{\tilde{C}_k}\left[\left(\left(\eta-\frac{\eta^2}{2}\right)\cdot\tilde{u}_{k.r}+\frac{\eta^2}{2}\cdot\tilde{u}_{k.r+1}\right)t_r\cdot b_r\right]_0^{\eta}\Bigg)\cdot b_r d\eta \\
&= b_r\Bigg[(\tau_{xs.k}t)_r\cdot\eta \\
&+ \frac{\widetilde{W}_{k,x}(x)}{\tilde{C}_k}\left[\left(\left(\frac{\eta^2}{2}-\frac{\eta^3}{6}\right)\cdot\tilde{u}_{k.r}+\frac{\eta^3}{6}\cdot\tilde{u}_{k.r+1}\right)t_r b_r\right]\Bigg]_0^1 \\
&= (\tau_{xs.k}t)_r b_r + \frac{\widetilde{W}_{k,x}(x)}{\tilde{C}_k}\frac{b_r^2 t_r}{6}(2\tilde{u}_{k.r}+\tilde{u}_{k.r+1})
\end{aligned}
$$

The programming ready shear force in plate element r is then defined as:

$$
S_{k.r} = (\tau_{xs.k}t)_r b_r + \frac{\widetilde{W}_{k,x}(x)}{\tilde{C}_k}\frac{b_r^2 t_r}{6}(2\tilde{u}_{k.r}+\tilde{u}_{k.r+1}) \tag{4.197}
$$

Where $(\tau_{xs.k}t)_r$ is calculated according to (4.195).

5 Implementation of GBT

This chapter will describe the implementation of GBT into calculation routines. Flowcharts showing the calculation will be presented, to make it possible for the reader to get a grip on how the main concepts are working.

Figure 5.1 below shows the basic calculation flow of the GBT implementation. The first step is to discretize the cross-section into plate elements and nodes and assign the geometry such as widths, thicknesses, nodal coordinates etc. The next step is to analyse the cross-section to determine the deformation modes and its corresponding constants which forms the basis for the member analysis. The user can after this step finish the calculation flow and present the modal results or continue with a member analysis. This step requires more information about the member such as member length, boundary conditions and loads so that the amplitude function $\tilde{\phi}_k$ can be determined for each deformation mode k. With the mode properties and amplitude function known, the total GBT solution can be calculated. Each mode property is then paired with the corresponding amplitude function and summed together to have the total deformation, stress and sectional forces.

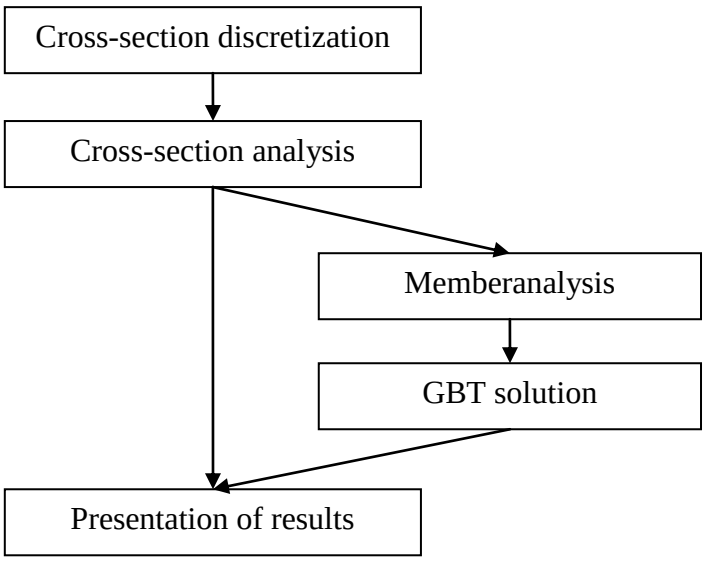

Figure 5.1: An overall main flowchart of how a application in the context of GBT is performed.

5.1 Cross-section discretization

To enable any kind of GBT calculation the cross-section has to be discretized. As shown in the flowchart in Figure 5.1 this is the first step during the calculations and the output are frequently used throughout the rest of the process. The required inputs in the discretization process are the geometry of the cross-section, plate thicknesses and number of sub-plates per plate element. The geometry is then defined by the nodal coordinates, i.e. the y- and z-coordinates of the natural nodes[4]. This can easily be managed by assigning different input vectors. Then the different input vectors will be one vector containing the nodal y-coordinates, one containing the nodal z-

[4]For the definition of a natural node, see Section 4.3.1.

coordinates, one with the plate element thicknesses and one vector that defines the number of sub-plates per plate element. If the "sub-plates per plate"-vector only contains ones it means that the analysis only will involve degrees of freedom associated with the natural nodes. The size of the input vectors will then depend if it contain nodal values or plate element values since there will always be one more node than elements.

Figure 5.2 describes the difference in the node and elements numbering when only a) considering natural nodes and when b) intermediate nodes are included. The main difference is, after the cross-sectional analysis is performed, the number of obtained deformation modes. When including intermediate nodes also local deformation modes will be obtained, i.e. the variation between the natural nodes will be included together with the rigid-body modes and distortional modes.

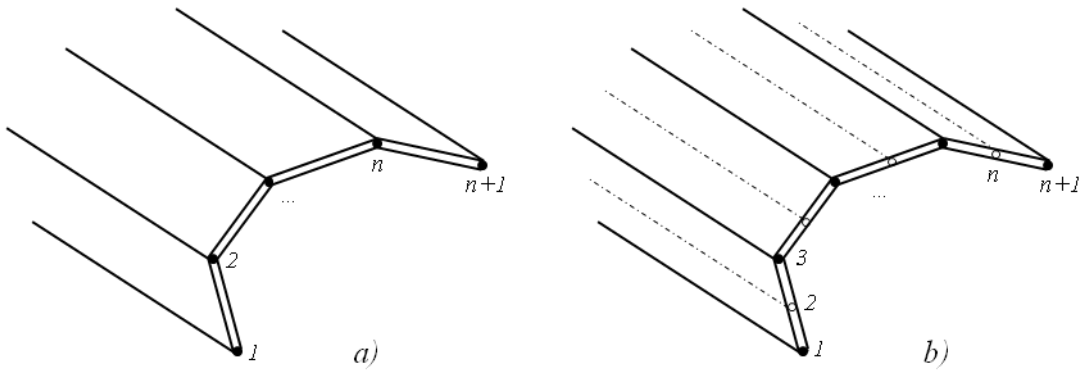

Figure 5.2: Discretized cross-sections where a) only considering natural nodes marked with filled dots (n = the total number of plate elements) and b) involving intermediate nodes marked with rings (n = the total number of sub-plate elements).

5.2 Cross-section analysis

The main subject of the cross-section analysis is to determine the cross-sectional deformation modes which form the basis within the concept of GBT. In Figure 5.3 the calculation flow within the cross-section analysis is prescribed. First the geometric $\overline{\boldsymbol{F}}_v$, $\overline{\boldsymbol{F}}_{w1}$, $\overline{\boldsymbol{F}}_{w2}$ and $\boldsymbol{\Delta}_{ik}$ matrices are constructed which are used in order to determine the other $\overline{\boldsymbol{F}}_w$, $\overline{\boldsymbol{F}}_\vartheta$, $\Delta\overline{\boldsymbol{F}}_\vartheta$ and $\overline{\boldsymbol{M}}$ matrices. For further knowledge about the different matrices the reader is referred to Section 4.2 and programming ready matrices are found in Appendix B. These geometric matrices are then used in order to construct the $\overline{\boldsymbol{B}}$-, $\overline{\boldsymbol{C}}$- and $\overline{\boldsymbol{D}}$-matrices. For further knowledge and definitions about this step, the reader is referred to Section 4.1 and 4.4 and for programming ready matrices and expressions, see Appendix B.

Once the GBT matrices are determined a transformation process into an eigenvector coordinate system is initiated in order to have an as uncoupled differential equation as possible. This process is performed in three steps by solving three different generalized eigenproblems in order to capture orthogonal eigenvectors including four eigenvectors that are associated with the four rigid body modes allied with the four technical beam theories, namely extension, major and minor axis bending and non-uniform torsion. For a more extensive description of this step the reader is referred to Section 4.5. Once the transformation is performed the deformation modes $\widetilde{\boldsymbol{u}}$ and the

other displacement components are completely defined which then forms the basis for the next major step in the GBT analysis, namely the member analysis.

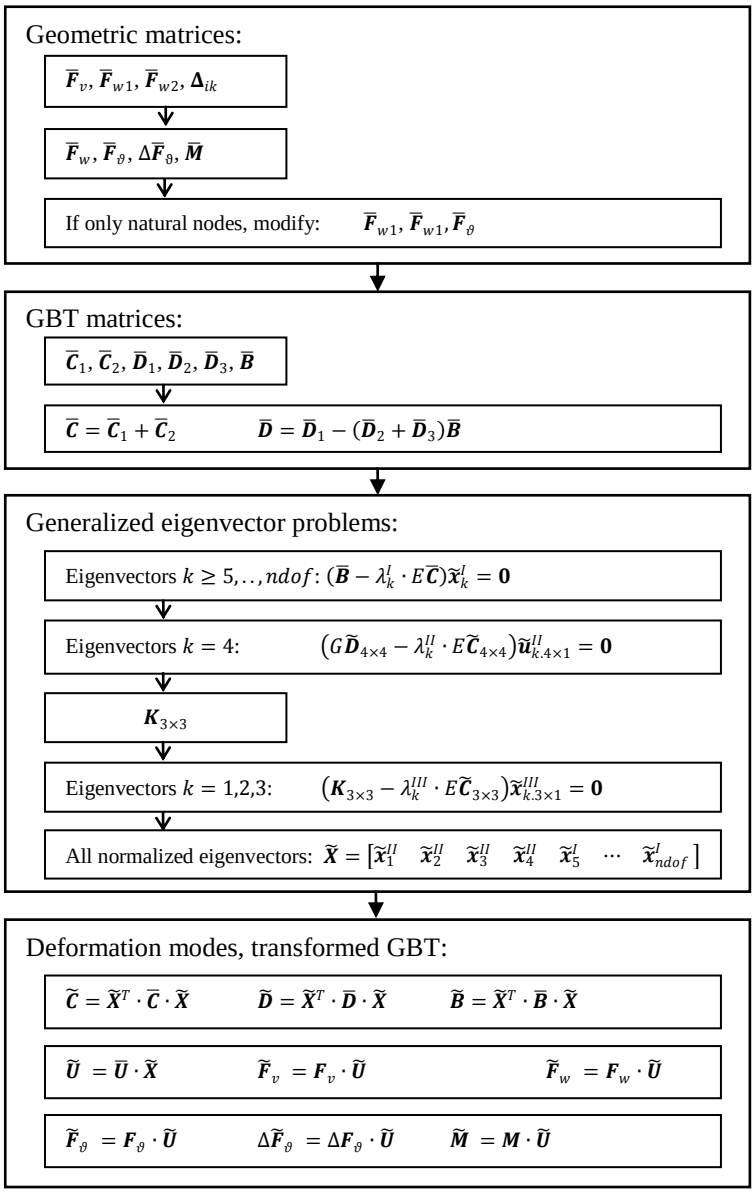

Figure 5.3: The calculation flow within the cross-sectional analysis is in this figure illustrated where in the first step all geometric matrices are assembled so that in the next step the GBT matrices can be determined. Out of these matrices three different eigenproblems are performed in order to transform the GBT differential equation as decoupled as possible. The last step is to define the deformation modes $\tilde{\boldsymbol{u}}$ and the other transformed displacement components.

5.3 Member analysis

After that the cross-sectional deformation modes have been determined the transformed GBT fundamental equation (4.151) can be established for each mode k. By solving the differential equation repeatedly for each mode the corresponding

amplitude function $\tilde{\phi}_k$ is determined which together with the modal cross-sectional properties is combined to get the total response of the member.

5.3.1 The solution to the GBT fundamental equation

There are two solution approaches available, namely analytical and numerical methods. The authors have chosen to only focus on the finite element method (FEM) which has advantages when programming the GBT. For further reading and knowledge about the FEM approach see Appendix D.

The transformed and uncoupled GBT fundamental equation (4.151) reminds of the differential equation for a beam on elastic foundation, hence finite beam elements will be used in order to descretitize the GBT equation. In order to find a unique solution more information about the member, in addition to the cross-sectional modal properties, is required. Boundary and support conditions, member length, loading conditions are needed, as well as a sufficient number of finite elements in order to obtain a satisfactory convergence of the solution. Figure 5.4 below illustrates how the member analysis is performed for deformation mode k when using a finite element approximation method on the uncoupled transformed GBT equation.

The first step is to extract the quantities associated with the deformation mode k, i.e. extraction of $\tilde{C}_k$, $\tilde{D}_k$, $\tilde{B}_k$ and the displacement components $(\widetilde{\boldsymbol{u}}_k, \widetilde{\boldsymbol{v}}_k, \widetilde{\boldsymbol{w}}_k)$[5] or $(\widetilde{\boldsymbol{U}}_k, \widetilde{\boldsymbol{V}}_k, \widetilde{\boldsymbol{W}}_k)$[6] depending on how the loads are defined. The next step is to calculate the modal loads $\tilde{q}_k$ and $\tilde{q}_{x.k,x}$ according to Section 4.6.2. At this stage the all constants in the transformed GBT fundamental equation are defined and the FEM approximation process can be initiated by determine the FE element stiffness matrices and loads. The next step is to assemble all element matrices and element load vectors to global stiffness matrices and load vectors and apply the essential boundary conditions so that a unique solution to the equation system $\boldsymbol{a}_k$ can be obtained. The last step is to extract the solution to obtain the approximated amplitude function $\tilde{\phi}_k$ and its first derivative $\tilde{\phi}_{k,x}$ but also the sectional forces $\widetilde{W}_k(x)$ and $\widetilde{W}_{k,x}(x)$.

[5]The $\widetilde{\boldsymbol{u}}_k$-, $\widetilde{\boldsymbol{v}}_k$- and $\widetilde{\boldsymbol{w}}_k$-displacement components are obtained as the columns in the $\widetilde{\boldsymbol{U}}$, $\widetilde{\boldsymbol{F}}_v$ and $\widetilde{\boldsymbol{F}}_w$ respectively.

[6]$\widetilde{\boldsymbol{U}}_k$, $\widetilde{\boldsymbol{V}}_k$ and $\widetilde{\boldsymbol{W}}_k$ are the global nodal displacement components calculated according to Section 4.6.4

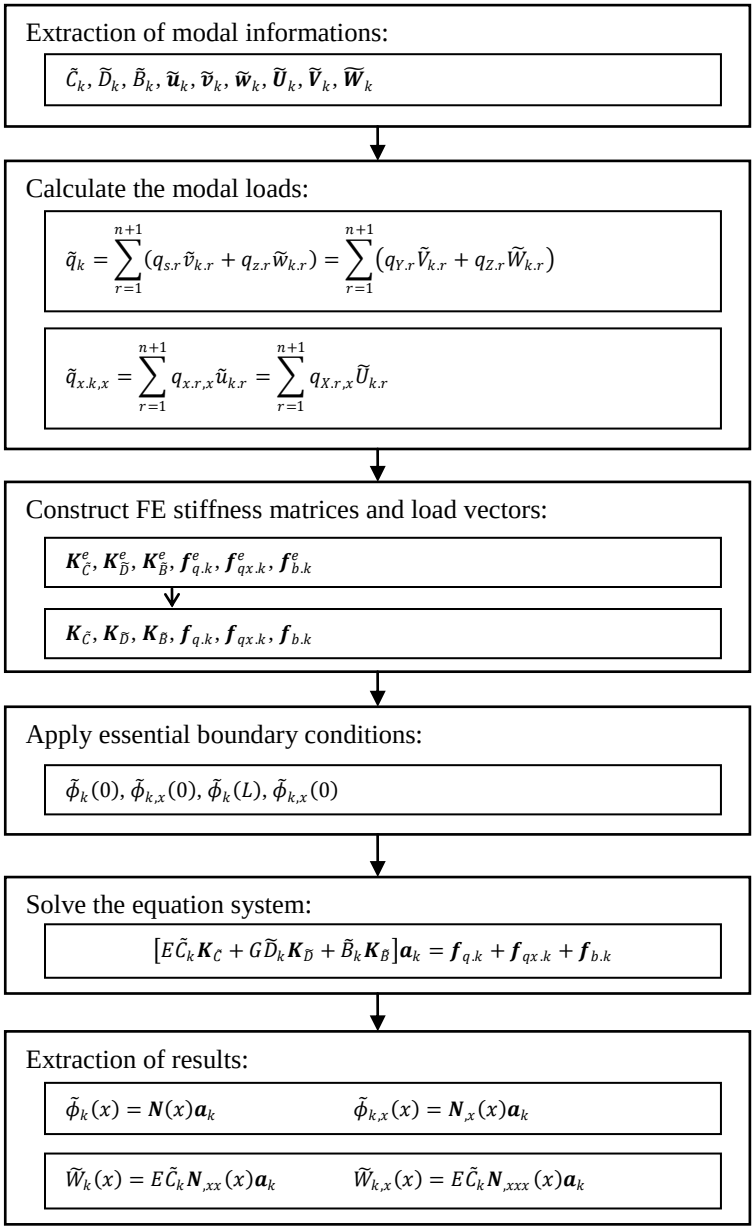

Figure 5.4: The flowchart over how the FE-solution of the amplitude functions $\tilde{\phi}_k$ and $\tilde{\phi}_{k,x}$ are obtained together with the sectional forces $\widetilde{W}_k(x)$ and $\widetilde{W}_{k,x}(x)$.

When utilizing the FEM approach there is also a possibility to solve the coupled GBT fundamental equation (4.149). This will not be illustrated here so for further reading about how to obtain the coupled solution, the reader is referred to Appendix D.

5.4 GBT Solution

When the amplitude function $\tilde{\phi}_k(x)$ and the sectional force $\widetilde{W}_k(x)$ are known, the total behaviour of the member can be determined. Since all deformation modes are orthogonal to each other, the total behaviour is obtained as the summation over all modal contributions, see Figure 5.5.

Global nodal displacements, node r:

$$U_r(x) = \sum_k \widetilde{U}_{k.r}\tilde{\phi}_{k,x}(x)$$

$$V_r(x) = \sum_k \tilde{V}_{k.r}\tilde{\phi}_k(x)$$

$$W_r(x) = \sum_k \widetilde{W}_{k.r}\tilde{\phi}_k(x)$$

Stresses, node r:

$$\sigma_x(x) = \sum_k \sigma_{x.k}(x)$$

$$\tau_{xs}(x) = \sum_k \tau_{xs.k}(x)$$

Transverse bending moments, node r:

$$m_{s.r}(x) = \sum_k m_{s.r.k}\tilde{\phi}_k(x)$$

Shear force, plate element r:

$$S_r(x) = \sum_k S_{r.k}(x)$$

Figure 5.5: Illustration and a summary of the total GBT resulting displacements, stresses and section forces of the member at cross-sectional node or element r and how they vary along the member lengths.

6 Application and verification of GBT

This chapter contains an application of the GBT on a predefined profile. During the literature review, all of the solved examples presented were performed for single symmetric cross sections. Therefore the authors have chosen to apply the GBT theory on a Z-profile in order to illustrate how the anti-symmetry affects the deformation modes. Another argument is that the Z-profile is a common profile in the construction industry and one common product is roof purlins.

6.1 Selected profile

The Z-profile used in the GBT analysis is Z200x1.2-profile manufactured by Borga AB [25]. The cross-section is depicted and defined according to Figure 6.1 below.

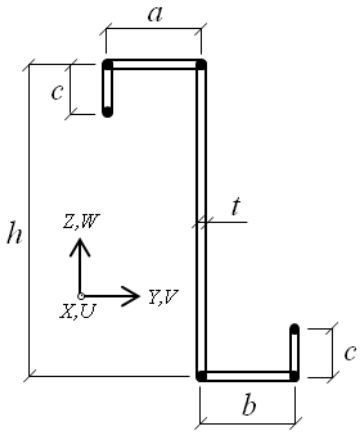

Parameter	Size $[mm]$
Height web, h:	200
Width upper flange, a:	52
Width lower flange, b:	59
Height lip, c:	14
Thickness, t:	1.17

Figure 6.1: The figure illustrates the cross-section of the chosen Z-profile. The table to the right contains the associated numbers according the labelling in the figure to the left. The figure also indicates the positive directions in the global (X,Y,Z)-coordinate system and the associated global (U,V,W)-displacements.

The material parameters used are the Young's modulus of elasticity $E = 210\,000\ N/mm^2$ and the Poisson's ratio $\nu = 0.3$ which gives the shear modulus of elasticity G according to the formula:

$$G = \frac{E}{2(1+\nu)} = 80\,769.23\ N/mm^2 \tag{6.1}$$

6.2 Cross-section analysis

This section presents the procedure of how the deformation modes are determined for the chosen Z-profile. This procedure is repeated twice, once when only the natural nodes are considered and once with imposed intermediate nodes so that the influence of intermediate nodes can be evaluated in an illustrative way.

6.2.1 Discretization

The first step is to discretize the cross-section into plate elements and nodes. The plate intersections and the free ends will form the natural nodes and the plate elements will be defined between them. The intermediate nodes are the imposed nodes defined between natural nodes.

6.2.1.1 Discretization with only natural nodes considered

When only considering natural nodes the discretization of the cross-section and all inherent sizes will be defined in Figure 6.2. In total there will be five plate elements and six nodes (natural nodes). The associated degrees of freedom are the warping values u_r at each natural node r, i.e. in total there are six degrees of freedom when only considering natural nodes.

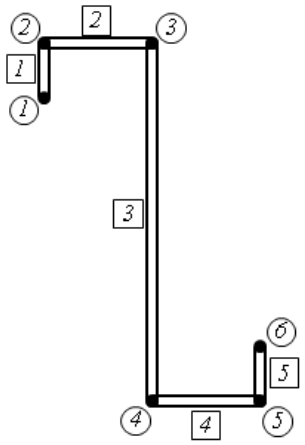

Element$r$	Widthb_r [mm]	Thicknesst_r [mm]	Angleα_r [rad]
1	14	1.17	$\pi/2$
2	52	1.17	0
3	200	1.17	$-\pi/2$
4	59	1.17	0
5	14	1.17	$\pi/2$

Figure 6.2: Discretization of the cross-section when only considering the natural nodes. The figure to the left define the node (rings) and element (squares) numbering. The table to the right contain the plate element information such as plate widths b_r, plate thickness t_r and the plate angle α_r.

6.2.1.2 Discretization including intermediate nodes

The authors have chosen to impose three intermediate nodes, one at the upper flange, one at the web and one at the lower flange. The node and element numbering along with each sub-plate information are defined in Figure 6.3.

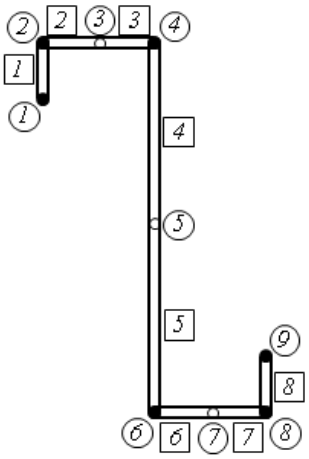

Element r	Width b_r [mm]	Thickness t_r [mm]	Angle α_r [rad]
1	14	1.17	$\pi/2$
2	26	1.17	0
3	26	1.17	0
4	100	1.17	$-\pi/2$
5	100	1.17	$-\pi/2$
6	29.5	1.17	0
7	29.5	1.17	0
8	14	1.17	$\pi/2$

Figure 6.3: Discretization of the cross-section when intermediate nodes are included. The figure to the left define the node (rings) and element (squares) numbering. The table to the right contain the plate and subplate element information such as plate widths b_r, plate thickness t_r and the plate angle α_r.

The increased number of nodes also increases the number of degrees of freedom. For this particular cross-section and set of nodes the degrees of freedom consists of:

- Node 1, 2, 4, 6, 8 and 9 are the defined natural nodes that give rise to six warping (u_r) degrees of freedom.
- Node 1 and 9 are the defined end nodes that give rise to two transverse (w_r) degrees of freedom.
- Node 3, 5 and 7 are the defined intermediate nodes that give rise to three transverse (w_r) degrees of freedom.

In total there are eight plate elements, nine nodes, six warping degrees of freedom and five transverse degrees of freedom which in total are eleven degrees of freedom.

6.2.2 Cross-section analysis

The cross-section analysis is fully described in Chapter 5, which involves a number of matrices which that has to be determined in order to have the setup of deformation modes. All the geometric matrices $(\overline{\boldsymbol{U}}, \overline{\boldsymbol{F}}_v, \overline{\boldsymbol{F}}_{w1}, \overline{\boldsymbol{F}}_{w2}, \overline{\boldsymbol{F}}_w, \overline{\boldsymbol{F}}_\vartheta, \Delta\overline{\boldsymbol{F}}_\vartheta, \boldsymbol{\Delta}_{ik}, \overline{\boldsymbol{M}})$, GBT matrices $(\overline{\boldsymbol{C}}, \overline{\boldsymbol{D}}, \overline{\boldsymbol{B}})$, all matrices in the transformation process $(\widetilde{\boldsymbol{C}}_{4\times4}, \widetilde{\boldsymbol{D}}_{4\times4}, \boldsymbol{K}_{3\times3}, \widetilde{\boldsymbol{C}}_{3\times3})$ and the transformed GBT matrices $\left(\widetilde{\boldsymbol{C}}, \widetilde{\boldsymbol{D}}, \widetilde{\boldsymbol{B}}, \widetilde{\boldsymbol{U}}, \widetilde{\boldsymbol{F}}_v, \widetilde{\boldsymbol{F}}_w, \widetilde{\boldsymbol{F}}_\vartheta, \Delta\widetilde{\boldsymbol{F}}_\vartheta, \widetilde{\boldsymbol{M}}\right)$ are all expressed in numbers for the two analyses with and without imposition of intermediate nodes in Appendix G.

6.2.3 Extracted deformation modes

Due to the differences between including intermediate nodes or not, a different set of modes are acquired for each case. When performing the analysis with only natural nodes, global and distortional modes are collected. Imposition of intermediate nodes contributes to the result with the addition of local modes. In this section the obtained deformation modes are shown. The values from this analysis are used later in the report when analysing the response of a beam.

6.2.3.1 Only natural nodes

The deformation modes $\tilde{\boldsymbol{u}}_k$ are expressed as a set of nodal warping values $\tilde{u}_r$ and the total number of deformation modes is obtained as the number of degrees of freedom, hence when only natural nodes are considered six deformation modes are obtained. These modes are depicted in Figure 6.4 below where the dotted black line represent the undeformed cross-section and the solid red line is the deformation mode expressed in the nodal warping values $\tilde{u}_r$. The first four modes represents the deformation modes associated with the four rigid body modes, i.e. axial extension, major and minor principle axis bending and torsion. Mode five and six are the possible distortional modes.

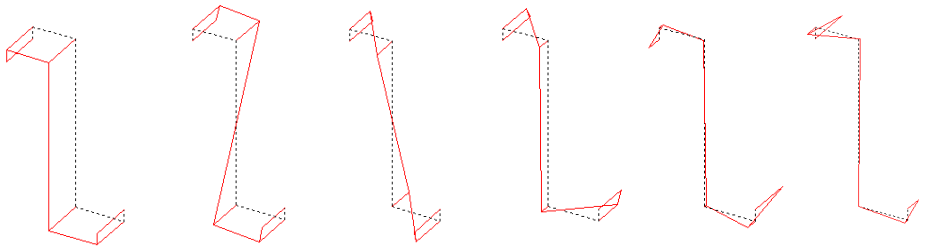

Figure 6.4: In total six deformation modes will be obtained when only natural nodes are considered. The black dotted line represents the undeformed cross-section and the solid red line is the corresponding deformation mode expressed in its nodal warping values $\tilde{u}_r$.

These deformation modes can also be expressed in terms of the global $\tilde{V}_r$ and $\tilde{W}_r$ displacement components, see Figure 6.5. The solid red line is the corresponding deformation mode expressed in terms of the nodal $\tilde{V}_r$ and $\tilde{W}_r$ displacement components. For further information about each deformation mode, see Appendix F. The variation between the nodes is plotted with a linear variation but actually the variation is non-linear and can be described in the shape functions $\Psi_{1-4}(\eta)$, see equation (4.108).

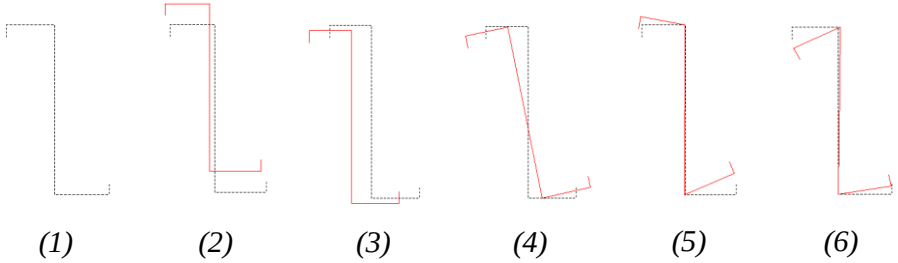

Figure 6.5: The deformation modes expressed in the global $\tilde{V}_r$ and $\tilde{W}_r$ displacement components. The black dotted lines represent the undeformed cross-section and the solid red lines are illustrating the corresponding deformation mode.

6.2.3.2 Including intermediate nodes

The deformation modes $\tilde{\boldsymbol{u}}_k$ obtained when imposing the intermediate nodes are illustrates in Figure 6.6. Eleven deformation modes are obtained, the same number as

the degrees of freedom. The four first deformation modes are identical to the four first obtained when only natural nodes are considered. The same colour scheme is used as for the natural nodes. Dotted black lines represents the undeformed cross-section and the solid red lines are the deformation modes expressed in the nodal warping values $\tilde{u}_r$.

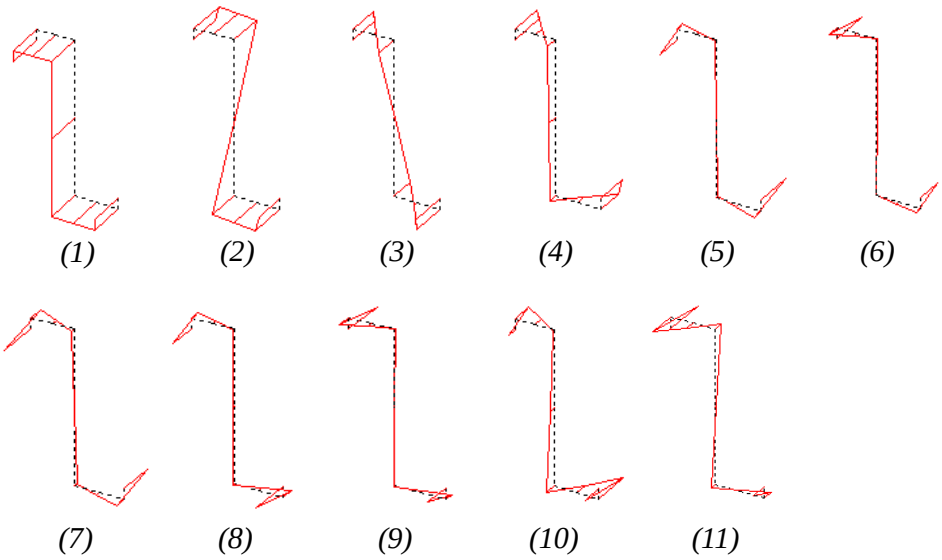

Figure 6.6: The eleven deformation modes obtained in the case of imposed intermediate nodes. The black dotted lines represent the undeformed cross-section and the solid red lines are illustrating the corresponding deformation mode expressed in its nodal warping values $\tilde{u}_r$.

These deformation modes can also be expressed in terms of the global $\tilde{V}_r$ and $\tilde{W}_r$ displacement components, as in Figure 6.7. The solid red lines are illustrating the corresponding deformation mode expressed in terms of the nodal $\tilde{V}_r$ and $\tilde{W}_r$ displacement components. For further information about each deformation mode, see Appendix F. The variation between the nodes is plotted with a linear variation but actually the variation is non-linear and can be described in the shape functions $\Psi_{1-4}(\eta)$, see equation (4.108).

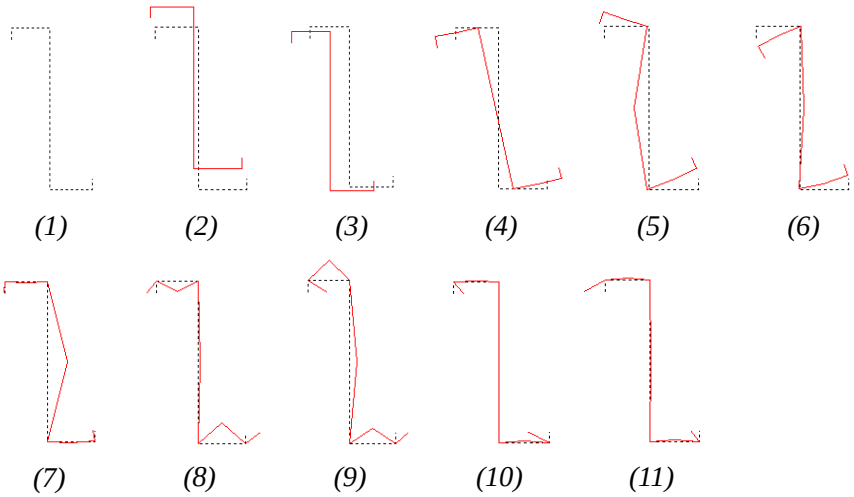

Figure 6.7: The deformation modes expressed in the nodal global $\tilde{V}_r$ and $\tilde{W}_r$ displacement components. The black dotted line represents the undeformed cross-section and the solid red line is the corresponding deformation mode.

6.3 Member analysis

Based on the deformation modes acquired in previous section, this section will present the results from the member analysis. Further information of the member is therefore required such as loads, boundary conditions and member length. Initially the modal loads are calculated, based on the loads acting on the member. Thereafter the amplitude function is solved for each mode, and finally the summation of mode contributions will form the total beam response.

6.3.1 The member conditions

Figure 6.8 illustrates the conditions for the chosen member. The Z-profile is fully fixed at both ends and the total member length L is 2.4 meters. The beam is subjected to two types of loads, namely the gravity load and an imposed uniformly distributed line-load. The gravity load ρg is defined by the density $\rho = 7800 kg/m^3$ and the gravity constant $g = 9.82 m/s^2$. The uniformly distributed line-load q_l has a magnitude of $5 kN/m$. Note that the loads are not aligned with any of the principle axes and also eccentric with regard to both the shear and gravity center. This application of loads will cause both skew bending and torsion effects.

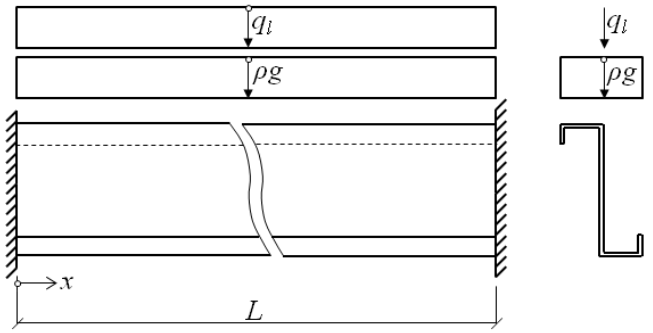

Member parameters		
Length, L:	2.4	$[m]$
Line-load, q_l:	5.0	$[kN/m]$
Gravity, ρg:	76.596	$[kN/m^3]$
BC:	Fixed-Fixed	

Figure 6.8: The applied GBT example is based on these conditions and loads. The Z-profile is fully fixed at both ends and subjected to both gravity loads and an uniformly distributed line-load acting at the intersection of the upper flange and the web. The table to the right contains the values used in the GBT member analysis.

6.3.2 Modal loads and boundary conditions

As a first step in the analysis process, the given loads have to be expressed in terms of nodal loads in the discretized cross-section. This is made according to Section 4.6.2 and the discretized cross-section including intermediate nodes, see Figure 6.3. Since all loads are acting in the (negative) Z-direction the nodal loads $q_{Y.r}$ and $q_{X.r}$ are obtained as zero for all deformation modes. The only retained and discretized nodal loads are the $q_{Z.r}$ loads, which are tabulated in Figure 6.9 below.

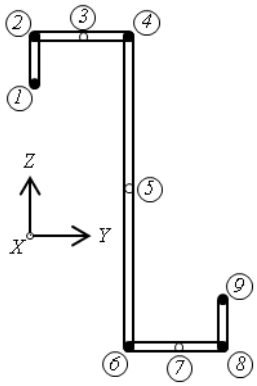

Node r	$q_{Z.r} \cdot 10^{-4}[kN/m]$
1	-6.273
2	-17.923
3	-23.301
4	-50056.000
5	-89.617
6	-58.027
7	-26.437
8	-19.492
9	-6.273

Figure 6.9: The loads on the Z-profile are only acting in (negative) Z-direction. When the gravity load ρg and the imposed line-load q_l have been discretized to corresponding node loads $q_{z.r}$ are tabulated to the right.

Before the GBT fundamental equation can be established, the modal loading term $\tilde{q}_k$ must be calculated. This is performed according to Section 4.6.2 and the numbers are presented in Figure 6.10 below. Deformation modes two, three and four have the greatest modal loads and will therefore have larger impact on the member than the other modes.

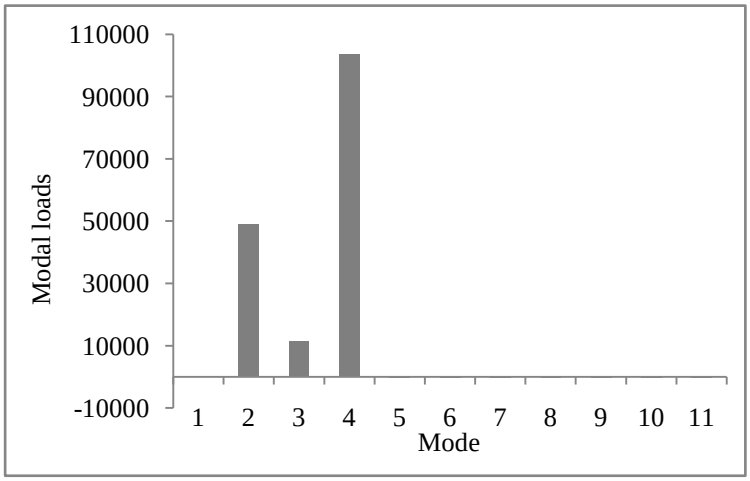

Mode k	$\tilde{q}_k \cdot 10^{-4}$
1	0
2	48965.0000
3	11528.0000
4	103470.0000
5	21.1200
6	-4.2164
7	7.6925
8	-13.5640
9	-43.7400
10	-2.0588
11	-4.0940

Figure 6.10: The modal loads $\tilde{q}_k$ obtained for the Z-profile. The histogram to the left shows the magnitudes of each modal load $\tilde{q}_k$ tabulated to the right.

The boundary conditions for the fully fixed Z-profile are of essential type. All displacements are locked at $X = 0$ and $X = L$ which expressed in terms of the modal amplitude functions $\tilde{\phi}_k$ and $\tilde{\phi}_{k,x}$ are defined as:

$$\left.\begin{matrix} \tilde{\phi}_k(0) = \tilde{\phi}_k(\mathrm{L}) = 0 \\ \tilde{\phi}_{k,x}(0) = \tilde{\phi}_{k,x}(\mathrm{L}) = 0 \end{matrix}\right\} \quad \text{for } k = 1, \dots, 11 \tag{6.2}$$

6.3.3 Solution of differential equations

The GBT fundamental equation is solved by means of FEM. In order to see how large the coupling terms in the GBT $\widetilde{\boldsymbol{D}}$-matrix are influencing the results, the GBT fundamental equation is solved both uncoupled (4.151) and coupled (4.149). For further knowledge about the FEM procedure, the reader is referred to Appendix D.

During the solution process a convergence study is performed, where the result are compared for different longitudinal discretizations. The authors used 10 mm finite elements during the analysis, even dough the result converges with relatively large element sizes. The argument to use these small elements is to get more data points available along the member.

The uncoupled and coupled GBT solutions are expressed in terms of the modal amplitude function $\tilde{\phi}_k(X)$ and tabulated in the quarter sections $X = 0,\ 0.25L,\ 0.5L$ and $0.75L$ in Table 6.1.

Table 6.1: The amplitude function $\tilde{\phi}_k(X)$ are expressed at the quarter sections $X = 0$, $0.25L$, $0.5L$ and $0.75L$ for both the uncoupled and coupled solutions

Mode k	$\tilde{\phi}_k(X)$ Uncoupled				$\tilde{\phi}_k(X)$ Coupled			
	$X = 0$	$0.25L$	$0.5L$	$0.75L$	$X = 0$	$0.25L$	$0.5L$	$0.75L$
1	0	1.29E-12	2.39E-12	1.35E-12	0	1.26E-12	2.34E-12	1.32E-12
2	0	4.36E-01	8.10E-01	4.56E-01	0	4.36E-01	8.10E-01	4.56E-01
3	0	2.30E00	4.28E00	2.41E00	0	2.30E00	4.28E00	2.41E00
4	0	1.35E-03	2.51E-03	1.41E-03	0	1.35E-03	2.51E-03	1.41E-03
5	0	1.77E00	2.06E00	1.81E00	0	1.73E00	1.83E00	1.75E00
6	0	-1.52E-01	-1.54E-01	-1.54E-01	0	-1.46E-01	-1.44E-01	-1.46E-01
7	0	1.50E-03	1.50E-03	1.50E-03	0	2.83E-03	2.16E-03	2.81E-03
8	0	-1.02E-04	-1.02E-04	-1.02E-04	0	-9.01E-05	-5.78E-05	-8.80E-05
9	0	-2.15E-04	-2.15E-04	-2.15E-04	0	-2.02E-04	-2.14E-04	-2.03E-04
10	0	-1.35E-05	-1.35E-05	-1.35E-05	0	-1.86E-05	3.27E-06	-1.74E-05
11	0	-2.33E-05	-2.33E-05	-2.33E-05	0	-9.04E-06	1.55E-04	1.22E-06

As a trend in the values, the amplitude function is decreasing its magnitude for the higher modes. This means that the influence of the mode, on the total response, will be smaller. In Appendix F the first order derivative of the amplitude function, as well as sectional forces, are shown.

6.4 GBT solution

When both the cross-section analysis and the member analysis are performed, the GBT solution can be obtained. Equation (4.183) and (4.191) shows how the displacements and stresses are calculated respectively, based on the known deformation modes and amplitude functions. In this section only relevant values are highlighted; see Appendix F for more detailed results for each node along the member.

Figure 6.11 illustrates how the Z-Profile responds to the applied load and boundary conditions. The colour represents the stresses with tensile stresses marked as red and compressive stresses marked as blue. To make the deformations visible, a scale factor of 50 is used on the plot to the right.

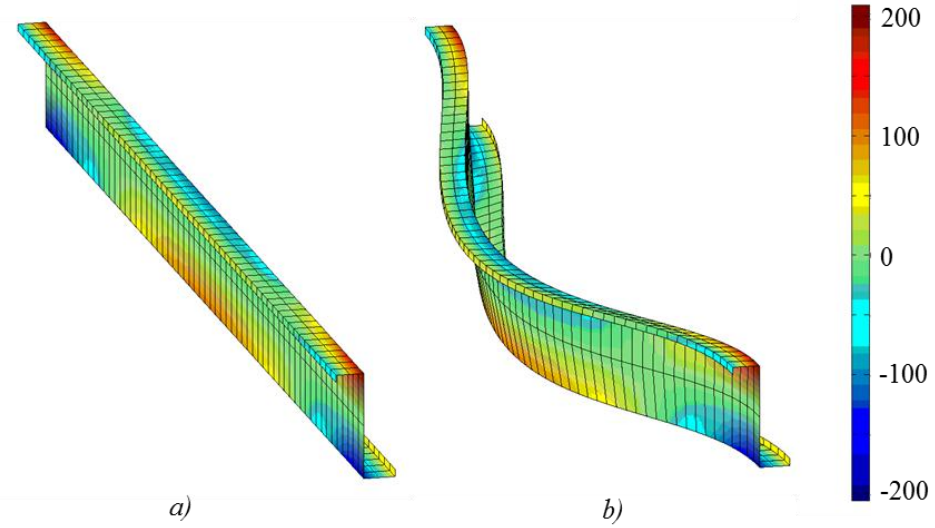

Figure 6.11: The Z-profile is here plotted in its undeformed and deformed shape (scale factor 50). The colour represents the normal stress σ_x and red colour denotes tensile stresses and blue colour for compressive stresses [MPa].

6.4.1 Displacements

The nodal displacements of the member are obtained as summation over all eleven modal contributions according to equation (4.183). Figure 6.12 illustrates the accumulation of modal contributions to the total displacements at node four in the midsection of the member. The contributions from the higher mode numbers $k > 5$ will not have any significant impact on this node at this section of the member. See Figure 6.9 for the nodal numbering.

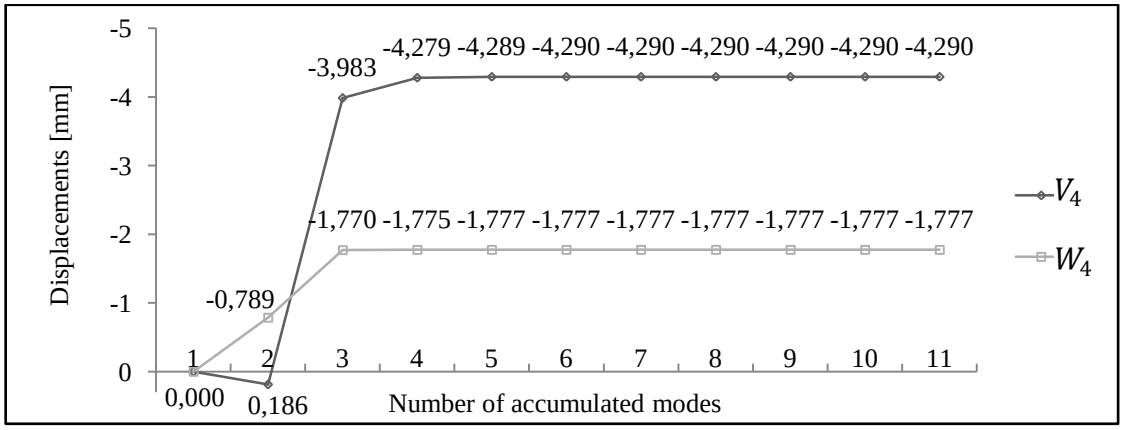

Figure 6.12: The accumulated V_4 and W_4 displacements at the midsection of the beam for node four.

6.4.2 Longitudinal stress

The accumulated nodal normal stresses $\sigma_{x.1}(X)$ and $\sigma_{x.4}(X)$ for node one and node four are plotted in Figure 6.13 and Figure 6.14 respectively for an increasing number of considered modes. These are calculated as shown in (4.191).The labelling refers to total number of accumulated modes, e.g. *Mode 1-4* stands for the sum of the contributions from deformation mode 1, 2, 3 and 4.

At node one there is a counteracting impact on the normal stresses but for node four there is contributory impact instead. The influence of the higher modes on node one is of greater importance than for node four, but not in the same magnitudes as for the first modes.

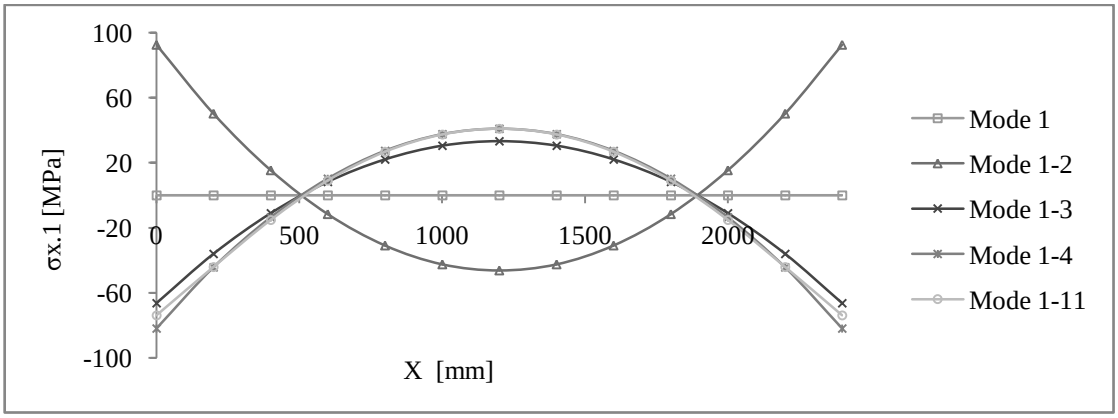

Figure 6.13: The variation along the member for the accumulated normal stress $\sigma_{x.1}(X)$ at node one. The labeling refers to total number of accumulated modes, e.g. Mode 1-4 stands for the sum of the contributions from deformation mode 1, 2, 3 and 4.

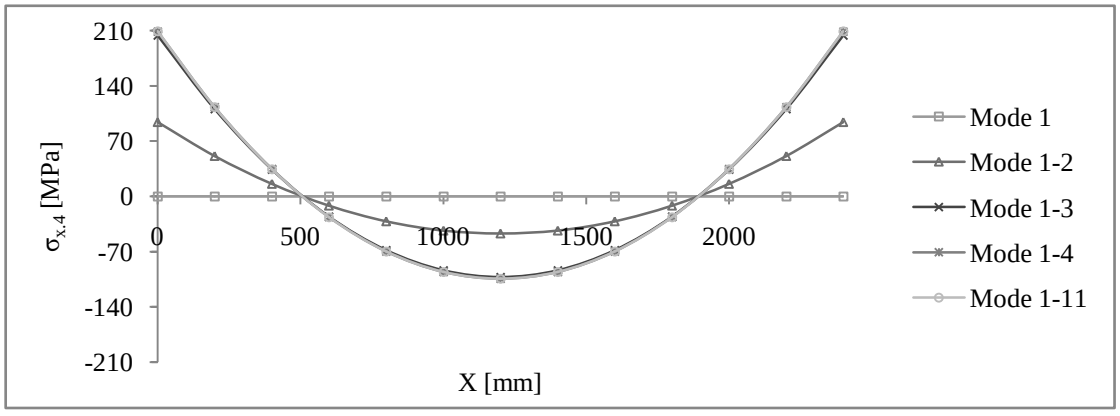

Figure 6.14: The variation along the member for the accumulated normal stress $\sigma_{x.4}(X)$ at node four. The labeling refers to total number of accumulated modes, e.g. Mode 1-4 stands for the sum of the contributions from deformation mode 1, 2, 3 and 4.

6.4.3 Extreme values

Table 6.2 contain all extreme values along the member, both for the uncoupled and coupled case. The minimum value of V_r is smaller than for W_r, an indication on that

the member is deflecting more in the horizontal direction than in the vertical direction. This can also be seen in the accompanying Figure 6.15 which illustrates each section where the respective extreme value occurs.

Table 6.2: All extreme values in terms of max and min values are here tabulated together with its associated node number and X-coordinate.

Parameter		Uncoupled			Coupled			Difference
		X[mm]	*Noder*	*Value*	*X*[mm]	*Noder*	*Value*	[%]
U_r [mm]	*Max*	1900	4	0.22968	1900	4	0.22965	0.013
	Min	500	4	-0.22968	500	4	-0.22965	0.013
V_r [mm]	*Max*	0	1	0	0	1	0	0
	Min	1200	1	-4.2976	1200	1	-4.2916	0.140
W_r [mm]	*Max*	0	1	0	0	1	0	0
	Min	1200	4	-1.7766	1200	3	-1.7795	-0.163
$\sigma_{x.r}$ [MPa]	*Max*	0	4	209.3	2400	4	209.33	-0.014
	Min	0	6	-206.03	0	6	-206.07	-0.019

Figure 6.15 illustrates the cross-sectional distribution at the sections for the corresponding extreme values. Due to the small difference between the uncoupled and coupled solution, only the uncoupled case is plotted.

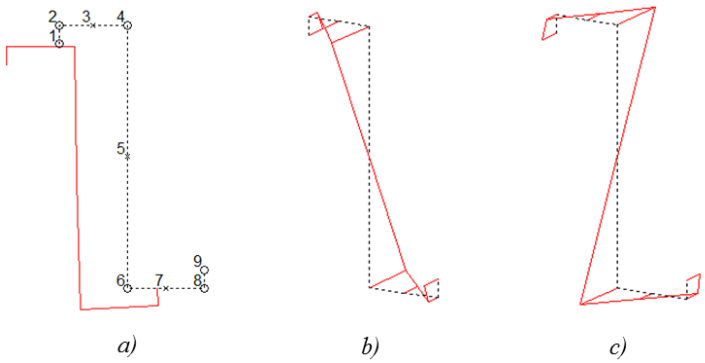

Figure 6.15: Illustration of a) the V and W displacements at midsection, b) the U displacements at $X = 500mm$ and c) the normal stress σ_x at the support. Note that different scale-factors are used for the three different sub-plots.

6.5 ABAQUS Comparison

A reference analysis is performed in a commercial FE-application in order to verify the GBT solution and also to evaluate the accuracy of the GBT method. The authors have chosen to use ABAQUS and model the Z-profile with shell-elements. See Appendix H for details on how the profile was modelled and also to see more results along the member length, than what is presented in this section. The GBT values that are used in the comparison are all calculated according to the uncoupled approach.

6.5.1 Displacements

Figure 6.16 to Figure 6.18 below shows the U_4, V_4 and W_4 displacements along the member length. The U and V displacements are almost the same for the two different analyse methods, where the graphs are placed on top of each other. The W displacements are slightly differing towards the middle of the beam.

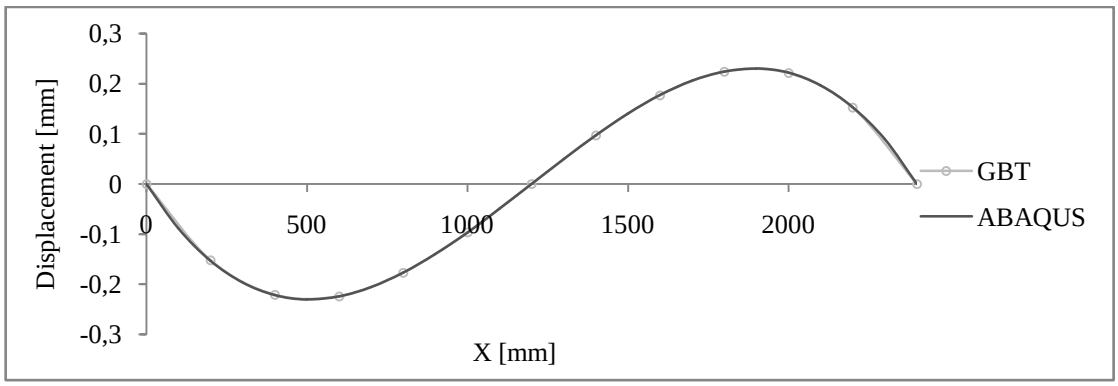

Figure 6.16: U_4 displacements along the member length, both for the GBT and ABAQUS case.

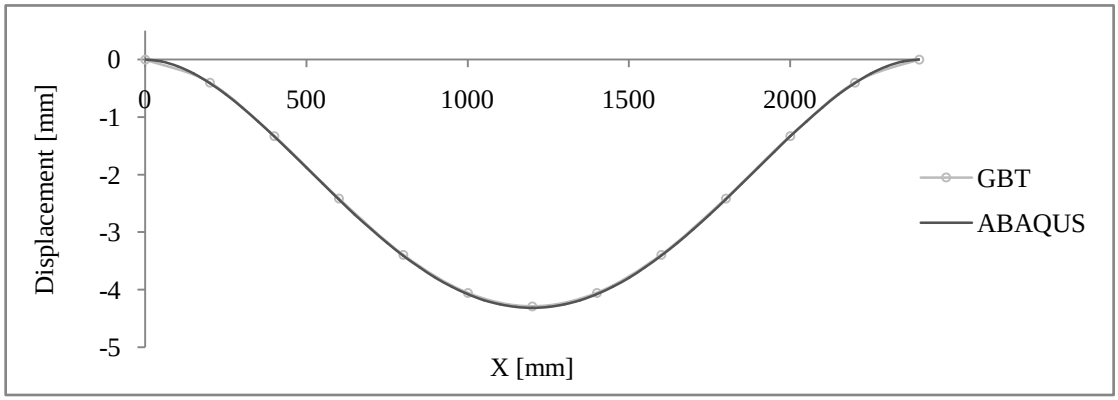

Figure 6.17: V_4 displacements along the member length, both for the GBT and ABAQUS case.

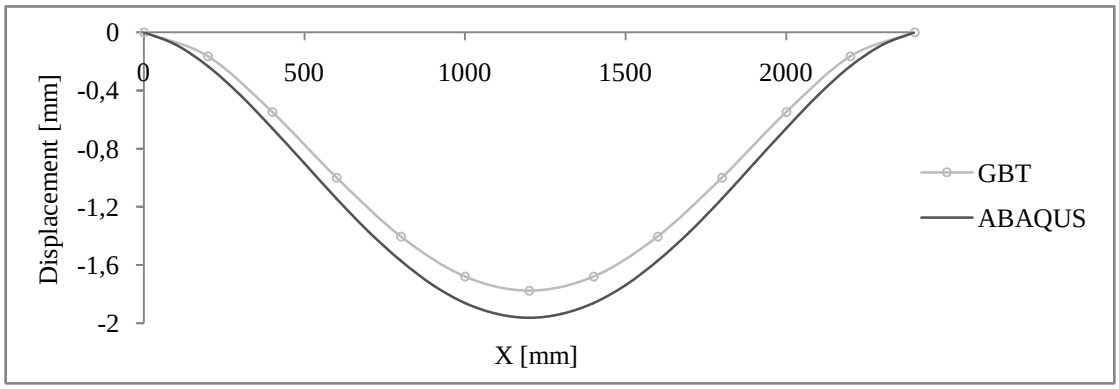

Figure 6.18: W_4 displacements along the member length, both for the GBT and ABAQUS case.

6.5.2 Longitudinal stress

Figure 6.19 shows the GBT and ABAQUS values for the longitudinal stress along the member. The values correlate very well in the middle part of the beam, where the curves are laying on each other. Close to the supports there are differences between the results, due to singularities in the ABAQUS model in these regions.

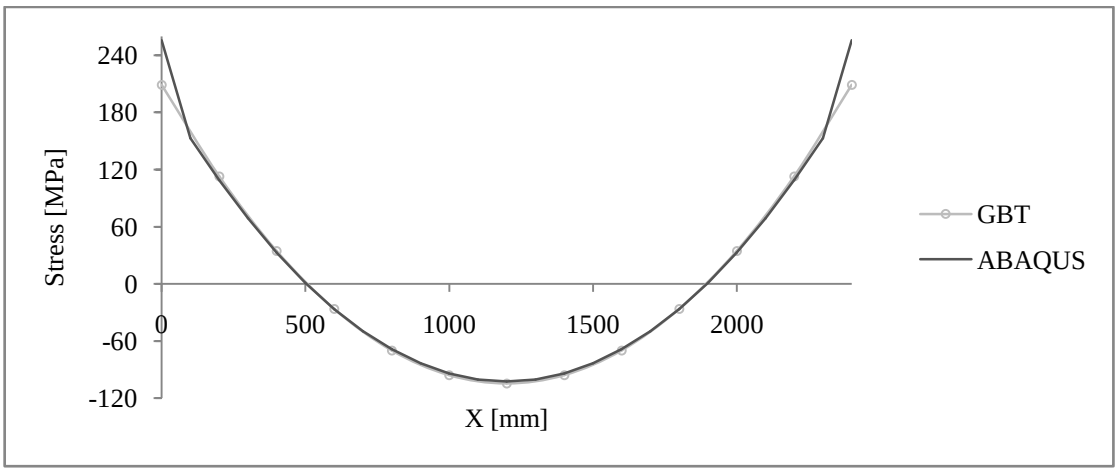

Figure 6.19: $\sigma_{x.4}$ magnitude along the member length, both for the GBT and ABAQUS case.

6.5.3 Extreme values

Table 6.3 presents all extreme values in terms of nodal displacements and normal stresses for the uncoupled GBT solution and the corresponding ABAQUS values at the same locations. The difference between the values is calculated, using the ABAQUS result as reference.

For the U and V displacements there are almost no difference at all, with a maximum of -0.24% for V. The difference for W is considerable larger, where the maximum displacement differs with 9.51%. The maximum and minimum values in normal stress σ_x at the support are not representative, since the ABAQUS values are affected by singularities at the boundaries. To get a representative comparison for the normal stress, the values are compared at the midpoint $X = 1200mm$. The difference in this section is about 0.6% to 1.59%.

Table 6.3: Comparison of the GBT extreme values to the ABAQUS values in the same points along the member.

Parameter		X[mm]	Node r	GBT	ABAQUS	Difference	
U_r [mm]	*Max*	1900	4	0.22968	0.2301	0.0004	0.18 %
	Min	500	4	-0.22968	-0.2301	-0.0004	0.18 %
V_r [mm]	*Max*	0	1	0	0	0	0 %
	Min	1200	1	-4.2976	-4.2874	0.0102	-0.24 %
W_r [mm]	*Max*	0	1	0	0	0	0 %
	Min	1200	4	-1.7766	-1.9633	-0.1867	9.51 %
$\sigma_{x.r}$ [MPa]	*Max*	0	4	209.3	275.8790	66.5790	24.13 %
	Min	0	6	-206.03	-266.3320	-60.3020	22.64 %
$\sigma_{x.r}$ [MPa]	*Max*	1200	6	102.8085	102.1890	-0.6195	-0.61 %
	Min	1200	4	-104.4486	-102.8170	1.6316	-1.59 %

7 Parameter study

To further enhance the understanding of GBT and the possibilities and restrictions, a parameter study will be undertaken. Throughout the chapter the same cross-section as defined in Section 6.1 will be used, and if nothing else is mentioned the discretization according to Figure 6.3 is used.

7.1 Boundary conditions

Here below follows the parameter study regarding different boundary conditions. Two boundary conditions are treated, namely one with fixed-free boundaries and one with fixed-guided boundaries.

7.1.1 Fixed - Free conditions

The Z-Profile is modelled as a cantilever where one end is fully fixed and the other is free. See Figure 7.1 for applied loads and conditions.

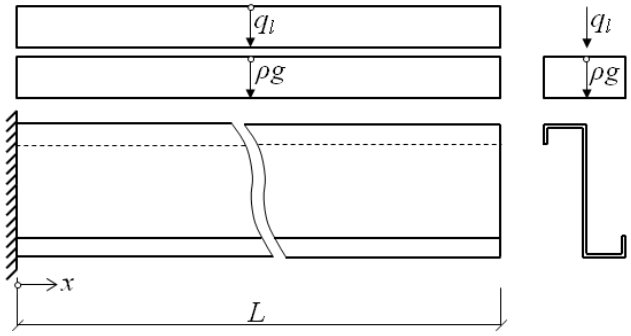

Member parameters		
Length, L:	2.4	$[m]$
Line-load, q_l:	0.5	$[kN/m]$
Gravity, ρg:	76.596	$[kN/m^3]$
BC:	Fixed-Free	

Figure 7.1: The Z-Profile is fully fixed at one end and free at the other. The member is subjected to both gravity loads and a uniformly distributed line-load acting at the intersection of upper flange and the web. The table to the right contains the values used in the analyses.

The essential GBT boundary conditions are defined below as:

$$\tilde{\phi}_k(0) = \tilde{\phi}_{k,x}(0) = 0 \qquad \text{for } k = 1, \dots, 11 \tag{7.1}$$

In the ABAQUS model all degrees of freedom are locked at the fixed end, i.e. all displacements and rotations are prevented.

The total response of the cantilever is depicted in Figure 7.2 in its deformed shape with a scale factor of 20 and the colour represents the normal stress distribution. The red colour denotes tensile stresses and blue colour for compressive stresses.

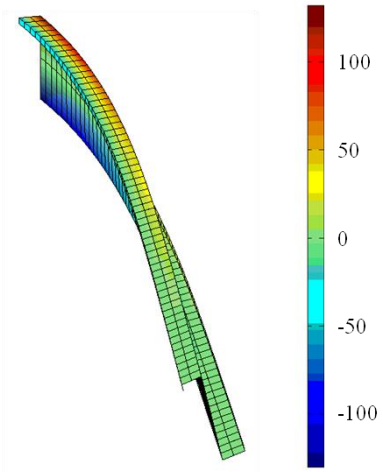

Figure 7.2: The Z-profile plotted in its deformed shape (scale factor 20). The colour represents the normal stress σ_x and red colour denotes tensile stresses and blue colour for compressive stresses [MPa].

The GBT and the ABAQUS results are compared to each other at node four, i.e. the intersection between the upper flange and the web. Figure 7.3 illustrates the difference between the U, V and W displacements and the longitudinal stress σ_x along the member. The values are obtained as the difference between ABAQUS and GBT over the maximum obtained value in ABAQUS in each category.

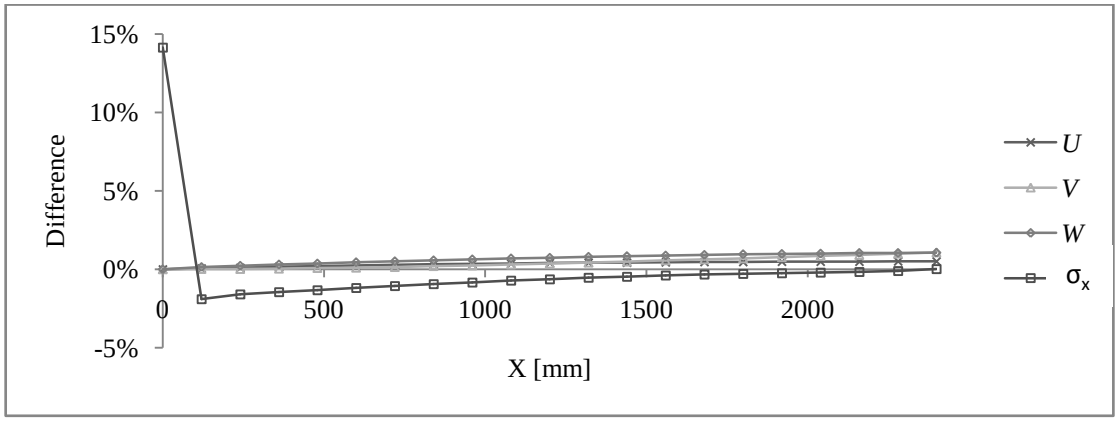

Figure 7.3: The difference between the GBT and ABAQUS results are plotted as the difference between them over the largest obtained value in ABAQUS in each category. This is performed for the U, V and W displacements and normal stress σ_x at node four along the member.

Table 7.1 contain the differences expressed in numbers at five sections. Also the average difference is calculated for each category given both in its actual difference and in percentage. See Appendix I for detailed plots over each displacement and stress variation along the member at node four.

Table 7.1: Differences between the ABAQUS and GBT results given at five different sections along the member. The average difference is also tabulated in its actual difference and in percentage.

X [mm]	0	600	1200	1800	2400	Average difference [mm] or [MPa]	[%]
U	0%	0.25%	0.40%	0.48%	0.51%	0.0018	0.35%
V	0%	0.11%	0.37%	0.71%	1.08%	0.0940	0.43%
W	0%	0.45%	0.75%	0.96%	1.07%	-0.0616	0.68%
σ_x	14.14%	-1.19%	-0.62%	-0.28%	0.02%	-0.0063	-0.71%[7]

7.1.2 Fixed - Guided conditions

The Z-Profile is modelled as with one end is fully fixed and the other is guided, i.e. the transverse displacements are permitted but no rotations are allowed. See Figure 7.4 for applied loads and conditions.

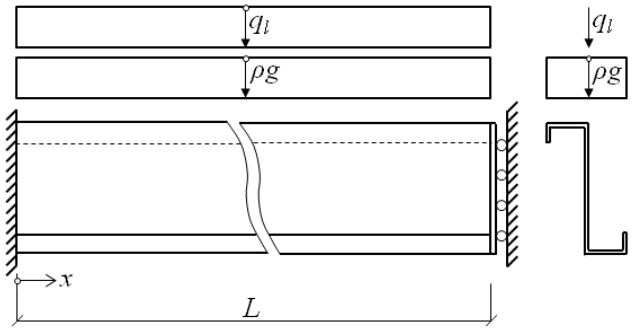

Member parameters		
Length, L:	2.4	$[m]$
Line-load, q_l:	0.5	$[kN/m]$
Gravity, ρg:	76.596	$[kN/m^3]$
BC:	Fixed-Guided	

Figure 7.4: The Z-Profile is fully fixed at one end and guided at the other. The member is subjected to both gravity loads and a uniformly distributed line-load acting at the intersection of upper flange and the web. The table to the right contains the values used in the analyses.

The essential GBT boundary conditions are defined as:

$$\tilde{\phi}_k(0) = \tilde{\phi}_{k,x}(0) = \tilde{\phi}_{k,x}(\mathrm{L}) = 0 \qquad \text{for } k = 1, \ldots, 11 \tag{7.2}$$

In the ABAQUS model all degrees of freedom are locked at the fixed end and at the guided end only the rotation degrees of freedom are locked.

The total response of the member is depicted in Figure 7.2 in its deformed shape with a scale factor of 50 and the colour represents the normal stress distribution. The red colour denotes tensile stresses and blue colour for compressive stresses.

[7]This value is calculated without considering the singularity at the fixed end

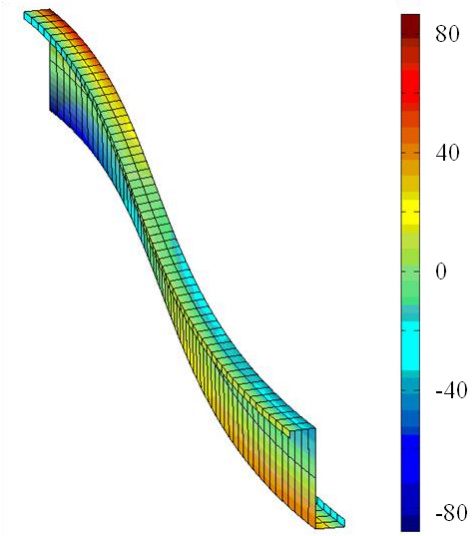

Figure 7.5: The Z-profile plotted in its deformed shape (scale factor 50). The colour represents the normal stress σ_x and red colour denotes tensile stresses and blue colour for compressive stresses [MPa].

The GBT and the ABAQUS results are compared to each other at node four, i.e. the intersection between the upper flange and the web. Figure 7.6 illustrates the difference betweenthe U, V and W displacements and the longitudinal stress σ_x along the member. The values are obtained as the difference between ABAQUS and GBT over the maximum obtained value in ABAQUS in each category.

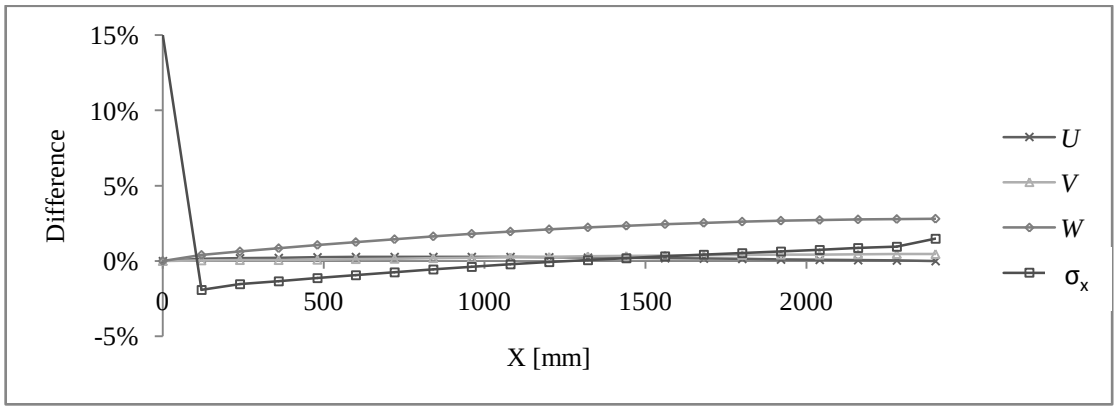

Figure 7.6: The difference between the GBT and ABAQUS results are plotted as the difference between them over the largest obtained value in ABAQUS in each category. This is performed for the U, V and W displacements and normal stress σ_x at node four along the member.

Table 7.2 contain the differences expressed in numbers at five different sections. Also the average difference is calculated for each category presented both in its actual difference and in percentage. See Appendix I for detailed plots over each displacement and stress variation along the member at node four.

Table 7.2: Differences between the ABAQUS and GBT results given at five different sections along the member. The average difference is also tabulated in its actual difference and in percentage.

X [mm]	0	600	1200	1800	2400	Average difference [mm] or [MPa]	[%]
U	0%	0.26%	0.25%	0.13%	0%	0.0003	0.17%
V	0%	0.11%	0.28%	0.39%	0.45%	0.0170	0.25%
W	0%	1.25%	2.08%	2.60%	2.78%	-0.0567	1.85%
σ_x	15.01%	-0.95%	-0.08%	0.51%	1.47%	0.5911	-0.14%[8]

7.2 Point loading

None of the used reference papers shows the full procedure of GBT analysis for point loading on a member. The authors thought that this is an important application and therefore this section is dedicated comparison and verification of that case.

The same Z-profile as used before is now modelled as a cantilever, where one of the ends is considered fully fixed and the other one as free. The member is subjected to a concentrated point-force $P_z = 75N$, which is applied at the free end. See Figure 7.7 for specifics concerning the model.

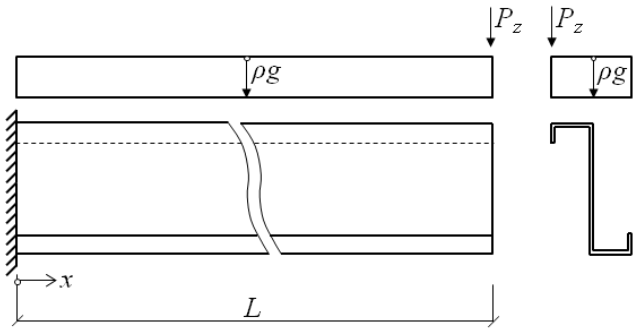

Member parameters		
Length, L:	2.4	$[m]$
Point-load, P_z:	75	$[N]$
Gravity, ρg:	76.596	$[kN/m^3]$
BC:	Fixed-Free	

Figure 7.7: The Z-Profile is fully fixed at one end and free at the other. The member is subjected to both gravity load and a concentrated point-force P_x acting at the tip of the member and at the intersection of upper flange and lip. The table to the right contains the values used in the analyses.

The total response of the member is depicted in Figure 7.2 in its deformed shape with a scale factor of 50 and the colour represents the normal stress distribution. The red colour denotes tensile stresses and blue colour for compressive stresses.

[8]This value is calculated without considering the singularity at the fixed end

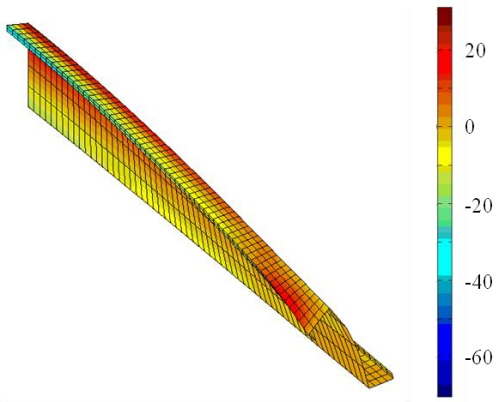

Figure 7.8: The Z-profile plotted in its deformed shape (scale factor 10). The colour represents the normal stress σ_x and red colour denotes tensile stresses and blue colour for compressive stresses [MPa].

The GBT and the ABAQUS results are compared to each other at node one, i.e. at the free end of the upper lip. Figure 7.9 illustrates the difference between the U, V and W displacements and the longitudinal stress σ_x along the member. The values are obtained as the difference between ABAQUS and GBT over the maximum obtained value in ABAQUS in each category.

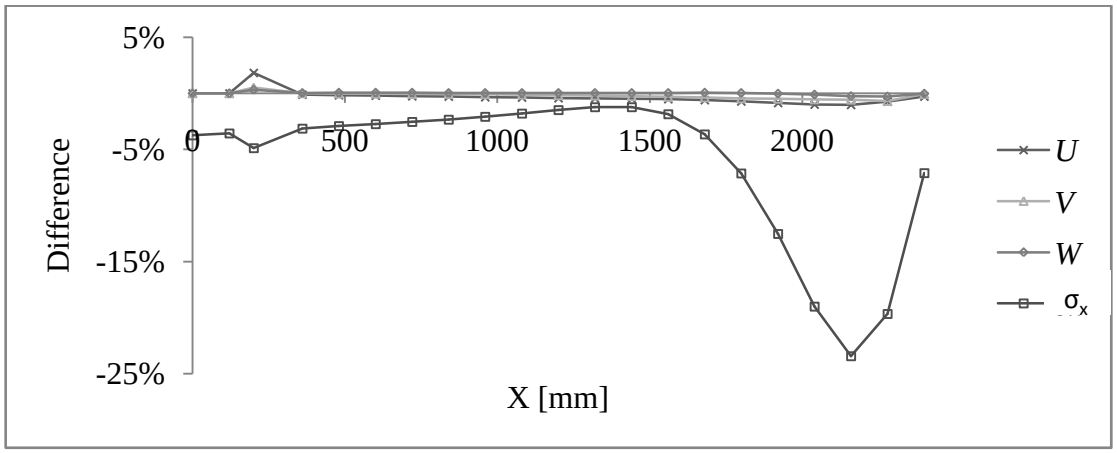

Figure 7.9: The difference between the GBT and ABAQUS results are plotted as the difference between them over the largest obtained value in ABAQUS in each category. This is performed for the U, V and W displacements and normal stress σ_x at node one along the member.

Table 7.3 contain the differences expressed in numbers at five different sections. Also the average difference is calculated for each category presented both in its actual difference and in percentage. See Appendix I for detailed plots over each displacement and stress variation along the member at node one.

Table 7.3: Differences between the ABAQUS and GBT results given at five different sections along the member. The average difference is also tabulated in its actual difference and in percentage.

X [mm]	0	600	1200	1800	2400	Average difference [mm] or [MPa]	[%]
U	0%	-0.20%	-0.41%	-0.70%	-0.29%	0.0011	-0.33%
V	0%	-0.02%	-0.15%	-0.44%	-0.04%	-0.0148	-0.18%
W	0%	0.06%	0.03%	0.04%	-0.02%	-0.0010	0.01%
σ_x	-3.74%	-2.72%	-1.47%	-7.13%	-7.10%	3.3928	-6.2%[9]

7.3 Varying slenderness

One of the major benefits by performing GBT analysis is that the result can be related to the response of each single independent deformation mode. In this section the influence of the different modes will be related to the length of the member.

During the analysis the member length was varied between 600 mm and 3000 mm, in steps of 200 mm. For each analysis the total displacement at the midsection of the member in node one and four was calculated. The total displacement for each step was then divided into the first four modes (rigid body) and the following distortional and local deformation modes. Figure 7.10 and Figure 7.11 shows the result from this separation.

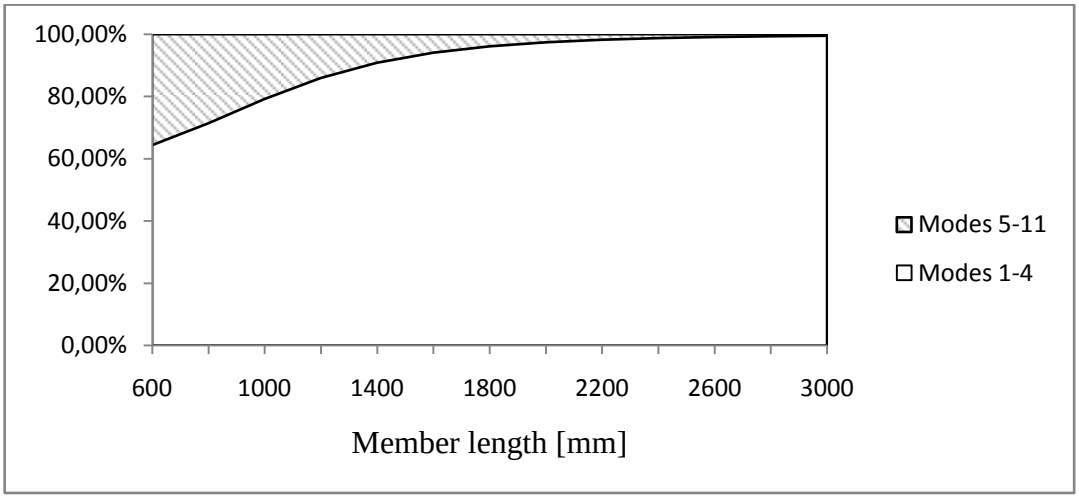

Figure 7.10: Mode influence, with varying length, on the total displacement of node one at midpoint.

For node one the influence of the distortional and local modes are greater than for node four. Similar to both cases is that with and increasing member length, the rigid body modes are influencing more of the results. This could be described as that the response for a stocky member has a local characteristic and the response for a slender member is more global.

[9]This value is calculated without considering the singularity at the fixed end

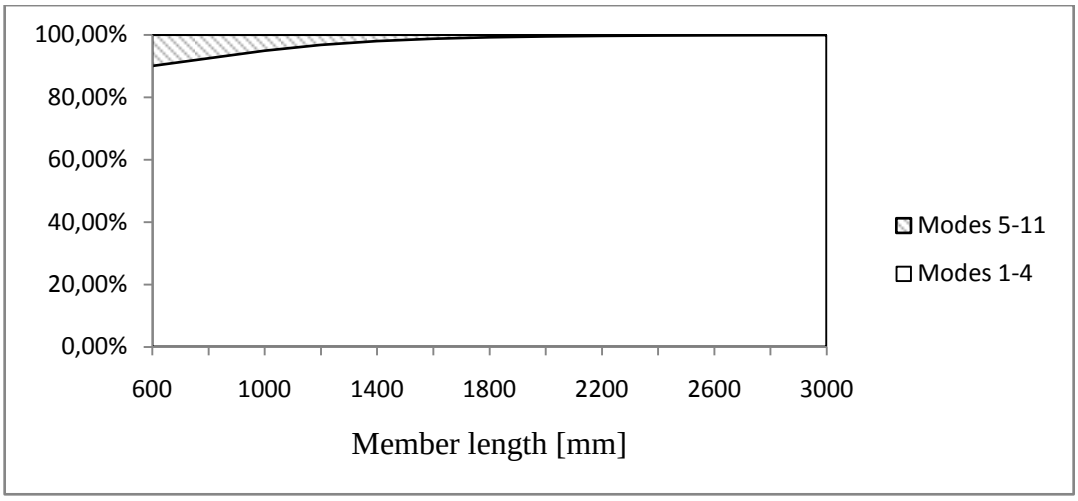

Figure 7.11: Modal influence, with varying length, on the total displacement of node four at midpoint.

7.4 Different discretization of the cross-section

The way of discretizing the cross-section will have different affects on the total response of the member. In order to present this a symmetric hat-profile is chosen treated as a cantilever with both an applied gravity force ρg and a uniformly distributed pressure q at the upper flange, see Figure 7.12.

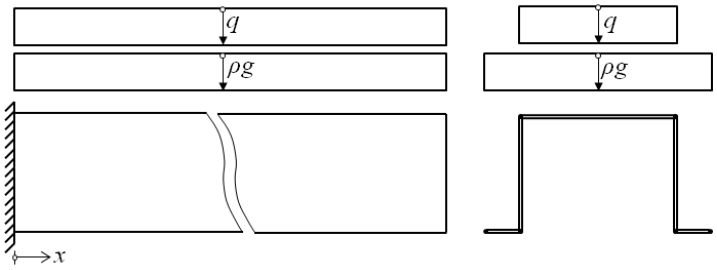

Figure 7.12: A symmetric hat-profile modelled as a cantilever subjected both a gravity load ρg and uniformly distributed pressure q at the upper flange.

The GBT analysis is performed for three different setups of nodes, namely a) only considering natural nodes, b) imposition of one intermediate node at the upper flange and c) a case when several intermediate nodes are considered. The total responses of the three setups are illustrated in Figure 7.13. One can there see that there is a difference in how the webs are inclined. In the case of only natural nodes the webs will have inwards inclinations compared to when imposition of intermediate nodes where an outwards inclination is obtained instead.

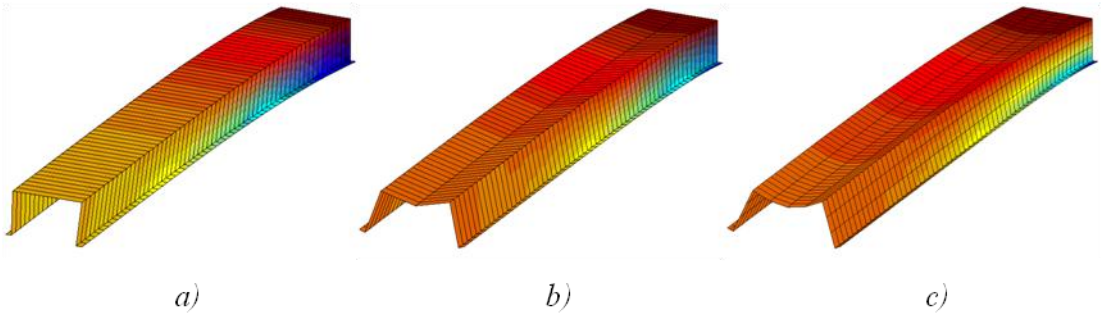

Figure 7.13: The GBT solution for three different setups of discretizations.a) only natural nodes, b) one imposed intermediate node and c) several imposed intermediate nodes.

When imposing intermediate nodes the resolution of the member gets better, but this mainly affects the local $w(s)$ displacements in the cross-section. The $u(s)$ will still vary linear between the natural nodes and $v(s)$ will still be the same and constant for all sub-plates. Since $u(s)$ varies linear also the normal stress $\sigma_x(s)$ will vary linear between the natural nodes. A way of overcoming this is to impose natural nodes instead of intermediate nodes. Due to the definition these imposed natural nodes must be inserted such that an angle difference arises over those nodes. Therefore, displace those imposed nodes with a small distance δ according to Figure 7.14.

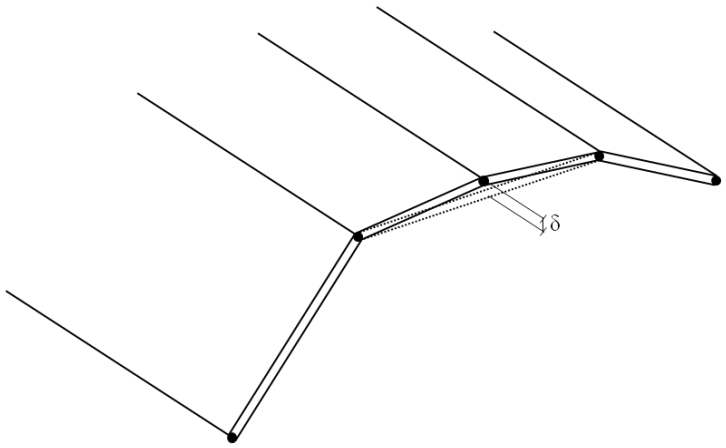

Figure 7.14: Imposition of a natural node instead of intermediate node requires an angle difference over that node, hence introduce that node with a small displacement δ.

Recall the Z-profile with fixed boundaries defined in Figure 6.2 and Figure 6.8. Instead of using intermediate nodes, natural nodes are imposed with a displacement $\delta = 0.1mm$. The variation in normal stresses σ_x at the mid-section of the member are illustrated in Figure 7.15 for the case of a) imposed intermediate nodes and b) imposed natural nodes. Note that the non-linear stress distribution in the lip is captured when natural nodes are imposed.

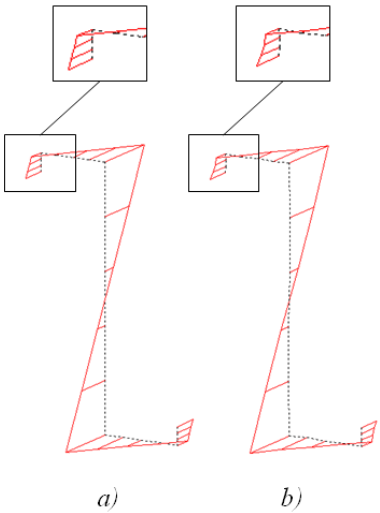

Figure 7.15: The variation in normal stress σ_x at the mid-section of the Z-profile in the case of a) imposed intermediate nodes and b) imposed natural node with the displacement $\delta = 0.1mm$

7.5 Calculation effort

The difference in computational effort, between GBT and ABAQUS, is difficult to estimate since the analyses are using different solution methods. To enable any kind of comparison the GBT solution has been clocked for two separate parts; the cross-sectional analysis and the member analysis. The cross-sectional analysis, which is GBT unique, is not compared with ABAQUS. The GBT member analysis is compared with the ABAQUS analysis, where the FEM solution is of interest. As model the same member and conditions as specified in Section 6.3 is used (fixed-fixed Z-profile with body force and line load).

7.5.1 Cross-sectional analysis

This particular study is carried out in order to see how large the computational effort is to determine the deformation modes. The time is measured from that the first matrix is assembled, until the final deformation mode has been determined. Calculation of geometrical and material parameters, as well as the following FEM solution is not included in this comparison.

Table 7.4 illustrates the elapsed time for different discretisations of the cross-section, where the number of intermediate nodes is the varying parameter. One can read that the case of only natural nodes requires a higher computational effort than if a few intermediate nodes are imposed, even though a larger number of degrees of freedom (dof) are considered. The computational effort per degree of freedom also increases for a larger number of considered intermediate nodes. Note that the degrees of freedom are calculated as the number of nodes in case of no intermediate nodes, otherwise it is the total number of nodes plus two.

Table 7.4: Elapsed time to carry out the cross-sectional analysis for different cross-sectional discretizations.

Intermediate nodes	Dofs	Time$[s]$	Rate $[s/dof]$	Change of rate $[s/dof]$
-	6	0.158	0.0263	-
3	11	0.056	0.0051	-
5	13	0.079	0.0061	0.0115
10	18	0.207	0.0115	0.0305
15	23	0.435	0.0189	0.0518
20	28	0.793	0.0283	0.0716
25	33	1.309	0.0397	0.1033
30	38	2.020	0.0532	0.1421

7.5.2 Member analysis

The member analysis of GBT is compared to the solution of the ABAQUS model. For the GBT part the time is measured for the assembly and solution of the FEM approximation, where the modes of deformation already have been determined. In ABAQUS the time is measured as the CPU time, as given in the .dat file. Table 7.5 shows the values of this comparison.

Table 7.5: Comparison between the elapsed times to have the GBT and ABAQUS solutions for an increasing set of finite elements.

	Element size $[mm]$	Dofs	Time $[s]$	Rate $[s/dof]$	Change of rate $[s/dof]$
GBT	53.33	1012	0.058	5.76E-05	-
	40	1342	0.066	4.95E-05	2.45E-05
	26.66	2002	0.095	4.76E-05	6.63E-05
	20	2662	0.102	3.84E-05	1.64E-05
	10	5302	0.246	4.64E-05	5.44E-05
	6.66	7942	0.533	6.71E-05	1.09E-04
	5	10582	0.853	8.06E-05	1.21E-04
ABAQUS	15	23184	1.6	6.90E-05	-
	10	50610	3.1	6.13E-05	5.47E-05
	7	103200	6.6	6.40E-05	6.66E-05
	5	202020	13.5	6.68E-05	6.98E-05
	3	557496	41.9	7.52E-05	7.99E-05

The elapsed time per degree of freedom is almost equal between the different solution methods. As shown for the cross-sectional analysis, the change of rate for a higher number of degrees of freedom is increasing also in this case. The degrees of freedom in ABAQUS are summed as the total number of nodes times six, which are the degrees of freedom in each node for S4R elements. In the GBT method the degrees of freedom are calculated as two times the number of nodes in the longitudinal direction times the number of modes. Since the elements used are four degrees of freedom beam elements, and the FEM system is assembled for each mode, this calculation is considered to be the best reference compared to ABAQUS.

8 Discussion

In this chapter the authors reasons about the whole project process, where difficulties and discoveries worth to mention are presented. Possible future research areas or masters project subjects are also discussed.

8.1 GBT

Most of the papers used in the background study are written at a very high academic level, where the reader is supposed to have an extensive knowledge in the field. This caused the authors to spend a lot of time to understand the core of the theory, as well as having to learning many new terms and physical relations.

Since most of the found papers about research in the context of GBT are brief and concerns only one specific area, they are not very comprehensive regarding the fundamental parts. For a deeper understanding of the basic theory as well as the underlying mathematics, the authors chose to present this in a thoroughly manner. The derivation of both the fundamental equation and the establishment of deformation modes will hopefully make it easier for fresh researchers in the field to understand these parts. The only reference, known to the authors, dealing with the theory behind both the fundamental equation and the cross-sectional analysis is the *Verallgemeinerte Technische Biegetheorie* [6]. This book is written all in german, so in order to simplify further research the cross-sectional derivation was translated into english. Also a more logical notation has been used, which makes it easier to understand the different meanings of the terms. Furthermore, the mathematical parts in the derivation have been written a lot more explicit. As an example the diagonalization procedure was hard to comprehend, so the authors have specifically written, step-by-step, how to perform this.

8.2 Implementation

During the implementation of the theory it was of great importance to distinguish between the cross sectional analysis and the member analysis. From the beginning the authors did not see this, but during the process a structure like this felt more logical. The documentation about the whole MATLAB application is a bit vague on other parts than the ones discussed below, but this is made deliberately since they have a more arbitrary nature. How the cross section is discretized and how the results are presented, expressed in MATLAB code, can be done in numerous ways.

8.2.1 Cross section analysis

The cross section analysis was the first step to implement. The authors followed the calculation procedure as shown in [6], without including intermediate nodes. Constructing the geometrical and material matrices was unproblematic, and could easily be verified to be correct. The most challenging part was the diagonalization process, where the three eigenvalues where solved. Since the orthogonal eigenvectors are infinitely many, it is not possible to verify all the numbers during the calculation. When the procedure was completed, the end result could be verified to be correct.

After succeeding the analysis once, the authors repeated the implementation again with the introduction of intermediate nodes. The reference material lacked specific

information on how to build some of the matrices, where the authors had to find out how to do that.

8.2.2 Member analysis

This part aims at solving the fundamental GBT equation, to get the amplitude functions known for each mode. The equation can be solved according to two different methods; analytical or approximate method. Analytical approach generates a solution that is exact and due to this no convergence needs to be verified, it is also provides a short computing time. When implementing an analytical solution, it has to be derived for each possible boundary condition and loading. This fact in combination with that only the uncoupled approach could be solved, made the authors to choose FEM as the solution method. FEM provides a good tool to approximate the solution both for the coupled and uncoupled case. Furthermore, it is easier to change boundary conditions and add arbitrarily placed loads on the member. A firm pre-existing knowledge base in the method made the choice easier for the authors and the implementation procedure went relatively easy.

8.3 Application of GBT

The authors chose to apply the GBT on a non-symmetric Z-profile and present the full solution, including numerical values both for the cross-sectional and member analysis. One of the factors to why this type of profile was chosen was that all reference examples concerns sections which are symmetrical around one axis. Hence the skew bending phenomena are not captured and illustrated, which the GBT is capable to handle. The extensive illustration and the fully solved example aim at helping subsequent readers to verify their own GBT implementations, both for the case of coupled and uncoupled approach as well as for different discretization methods.

In Table 6.3 the GBT results and ABAQUS results for the member are compared. There is a good correlation between the U and V displacements and also the normal stresses σ_x correlates good if one neglect the singularities at the boundaries. The major difference is in the W displacements and the reason to this is a bit concerning and the authors have not found the actual cause to the difference. Also the stress differs a bit at the boundaries, a fact caused by the singularities when analysing these regions in ABAQUS.

To verify and understand the behaviour of GBT, with its limitations and possibilities, different analysis parameters have been studied. Boundary conditions, loading, varying slenderness are some of the areas that are covered in the following sections.

8.3.1 Different loading and boundary conditions

During parametric studies different boundary conditions and load applications was tested in the implementation and verified with ABAQUS. Since the boundary conditions in GBT are specified on a modal basis it is hard to mimic some of them in ABAQUS. Fixed, free and guided was easy to model in ABAQUS, while pinned where troublesome. The authors tried it but the system was unsolvable and due to this no comparison could be made for this condition. During all of the different models the body force where considered, while the external loading was varying. Line loads and point loads in different directions was tested.

Overall the results seem to correspond well between the different cases, where the deflections are almost exactly the same. For the longitudinal stress there are larger differences at locations close to supports or concentrated forces. One cause for these variances could be the already mentioned singularities, which causes local stress raiser at specific nodes. Another cause could be how the values have been extracted from ABAQUS. Since the S4R element type has several integration points in the thickness direction and also across the elements. The values used for comparison has been difficult to choose. In GBT stress across the thickness of the element is considered to be constant, an assumption which make the comparison to the shell model a bit more difficult. Furthermore ABAQUS returns two different values from a node line along the intersection of two plates, where the authors have been using the mean value for comparison. Although these uncertainties exist, the values seem to correlate in a very convincing way. Also it is interesting to see how good the theory performs for the point loading cases, since no verified calculation for this exists in the used reference literature. In the treatment of the free end boundary condition in GBT the more simplified method was utilized, see Section 4.6.1. Due to this assumption a larger difference in stresses for this case was expected and also obtained, even though the magnitude was small in comparison to the other more restraint conditions.

8.3.2 Different discretizations of the cross-section

When the intermediate nodes were modelled as natural nodes with a small angle between connecting plates, the resolution of the normal stress was shown to increase. In the case of intermediate nodes the value of the normal stress in these is an interpolation based on the distance from the previous natural node. The authors think that this is a good method to investigate how the stress varies along a plate in the cross-section. Also it was discovered that a really small offset of the nodes were required to perform the calculation, which minimizes the geometrical distortion compared to the unadjusted shape of the section. If no intermediate nodes had been implemented in the project, this approach would have been used to capture higher modes.

The lipped U-section that was modelled with only natural nodes and a varying number of intermediate ones, showed how important the imposition of nodes at strategic locations are during analysis, see Figure 7.12. When only natural nodes at intersections between plates were used, the beam responded in a way that does not capture the real phenomena in the member. By imposing intermediate nodes the response seems adequate, which could be proven to be the case also when imposing one single node in the middle of the beam. This shows how important the intermediate nodes are and the locations that they are placed in. As a rule of thumb the authors estimate that one intermediate node per plate will provide a trustworthy result. This harsh method could off course be optimized, as shown when only one node was imposed at the right location.

8.3.3 Modal influence depending on slenderness

Figure 7.10 and Figure 7.11 illustrates the relation between the four rigid-body modes and the higher ones, for a transversally loaded beam with varying slenderness. The figures show clearly how the local and distortional modes have a larger impact on the results for shorter members. For more slender beams the total response of the beam is captured in a satisfactory way with only the rigid-body modes. The result is not

surprising, due to the knowledge of the different phenomena in slender and stocky members. Stocky beams are exposed to local and distortional deformations, while slender members have a more global response. One has to remember the instability issues with slender beams, which probably causes a failure before the yield limit is reached for the material. This kind of instability is not considered in this project, since it is related to the second order theory. The figures previously referred to also shows how the relation varies in different parts of the beam. For the node that is far away from the centreline the influence from the local and distortional modes are greater than for the node closer to the centreline. The reason for this is that more distortional and local effects occur in these outermost regions, while the centre of the beam is governed by the global effects.

8.3.4 Computational effort

The computational effort is similar per degree of freedom in both the GBT and ABAQUS analyses. Since the GBT method is using fewer degrees of freedom to reach a satisfactory result, this method is considered to be more computing efficient. It should also be mentioned that the GBT implementation is not optimized in any way, which most likely is the case for ABAQUS. If the application had been optimized, the authors thinks that the solution time per degree of freedom could be lowered and outperformance ABAQUS. Another approach could have been to use analytical method, where the calculation time probably would have been almost nullified.

Although the previous paragraph presents GBT as very efficient in comparison to ABAQUS, one has to remember that the calculation effort for static first order analysis is not that high. With modern computers these kinds of problems are easy to solve, and the usage of shell elements gives the user a greater versatility to model more complex cases. However, if second order theory is considered, the authors think that this comparison will be of greater importance. More about the efficiency for second order calculation are written in Section 2.3.

8.4 General remarks

During the usage of the theory one of the major positive experiences is how the result is built up, where each mode has its contribution on the total member response. In the analysis the user can specify which modes to include, and see which modes that influence different behaviours. From a pedagogical point of view, this possibility contributes to a deeper understanding on the structural behaviour of a member. Since the theory is rather sophisticated to derive and implement the pedagogical benefits arrives when the implementation is done and a member is analysed.

Due to the limited time of the project only first order theory was applied, where deflections and stresses were of interest. The authors thinks that the real benefits of the theory concerns the second order analysis, where critical loads and buckling shapes are in focus. A lot of research in this field has been done and it would have been very interesting for the project to reach these areas, but the fundamental knowledge has to be known to achieve this in a methodical way.

8.5 Further research

The project has neglected some areas concerning first order theory, which was considered as too time consuming to include. For instance this thesis only presents the theory for thin-walled open cross-sections, which disables analysis of common shapes like I beams. There are written articles, [8] and [10], about GBT applied on arbitrary cross-section geometries. The basic concept is to discretize and handle the cross-sectional analysis in a different manner than what is implemented throughout this project. There are also further possibilities to include cross-sectional restraints, e.g. preventing one node in the cross-section to translate or rotate. The way of treating this is to redefine the $\boldsymbol{\Delta}_{ik}$-matrix during the cross-sectional analysis. Boundary conditions are also one of area that perhaps would benefit from further investigations. The authors tried to model as many types as possible, with the given timeframe, but thinks that this could be further explored. Unfortunately it is hard to mimic some of the conditions in ABAQUS, hence the comparison gets difficult between the different methods.

After the previous mentioned subjects have been studied, or neglected, the authors think that there are two different possible paths to follow in the future. One of them concerns the theory applied on frames, where several members are connected by joints. Reference papers concerning the theory applied on frames exists, where the crucial part is how to model the joints. Warping transmission and other kinematical connections are of great importance to model the behaviour of the structure. The other path concerns the second order theory. A lot of research on second order theory has been done, and the main reason to expand the research into this field is to get bifurcation loads and buckling shapes. The authors will not discuss all the areas in second order theory here, since that theory is as wide as for first order. Also the background chapter gives a picture about the different topics there is.

9 Conclusions

The derivation in the context of GBT has been a major challenge, with all its lengthy and comprehensive calculation steps. During implementation the cross-sectional analysis was the most demanding obstacle due to its mathematical complexity in establishment of the deformation modes. Once the GBT fundamental equation and all deformation modes were determined, the FEM based member analysis could be solved and the solution could be obtained without difficulties.

The GBT provides accurate values compared to the reference shell-models used. No singularities are occurring in the solution and the extraction of results is easy due to the orthogonality condition between the modes. The commonly used assumption of an uncoupled equation system was verified to be adequate, since the coupling terms did not have any noticeable effect on the results. The GBT boundary conditions that are possible to mimic with finite shell-elements have been tested and verified. Computational efficiency is higher for GBT than for the reference FEM model, due to lower total number degrees of freedom.

The cross-section discretization has been found to be crucial and the imposed nodes must carefully be placed in the cross-section in order to capture the real behaviour of the member. If this is so and the analysis is performed correctly, the GBT provides a fast, pedagogical and an elegant solution approach. Furthermore, it enables new possibilities to evaluate the member and enhance the understanding of the response in the case of different cross-sections, boundary and loading conditions.

10 References

[1] C. Basaglia, D. Camotim and N. Silvestre, "Global buckling analysis of plane and space thin-walled frames in the context of GBT," *Thin-Walled Structures,* vol. 46, pp. 79-101, 2008.

[2] Y. Fang, "A geometrically exact thin-walled beam theory considering in-plane cross-section distortion," Cornell University, 2005.

[3] M. Nedelcu, "GBT formulation to analyse the behaviour of thin-walled members with variable cross-section," *Thin-Walled Structures,* vol. 48, pp. 629-638, 2010.

[4] B. W. Schafer and S. Ádány, "Understanding and classyfying local, distortional and global buckling in open thin-walled members," in *SSRC Annual Stability Conference*, Montreal, Canada, 2005.

[5] F. P. S. d. S. D. Simão, "Post-buckling bifurcational analysis of thin walled prismatic members in the context of the Generalized Beam Theory," University of Coimbra, Coimbra, 2007.

[6] R. Schardt, Verallgemeinerte Technische Biegetheorie - Lineare Probleme, Darmstadt: metrum-Verlag, 1989.

[7] J. M. Davies and L. Philip, "First-order generalised beam theory," *Journal of Constructional Steel Research,* vol. 31, pp. 187-220, 1994.

[8] P. Borges Dinis, D. Camotim and N. Silvestre, "GBT formulation to analyse the buckling behaviour of thin-walled members with arbitrarily "branched" open cross-sections," *Thin-Walled Structures,* vol. 44, pp. 20-38, 2006.

[9] R. Kindmann and M. Kraus, Steel Structures - Design using FEM, Berlin, Germany: Wilhelm Ernst & Sohn, 2011.

[10] D. Camotim, N. Silvestre, R. Goncalves and P. Borges Dinis, "GBT - based Structural Analysis of Thin-walled member: Overview, Recent Progress and Future Developments," *Solid Mechanics and Its Applications,* vol. 140, pp. 187-204, 2006.

[11] N. Silvestre and D. Camotim, "A shear deformable generalized beam theory for the analysis of thin-walled composite members," *Journal of Engineering Mechanics,* 2012.

[12] C. Basaglia, D. Camotim and N. Silvestre, "Torsion warping transmission at thin-walled frame joints: Kinematics, modelling and structural response," *Journal of Constructional Steel Research,* vol. 69, pp. 39-53, 2012.

[13] J. M. Davies and L. Philip, "Some applications of generalized beam theory," in *Eleventh International Specialty Conference on Cold-Formed Steel Structures*, St

Louis, Missouri, U.S.A., 1992.

[14] J. M. Davies and L. Philip, "Second-Order Generalised Beam Theory," *Journal of Constructional Steel Research,* vol. 31, pp. 221-241, 1994.

[15] N. Silvestre and D. Camotim, "Nonlinear generalized beam theory for cold-formed steel members," *International Journal of Structural Stability and Dynamics,* vol. 3, no. 4, pp. 461-490, 2003.

[16] R. Goncalves and D. Camotim, "GBT local and global buckling analysis of aluminium and stainless steel columns," vol. 82, pp. 1473-1484, 2004.

[17] R. Goncalves and D. Camotim, "Thin-walled member plastic bifurcation analysis using generalised beam theory," *Advances in Engineering Software,* vol. 38, pp. 637-646, 2007.

[18] D. Camotim, S. Nuno, B. Cilmar and R. Bebiano, "GBT-based buckling analysis of thin-walled members with non-standard support conditions," *Thin-Walled Structures,* vol. 46, pp. 800-815, 2008.

[19] D. A. Heinz, "Application of Generalized Beam Theory to the Design of Thin-Walled Purlins," *Thin-Walled Structures,* vol. 19, pp. 311-335, 1994.

[20] M. Nedelcu, "GBT-based analysis of tapered thin-walled members: Recent developments," *Civil Engineering & Architecture,* vol. 54, no. 1, pp. 38-49, 2011.

[21] C. Basaglia, D. Camotim and N. Silvestre, "Non-linear GBT formulation for open-section thin-walled members with arbitrary support conditions," *Computers and Structures,* vol. 89, pp. 1906-1919, 2011.

[22] M. Casafont, M. Frederic, M. Pastor and M. Ferrer, "Linear buckling analysis of thin-walled members combinding the Generalised Beam Theory and the Finite Element Method," *Computers and Structures,* vol. 89, pp. 1982-2000, 2011.

[23] N. Silvestre and D. Camotim, "First-order generalised beam theory for arbitrary orthotropic materials," *Thin-Walled Structures,* vol. 40, pp. 755-789, 2002.

[24] N. Silvestre and D. Camotim, "Second-order generalised beam theory for arbitrary orthotropic materials," *Thin-Walled Structures,* vol. 40, pp. 791-820, 2002.

[25] Borga Gruppen AB, [Online]. Available: http://borga.se/new_se/Produkter/purlins.html. [Accessed 18 04 2013].

[26] N. Ottosen and H. Petersson, Introduction to the Finite Element Method, Dorchester: Prentice Hall, 1992.

Appendices

Contents

Appendix A **Evaluation of the GBT stiffness terms**

The following stiffness terms are derived in Section 4.1 and are here stated and evaluated by integration over the element plate thickness. The plate stiffness K is also introduced where it is suitable:

$$B_{ik} = \frac{E}{1-\upsilon^2}\iint_{b,t} z^2 w_{k,ss} w_{i,ss}\, dzds = \frac{E}{1-\upsilon^2}\int_b \left[\frac{z^3}{3}\right]_{-t/2}^{t/2} w_{k,ss} w_{i,ss}\, ds$$
$$= \frac{Et^3}{12(1-\upsilon^2)}\int_b w_{k,ss} w_{i,ss}\, ds = K\int_b w_{k,ss} w_{i,ss}\, ds \tag{A.1}$$

$$C_{ik}^{I} = \iint_{b,t} u_k u_i\, dzds = \int_b [z]_{-t/2}^{t/2} u_k u_i\, ds = t\int_b u_k u_i\, ds \tag{A.2}$$

$$C_{ik}^{II} = \frac{1}{1-\nu^2}\iint_{b,t} z^2 w_k w_i\, dzds = \frac{1}{1-\nu^2}\int_b \left[\frac{z^3}{3}\right]_{-t/2}^{t/2} w_k w_i\, ds$$
$$= \frac{t^3}{12(1-\nu^2)}\int_b w_k w_i\, ds = \frac{K}{E}\int_b w_k w_i\, ds \tag{A.3}$$

$$C_{ik}^{III} = \frac{1}{1-\nu^2}\iint_{b,t} z w_k u_i\, dzds = \frac{1}{1-\nu^2}\int_b \left[\frac{z^2}{2}\right]_{-t/2}^{t/2} w_k u_i\, ds = 0 \tag{A.4}$$

$$C_{ik}^{IV} = \iint_{b,t} z u_k w_i\, dzds = \int_b \left[\frac{z^2}{2}\right]_{-t/2}^{t/2} u_k w_i\, ds = 0 \tag{A.5}$$

$$D_{ik}^{I} = 4\iint_{b,t} z^2 w_{k,s} w_{i,s}\, dzds = 4\int_b \left[\frac{z^3}{3}\right]_{-t/2}^{t/2} w_{k,s} w_{i,s}\, ds = \frac{t^3}{3}\int_b w_{k,s} w_{i,s}\, ds \tag{A.6}$$

$$D_{ik}^{II} = \frac{1}{G}\frac{\nu E}{1-\nu^2}\iint_{b,t} z^2 w_{k,ss} w_i\, dzds = \frac{1}{G}\frac{\nu E}{1-\nu^2}\int_b \left[\frac{z^3}{3}\right]_{-t/2}^{t/2} w_{k,ss} w_i\, ds$$
$$= \frac{1}{G}\frac{\nu E t^3}{12(1-\nu^2)}\int_b w_{k,ss} w_i\, ds = \frac{\nu K}{G}\int_b w_{k,ss} w_i\, ds \tag{A.7}$$

$$D_{ik}^{III} = \frac{1}{G}\frac{\nu E}{1-\nu^2}\iint_{b,t} z^2 w_k w_{i,ss} dz ds = \frac{1}{G}\frac{\nu E}{1-\nu^2}\int_b \left[\frac{z^3}{3}\right]_{-t/2}^{t/2} w_k w_{i,ss} ds$$
$$= \frac{1}{G}\frac{\nu E t^3}{12(1-\nu^2)}\int_b w_k w_{i,ss} ds = \frac{\nu K}{G}\int_b w_k w_{i,ss} ds \quad \text{(A.8)}$$

$$D_{ik}^{IV} = \frac{1}{G}\frac{\nu E}{1-\nu^2}\iint_{b,t} z w_{k,ss} u_i dz ds = \frac{1}{G}\frac{\nu E}{1-\nu^2}\int_b \left[\frac{z^2}{2}\right]_{-t/2}^{t/2} w_{k,ss} u_i ds = 0 \quad \text{(A.9)}$$

Where the plate stiffness K is defined as:

$$K = \frac{E t^3}{12(1-\nu^2)} \quad \text{(A.10)}$$

Appendix B **Programmable matrices**

Here in this appendix all programmable expressions derived in Chapter 4 are stated and expanded into programming ready matrices. The matrices that follow here are stated by only considering natural nodes, i.e. no intermediate nodes are accounted for. However, these matrices can be expanded so that intermediate nodes could be considered, see Section 4.3.

Geometric matrices

The $\boldsymbol{F}_v$-matrix defines the relation between the nodal warping values u_r and the transverse in-plane plate element displacements v_r, see equation (4.40).

$$\boldsymbol{F}_v = \begin{bmatrix} \frac{1}{b_1} & -\frac{1}{b_1} & & 0 \\ & \ddots & \ddots & \\ 0 & & \frac{1}{b_n} & -\frac{1}{b_n} \end{bmatrix} \tag{B.1}$$

The $\mathbf{F}_{w1}$- and $\mathbf{F}_{w2}$-matrices defines the relation between the nodal warping value u_r and the nodal transverse out-of-plane displacements $w_{1.r}$ and $w_{2.r}$, one at each end of the element, see equation (4.45) and (4.46).

$$\boldsymbol{F}_{w1} = \begin{bmatrix} -\frac{1}{b_1 \sin\Delta\alpha_2} & \left(\frac{1}{b_1 \sin\Delta\alpha_2} + \frac{1}{b_2 \tan\Delta\alpha_2}\right) & -\frac{1}{b_2 \tan\Delta\alpha_2} & & 0 \\ & \ddots & \ddots & & \\ 0 & & -\frac{1}{b_{n-1} \sin\Delta\alpha_n} & \left(\frac{1}{b_{n-1} \sin\Delta\alpha_n} + \frac{1}{b_n \tan\Delta\alpha_n}\right) & -\frac{1}{b_n \tan\Delta\alpha_n} \end{bmatrix} \tag{B.2}$$

$$\boldsymbol{F}_{w2} = \begin{bmatrix} -\frac{1}{b_1 \tan\Delta\alpha_2} & \left(\frac{1}{b_1 \tan\Delta\alpha_2} + \frac{1}{b_2 \sin\Delta\alpha_2}\right) & -\frac{1}{b_2 \sin\Delta\alpha_2} & & 0 \\ & \ddots & \ddots & & \\ 0 & & -\frac{1}{b_{n-1} \tan\Delta\alpha_n} & \left(\frac{1}{b_{n-1} \tan\Delta\alpha_n} + \frac{1}{b_n \sin\Delta\alpha_n}\right) & -\frac{1}{b_n \sin\Delta\alpha_n} \end{bmatrix} \tag{B.3}$$

These two matrices can later be used in order to evaluate the $\mathbf{F}_w$- and $\mathbf{F}_\vartheta$-matrices which relates the nodal warping values u_r to the plate element transverse out-of-plane displacement w_r and the plate element rotation ϑ_r, see equation (4.49) and (4.52).

The $\boldsymbol{\Delta}_{ik}$-matrix is such that the transverse nodal bending moments m_s can be expressed in terms of the nodal warping values u_r, see equations (4.71), (4.72) and (4.73).

$$\boldsymbol{\Delta}_{ik} = \begin{bmatrix} 0 & & & & & & & & 0 \\ & 0 & & & & & & & \\ & & \left(\frac{b_2}{3K_2}+\frac{b_3}{3K_3}\right) & \frac{b_3}{6K_3} & & & & & \\ & & \frac{b_3}{6K_3} & \left(\frac{b_3}{3K_3}+\frac{b_4}{3K_4}\right) & \frac{b_4}{3K_4} & & & & \\ & & & \ddots & \ddots & \ddots & & & \\ & & & & \frac{b_{n-3}}{6K_{n-3}} & \left(\frac{b_{n-3}}{3K_{n-3}}+\frac{b_{n-2}}{3K_{n-2}}\right) & \frac{b_{n-2}}{6K_{n-2}} & & \\ & & & & & \frac{b_{n-2}}{6K_{n-2}} & \left(\frac{b_{n-2}}{3K_{n-2}}+\frac{b_{n-1}}{3K_{n-1}}\right) & & \\ & & & & & & & 0 & \\ 0 & & & & & & & & 0 \end{bmatrix} \tag{B.4}$$

GBT matrices

The $\boldsymbol{C}_1$-matrix is also possible to have a programming ready matrix for, see equation (4.119).

$$\boldsymbol{C}_1 = \frac{1}{3}\begin{bmatrix} t_1 b_1 & \frac{t_1 b_1}{2} & & & & & & 0 \\ \frac{t_1 b_1}{2} & (t_1 b_1 + t_2 b_2) & \frac{t_2 b_2}{2} & & & & & \\ & \frac{t_2 b_2}{2} & (t_2 b_2 + t_3 b_3) & \frac{t_3 b_3}{2} & & & & \\ & & \ddots & \ddots & \ddots & & & \\ & & & \frac{t_{n-2} b_{n-2}}{2} & (t_{n-1} b_{n-1} + t_n b_n) & \frac{t_{n-1} b_{n-1}}{2} & & \\ & & & & \frac{t_{n-1} b_{n-1}}{2} & t_{n-1} b_{n-1} + t_n b_n & \frac{t_n b_n}{2} & \\ & & & & & \frac{t_n b_n}{2} & t_n b_n & \\ 0 & & & & & & & \end{bmatrix} \tag{B.5}$$

The other matrices is in the GBT analysis is not possible to have a presentation in a distinct programmable matrix as above. Instead a calculation scheme is presented in terms of a MATLAB routine. Here follow first a translation of the notations used in the derivation chapter to the used notations in the MATLAB code.

Table B.1: Here follows the matrix notations used in Chapter 4 and the corresponding matrix notations used in the MATLAB-code defined within this appendix

Matrix notations	MATLAB notations
$\bar{\boldsymbol{F}}_v$	`Fv`
$\bar{\boldsymbol{F}}_w$	`Fw`
$\bar{\boldsymbol{F}}_\vartheta$	`Ftheta`
$\bar{\boldsymbol{M}}$[10]	`M`
$\tilde{\boldsymbol{U}}^{III}$	`U_III`
$\bar{m}_{s.r.k}, \bar{m}_{s.r.i}$[11]	`mrk_bar, mri_bar`
$\hat{m}_{s.r.k}, \hat{m}_{s.r.i}$	`mrk_hat, mri_hat`

The $\boldsymbol{B}$-matrix defined in (4.114):

```
M_bar = zeros(nrOfElements,nrOfDofs);
M_hat = zeros(nrOfElements,nrOfDofs);
for r = 1:nrOfElements
    M_bar(r,:) = (M(r+1,:)+M(r,:))/2;
    M_hat(r,:) = (M(r+1,:)-M(r,:))/2;
end

B = zeros(nrOfDofs,nrOfDofs);
for k = 1:nrOfDofs
    for i = 1:nrOfDofs
        sum_terms = 0;
    for r = 1:nrOfElements
            element = elements(r).Value;
            br = element(r).Value.width;
            Kr = element(r).Value.K;
            mrk_bar = M_bar(r,k);
            mri_bar = M_bar(r,i);
            mrk_hat = M_hat(r,k);
            mri_hat = M_hat(r,i);

            sum_terms = sum_terms + ...
               Kr*br*(mrk_bar*mri_bar*1/(Kr*Kr) + ...
               mrk_hat*mri_hat*1/(3*Kr*Kr));
    end
        B(k,i) = sum_terms;
    end
end
```

[10] $\bar{\boldsymbol{M}}$ is the matrix which translates the nodal unit transverse bending moments $\bar{m}_{s.r}$ to the corresponding unit warping $\bar{u}_r$ and should not be mistaken for the "average" element moments $\bar{m}_{s.r}$ defined in (4.100)
[11] "Average" element moments defined in (4.100)

Note: The $\boldsymbol{B}$-matrix can also be obtained as $\boldsymbol{B} = -\Delta\bar{\boldsymbol{F}}_{\vartheta} \cdot \bar{\boldsymbol{M}}$

The $\boldsymbol{C}_2$-matrix is defined in (4.122):

```
C2 = zeros(nrOfDofs,nrOfDofs);
for k = 1:nrOfDofs
    for i = 1:nrOfDofs
        sum_terms = 0;
        for r = 1:nrOfElements
            element = elements(r).Value;
            br = element.width;
            Kr = element.K;
            w_rk = Fw(r,k);
            w_ri = Fw(r,i);
            theta_rk = Ftheta(r,k);
            theta_ri = Ftheta(r,i);
            mrk_bar = M_bar(r,k);
            mri_bar = M_bar(r,i);
            mrk_hat = M_hat(r,k);
            mri_hat = M_hat(r,i);

            sum_terms = sum_terms + ...
               Kr*br*(w_rk*w_ri + ...
               theta_rk*theta_ri*br^2/12 + ...
               (w_rk*mri_bar+mrk_bar*w_ri)*br^2/(12*Kr) + ...
               (mrk_hat*theta_ri+theta_rk*mri_hat)*br^3/(360*Kr) + ...
               (mrk_bar*mri_bar+1/63*mrk_hat*mri_hat)*br^4/(120*Kr^2));

        end
        C2(k,i) = 1/E*sum_terms;
    end
end
```

The $\boldsymbol{D}_1$-matrix defined in (4.126):

```
D1 = zeros(nrOfDofs,nrOfDofs);
for k = 1:nrOfDofs
    for i = 1:nrOfDofs
        sum_terms = 0;
        for r = 1:nrOfElements
            element = elements(r).Value;
            br = element.width;
            tr = element.thickness;
            Kr = element.K;
            theta_rk = Ftheta(r,k);
            theta_ri = Ftheta(r,i);
            mrk_bar = M_bar(r,k);
            mri_bar = M_bar(r,i);
            mrk_hat = M_hat(r,k);
            mri_hat = M_hat(r,i);

            sum_terms = sum_terms + ...
               br*tr^3/3*(theta_rk*theta_ri + ...
               (mrk_bar*mri_bar+1/15*mrk_hat*mri_hat)*br^2/(12*Kr^2));
        end
        D1(k,i) = sum_terms;
    end
end
```

The $\boldsymbol{D}_2$-matrix defined in (4.129):

```
D2 = zeros(nrOfDofs,nrOfDofs);
for k = 1:nrOfDofs
    for i = 1:nrOfDofs
        sum_terms = 0;
        for r = 1:nrOfElements
            element = elements(r).Value;
            br = element.width;
            tr = element.thickness;
```

```
            Kr = element.K;
            w_rk = Fw(r,k);
            w_ri = Fw(r,i);
            theta_rk = Ftheta(r,k);
            theta_ri = Ftheta(r,i);
            mrk_bar = M_bar(r,k);
            mri_bar = M_bar(r,i);
            mrk_hat = M_hat(r,k);
            mri_hat = M_hat(r,i);

            sum_terms = sum_terms + ...
               br*(-mrk_bar*w_ri - ...
               mrk_hat*theta_ri*br/6 - ...
                (mrk_bar*mri_bar+1/15*mrk_hat*mri_hat)*br^2/(12*Kr));
        end
        D2(k,i) = ny/G*sum_terms;
    end
end
```

The $\boldsymbol{D}_3$-matrixdefined in (4.130):

```
D3 = zeros(nrOfDofs,nrOfDofs);
for k = 1:nrOfDofs
    for i = 1:nrOfDofs
        sum_terms = 0;
        for r = 1:nrOfElements
            element = elements(r).Value;
            br = element.width;
            tr = element.thickness;
            Kr = element.K;
            w_rk = Fs_hat(r,k);
            w_ri = Fs_hat(r,i);
            theta_rk = Ftheta(r,k);
            theta_ri = Ftheta(r,i);
            mrk_bar = M_bar(r,k);
            mri_bar = M_bar(r,i);
            mrk_hat = M_hat(r,k);
            mri_hat = M_hat(r,i);

            sum_terms = sum_terms + ...
               br*(-mri_bar*w_rk - ...
               mri_hat*theta_rk*br/6 - ...
                (mri_bar*mrk_bar+1/15*mri_hat*mrk_hat)*br^2/(12*Kr));
        end
        D3(k,i) = ny/G*sum_terms;
    end
end
```

The $\boldsymbol{K}$-matrix defined in (4.140):

```
K = zeros(size(U_III,2),size(U_III,2));
for k = 1:size(U_III,2)
    for i = 1:size(U_III,2)
        sum_terms = 0;
        for r = 1:nrOfElements
            element = elements(r).Value;
            br = element.width;
            tr = element.thickness;
            v_rk = Fv(r,:)*U_III (:,k);
            v_ri = Fv(r,:)*U_III (:,i);
            w_rk = Fw(r,:)*U_III (:,k);
            w_ri = Fw(r,:)*U_III (:,k);

            sum_terms = sum_terms +...
              (v_rk*v_ri+w_rk*w_ri)*br*tr;
        end
        K(k,i) = sum_terms;
    end
end
K = -1/A*K;
```

Appendix C **Analogy between the rod and GBT differential equation**

This chapter shows the analogy between the rod equation which is a second order differential equation and the first deformation mode which is a forth order differential equation. The physical meaning of the two extra boundary conditions needed in order to solve the GBT fundamental differential equation is here stated and evaluated.

The rod differential equation

The rod-equation is defined and stated below for a member with an arbitrary and constant cross-section and elastic modulus.

$$EAu_{,xx} = -q_x \tag{C.1}$$

In order to have a solution to (C.1) integrate the equation twice:

$$EAu_{,x} = -q_x x + C_1 \tag{C.2}$$

$$EAu = -q_x \frac{x^2}{2} + C_1 x + C_2 \tag{C.3}$$

Two integration constants are obtained, hence two boundary conditions is needed in order to have complete determined variation along the member. There are two types of boundary conditions, namely essential and natural boundary conditions.

To have a representative comparison between the rod equation and the GBT fundamental equation an example is introduced, see Figure C.1.

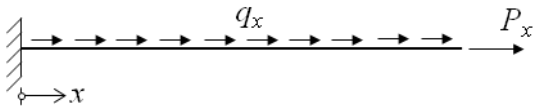

Figure C.1: This example is used in order to have a representative comparison between the rod equation and the GBT fundamental equation. The rod is subjected to a uniform load q_x and a point force P_x at $x = L$ and is clamped at $x = 0$.

The associated boundary conditions for the clamped rod are given as:

$$u(0) = 0 \tag{C.4}$$

$$EAu_{,x}(L) = P_x \tag{C.5}$$

The first boundary condition gives that $C_2 = 0$ and the other gives that $C_1 = P_x + q_x L$. The u-displacement variation along the member is then defined as:

$$u(x) = \frac{1}{EA}\left[-q_x \frac{x^2}{2} + (P_x + q_x L)x\right] \tag{C.6}$$

The GBT equation for the first deformation mode

The GBT fundamental equation is defined in (4.151). For the first deformation mode $(k = 1)$ it appears that $\tilde{D}_1$, $\tilde{B}_1$ and $\tilde{q}_1$ is zero, hence the only non-zero terms are $\tilde{C}_1$ and $\tilde{q}_{x.1,x}$. The warping function for the first mode is defined as $\tilde{u}_1 = -1$ which gives that $u(x)$ and $\tilde{q}_{x.1,x}$ are defined as:

$$u(x) = \tilde{u}_1 \tilde{\phi}_{1,x}(x) = -\tilde{\phi}_{1,x}(x) \tag{C.7}$$

$$q_{x.1,x} = q_{x,x} \tilde{u}_1 = -q_{x,x} \tag{C.8}$$

Insert all conditions for the first mode into the GBT equation gives:

$$E\tilde{C}_1 \tilde{\phi}_{1,xxxx} = q_{x,x} \tag{C.9}$$

This equation is a forth order differential equation and must be integrated four times:

$$E\tilde{C}_1 \tilde{\phi}_{1,xxx} = q_x + C_1 \tag{C.10}$$

$$E\tilde{C}_1 \tilde{\phi}_{1,xx} = (q_x + C_1)x + C_2 \tag{C.11}$$

$$E\tilde{C}_1 \tilde{\phi}_{1,x} = (q_x + C_1)\frac{x^2}{2} + C_2 x + C_3 \tag{C.12}$$

$$E\tilde{C}_1 \tilde{\phi}_1 = (q_x + C_1)\frac{x^3}{6} + C_2 \frac{x^2}{2} + C_3 x + C_4 \tag{C.13}$$

Four boundary conditions are needed in order to have a complete description of the variation in the amplitude function $\tilde{\phi}_1$ along the member. However, since for the first deformation mode only the u-displacements is of interest (the v- and w-displacements are by definition zero) there is only a need of determine the first derivative of the amplitude function $\tilde{\phi}_{1,x}$, hence three boundary conditions is needed. The forth integration constant can therefore be left undefined since it will not contribute to the variation of u-displacements along the member. From Figure C.1 two boundary conditions are obtained by simply translate them to the GBT notations as:

$$u(0) = 0 \quad \Rightarrow \quad -\tilde{\phi}_{1,x}(0) = 0 \tag{C.14}$$

$$EAu_{,x}(L) = P_x \quad \Rightarrow \quad -E\tilde{C}_1 \tilde{\phi}_{1,xx}(L) = P_x \tag{C.15}$$

The third condition is obtained by equilibrium condition of an infinitesimal part of the rod. The third condition is then given as:

$$N_{,x} = -q_x \quad \Rightarrow \quad -E\tilde{C}_1 \tilde{\phi}_{1,xxx} = -q_x \tag{C.16}$$

Utilize the third condition to determine the C_1-constant by inserting (C.16) into (C.10). It appears that the C_1-constant must be zero in order to fulfil the equilibrium condition as:

$$N_{,x} = -E\tilde{C}_1 \tilde{\phi}_{,xxx} = -(q_x + C_1) = -q_x \quad \Rightarrow \quad C_1 = 0 \tag{C.17}$$

Apply the first boundary condition (C.14) on (C.12). From this condition the C_3-constant must also be zero in order to be fulfilled:

$$-\tilde{\phi}_{1,x}(0) = -\frac{1}{E\tilde{C}_1}C_3 = 0 \quad \Rightarrow \quad C_3 = 0 \tag{C.18}$$

The last constant is determined by using the boundary load term (C.15) and introducing it into (C.11). The C_2-constant is then obtained as:

$$-E\tilde{C}_1\tilde{\phi}_{1,xx}(L) = -[q_x L + C_2] = P_x \quad \Rightarrow \quad C_2 = -(P_x + q_x L) \tag{C.19}$$

The variation in u-displacement along the member is then obtained by inserting the integration constants C_1 (C.17), C_2 (C.19) and C_3 (C.18) into (C.12) gives:

$$\tilde{\phi}_{1,x} = \frac{1}{E\tilde{C}_1}\left[q_x\frac{x^2}{2} - (P_x + q_x L)x\right] \tag{C.20}$$

$$u(x) = -\tilde{\phi}_{1,x} = \frac{1}{E\tilde{C}_1}\left[-q_x\frac{x^2}{2} + (P_x + q_x L)x\right] \tag{C.21}$$

Expression (C.21) is the same as (C.6) derived using the rod-equation, hence the analogy between the two equations are proofed and there are only two boundary conditions with physical meaning in order to solve the GBT fundamental differential equation for the first mode. The other two conditions are simply just to get rid of integration constants.

Another interesting comparison could be by relating the first deformation mode and its quantities to known beam quantities, see Figure C.2.

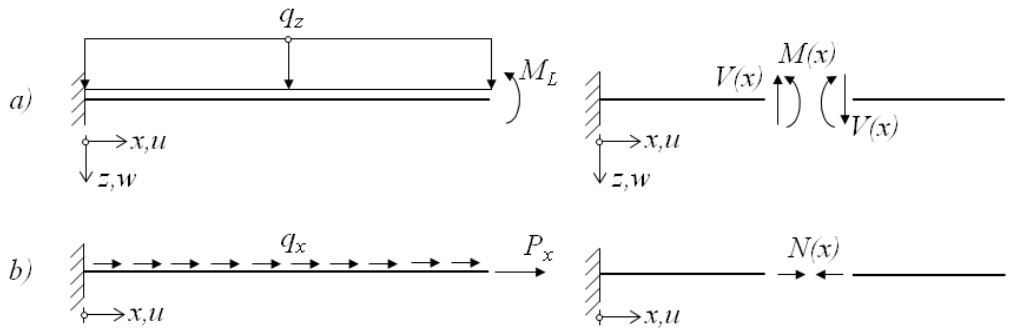

Figure C.2: The analogy between the GBT equation for the first deformation mode and the Euler-Bernoulli equation. a) Illustrates a cantilevering beam subjected to a uniformly distributed load q_z and a point moment M_L together with its sectional forces. b) Illustrates a clamped rod subjected to uniformly distributed load q_x and a point load P_x together with its sectional force.

The GBT quantities for the first deformation mode and the corresponding beam quantities are tabulated in Table C.1 below. One can read that the u-displacements corresponds to the slope of the beam deflections $w_{,x}$, the normal force $N(x)$ to the bending moments $M(x)$, the uniformly distributed load q_x to the shear force distribution $V(x)$ and a concentrated point force P_x to a point moment M_L.

Table C.1: This table contains the GBT differential equation according to the first deformation mode and its corresponding quantities and the ordinary Euler-Bernoulli beam equation with its corresponding quantities, both related to the members defined in Figure C.2

GBT, deformation mode 1	Euler-Bernoulli beam
$E\tilde{C}_1\tilde{\phi}_{1,xxxx} = -\tilde{q}_{x.1,x} = q_{x,x}$	$-EI_z w_{,xxxx} = q_Z$
$E\tilde{C}_1\tilde{\phi}_{1,xxx} = q_x$	$EI_z w_{,xxx} = V(x)$
$-E\tilde{C}_1\tilde{\phi}_{1,xx} = \widetilde{W}(x) = N(x)$	$EI_z w_{,xx} = M(x)$
$-E\tilde{C}_1\tilde{\phi}_{1,xx}(L) = P_x$	$EI_z w_{,xx}(L) = M_L$
$u(0) = -\tilde{\phi}_{1,x}(0) = 0$	$w_{,x}(0) = 0$
–	$w(0) = 0$

Appendix D **Finite element solution**

This appendix will show the theory behind the FEM implementation used by the authors when solving the GBT equation for each mode. Note that the procedure to perform this is analogue with the one for beam on elastic foundation.

The transformed and uncoupled GBT equation

The uncoupled GBT differential equation (4.151) is derived in Section 4.6 and is redefined here as:

$$E\tilde{C}_k\tilde{\phi}_{k,xxxx} - G\tilde{D}_k\tilde{\phi}_{k,xx} + \tilde{B}_k\tilde{\phi}_k = \tilde{q}_k - \tilde{q}_{x.k,x} \tag{D.1}$$

The weak form

The first step in the finite element approach is to rewrite the uncoupled GBT-equation on weak form. This is obtained by multiplication of an arbitrary weight-function $v(x)$ and integration over the member length as shown below:

$$\int_0^L v\left[E\tilde{C}_k\tilde{\phi}_{k,xxxx} - G\tilde{D}_k\tilde{\phi}_{k,xx} + \tilde{B}_k\tilde{\phi}_k\right]dx = \int_0^L v\tilde{q}_k\,dx - \int_0^L v\tilde{q}_{x.k,x}\,dx \tag{D.2}$$

The next step is to carry out the integration such that the same order of derivatives on the weight-function $v(x)$ and the amplitude function $\tilde{\phi}(x)$ is obtained. Integration by parts on the terms gives:

$$\begin{aligned}\int_0^L vE\tilde{C}_k\tilde{\phi}_{k,xxxx}\,dx &= \left[vE\tilde{C}_k\tilde{\phi}_{k,xxx}\right]_0^L - \int_0^L v_{,x}E\tilde{C}_k\tilde{\phi}_{k,xxx}\,dx \\ &= \left[vE\tilde{C}_k\tilde{\phi}_{k,xxx}\right]_0^L - \left[v_{,x}E\tilde{C}_k\tilde{\phi}_{k,xx}\right]_0^L + \int_0^L v_{,xx}E\tilde{C}_k\tilde{\phi}_{k,xx}\,dx\end{aligned} \tag{D.3}$$

$$\int_0^L vG\tilde{D}_k\tilde{\phi}_{k,xx}\,dx = \left[vG\tilde{D}_k\tilde{\phi}_{k,x}\right]_0^L - \int_0^L v_{,x}G\tilde{D}_k\tilde{\phi}_{k,x}\,dx \tag{D.4}$$

$$\int_0^L v\tilde{q}_{xk,x}\,dx = [v\tilde{q}_{x.k}]_0^L - \int_0^L v_{,x}\tilde{q}_{x.k}\,dx \tag{D.5}$$

The weak form of the differential equation is then formulated by putting all terms together as:

$$\int_0^L v_{,xx} E\tilde{C}_k \tilde{\phi}_{k,xx}\, dx + \int_0^L v_{,x} G\widetilde{D}_k \tilde{\phi}_{k,x}\, dx + \int_0^L v\tilde{B}_k \tilde{\phi}_k\, dx$$

$$= \int_0^L v\tilde{q}_k\, dx + \int_0^L v_{,x}\tilde{q}_{x.k}\, dx - \left[vE\tilde{C}_k \tilde{\phi}_{k,xxx}\right]_0^L \tag{D.6}$$

$$+ \left[v_{,x} E\tilde{C}_k \tilde{\phi}_{k,xx}\right]_0^L + \left[vG\widetilde{D}_k \tilde{\phi}_{k,x}\right]_0^L - \left[v\tilde{q}_{x.k}\right]_0^L$$

Finite element approximation

Once the weak form of the equation is known, the finite element approximation could be introduced. Discretize the member into a number of finite elements and nodes. The amplitude function $\tilde{\phi}_k$ is then determined by the nodal values and the variation within the elements are defined by element shape functions. The amplitude function is discretized as:

$$\tilde{\phi}_k(x) = \boldsymbol{N}(x) \cdot \boldsymbol{a}_k \tag{D.7}$$

Where $\boldsymbol{N}(x)$ is a vector containing the element shape functions, one per degree of freedom and $\boldsymbol{a}$ is a vector containing all the nodal degrees of freedom. The arbitrary weight-function is chosen according to Galerkin's method presented in [26] defined as:

$$v(x) = \boldsymbol{N}(x) \cdot \boldsymbol{c} \tag{D.8}$$

Where $\boldsymbol{N}(x)$ is the shape function vector and $\boldsymbol{c}$ is a vector contain arbitrary chosen constants.

Insert the finite element approximations into the weak form (D.6). Since it is only the shape functions $\boldsymbol{N}(x)$ that vary with x the $\boldsymbol{a}_k$- and $\boldsymbol{c}$-vectors can be left outside the integrals. This give:

$$\boldsymbol{c}^T \left[E\tilde{C}_k \int_0^L \boldsymbol{N}_{,xx}^T \boldsymbol{N}_{,xx}\, dx + G\widetilde{D}_k \int_0^L \boldsymbol{N}_{,x}^T \boldsymbol{N}_{,x}\, dx + \tilde{B}_k \int_0^L \boldsymbol{N}^T \boldsymbol{N} dx \right] \boldsymbol{a}_k$$

$$= \boldsymbol{c}^T \left[\int_0^L \boldsymbol{N}^T \tilde{q}_k\, dx + \int_0^L \boldsymbol{N}_{,x}^T \tilde{q}_{x.k}\, dx - \left[\boldsymbol{N}^T E\tilde{C}_k \tilde{\phi}_{k,xxx}\right]_0^L \right. \tag{D.9}$$

$$\left. + \left[\boldsymbol{N}_{,x}^T E\tilde{C}_k \tilde{\phi}_{k,xx}\right]_0^L + \left[\boldsymbol{N}^T G\widetilde{D}_k \tilde{\phi}_{k,x}\right]_0^L - \left[\boldsymbol{N}^T \tilde{q}_{x.k}\right]_0^L \right]$$

Since $\boldsymbol{c}$-vector only consist arbitrary constants it can be neglected and the final finite element approximation can be written as:

$$\left[E\tilde{C}_k\boldsymbol{K}_{\tilde{C}} + G\tilde{D}_k\boldsymbol{K}_{\tilde{D}} + \tilde{B}_k\boldsymbol{K}_{\tilde{B}}\right]\boldsymbol{a}_k = \boldsymbol{f}_{q.k} + \boldsymbol{f}_{qx.k} + \boldsymbol{f}_{b.k} \tag{D.10}$$

Where $\boldsymbol{K}_{\tilde{C}}$, $\boldsymbol{K}_{\tilde{D}}$ and $\boldsymbol{K}_{\tilde{B}}$ are global stiffness matrices and the three global loading vectors $\boldsymbol{f}_{q.k}$, $\boldsymbol{f}_{qx.k}$ and $\boldsymbol{f}_{b.k}$ correspond to the applied modal loads and boundary loads respectively. They are defined as:

$$\boldsymbol{K}_{\tilde{C}} = \int_0^L \boldsymbol{N}_{,xx}^T\boldsymbol{N}_{,xx}\,dx \qquad \boldsymbol{K}_{\tilde{D}} = \int_0^L \boldsymbol{N}_{,x}^T\boldsymbol{N}_{,x}\,dx \qquad \boldsymbol{K}_{\tilde{B}} = \int_0^L \boldsymbol{N}^T\boldsymbol{N}dx \tag{D.11}$$

$$\boldsymbol{f}_{q.k} = \tilde{q}_k\int_0^L \boldsymbol{N}^T dx \qquad \boldsymbol{f}_{qx.k} = \tilde{q}_{x.k}\int_0^L \boldsymbol{N}_{,x}^T dx \tag{D.12}$$

$$\begin{aligned}\boldsymbol{f}_{b.k} = -\left[\boldsymbol{N}^T E\tilde{C}_k\tilde{\phi}_{k,xxx}\right]_0^L + \left[\boldsymbol{N}_{,x}^T E\tilde{C}_k\tilde{\phi}_{k,xx}\right]_0^L + \left[\boldsymbol{N}^T G\tilde{D}_k\tilde{\phi}_{k,x}\right]_0^L \\ - \left[\boldsymbol{N}^T\tilde{q}_{x.k}\right]_0^L\end{aligned} \tag{D.13}$$

Evaluation of the element stiffness matrices

The global stiffness matrices defined in (D.11) is obtained by assembling element stiffness matrices $\boldsymbol{K}_{\tilde{C}}^e$, $\boldsymbol{K}_{\tilde{D}}^e$ and $\boldsymbol{K}_{\tilde{B}}^e$. In order to calculate the element stiffness matrices, the shape functions must be defined in first place. The differential equation (D.1) reminds on the equation for a beam on elastic foundation, hence finite beam elements will be used. These contain four degrees of freedom per element or two per node. The finite element approximation for one element is then defined as:

$$\tilde{\phi}_k(x) = \boldsymbol{N}^e(x)\cdot\boldsymbol{a}_k^e \tag{D.14}$$

Where the element shape function vector is defined as:

$$\boldsymbol{N}^e(x) = \begin{bmatrix}N_1^e(x) & N_2^e(x) & N_3^e(x) & N_4^e(x)\end{bmatrix} \tag{D.15}$$

And the element degrees of freedom vector is defined as the nodal value and the nodal slope of the amplitude function as:

$$\boldsymbol{a}_k^e = \begin{bmatrix}\tilde{\phi}_{k.1} & \tilde{\phi}_{k.1,x} & \tilde{\phi}_{k.2} & \tilde{\phi}_{k.2,x}\end{bmatrix} \tag{D.16}$$

The superscript $(\cdot)^e$ is introduced to indicate that they are related to one finite element. The shape functions are derived by means of the C-method [26].

Those shape functions are defined below together with the first and second derivative respectively.

$$
\begin{aligned}
N_1^e &= 1 - 3\frac{x^2}{L_e^2} + 2\frac{x^3}{L_e^3} & N_{1,x}^e &= -\frac{6x(L_e - x)}{L_e^3} & N_{1,xx}^e &= -\frac{6\,(L_e - 2\,x)}{L_e^3} \\
N_2^e &= x\left(1 - 2\frac{x}{L_e} + \frac{x^2}{L_e^2}\right) & N_{2,x}^e &= \frac{(L_e - 3\,x)(L_e - x)}{L_e^2} & N_{2,xx}^e &= \frac{6\,x - 4\,L_e}{L_e^2} \\
N_3^e &= \frac{x^2}{L_e^2}\left(3 - 2\frac{x}{L_e}\right) & N_{3,x}^e &= \frac{6\,x(L_e - x)}{L_e^3} & N_{3,xx}^e &= \frac{6\,(L_e - 2\,x)}{L_e^3} \\
N_4^e &= \frac{x^2}{L_e}\left(\frac{x}{L_e} - 1\right) & N_{4,x}^e &= \frac{x(3\,x - 2\,L_e)}{L_e^2} & N_{4,xx}^e &= -\frac{2\,(L_e - 3\,x)}{L_e^2}
\end{aligned}
\tag{D.17}
$$

The finite element stiffness matrices $\boldsymbol{K}_{\tilde{C}}^e$, $\boldsymbol{K}_{\tilde{D}}^e$ and $\boldsymbol{K}_{\tilde{B}}^e$ can now be completely determined by performing the vector multiplication and integration over the element length L_e gives:

$$
\boldsymbol{K}_{\tilde{C}}^e = \int_0^{L_e} \begin{bmatrix} N_{1,xx}^e N_{1,xx}^e & N_{1,xx}^e N_{2,xx}^e & N_{1,xx}^e N_{3,xx}^e & N_{1,xx}^e N_{4,xx}^e \\ N_{2,xx}^e N_{1,xx}^e & N_{2,xx}^e N_{2,xx}^e & N_{2,xx}^e N_{3,xx}^e & N_{2,xx}^e N_{4,xx}^e \\ N_{3,xx}^e N_{1,xx}^e & N_{3,xx}^e N_{2,xx}^e & N_{3,xx}^e N_{3,xx}^e & N_{3,xx}^e N_{4,xx}^e \\ N_{4,xx}^e N_{1,xx}^e & N_{4,xx}^e N_{2,xx}^e & N_{4,xx}^e N_{3,xx}^e & N_{4,xx}^e N_{4,xx}^e \end{bmatrix} dx \tag{D.18}
$$

$$
\boldsymbol{K}_{\tilde{D}}^e = \int_0^{L_e} \begin{bmatrix} N_{1,x}^e N_{1,x}^e & N_{1,x}^e N_{2,x}^e & N_{1,x}^e N_{3,x}^e & N_{1,x}^e N_{4,x}^e \\ N_{2,x}^e N_{1,x}^e & N_{2,x}^e N_{2,x}^e & N_{2,x}^e N_{3,x}^e & N_{2,x}^e N_{4,x}^e \\ N_{3,x}^e N_{1,x}^e & N_{3,x}^e N_{2,x}^e & N_{3,x}^e N_{3,x}^e & N_{3,x}^e N_{4,x}^e \\ N_{4,x}^e N_{1,x}^e & N_{4,x}^e N_{2,x}^e & N_{4,x}^e N_{3,x}^e & N_{4,x}^e N_{4,x}^e \end{bmatrix} dx \tag{D.19}
$$

$$
\boldsymbol{K}_{\tilde{B}}^e = \int_0^{L_e} \begin{bmatrix} N_1^e N_1^e & N_1^e N_2^e & N_1^e N_3^e & N_1^e N_4^e \\ N_2^e N_1^e & N_2^e N_2^e & N_2^e N_3^e & N_2^e N_4^e \\ N_3^e N_1^e & N_3^e N_2^e & N_3^e N_3^e & N_3^e N_4^e \\ N_4^e N_1^e & N_4^e N_2^e & N_4^e N_3^e & N_4^e N_4^e \end{bmatrix} dx \tag{D.20}
$$

Evaluating these integrals results in the following programmable matrices:

$$
\boldsymbol{K}_{\tilde{C}}^e = \begin{bmatrix} \frac{12}{L_e^3} & \frac{6}{L_e^2} & -\frac{12}{L_e^3} & \frac{6}{L_e^2} \\ \frac{6}{L_e^2} & \frac{4}{L_e} & -\frac{6}{L_e^2} & \frac{2}{L_e} \\ -\frac{12}{L_e^3} & -\frac{6}{L_e^2} & \frac{12}{L_e^3} & -\frac{6}{L_e^2} \\ \frac{6}{L_e^2} & \frac{2}{L_e} & -\frac{6}{L_e^2} & \frac{4}{L_e} \end{bmatrix} \tag{D.21}
$$

$$\boldsymbol{K}^e_{\tilde{D}} = \begin{bmatrix} \frac{6}{5L_e} & \frac{1}{10} & -\frac{6}{5L_e} & \frac{1}{10} \\ \frac{1}{10} & \frac{2L_e}{15} & -\frac{1}{10} & -\frac{L_e}{30} \\ -\frac{6}{5L_e} & -\frac{1}{10} & \frac{6}{5L_e} & -\frac{1}{10} \\ \frac{1}{10} & -\frac{L_e}{30} & -\frac{1}{10} & \frac{2L_e}{15} \end{bmatrix} \tag{D.22}$$

$$\boldsymbol{K}^e_{\tilde{B}} = \begin{bmatrix} \frac{13L_e}{35} & \frac{11L_e^2}{210} & \frac{9L_e}{70} & -\frac{13L_e^2}{420} \\ \frac{11L_e^2}{210} & \frac{L_e^3}{105} & \frac{13L_e^2}{420} & -\frac{L_e^3}{140} \\ \frac{9L_e}{70} & \frac{13L_e^2}{420} & \frac{13L_e}{35} & -\frac{11L_e^2}{210} \\ -\frac{13L_e^2}{420} & -\frac{L_e^3}{140} & -\frac{11L_e^2}{210} & \frac{L_e^3}{105} \end{bmatrix} \tag{D.23}$$

The finite element loading vectors

The global loading vectors $\boldsymbol{f}_{q.k}$ and $\boldsymbol{f}_{qx.k}$ defined in (D.12) can be determined by assemble the element loading vectors $\boldsymbol{f}^e_{q.k}$ and $\boldsymbol{f}^e_{qx.k}$ in a similar way as the for the stiffness matrices. The element loading vectors is determined by integration over the element length L_e as:

$$\boldsymbol{f}^e_{q.k} = \tilde{q}_k \int_0^{L_e} \begin{bmatrix} N_1 \\ N_2 \\ N_3 \\ N_4 \end{bmatrix} dx = \tilde{q}_k \begin{bmatrix} \frac{L_e}{2} \\ \frac{L_e^2}{12} \\ \frac{L_e}{2} \\ -\frac{L_e^2}{12} \end{bmatrix} \tag{D.24}$$

$$\boldsymbol{f}^e_{qx.k} = \tilde{q}_{x.k} \int_0^{L_e} \begin{bmatrix} N_{1,x} \\ N_{2,x} \\ N_{3,x} \\ N_{4,x} \end{bmatrix} dx = \tilde{q}_{x.k} \begin{bmatrix} -1 \\ 0 \\ 1 \\ 0 \end{bmatrix} \tag{D.25}$$

In case of a point force the loading term cannot be left outside the integral since the Dirac's delta function depends on x, hence the element load vector for an applied point force P acting at $x = x_P$ is obtained as:

$$\boldsymbol{f}^e_{q.k} = \int_0^{L_e} \tilde{q}_k \begin{bmatrix} N_1 \\ N_2 \\ N_3 \\ N_4 \end{bmatrix} dx = \int_{x_P^-}^{x_P^+} \tilde{q}_k \begin{bmatrix} N_1 \\ N_2 \\ N_3 \\ N_4 \end{bmatrix} dx = (P_s \tilde{v}_{k.r} + P_z \tilde{w}_{k.r}) \begin{bmatrix} N_1(x_P) \\ N_2(x_P) \\ N_3(x_P) \\ N_4(x_P) \end{bmatrix} \tag{D.26}$$

$$\boldsymbol{f}^e_{qx.k} = \int_0^{L_e} \tilde{q}_{x.k} \begin{bmatrix} N_{1,x} \\ N_{2,x} \\ N_{3,x} \\ N_{4,x} \end{bmatrix} dx = \int_{x_P^-}^{x_P^+} \tilde{q}_{x.k} \begin{bmatrix} N_{1,x} \\ N_{2,x} \\ N_{3,x} \\ N_{4,x} \end{bmatrix} dx = P_x \tilde{u}_{k.r} \begin{bmatrix} N_{1,x}(x_P) \\ N_{2,x}(x_P) \\ N_{3,x}(x_P) \\ N_{4,x}(x_P) \end{bmatrix} \tag{D.27}$$

Where the modal loads are defined as $\tilde{q}_k = \delta(x - x_P)(P_s \tilde{v}_{k.r} + P_z \tilde{w}_{k.r}) = \delta(X - X_P)\left(P_Y \tilde{V}_{k.r} + P_Z \widetilde{W}_{k.r}\right)$ and $\tilde{q}_{x.k} = \delta(x - x_P) P_x \tilde{u}_{k.r} = \delta(X - X_P) P_X \widetilde{U}_{k.r}$ depending if the loads are defined in the local (x, s, z)-coordinate system or the global (X, Y, Z)-coordinate system, see Section 4.6.2.2

The finite element boundary load vector $\boldsymbol{f}_{k.b}$ defined in (D.13) can be developed further by inserting the respective coordinates $x = 0$ and $x = L_e$ into the expressions:

$$\begin{aligned} \boldsymbol{f}_{b.k} = & -\left[\boldsymbol{N}^T E \tilde{C}_k \tilde{\phi}_{k,xxx}\right]_0^L + \left[\boldsymbol{N}_{,x}^T E \tilde{C}_k \tilde{\phi}_{k,xx}\right]_0^L + \left[\boldsymbol{N}^T G \widetilde{D}_k \tilde{\phi}_{k,x}\right]_0^L \\ & - \left[\boldsymbol{N}^T \tilde{q}_{x.k}\right]_0^L \\ & = -\left[\left(\boldsymbol{N}^T(L) E \tilde{C}_k \tilde{\phi}_{k,xxx}(L)\right) - \left(\boldsymbol{N}^T(0) E \tilde{C}_k \tilde{\phi}_{k,xxx}(0)\right)\right] \\ & + \left[\left(\boldsymbol{N}_{,x}^T(L) E \tilde{C}_k \tilde{\phi}_{k,xx}(L)\right) - \left(\boldsymbol{N}_{,x}^T(0) E \tilde{C}_k \tilde{\phi}_{k,xx}(0)\right)\right] \\ & + \left[\left(\boldsymbol{N}^T(L) G \widetilde{D}_k \tilde{\phi}_{k,x}(L)\right) - \left(\boldsymbol{N}^T(0) G \widetilde{D}_k \tilde{\phi}_{k,x}(0)\right)\right] \\ & - \left[\left(\boldsymbol{N}^T(L) \tilde{q}_{x.k}\right) - \left(\boldsymbol{N}^T(0) \tilde{q}_{x.k}\right)\right] \\ & = \begin{bmatrix} E \tilde{C}_k \tilde{\phi}_{k,xxx}(0) - G \widetilde{D}_k \tilde{\phi}_{k,x}(0) + \tilde{q}_{x.k}(0) \\ -E \tilde{C}_k \tilde{\phi}_{k,xx}(0) \\ 0 \\ \vdots \\ 0 \\ -E \tilde{C}_k \tilde{\phi}_{k,xxx}(L) + G \widetilde{D}_k \tilde{\phi}_{k,x}(L) - \tilde{q}_{x.k}(L) \\ E \tilde{C}_k \tilde{\phi}_{k,xx}(L) \end{bmatrix} \end{aligned} \tag{D.28}$$

Introduce the sectional forces and the boundary load vector is obtained as:

$$\boldsymbol{f}_{b.k} = \begin{bmatrix} -\widetilde{W}_{k,x}(0) - G\widetilde{D}_k\tilde{\phi}_{k,x}(0) + \tilde{q}_{x.k}(0) \\ \widetilde{W}_k(0) \\ 0 \\ \vdots \\ 0 \\ \widetilde{W}_{k,x}(L) + G\widetilde{D}_k\tilde{\phi}_{k,x}(L) - \tilde{q}_{x.k}(L) \\ -\widetilde{W}_k(L) \end{bmatrix} \tag{D.29}$$

The transformed and coupled GBT equation

The transformed and coupled GBT differential equation is written on the form:

$$E\widetilde{\boldsymbol{C}}\widetilde{\boldsymbol{\phi}}_{,xxxx} - G\widetilde{\boldsymbol{D}}\widetilde{\boldsymbol{\phi}}_{,xx} + \widetilde{\boldsymbol{B}}\widetilde{\boldsymbol{\phi}} = \widetilde{\boldsymbol{q}} - \widetilde{\boldsymbol{q}}_{x,x} \tag{D.30}$$

Where the $\widetilde{\boldsymbol{B}}$, $\widetilde{\boldsymbol{C}}$ and $\widetilde{\boldsymbol{D}}$ are the transformed GBT matrices. The $\widetilde{\boldsymbol{B}}$- and $\widetilde{\boldsymbol{C}}$-matrix are completely diagonalized in the simultaneous diagonalization process, see Section 4.5.1. The $\widetilde{\boldsymbol{D}}$-matrix will still have some non-zero off-diagonal terms which means that the differential equation (D.1) will still be coupled.

The weak form

The same procedure is carried out as for an uncoupled differential equation, namely rewriting the differential on the weak form. Multiply with an arbitrary weight-function $\boldsymbol{v}(x)$ which is defined in a vector and finally integrate over the length. The weak form of the coupled differential equation is obtained as:

$$\begin{aligned} &\int_0^L \boldsymbol{v}_{,xx} E\widetilde{\boldsymbol{C}}\widetilde{\boldsymbol{\phi}}_{,xx}\,dx + \int_0^L \boldsymbol{v}_{,x} G\widetilde{\boldsymbol{D}}\widetilde{\boldsymbol{\phi}}_{,x}\,dx + \int_0^L \boldsymbol{v}\widetilde{\boldsymbol{B}}\widetilde{\boldsymbol{\phi}}\,dx \\ &\qquad = \int_0^L \boldsymbol{v}\widetilde{\boldsymbol{q}}\,dx + \int_0^L \boldsymbol{v}_{,x}\widetilde{\boldsymbol{q}}_x\,dx - \left[\boldsymbol{v}E\widetilde{\boldsymbol{C}}\widetilde{\boldsymbol{\phi}}_{,xxx}\right]_0^L + \left[\boldsymbol{v}_{,x}E\widetilde{\boldsymbol{C}}\widetilde{\boldsymbol{\phi}}_{,xx}\right]_0^L \\ &\qquad + \left[\boldsymbol{v}G\widetilde{\boldsymbol{D}}\widetilde{\boldsymbol{\phi}}_{,x}\right]_0^L - \left[\boldsymbol{v}\widetilde{\boldsymbol{q}}_x\right]_0^L \end{aligned} \tag{D.31}$$

Finite element approximation

Introduce the finite element approximation into the weak form. The amplitude function $\widetilde{\boldsymbol{\phi}}$ and the weight-function is approximated as for the uncoupled case, namely:

$$\widetilde{\boldsymbol{\phi}}(x) = \boldsymbol{N}(x) \cdot \boldsymbol{a}^{tot} \tag{D.32}$$

$$\boldsymbol{v}(x) = \boldsymbol{N}(x) \cdot \boldsymbol{c} \tag{D.33}$$

Insert the finite element approximation into weak form which gives:

$$\boldsymbol{c}^T\left[E\widetilde{\boldsymbol{C}}\int_0^L \boldsymbol{N}_{,xx}^T\boldsymbol{N}_{,xx}dx + G\widetilde{\boldsymbol{D}}\int_0^L \boldsymbol{N}_{,x}^T\boldsymbol{N}_{,x}dx + \widetilde{\boldsymbol{B}}\int_0^L \boldsymbol{N}^T\boldsymbol{N}dx\right]\boldsymbol{a}^{tot}$$
$$= \boldsymbol{c}^T\left[\int_0^L \boldsymbol{N}^T\widetilde{\boldsymbol{q}}dx + \int_0^L \boldsymbol{N}_{,x}^T\widetilde{\boldsymbol{q}}_x dx - \left[\boldsymbol{N}^T E\widetilde{\boldsymbol{C}}\widetilde{\boldsymbol{\phi}}_{,xxx}\right]_0^L\right. \tag{D.34}$$
$$\left. + \left[\boldsymbol{N}_{,x}^T E\widetilde{\boldsymbol{C}}\widetilde{\boldsymbol{\phi}}_{,xx}\right]_0^L + \left[\boldsymbol{N}^T G\widetilde{\boldsymbol{D}}\widetilde{\boldsymbol{\phi}}_{,x}\right]_0^L - \left[\boldsymbol{N}^T\widetilde{\boldsymbol{q}}_x\right]_0^L\right]$$

Since the $\boldsymbol{c}$-vector only consists of arbitrary constants it can be cancelled out since the expression within the parentheses will hold any way. The final finite element approximation of the differential equation can then be written as:

$$\left[\boldsymbol{K}_{\tilde{C}}^{tot} + \boldsymbol{K}_{\tilde{D}}^{tot} + \boldsymbol{K}_{\tilde{B}}^{tot}\right]\boldsymbol{a}^{tot} = \boldsymbol{q}^{tot} \tag{D.35}$$

The finite element stiffness matrices are here defined as:

$$\boldsymbol{K}_{\tilde{C}}^{tot} = \begin{bmatrix} E\tilde{C}_{11}\boldsymbol{K}_{\tilde{C}}^{11} & & \boldsymbol{0} \\ & \ddots & \\ \boldsymbol{0} & & E\tilde{C}_{nn}\boldsymbol{K}_{\tilde{C}}^{nn} \end{bmatrix} \tag{D.36}$$

$$\boldsymbol{K}_{\tilde{D}}^{tot} = \begin{bmatrix} G\widetilde{D}_{11}\boldsymbol{K}_{\tilde{D}}^{11} & \cdots & G\widetilde{D}_{1n}\boldsymbol{K}_{\tilde{D}}^{1n} \\ \vdots & \ddots & \vdots \\ G\widetilde{D}_{n1}\boldsymbol{K}_{\tilde{D}}^{n1} & \cdots & G\widetilde{D}_{nn}\boldsymbol{K}_{\tilde{D}}^{nn} \end{bmatrix} \tag{D.37}$$

$$\boldsymbol{K}_{\tilde{B}}^{tot} = \begin{bmatrix} \tilde{B}_{11}\boldsymbol{K}_{\tilde{B}}^{11} & & \boldsymbol{0} \\ & \ddots & \\ \boldsymbol{0} & & \tilde{B}_{nn}\boldsymbol{K}_{\tilde{B}}^{nn} \end{bmatrix} \tag{D.38}$$

Where the sub-matrices $\boldsymbol{K}_{\tilde{C}}^{kk}$, $\boldsymbol{K}_{\tilde{D}}^{kj}$ and $\boldsymbol{K}_{\tilde{B}}^{kk}$ are the global finite element stiffness matrices corresponding to deformation mode j and k. The subscript and superscript$n$ stands for total number of deformation modes. The global stiffness matrices are assembled from the element stiffness matrices $\boldsymbol{K}_{\tilde{C}}^{e}$, $\boldsymbol{K}_{\tilde{D}}^{e}$ and $\boldsymbol{K}_{\tilde{B}}^{e}$ which are defined in (D.21), (D.22) and (D.23) respectively.

The total solution vector $\boldsymbol{a}^{tot}$ contain all modal solutions $\boldsymbol{a}_k$ which contains all degrees of freedom of the approximated amplitude function $\tilde{\phi}_k$. The vector is defined as:

$$\boldsymbol{a}^{tot} = [\boldsymbol{a}_1 \quad \cdots \quad \boldsymbol{a}_n]^T \tag{D.39}$$

The total load vector $\boldsymbol{q}^{tot}$ is defined in the same way as the solution vector, namely each the modal load vectors are stated after each other as:

$$\boldsymbol{q}^{tot} = \left[\left(\boldsymbol{f}_{q.1} + \boldsymbol{f}_{qx.1} + \boldsymbol{f}_{b.1}\right) \quad \cdots \quad \left(\boldsymbol{f}_{q.n} + \boldsymbol{f}_{qx.n} + \boldsymbol{f}_{b.n}\right)\right]^T \tag{D.40}$$

Where the load vectors are defined as in (D.12) and (D.13).

Extraction of modal results

Once the equation system is solved and the solution vector $\boldsymbol{a}_k$ is determined, the amplitude functions $\tilde{\phi}_k(x)$ and $\tilde{\phi}_{k,x}(x)$ are obtained as:

$$\tilde{\phi}_k(x) = \boldsymbol{N}(x) \cdot \boldsymbol{a}_k \qquad \tilde{\phi}_{k,x}(x) = \boldsymbol{N}_{,x}(x) \cdot \boldsymbol{a}_k \tag{D.41}$$

And the sectional forces $\widetilde{W}_k(x)$ and $\widetilde{W}_{k,x}(x)$ are obtained as:

$$\widetilde{W}_k(x) = E\tilde{C}_k \boldsymbol{N}_{,xx}(x) \cdot \boldsymbol{a}_k \qquad \widetilde{W}_{k,x}(x) = E\tilde{C}_k \boldsymbol{N}_{,xxx}(x) \cdot \boldsymbol{a}_k \tag{D.42}$$

Appendix E **Beam theory analogies to GBT**

Table E.1: This table contain the analogies between the four fundamental beam theories and there corresponding quantities and how the notations is handled in the GBT for the corresponding deformation mode k

Process	Elongation	Bending 1	Bending 2	Warping Torsion	GBT
Deformation	u	v	w	ϑ	$\tilde{\phi}_k$
Unit warping function	-1	$-y$	$-z$	ω	$\tilde{u}_k$
Warping function	u	$u = -yv_{,x}$	$u = -zw_{,x}$	$u = \omega\vartheta_{,x}$	$u_k = \tilde{u}_k\tilde{\phi}_{k,x}$
Area	$A = \int_A dA$				$\tilde{C}_{ik} = \int_A \tilde{u}_i\tilde{u}_k dA$ $\tilde{C}_k = \int_A \tilde{u}_k^2 dA$
First moment of inertia		$S_1 = \int_A ydA$	$S_2 = \int_A zdA$		
Second moment of inertia		$I_1 = \int_A y^2 dA$	$I_2 = \int_A z^2 dA$		
Warping stiffness constant				$C_M = \int_A \omega^2 dA$	
Cross-sectional forces	$N = \int_A \sigma dA$	$M_1 = \int_A \sigma y dA$	$M_2 = \int_A \sigma z dA$	$W = -\int_A \sigma\omega dA$	$\widetilde{W}_k = -\int_A \sigma\tilde{u}_k dA$
Elasticity (Hook's law)	$N = EAu_{,x}$	$M_1 = -EI_1v_{,xx}$	$M_2 = -EI_2w_{,xx}$	$W = -EC_M\vartheta_{,xx}$	$\widetilde{W}_k = -E\tilde{C}_k\tilde{\phi}_{k,xx}$
Normal stresses	$\sigma_N = \frac{N}{A}$	$\sigma_1 = \frac{M_1}{I_1}y$	$\sigma_2 = \frac{M_2}{I_2}z$	$\sigma_\vartheta = -\frac{W}{C_M}\omega$	$\sigma_k = -\frac{\widetilde{W}_k}{\tilde{C}_k}\tilde{u}_k$
Shear stresses		$\tau_1(s) = \frac{Q_1S_1}{I_1t(s)}$	$\tau_2(s) = \frac{Q_2S_2}{I_2t(s)}$	$\tau_\vartheta(s) = \frac{W_{,x}\int_0^s \omega dA}{C_M t(s)}$	$\tau_k(s) = \frac{\widetilde{W}_{k,x}\int_0^s \tilde{u}_k dA}{\tilde{C}_k t(s)}$
Differantial equation	$(EAu_{,x})_{,x} = -q_x$	$(EI_1v_{,xx})_{,xx} = q_1$	$(EI_2w_{,xx})_{,xx} = q_2$	$(EC_M\vartheta_{,xx})_{,xx} - (GI_D\vartheta_{,x})_{,x} = m_D$	$(E\tilde{C}_k\tilde{\phi}_{k,xx})_{,xx} - (G\tilde{D}_k\tilde{\phi}_{k,x})_{,x} + \tilde{B}_k\tilde{\phi}_k = \tilde{q}_k - \tilde{q}_{x.k,x}$

Appendix F **Application of GBT– Results**

This appendix presents the numerical results of the Z-profile from the three major steps in GBT, namely the cross-section analysis, the member analysis and the GBT solution. The cross-section analysis is a fundamental part of GBT, therefore this step is carried out twice where one case is by only considering natural nodes and one case when three intermediate nodes are imposed. In the member analysis and GBT solution there is no difference in procedure of how the cross-section is discretized, hence only the results for the case of intermediate nodes are presented. But instead two cases of solutions of the GBT fundamental equation is tabulated, namely the solution to the uncoupled and the solution to the coupled equation.

Cross-sectional analysis

The cross-section analysis is carried out for two cases, one for only natural nodes and one for the case of three imposed intermediate nodes.

Only natural nodes considered

Table F.1 to Table F.6 presents each deformation mode in terms of the global nodal $\widetilde{U}_r$, $\widetilde{V}_r$ and $\widetilde{W}_r$ displacement components, the local nodal transverse bending moment $\widetilde{m}_{s.r}$, the element $\tilde{v}_r$, $\tilde{w}_r$, $\tilde{\vartheta}_r$ displacement components together with the element shear force $\tilde{S}_r$. Note that the same subscript $(\cdot)_r$ is used to denote either which node or which plate element the corresponding value is associated with. The table also contains the diagonal terms in the transformed GBT $\widetilde{\boldsymbol{C}}$-, $\widetilde{\boldsymbol{D}}$- and $\widetilde{\boldsymbol{B}}$-matrices which then spans the decoupled GBT fundamental equation.

Table F.1: Characteristics of deformation mode 1

Node r	$\widetilde{U}_r$	$\widetilde{V}_r$	$\widetilde{W}_r$	$\tilde{v}_r$	$\tilde{w}_r$	$\tilde{\vartheta}_r$	$\widetilde{m}_{s.r}$	$\tilde{S}_r$
1	-1	0	0	0	0	0	0	-0.2891
2	-1	0	0	0	0	0	0	-6.1357
3	-1	0	0	0	0	0	0	-97.9350
4	-1	0	0	0	0	0	0	-51.4290
5	-1	0	0	0	0	0	0	-13.7110
6	-1	0	0	-	-	-	0	-
$\tilde{C}_1$ = 396.6300				$\widetilde{D}_1 = 0$			$\tilde{B}_1 = 0$	

Table F.2: Characteristics of deformation mode 2

Node r	$\widetilde{U}_r$	$\widetilde{V}_r$	$\widetilde{W}_r$	$\tilde{v}_r$	$\tilde{w}_r$	$\tilde{\vartheta}_r$	$\widetilde{m}_{s.r}$	$\tilde{S}_r$
1	97.9670	-0.2292	0.9734	-0.9734	0.2292	0	0	0.0047
2	111.5900	-0.2292	0.9734	0.2292	0.9734	0	0	0.1044
3	99.6780	-0.2292	0.9734	0.9734	-0.2292	0	0	0.9827
4	-95.0000	-0.2292	0.9734	0.2292	0.9734	0	0	0.1248
5	-108.5200	-0.2292	0.9734	-0.9734	0.2292	0	0	0.0046
6	-94.8930	-0.2292	0.9734	-	-	-	0	-
$\tilde{C}_2$ = 2485600.0000				$\widetilde{D}_2 = 0$			$\tilde{B}_2 = 0$	

Table F.3: Characteristics of deformation mode 3

Node r	$\tilde{U}_r$	$\tilde{V}_r$	$\tilde{W}_r$	$\tilde{v}_r$	$\tilde{w}_r$	$\tilde{\vartheta}_r$	$\tilde{m}_{s.r}$	$\tilde{S}_r$
1	31.8320	-0.9734	-0.2292	0.2292	0.9734	0	0	0.0318
2	28.6240	-0.9734	-0.2292	0.9734	-0.2292	0	0	0.4003
3	-21.9920	-0.9734	-0.2292	-0.2292	-0.9734	0	0	-0.1603
4	23.8400	-0.9734	-0.2292	0.9734	-0.2292	0	0	0.5728
5	-33.5900	-0.9734	-0.2292	0.2292	0.9734	0	0	0.0370
6	-36.7990	-0.9734	-0.2292	-	-	-	0	-
$\tilde{C}_3 = 110750.0000$				$\tilde{D}_3 = 0$			$\tilde{B}_3 = 0$	

Table F.4: Characteristics of deformation mode 4

Node r	$\tilde{U}_r$	$\tilde{V}_r$	$\tilde{W}_r$	$\tilde{v}_r$	$\tilde{w}_r$	$\tilde{\vartheta}_r$	$\tilde{m}_{s.r}$	$\tilde{S}_r$
1	5292.8000	-103.7700	-54.0660	54.0660	110.7700	1	0	0.0003
2	4535.9000	-117.7700	-54.0660	117.7700	-28.0660	1	0	0.0048
3	-1588.1000	-117.7700	-2.0656	-2.0656	-17.7680	1	0	0.0001
4	-1174.9000	82.2320	-2.0656	-82.2320	27.4340	1	0	-0.0048
5	3676.7000	82.2320	56.9340	-56.9340	-75.2320	1	0	-0.0003
6	4473.8000	68.2320	56.9340	-	-	-	0	-
$\tilde{C}_4$ = 1685100000				$\tilde{D}_4 = 180.9800$			$\tilde{B}_4 = 0$	

Table F.5: Characteristics of deformation mode 5

Node r	$\tilde{U}_r$	$\tilde{V}_r$	$\tilde{W}_r$	$\tilde{v}_r$	$\tilde{w}_r$	$\tilde{\vartheta}_r$	$\tilde{m}_{s.r}$	$\tilde{S}_r$
1	-0.3870	-0.0134	0.0358	-0.0358	0.0081	-0.0007	0	-3.5555
2	0.1146	-0.0029	0.0358	0.0029	0.0177	-0.0007	0	-1.8953
3	-0.0348	-0.0029	-0.0004	-0.0004	-0.0043	0	-0.1868	-12.8570
4	0.0528	-0.0058	-0.0004	0.0058	0.0458	0.0016	-0.5431	1.7064
5	-0.2886	-0.0058	0.0920	-0.0920	0.0180	0.0017	0	-9.2301
6	1	-0.0302	0.0920	-	-	-	0	-
$\tilde{C}_5 = 7.0868$				$\tilde{D}_5 = 0.0002$			$\tilde{B}_5 = 0.0010$	

Table F.6: Characteristics of deformation mode 6

Node r	$\tilde{U}_r$	$\tilde{V}_r$	$\tilde{W}_r$	$\tilde{v}_r$	$\tilde{w}_r$	$\tilde{\vartheta}_r$	$\tilde{m}_{s.r}$	$\tilde{S}_r$
1	1	0.0351	-0.0941	0.0941	-0.0210	0.0020	0	8.9386
2	-0.3177	0.0069	-0.0941	-0.0069	-0.0470	0.0018	0	-3.2873
3	0.0395	0.0069	0.0002	0.0002	0.0025	0	0.7175	5.5176
4	-0.0002	-0.0019	0.0002	0.0019	0.0178	0.0006	-0.3097	3.3915
5	-0.1132	-0.0019	0.0353	-0.0353	0.0068	0.0007	0	-3.4484
6	0.3811	-0.0116	0.0353	-	-	-	0	-
$\tilde{C}_6 = 7.1932$				$\tilde{D}_6 = 0.0002$			$\tilde{B}_6 = 0.0015$	

Imposition of three intermediate nodes

Table F.7 to Table F.17 below present the characteristics for each deformation mode, in the same fashion as for the case of natural nodes. Note that for deformation mode $k = 1, 2, 3, 4$ the GBT $\tilde{C}, \widetilde{D}$ and $\tilde{B}$ constants are identical to the case when only natural nodes are considered. Node $r = 3, 5, 7$ are the imposed intermediate nodes.

Table F.7: Characteristics of deformation mode 1

Node r	$\widetilde{U}_r$	$\widetilde{V}_r$	$\widetilde{W}_r$	$\tilde{v}_r$	$\tilde{w}_r$	$\tilde{\vartheta}_r$	$\tilde{m}_{s.r}$	$\tilde{S}_r$
1	-1	0	0	0	0	0	0	-0.2891
2	-1	0	0	0	0	0	0	-2.0708
3	-1	0	0	0	0	0	0	-4.0649
4	-1	0	0	0	0	0	0	-34.2180
5	-1	0	0	0	0	0	0	-63.7170
6	-1	0	0	0	0	0	0	-24.4310
7	-1	0	0	0	0	0	0	-26.9980
8	-1	0	0	0	0	0	0	-13.7110
9	-1	0	0	-	-	-	0	-
$\tilde{C}_1 = 396.63$				$\widetilde{D}_1 = 0$			$\tilde{B}_1 = 0$	

Table F.8: Characteristics of deformation mode 2

Node r	$\widetilde{U}_r$	$\widetilde{V}_r$	$\widetilde{W}_r$	$\tilde{v}_r$	$\tilde{w}_r$	$\tilde{\vartheta}_r$	$\tilde{m}_{s.r}$	$\tilde{S}_r$
1	-97.9670	0.2292	-0.9734	0.9734	-0.2292	0	0	-0.0047
2	-111.590	0.2292	-0.9734	-0.2292	-0.9734	0	0	-0.0354
3	-105.640	0.2292	-0.9734	-0.2292	-0.9734	0	0	-0.0690
4	-99.6780	0.2292	-0.9734	-0.9734	0.2292	0	0	-0.4858
5	-2.3388	0.2292	-0.9734	-0.9734	0.2292	0	0	-0.4969
6	95.0000	0.2292	-0.9734	-0.2292	-0.9734	0	0	-0.0832
7	101.7600	0.2292	-0.9734	-0.2292	-0.9734	0	0	-0.0415
8	108.5200	0.2292	-0.9734	0.9734	-0.2292	0	0	-0.0046
9	94.8930	0.2292	-0.9734	-	-	-	0	-
$\tilde{C}_2$ = 2485600.0000				$\widetilde{D}_2 = 0$			$\tilde{B}_2 = 0$	

Table F.9: Characteristics of deformation mode 3

Node r	$\widetilde{U}_r$	$\widetilde{V}_r$	$\widetilde{W}_r$	$\tilde{v}_r$	$\tilde{w}_r$	$\tilde{\vartheta}_r$	$\tilde{m}_{s.r}$	$\tilde{S}_r$
1	31.8320	-0.9734	-0.2292	0.2292	0.9734	0	0	0.0318
2	28.6240	-0.9734	-0.2292	0.9734	-0.2292	0	0	0.1883
3	3.3160	-0.9734	-0.2292	0.9734	-0.2292	0	0	0.2120
4	-21.9920	-0.9734	-0.2292	-0.2292	-0.9734	0	0	-0.1289
5	0.9237	-0.9734	-0.2292	-0.2292	-0.9734	0	0	-0.0313
6	23.8400	-0.9734	-0.2292	0.9734	-0.2292	0	0	0.3088
7	-4.8754	-0.9734	-0.2292	0.9734	-0.2292	0	0	0.2640
8	-33.5900	-0.9734	-0.2292	0.2292	0.9734	0	0	0.0370
9	-36.7990	-0.9734	-0.2292	-	-	-	0	-
$\tilde{C}_3$ = 110750.0				$\widetilde{D}_3 = 0$			$\tilde{B}_3 = 0$	

Table F.10: Characteristics of deformation mode 4

Node r	$\tilde{U}_r$	$\tilde{V}_r$	$\tilde{W}_r$	$\tilde{v}_r$	$\tilde{w}_r$	$\tilde{\vartheta}_r$	$\tilde{m}_{s.r}$	$\tilde{S}_r$
1	5292.8000	-103.7700	-54.0660	54.0660	110.7700	1	0	0.0003
2	4535.9000	-117.7700	-54.0660	117.7700	-41.0660	1	0	0.0021
3	1473.9000	-117.7700	-28.0660	117.7700	-15.0660	1	0	0.0028
4	-1588.1000	-117.7700	-2.0656	-2.0656	-67.7680	1	0	0.0048
5	-1381.5000	-17.7680	-2.0656	-2.0656	32.2320	1	0	-0.0048
6	-1174.9000	82.2320	-2.0656	-82.2320	12.6840	1	0	-0.0028
7	1250.9000	82.2320	27.4340	-82.2320	42.1840	1	0	-0.0020
8	3676.7000	82.2320	56.9340	-56.9340	-75.2320	1	0	-0.0003
9	4473.8000	68.2320	56.9340	-	-	-	0	-
$\tilde{C}_4$ = 685100000.0000			$\tilde{D}_4 = 180.9800$				$\tilde{B}_4 = 0$	

Table F.11: Characteristics of deformation mode 5

Node r	$\tilde{U}_r$	$\tilde{V}_r$	$\tilde{W}_r$	$\tilde{v}_r$	$\tilde{w}_r$	$\tilde{\vartheta}_r$	$\tilde{m}_{s.r}$	$\tilde{S}_r$
1	-0.6897	-0.0235	0.0643	-0.0643	0.0142	-0.0013	0	-4.9364
2	0.2101	-0.0050	0.0643	0.0050	0.0473	-0.0013	0	-3.9871
3	0.0807	-0.0050	0.0304	0.0050	0.0149	-0.0012	-0.1358	3.0595
4	-0.0488	-0.0050	-0.0005	-0.0005	-0.0349	-0.0006	-0.2727	-9.1802
5	0.0047	-0.0649	-0.0005	-0.0005	-0.0354	0.0006	-0.3679	-3.0523
6	0.0583	-0.0059	-0.0005	0.0059	0.0210	0.0015	-0.4529	6.8407
7	-0.1148	-0.0059	0.0425	0.0059	0.0673	0.0017	-0.2257	-6.0662
8	-0.2878	-0.0059	0.0920	-0.0920	0.0179	0.0017	0	-7.2285
9	1	-0.0298	0.0920	-	-	-	0	-
$\tilde{C}_5$ = 9.0532			$\tilde{D}_5 = 0.0002$				$\tilde{B}_5 = 0.0011$	

Table F.12: Characteristics of deformation mode 6

Node r	$\tilde{U}_r$	$\tilde{V}_r$	$\tilde{W}_r$	$\tilde{v}_r$	$\tilde{w}_r$	$\tilde{\vartheta}_r$	$\tilde{m}_{s.r}$	$\tilde{S}_r$
1	1	0.0361	-0.0943	0.0943	-0.0215	0.0021	0	6.9301
2	-0.3199	0.0068	-0.0943	-0.0068	-0.0680	0.0020	0.0001	4.4934
3	-0.1428	0.0068	-0.0416	-0.0068	-0.0208	0.0016	0.4964	-7.6975
4	0.0343	0.0068	0.0001	0.0001	0.0128	0.0001	0.9960	-14.1560
5	0.0241	0.0188	0.0001	0.0001	0.0075	-0.0002	0.1070	16.2530
6	0.0139	-0.0037	0.0001	0.0037	0.0132	0.0009	-0.7894	6.7938
7	-0.0941	-0.0037	0.0263	0.0037	0.0449	0.0013	-0.3938	-3.5467
8	-0.2021	-0.0037	0.0636	-0.0636	0.0130	0.0013	0	-4.8424
9	0.6880	-0.0222	0.0636	-	-	-	0	-
$\tilde{C}_6 = 9.2657$			$\tilde{D}_6 = 0.0002$				$\tilde{B}_6 = 0.0028$	

Table F.13: Characteristics of deformation mode 7

Node r	$\tilde{U}_r$	$\tilde{V}_r$	$\tilde{W}_r$	$\tilde{v}_r$	$\tilde{w}_r$	$\tilde{\vartheta}_r$	$\tilde{m}_{s.r}$	$\tilde{S}_r$
1	-0.0940	-0.0527	0.0093	-0.0093	0.0268	-0.0037	0	-0.4700
2	0.0358	-0.0009	0.0093	0.0009	-0.0272	-0.0028	0.1276	-0.0967
3	0.0133	-0.0009	-0.0638	0.0009	-0.0319	0.0024	-6.7344	0.7529
4	-0.0092	-0.0009	-0.0001	-0.0001	0.4996	0.0100	-10.5570	-0.2682
5	-0.0003	1	-0.0001	-0.0001	0.4997	-0.0100	14.3830	-0.5431
6	0.0086	-0.0006	-0.0001	0.0006	-0.0406	-0.0027	-9.9889	0.7314
7	-0.0099	-0.0006	-0.0811	0.0006	-0.0367	0.0030	-6.5469	-0.0813
8	-0.0284	-0.0006	0.0077	-0.0077	0.0286	0.0040	0.1312	-0.4027
9	0.0794	-0.0565	0.0077	-	-	-	0	-
$\tilde{C}_7$ = 12.3800			$\tilde{D}_7 = 0.0183$				$\tilde{B}_7 = 0.5131$	

Table F.14: Characteristics of deformation mode 8

Node r	$\tilde{U}_r$	$\tilde{V}_r$	$\tilde{W}_r$	$\tilde{v}_r$	$\tilde{w}_r$	$\tilde{\vartheta}_r$	$\tilde{m}_{s.r}$	$\tilde{S}_r$
1	-0.0357	-0.4555	0.0035	-0.0035	0.2279	-0.0325	0	-0.1864
2	0.0128	-0.0003	0.0035	0.0003	-0.2755	-0.0215	0.9819	-0.0608
3	0.0057	-0.0003	-0.5545	0.0003	-0.2772	0.0213	-81.5860	0.3175
4	-0.0013	-0.0003	0	0	0.0425	0.0009	21.2490	0.6672
5	-0.0015	0.0853	0	0	0.0428	-0.0009	5.4958	-0.8074
6	-0.0017	0.0003	0	-0.0003	0.5000	0.0339	-40.0780	-0.4216
7	0.0069	0.0003	1	-0.0003	0.4976	-0.0341	115.5600	0.1654
8	0.0155	0.0003	-0.0047	0.0047	-0.3795	-0.0542	3.5363	0.2715
9	-0.0505	0.7587	-0.0047	-	-	-	0	-
$\tilde{C}_8$ = 12.0220			$\tilde{D}_8 = 0.1475$			$\tilde{B}_8 = 13.2410$		

Table F.15: Characteristics of deformation mode 9

Node r	$\tilde{U}_r$	$\tilde{V}_r$	$\tilde{W}_r$	$\tilde{v}_r$	$\tilde{w}_r$	$\tilde{\vartheta}_r$	$\tilde{m}_{s.r}$	$\tilde{S}_r$
1	0.0397	0.9210	-0.0038	0.0038	-0.4607	0.0658	0	0.2597
2	-0.0131	0.0003	-0.0038	-0.0003	0.4981	0.0386	14.7720	0.1497
3	-0.0056	0.0003	1	-0.0003	0.5000	-0.0385	147.6000	-0.3043
4	0.0019	0.0003	0	0	0.1887	0.0038	-57.3800	-0.4220
5	0.0003	0.3772	0	0	0.1887	-0.0038	28.1800	-0.0351
6	-0.0013	0.0001	0	-0.0001	0.3741	0.0254	-41.4090	-0.1383
7	0.0029	0.0001	0.7483	-0.0001	0.3730	-0.0254	85.5120	0.1623
8	0.0070	0.0001	-0.0023	0.0023	-0.3320	-0.0474	17.6470	0.1724
9	-0.0255	0.6638	-0.0023	-	-	-	0	-
$\tilde{C}_9 = 9.7490$			$\tilde{D}_9 = 0.1869$			$\tilde{B}_9 = 20.3500$		

Table F.16: Characteristics of deformation mode 10

Node r	$\tilde{U}_r$	$\tilde{V}_r$	$\tilde{W}_r$	$\tilde{v}_r$	$\tilde{w}_r$	$\tilde{\vartheta}_r$	$\tilde{m}_{s.r}$	$\tilde{S}_r$
1	-0.0003	0.4700	0.0001	-0.0001	-0.2350	0.0336	0	-0.0005
2	0.0006	0	0.0001	0	0.0156	0.0012	79.8620	0.2766
3	0.0003	0	0.0312	0	0.0156	-0.0012	-15.6010	0.5023
4	-0.0001	0	0	0	0.0142	0.0003	-0.4151	1.2581
5	-0.0002	0.0284	0	0	0.0142	-0.0003	2.3596	-1.3419
6	-0.0004	0	0	0	0.0239	0.0016	-7.9750	-1.0010
7	0.0004	0	0.0477	0	0.0238	-0.0016	50.1090	-0.5926
8	0.0012	0	-0.0001	0.0001	0.5000	0.0714	-172.170	0.0041
9	-0.0006	-1	-0.0001	-	-	-	0	-
$\tilde{C}_{10}$ = 0.9892			$\tilde{D}_{10} = 0.0558$			$\tilde{B}_{10} = 15.3050$		

Table F.17: Characteristics of deformation mode 11

Node r	$\tilde{U}_r$	$\tilde{V}_r$	$\tilde{W}_r$	$\tilde{v}_r$	$\tilde{w}_r$	$\tilde{\vartheta}_r$	$\tilde{m}_{s.r}$	$\tilde{S}_r$
1	0.0032	-1	-0.0004	0.0004	0.5000	-0.0714	0	0.1758
2	-0.0022	0.0001	-0.0004	-0.0001	0.0378	0.0029	-191.640	-0.4898
3	-0.0007	0.0001	0.0760	-0.0001	0.0380	-0.0029	61.0680	-1.1239
4	0.0007	0.0001	0	0	0.0311	0.0006	-10.9940	-0.7518
5	0.0001	0.0622	0	0	0.0311	-0.0006	5.2788	0.7850
6	-0.0005	0	0	0	0.0387	0.0026	-7.8239	-0.3973
7	0.0002	0	0.0774	0	0.0386	-0.0026	30.4620	-0.2023
8	0.0008	0	-0.0002	0.0002	0.2148	0.0307	-81.1130	0.0741
9	-0.0013	-0.4297	-0.0002	-	-	-	0	-
$\tilde{C}_{11} = 0.9241$			$\tilde{D}_{11} = 0.0541$			$\tilde{B}_{11} = 17.5440$		

Member analysis

Here follows the solutions to the uncoupled and coupled GBT fundamental equation in terms of the modal amplitude function $\tilde{\phi}_k$, $\tilde{\phi}_{k,x}$ and in terms of the modal sectional force $\widetilde{W}_k$, $\widetilde{W}_{k,x}$.

Uncoupled solution

The uncoupled solution is tabulated in terms of the modal amplitude function $\tilde{\phi}_k(X)$ and $\tilde{\phi}_{k.x}(X)$ in Table F.18 and in terms of the sectional force $\widetilde{W}_k(X)$ and $\widetilde{W}_{k,x}(X)$ in Table F.*19.* The values are given at four different positions along the beam; at the first support, in the middle and at the quarter points. Note that $\widetilde{W}_k(X)$ and $\widetilde{W}_{k.x}(X)$ for deformation mode two and three can be interpret as the moment and shear distribution along the member respectively.

Table F.18: The solution to the uncoupled GBT fundamental equation is in this table expressed in terms of the modal amplitude function $\tilde{\phi}_k(X)$ and its first ordered derivative $\tilde{\phi}_{k,x}(X)$ at the sections $X = 0, 0.25L, 0.5L$ and $0.75L$.

Mode k	$\tilde{\phi}_k(X)$				$\tilde{\phi}_{k.x}(X)$			
	$X = 0$	$0.25L$	$0.5L$	$0.75L$	$X = 0$	$0.25L$	$0.5L$	$0.75L$
1	0	1.29E-12	2.39E-12	1.35E-12	0	3.02E-15	-1.11E-25	-2.99E-15
2	0	4.36E-01	8.10E-01	4.56E-01	0	1.02E-03	-1.33E-14	-1.01E-03
3	0	2.30E00	4.28E00	2.41E00	0	5.41E-03	-1.24E-14	-5.35E-03
4	0	1.35E-03	2.51E-03	1.41E-03	0	3.17E-06	-3.66E-17	-3.14E-06
5	0	1.77E00	2.06E00	1.81E00	0	1.70E-03	-7.62E-15	-1.56E-03
6	0	-1.52E-01	-1.54E-01	-1.54E-01	0	-6.92E-05	-3.90E-16	5.76E-05
7	0	1.50E-03	1.50E-03	1.50E-03	0	-1.03E-09	1.68E-21	6.29E-10
8	0	-1.02E-04	-1.02E-04	-1.02E-04	0	-4.27E-16	-5.77E-22	1.83E-16
9	0	-2.15E-04	-2.15E-04	-2.15E-04	0	-5.02E-16	0	2.16E-16
10	0	-1.35E-05	-1.35E-05	-1.35E-05	0	-1.33E-22	4.43E-23	4.43E-23
11	0	-2.33E-05	-2.33E-05	-2.33E-05	0	-9.02E-23	-9.02E-23	-9.02E-23

Table F.19: The solution to the uncoupled GBT fundamental equation is in this table expressed in terms of the modal sectional force $\widetilde{W}_k(X)$ and its first ordered derivative $\widetilde{W}_{k,x}(X)$ at the sections $X = 0, 0.25L, 0.5L$ and $0.75L$.

Mode k	$\widetilde{W}_k(X)$				$\widetilde{W}_{k.x}(X)$			
	$X = 0$	$0.25L$	$0.5L$	$0.75L$	$X = 0$	$0.25L$	$0.5L$	$0.75L$
1	-1.11E-09	1.10E-10	5.54E-10	1.39E-10	2.75E-12	1.41E-12	-2.31E-14	-1.41E-12
2	-2.35E06	2.34E05	1.18E06	2.94E05	5.83E03	2.99E03	-4.90E01	-2.99E03
3	-5.53E05	5.51E04	2.77E05	6.92E04	1.37E03	7.03E02	-1.15E01	-7.03E02
4	-4.95E06	4.95E05	2.47E06	6.20E05	1.23E04	6.27E03	-1.02E02	-6.27E03
5	-8.94E01	1.40E01	4.59E-01	1.34E01	6.46E-01	-3.26E-02	7.26E-04	3.26E-02
6	1.12E01	-1.18E00	1.19E-01	-1.07E00	-9.75E-02	5.66E-03	-2.18E-05	-5.66E-03
7	-1.68E00	-6.30E-05	-7.08E-10	-4.19E-05	5.06E-02	1.06E-06	6.09E-14	-1.06E-06
8	5.08E-01	-4.37E-11	-6.80E-16	-1.79E-11	-2.82E-02	1.29E-12	2.19E-17	-1.29E-12
9	1.13E00	-4.15E-11	2.39E-16	-1.70E-11	-6.88E-02	1.22E-12	-3.58E-17	-1.22E-12
10	1.53E-02	-9.20E-19	9.20E-19	1.84E-18	-1.18E-03	8.25E-19	-1.38E-19	-2.76E-19
11	2.69E-02	-1.75E-18	-1.75E-18	-1.75E-18	-2.12E-03	2.63E-19	2.63E-19	2.63E-19

Coupled solution

The coupled solution is tabulated in terms of the modal amplitude function $\tilde{\phi}_k(X)$ and $\tilde{\phi}_{k.x}(X)$ in Table F.20 and in terms of the sectional force $\widetilde{W}_k(X)$ and $\widetilde{W}_{k,x}(X)$ in

Table F.21. The values are given at the same four sections along the beam as for the uncoupled case so that the coupling influence can be evaluated.

Table F.20: The solution to the coupled GBT fundamental equation is in this table expressed in terms of the modal amplitude function $\tilde{\phi}_k(X)$ and its first ordered derivative $\tilde{\phi}_{k,x}(X)$ at the sections $X = 0$, $0.25L$, $0.5L$ and $0.75L$.

Mode k	$\tilde{\phi}_k(X)$				$\tilde{\phi}_{k.x}(X)$			
	$X = 0$	$0.25L$	$0.5L$	$0.75L$	$X = 0$	$0.25L$	$0.5L$	$0.75L$
1	0	1.26E-12	2.34E-12	1.32E-12	0	2.96E-15	-6.05E-26	-2.93E-15
2	0	4.36E-01	8.10E-01	4.56E-01	0	1.02E-03	2.06E-14	-1.01E-03
3	0	2.30E00	4.28E00	2.41E00	0	5.41E-03	-3.77E-14	-5.35E-03
4	0	1.35E-03	2.51E-03	1.41E-03	0	3.17E-06	6.45E-17	-3.14E-06
5	0	1.73E00	1.83E00	1.75E00	0	1.27E-03	4.73E-14	-1.12E-03
6	0	-1.46E-01	-1.44E-01	-1.46E-01	0	-4.96E-05	-9.19E-15	3.94E-05
7	0	2.83E-03	2.16E-03	2.81E-03	0	-1.09E-06	7.05E-17	1.32E-06
8	0	-9.01E-05	-5.78E-05	-8.80E-05	0	1.05E-07	1.26E-17	-1.01E-07
9	0	-2.02E-04	-2.14E-04	-2.03E-04	0	-2.93E-08	9.52E-18	3.04E-08
10	0	-1.86E-05	3.27E-06	-1.74E-05	0	5.94E-08	-1.17E-17	-5.96E-08
11	0	-9.04E-06	1.55E-04	1.22E-06	0	5.20E-07	-2.86E-17	-5.06E-07

Table F.21: The solution to the coupled GBT fundamental equation is in this table expressed in terms of the modal sectional force $\widetilde{W}_k(X)$ and its first ordered derivative $\widetilde{W}_{k,x}(X)$ at the sections $X = 0$, $0.25L$, $0.5L$ and $0.75L$.

Mode k	$\widetilde{W}_k(X)$				$\widetilde{W}_{k.x}(X)$			
	$X = 0$	$0.25L$	$0.5L$	$0.75L$	$X = 0$	$0.25L$	$0.5L$	$0.75L$
1	-1.08E-09	1.08E-10	5.42E-10	1.35E-10	2.69E-12	1.38E-12	-2.27E-14	-1.38E-12
2	-2.35E06	2.34E05	1.18E06	2.94E05	5.83E03	2.99E03	-4.90E01	-2.99E03
3	-5.53E05	5.51E04	2.77E05	6.92E04	1.37E03	7.03E02	-1.15E01	-7.03E02
4	-4.95E06	4.94E05	2.47E06	6.20E05	1.23E04	6.26E03	-1.02E02	-6.26E03
5	-9.71E01	1.50E01	-1.85E00	1.41E01	7.42E-01	-4.41E-02	8.46E-04	4.41E-02
6	1.20E01	-1.05E00	1.22E-01	-9.38E-01	-1.14E-01	5.78E-03	-1.19E-05	-5.78E-03
7	3.96E00	3.25E-02	-9.17E-03	2.54E-02	-1.54E-01	-3.55E-04	-1.23E-06	3.55E-04
8	9.58E-01	4.85E-04	4.34E-04	4.70E-04	-5.36E-02	-7.90E-07	-5.74E-09	7.90E-07
9	1.53E00	1.44E-04	-1.15E-04	9.52E-05	-9.45E-02	-2.44E-06	-1.14E-08	2.44E-06
10	7.03E-03	-3.60E-06	2.51E-05	7.29E-08	-5.84E-05	1.84E-07	2.80E-10	-1.84E-07
11	2.85E-01	1.25E-04	1.64E-04	1.34E-04	-2.20E-02	4.10E-07	2.16E-09	-4.10E-07

GBT solution

Here follows the numerical values of the GBT results. The nodal U_r, V_r and W_r displacements and stresses σ_x and τ_{xs} are defined at the quarter sections $X = 0$, $0.25L$, $0.5L$ and $0.75L$ for both the uncoupled and the coupled GBT fundamental equation. The nodal displacements are tabulated in Table F.22, Table F.23 and Table F.24. The nodal stresses are tabulated in Table F.25.

Table F.22: The total nodal U_r-displacements at the sections $X = 0$, $0.25L$, $0.5L$ and $0.75L$ calculated for both the uncoupled and coupled GBT fundamental equation expressed in [mm].

Node r	$U_r(X)$ uncoupled				$U_r(X)$ coupled			
	$X = 0$	$0.25L$	$0.5L$	$0.75L$	$X = 0$	$0.25L$	$0.5L$	$0.75L$
1	0	0.0870	0	-0.0866	0	0.0873	0	-0.0869
2	0	0.0551	0	-0.0548	0	0.0549	0	-0.0546
3	0	-0.0850	0	0.0845	0	-0.0850	0	0.0846
4	0	-0.2250	0	0.2238	0	-0.2249	0	0.2237
5	0	-0.0018	0	0.0018	0	-0.0018	0	0.0018
6	0	0.2214	0	-0.2203	0	0.2214	0	-0.2202
7	0	0.0812	0	-0.0807	0	0.0812	0	-0.0808
8	0	-0.0591	0	0.0588	0	-0.0590	0	0.0586
9	0	-0.0857	0	0.0853	0	-0.0861	0	0.0857

Table F.23: The total nodal V_r-displacements at the sections $X = 0$, $0.25L$, $0.5L$ and $0.75L$ calculated for both the uncoupled and coupled GBT fundamental equation expressed in [mm].

Node r	$V_r(X)$ uncoupled				$V_r(X)$ coupled			
	$X = 0$	$0.25L$	$0.5L$	$0.75L$	$X = 0$	$0.25L$	$0.5L$	$0.75L$
1	0	-2.3816	-4.2976	-2.4352	0	-2.3800	-4.2916	-2.4335
2	0	-2.3631	-4.2898	-2.4168	0	-2.3626	-4.2883	-2.4163
3	0	-2.3631	-4.2898	-2.4168	0	-2.3626	-4.2883	-2.4163
4	0	-2.3631	-4.2898	-2.4168	0	-2.3626	-4.2883	-2.4163
5	0	-2.3325	-4.1627	-2.3841	0	-2.3275	-4.1463	-2.3787
6	0	-2.0867	-3.7878	-2.1341	0	-2.0863	-3.7863	-2.1337
7	0	-2.0867	-3.7878	-2.1341	0	-2.0863	-3.7863	-2.1337
8	0	-2.0867	-3.7878	-2.1341	0	-2.0863	-3.7863	-2.1337
9	0	-2.1464	-3.8698	-2.1946	0	-2.1449	-3.8629	-2.1930

Table F.24: The total nodal W_r-displacements at the sections $X = 0$, $0.25L$, $0.5L$ and $0.75L$ calculated for both the uncoupled and coupled GBT fundamental equation expressed in [mm].

Node r	$W_r(X)$ uncoupled				$W_r(X)$ coupled			
	$X = 0$	$0.25L$	$0.5L$	$0.75L$	$X = 0$	$0.25L$	$0.5L$	$0.75L$
1	0	-0.9188	-1.7589	-0.9416	0	-0.9228	-1.7749	-0.9459
2	0	-0.9188	-1.7589	-0.9416	0	-0.9228	-1.7749	-0.9459
3	0	-0.9519	-1.7719	-0.9744	0	-0.9538	-1.7795	-0.9765
4	0	-0.9774	-1.7766	-0.9997	0	-0.9774	-1.7764	-0.9996
5	0	-0.9774	-1.7766	-0.9997	0	-0.9774	-1.7764	-0.9996
6	0	-0.9774	-1.7766	-0.9997	0	-0.9774	-1.7764	-0.9996
7	0	-0.8639	-1.6181	-0.8846	0	-0.8661	-1.6278	-0.8869
8	0	-0.7399	-1.4473	-0.7589	0	-0.7444	-1.4684	-0.7637
9	0	-0.7399	-1.4473	-0.7589	0	-0.7444	-1.4684	-0.7637

Table F.25: The total nodal longitudinal normal stress $\sigma_{x.r}$ at the sections $X = 0$, $0.25L$, $0.5L$ and $0.75L$ calculated for both the uncoupled and coupled GBT fundamental equation expressed in [MPa].

Node r	$\sigma_{x.r}(X)$ uncoupled				$\sigma_{x.r}(X)$ coupled			
	$X = 0$	$0.25L$	$0.5L$	$0.75L$	$X = 0$	$0.25L$	$0.5L$	$0.75L$
1	-73.8960	8.0503	40.9280	9.1137	-73.2450	7.9999	41.1000	9.0720
2	-53.2770	6.0728	25.3910	6.7030	-53.4570	6.0838	25.3330	6.7112
3	78.0180	-8.7388	-39.5020	-9.7384	77.9440	-8.7342	-39.5230	-9.7349
4	209.3100	-23.5500	-104.3900	-26.1800	209.3500	-23.5520	-104.3800	-26.1810
5	1.6345	-0.1828	-0.8196	-0.2035	1.6316	-0.1818	-0.8204	-0.2025
6	-206.0400	23.1850	102.7600	25.7730	-206.0800	23.1890	102.7400	25.7760
7	-74.5110	8.3300	37.7570	9.2855	-74.4270	8.3186	37.7860	9.2756
8	57.0210	-6.5248	-27.2420	-7.2019	57.2300	-6.5515	-27.1660	-7.2249
9	71.9160	-7.6693	-40.4560	-8.7229	71.1530	-7.5693	-40.7090	-8.6355

Appendix G **Application of GBT - Matrices**

This appendix present all matrices used in the cross-section analysis of the Z-profile defined in Section 6.1. The matrices are expressed for both the cases when only natural nodes are considered as well as the imposition of three intermediate nodes.

Natural nodes

$$\overline{\boldsymbol{F}}_{w1} = \begin{bmatrix} -0.0212 & 0.0406 & -0.0209 & 0.0013 & 0.0003 & -0.0002 \\ -0.0714 & 0.0714 & 0 & 0 & 0 & 0 \\ 0 & -0.0192 & 0.0192 & 0 & 0 & 0 \\ 0 & 0 & 0.0050 & -0.0050 & 0 & 0 \\ 0 & 0 & 0 & 0.0169 & -0.0169 & 0 \end{bmatrix}$$

$$\overline{\boldsymbol{F}}_{w2} = \begin{bmatrix} 0 & 0.0192 & -0.0192 & 0 & 0 & 0 \\ 0 & 0 & 0.0050 & -0.0050 & 0 & 0 \\ 0 & 0 & 0 & -0.0169 & 0.0169 & 0 \\ 0 & 0 & 0 & 0 & -0.0714 & 0.0714 \\ 0.0003 & -0.0004 & -0.0011 & 0.0184 & -0.0360 & 0.0189 \end{bmatrix}$$

$$\overline{\boldsymbol{F}}_{v} = \begin{bmatrix} 0.0714 & -0.0714 & 0 & 0 & 0 & 0 \\ 0 & 0.0192 & -0.0192 & 0 & 0 & 0 \\ 0 & 0 & 0.0050 & -0.0050 & 0 & 0 \\ 0 & 0 & 0 & 0.0169 & -0.0169 & 0 \\ 0 & 0 & 0 & 0 & 0.0714 & -0.0714 \end{bmatrix}$$

$$\overline{\boldsymbol{F}}_{w} = \begin{bmatrix} -0.0106 & 0.0299 & -0.0200 & 0.0007 & 0.0002 & -0.0001 \\ -0.0357 & 0.0357 & 0.0025 & -0.0025 & 0 & 0 \\ 0 & -0.0096 & 0.0096 & -0.0085 & 0.0085 & 0 \\ 0 & 0 & 0.0025 & -0.0025 & -0.0357 & 0.0357 \\ 0.0001 & -0.0002 & -0.0006 & 0.0177 & -0.0265 & 0.0095 \end{bmatrix}$$

$$\overline{\boldsymbol{F}}_{\vartheta} = \begin{bmatrix} 0.0015 & -0.0015 & 0.0001 & -0.0001 & 0 & 0 \\ 0.0014 & -0.0014 & 0.0001 & -0.0001 & 0 & 0 \\ 0 & 0.0001 & -0.0001 & -0.0001 & 0.0001 & 0 \\ 0 & 0 & -0.0001 & 0.0001 & -0.0012 & 0.0012 \\ 0 & 0 & -0.0001 & 0.0001 & -0.0014 & 0.0014 \end{bmatrix}$$

$$\Delta\overline{\boldsymbol{F}}_{\vartheta} = \begin{bmatrix} 0 & 0 & 0 & 0 & 0 & 0 \\ 0 & 0 & 0 & 0 & 0 & 0 \\ -0.1374 & 0.1470 & -0.0192 & 0.0011 & 0.0085 & 0 \\ 0 & -0.0096 & 0.0011 & 0.0169 & -0.1295 & 0.1211 \\ 0 & 0 & 0 & 0 & 0 & 0 \\ 0 & 0 & 0 & 0 & 0 & 0 \end{bmatrix} \cdot 10^{-2}$$

$$\boldsymbol{\Delta}_{Ik} = \begin{bmatrix} 1 & 0 & 0 & 0 & 0 & 0 \\ 0 & 1 & 0 & 0 & 0 & 0 \\ 0 & 0 & 0.0027 & 0.0003 & 0 & 0 \\ 0 & 0 & 0.0003 & 0.0028 & 0 & 0 \\ 0 & 0 & 0 & 0 & 1 & 0 \\ 0 & 0 & 0 & 0 & 0 & 1 \end{bmatrix}$$

$$\boldsymbol{\Delta}_{Ik}^{-1} = \begin{bmatrix} 0 & 0 & 0 & 0 & 0 & 0 \\ 0 & 1 & 0 & 0 & 0 & 0 \\ 0 & 0 & 371.6247 & -42.3279 & 0 & 0 \\ 0 & 0 & -42.3279 & 361.5808 & 0 & 0 \\ 0 & 0 & 0 & 0 & 1 & 0 \\ 0 & 0 & 0 & 0 & 0 & 0 \end{bmatrix}$$

$$\bar{\boldsymbol{M}} = \begin{bmatrix} 0 & 0 & 0 & 0 & 0 & 0 \\ 0 & 0 & 0 & 0 & 0 & 0 \\ 0.5105 & -0.5503 & 0.0719 & 0.0029 & -0.0863 & 0.0512 \\ -0.0581 & 0.0970 & -0.0123 & -0.0608 & 0.4720 & -0.4377 \\ 0 & 0 & 0 & 0 & 0 & 0 \\ 0 & 0 & 0 & 0 & 0 & 0 \end{bmatrix}$$

$$\bar{\boldsymbol{C}}_{\boldsymbol{1}} = \begin{bmatrix} 5.4600 & 2.7300 & 0 & 0 & 0 & 0 \\ 2.7300 & 25.7400 & 10.1400 & 0 & 0 & 0 \\ 0 & 10.1400 & 98.2800 & 39.0000 & 0 & 0 \\ 0 & 0 & 39.0000 & 101.0100 & 11.5050 & 0 \\ 0 & 0 & 0 & 11.5050 & 28.4700 & 2.7300 \\ 0 & 0 & 0 & 0 & 2.7300 & 5.4600 \end{bmatrix}$$

$$\bar{\boldsymbol{C}}_{\boldsymbol{2}} = \begin{bmatrix} 0.0340 & -0.0420 & 0.0103 & -0.0078 & 0.0232 & -0.0177 \\ -0.0420 & 0.0545 & -0.0158 & 0.0102 & -0.0300 & 0.0231 \\ 0.0103 & -0.0158 & 0.0070 & -0.0037 & 0.0095 & -0.0073 \\ -0.0078 & 0.0102 & -0.0037 & 0.0056 & -0.0121 & 0.0078 \\ 0.0232 & -0.0300 & 0.0095 & -0.0121 & 0.0450 & -0.0356 \\ -0.0177 & 0.0231 & -0.0073 & 0.0078 & -0.0356 & 0.0296 \end{bmatrix}$$

$$\bar{\boldsymbol{C}} = \begin{bmatrix} 5.4940 & 2.6880 & 0.0103 & -0.0078 & 0.0232 & -0.0177 \\ 2.6880 & 25.7945 & 10.1242 & 0.0102 & -0.0300 & 0.0231 \\ 0.0103 & 10.1242 & 98.2870 & 38.9963 & 0.0095 & -0.0073 \\ -0.0078 & 0.0102 & 38.9963 & 101.0156 & 11.4929 & 0.0078 \\ 0.0232 & -0.0300 & 0.0095 & 11.4929 & 28.5150 & 2.6944 \\ -0.0177 & 0.0231 & -0.0073 & 0.0078 & 2.6944 & 5.4896 \end{bmatrix}$$

$$\bar{\boldsymbol{D}}_{\boldsymbol{1}} = \begin{bmatrix} 0.0913 & -0.0918 & 0.0079 & -0.0070 & 0.0138 & -0.0142 \\ -0.0918 & 0.0933 & -0.0089 & 0.0060 & -0.0125 & 0.0138 \\ 0.0079 & -0.0089 & 0.0020 & 0 & 0.0050 & -0.0059 \\ -0.0070 & 0.0060 & 0 & 0.0017 & -0.0074 & 0.0066 \\ 0.0138 & -0.0125 & 0.0050 & -0.0074 & 0.0773 & -0.0761 \\ -0.0142 & 0.0138 & -0.0059 & 0.0066 & -0.0761 & 0.0758 \end{bmatrix} \cdot 10^{-3}$$

$$\bar{\boldsymbol{D}}_{\boldsymbol{2}} = \begin{bmatrix} -0.0035 & 0.0058 & -0.0031 & 0.0014 & -0.0040 & 0.0033 \\ 0.0035 & -0.0059 & 0.0032 & -0.0014 & 0.0040 & -0.0033 \\ 0 & 0 & 0 & 0 & 0 & 0 \\ 0 & 0 & 0 & 0 & 0 & 0 \\ -0.0032 & 0.0039 & -0.0013 & 0.0025 & -0.0041 & 0.0022 \\ 0.0032 & -0.0040 & 0.0013 & -0.0024 & 0.0041 & -0.0023 \end{bmatrix} \cdot 10^{-3}$$

$$\bar{\boldsymbol{D}}_{\boldsymbol{3}} = \begin{bmatrix} -0.0035 & 0.0035 & 0 & 0 & -0.0032 & 0.0032 \\ 0.0058 & -0.0059 & 0 & 0 & 0.0039 & -0.0040 \\ -0.0031 & 0.0032 & 0 & 0 & -0.0013 & 0.0013 \\ 0.0014 & -0.0014 & 0 & 0 & 0.0025 & -0.0024 \\ -0.0040 & 0.0040 & 0 & 0 & -0.0041 & 0.0041 \\ 0.0033 & -0.0033 & 0 & 0 & 0.0022 & -0.0023 \end{bmatrix} \cdot 10^{-3}$$

$$\bar{\boldsymbol{D}} = \begin{bmatrix} 0.0982 & -0.1011 & 0.0114 & -0.0089 & 0.0210 & -0.0207 \\ -0.1011 & 0.1052 & -0.0129 & 0.0080 & -0.0204 & 0.0211 \\ 0.0114 & -0.0129 & 0.0028 & 0 & 0.0068 & -0.0077 \\ -0.0089 & 0.0080 & 0 & 0.0024 & -0.0105 & 0.0094 \\ 0.0210 & -0.0204 & 0.0068 & -0.0105 & 0.0855 & -0.0824 \\ -0.0207 & 0.0211 & -0.0077 & 0.0094 & -0.0824 & 0.0804 \end{bmatrix} \cdot 10^{-3}$$

$$\bar{\boldsymbol{B}} = \begin{bmatrix} 0.7012 & -0.7559 & 0.0988 & 0.0040 & -0.1186 & 0.0704 \\ -0.7559 & 0.8181 & -0.1069 & -0.0102 & 0.1723 & -0.1174 \\ 0.0988 & -0.1069 & 0.0140 & 0.0013 & -0.0220 & 0.0148 \\ 0.0040 & -0.0102 & 0.0013 & 0.0103 & -0.0790 & 0.0736 \\ -0.1186 & 0.1723 & -0.0220 & -0.0790 & 0.6187 & -0.5714 \\ 0.0704 & -0.1174 & 0.0148 & 0.0736 & -0.5714 & 0.5300 \end{bmatrix} \cdot 10^{-3}$$

$$\widetilde{\boldsymbol{X}}^{I} = \begin{bmatrix} 0.0470 & 0.0729 & 1.0000 & 0.0119 & -0.3869 & 1.0000 \\ 0.1516 & 0.2212 & 0.9112 & -0.0266 & 0.1146 & -0.3177 \\ 0.9593 & 1.0000 & -0.1752 & 0.1007 & -0.0348 & 0.0395 \\ 1.0000 & -0.9509 & 0.0741 & -0.2071 & 0.0528 & -0.0002 \\ 0.1746 & -0.2575 & -0.0022 & 0.9103 & -0.2886 & -0.1132 \\ 0.0498 & -0.1343 & 0.0613 & 1.0000 & 1.0000 & 0.3811 \end{bmatrix}$$

$$\widetilde{\boldsymbol{X}}^{II} = \begin{bmatrix} 0.0123 & 0.2438 & 1.0054 & 0.9984 \\ 0.1695 & 0.1423 & 0.9846 & 0.8557 \\ 1.4475 & -0.0079 & 0.0028 & -0.2996 \\ -0.7977 & 1.4428 & 0.2989 & -0.2216 \\ 0.6524 & 1.2725 & -0.8152 & 0.6936 \\ 0.8095 & 1.1709 & -0.8359 & 0.8439 \end{bmatrix}$$

$$\bar{\boldsymbol{K}} = \begin{bmatrix} -0.7301 & 0.1524 & 0.4807 \\ 0.1524 & -0.0609 & -0.0653 \\ 0.4807 & -0.0653 & -0.3587 \end{bmatrix} \cdot 10^{-3}$$

$$\widetilde{\boldsymbol{X}}^{III} = \begin{bmatrix} -1.0000 & 97.9665 & 31.8323 \\ -1.0000 & 111.5940 & 28.6241 \\ -1.0000 & 99.6777 & -21.9921 \\ -1.0000 & -95.0001 & 23.8396 \\ -1.0000 & -108.5204 & -33.5904 \\ -1.0000 & -94.8930 & -36.7986 \end{bmatrix}$$

$$\widetilde{\boldsymbol{X}} = \begin{bmatrix} -1.0000 & 97.9665 & 31.8323 & 5292.7866 & -0.3869 & 1.0000 \\ -1.0000 & 111.5940 & 28.6241 & 4535.8682 & 0.1146 & -0.3177 \\ -1.0000 & 99.6777 & -21.9921 & -1588.0643 & -0.0348 & 0.0395 \\ -1.0000 & -95.0001 & 23.8396 & -1174.9435 & 0.0528 & -0.0002 \\ -1.0000 & -108.5204 & -33.5904 & 3676.7485 & -0.2886 & -0.1132 \\ -1.0000 & -94.8930 & -36.7986 & 4473.8301 & 1.0000 & 0.3811 \end{bmatrix}$$

$$\bar{\boldsymbol{U}} = \begin{bmatrix} 1.0000 & 0 & 0 & 0 & 0 & 0 \\ 0 & 1.0000 & 0 & 0 & 0 & 0 \\ 0 & 0 & 1.0000 & 0 & 0 & 0 \\ 0 & 0 & 0 & 1.0000 & 0 & 0 \\ 0 & 0 & 0 & 0 & 1.0000 & 0 \\ 0 & 0 & 0 & 0 & 0 & 1.0000 \end{bmatrix}$$

$$\tilde{\boldsymbol{U}} = \begin{bmatrix} -1.0000 & 97.9665 & 31.8323 & 5292.7866 & -0.3869 & 1.0000 \\ -1.0000 & 111.5940 & 28.6241 & 4535.8682 & 0.1146 & -0.3177 \\ -1.0000 & 99.6777 & -21.9921 & -1588.0643 & -0.0348 & 0.0395 \\ -1.0000 & -95.0001 & 23.8396 & -1174.9435 & 0.0528 & -0.0002 \\ -1.0000 & -108.5204 & -33.5904 & 3676.7485 & -0.2886 & -0.1132 \\ -1.0000 & -94.8930 & -36.7986 & 4473.8301 & 1.0000 & 0.3811 \end{bmatrix}$$

$$\tilde{\boldsymbol{C}} = \begin{bmatrix} 396.6300 & 0 & 0 & 0 & 0 & 0 \\ 0 & 2485614.0056 & 0 & 0 & 0 & 0 \\ 0 & 0 & 110749.2464 & 0 & 0 & 0 \\ 0 & 0 & 0 & 1685093945.1568 & 0 & 0 \\ 0 & 0 & 0 & 0 & 7.0868 & 0 \\ 0 & 0 & 0 & 0 & 0 & 7.1932 \end{bmatrix}$$

$$\tilde{\boldsymbol{B}} = \begin{bmatrix} 0 & 0 & 0 & 0 & 0 & 0 \\ 0 & 0 & 0 & 0 & 0 & 0 \\ 0 & 0 & 0 & 0 & 0 & 0 \\ 0 & 0 & 0 & 0 & 0 & 0 \\ 0 & 0 & 0 & 0 & 0.9868 & 0 \\ 0 & 0 & 0 & 0 & 0 & 1.5308 \end{bmatrix} \cdot 10^{-3}$$

$$\tilde{\boldsymbol{D}} = \begin{bmatrix} 0 & 0 & 0 & 0 & 0 & 0 \\ 0 & 0 & 0 & 0 & -0.0134 & 0 \\ 0 & 0 & 0 & 0 & 0.2817 & -0.1555 \\ 0 & 0 & 0 & 180982.2690 & 35.5691 & 67.3127 \\ 0 & -0.0134 & 0.2817 & 35.5691 & 0.1899 & -0.0456 \\ 0 & 0 & -0.1555 & 67.3127 & -0.0456 & 0.1667 \end{bmatrix} \cdot 10^{-3}$$

Intermediate nodes

$$\overline{\boldsymbol{F}}_{v} = \begin{bmatrix} 0.0714 & -0.0714 & 0 & 0 & 0 & 0 & 0 & 0 & 0 & 0 & 0 & 0 \\ 0 & 0.0192 & -0.0192 & 0 & 0 & 0 & 0 & 0 & 0 & 0 & 0 & 0 \\ 0 & 0.0192 & -0.0192 & 0 & 0 & 0 & 0 & 0 & 0 & 0 & 0 & 0 \\ 0 & 0 & 0 & 0.0050 & -0.0050 & 0 & 0 & 0 & 0 & 0 & 0 & 0 \\ 0 & 0 & 0 & 0.0050 & -0.0050 & 0 & 0 & 0 & 0 & 0 & 0 & 0 \\ 0 & 0 & 0 & 0 & 0 & 0.0169 & -0.0169 & 0 & 0 & 0 & 0 & 0 \\ 0 & 0 & 0 & 0 & 0 & 0.0169 & -0.0169 & 0 & 0 & 0 & 0 & 0 \\ 0 & 0 & 0 & 0 & 0 & 0 & 0 & 0.0714 & -0.0714 & 0 & 0 & 0 \end{bmatrix}$$

$$\overline{\boldsymbol{F}}_{w2} = \begin{bmatrix} -0 & 0.0192 & -0.0192 & 0 & 0 & 0 & 0 & 0 & 0 & 0 & 0 & 0 \\ 0 & 0 & 0 & 0 & 0 & 0 & 0 & 0 & 1.0000 & 0 & 0 & 0 \\ 0 & 0 & 0 & 0.0050 & -0.0050 & 0 & 0 & 0 & 0 & 0 & 0 & 0 \\ 0 & 0 & 0 & 0 & 0 & -0.0169 & 0.0169 & 0 & 0 & 0 & 0 & 0 \\ 0 & 0 & 0 & 0 & 0 & 0 & 0 & -0.0714 & 0.0714 & 0 & 0 & 0 \\ 0 & 0 & 0 & 0 & 0 & 0 & 0 & 0 & 0 & 1.0000 & 0 & 0 \\ 0 & 0 & 0 & 0 & 0 & 0 & 0 & 0 & 0 & 0 & 1.0000 & 0 \\ 0 & 0 & 0 & 0 & 0 & 0 & 0 & 0 & 0 & 0 & 0 & 1.0000 \end{bmatrix}$$

$$\overline{\boldsymbol{F}}_{w1} = \begin{bmatrix} 0 & 0 & 0 & 0 & 0 & 0 & 1.0000 & 0 & 0 & 0 & 0 & 0 \\ -0.0714 & 0.0714 & 0 & 0 & 0 & 0 & 0 & 0 & 0 & 0 & 0 & 0 \\ 0 & 0 & -0.0192 & 0.0192 & 0 & 0 & 0 & 1.0000 & 0 & 0 & 0 & 0 \\ 0 & 0 & 0 & 0 & 0.0050 & -0.0050 & 0 & 0 & 1.0000 & 0 & 0 & 0 \\ 0 & 0 & 0 & 0 & 0 & 0 & 0 & 0 & 0 & 1.0000 & 0 & 0 \\ 0 & 0 & 0 & 0 & 0 & 0 & 0 & 0 & 0 & 0 & 1.0000 & 0 \\ 0 & 0 & 0 & 0 & 0 & 0 & 0 & 0 & 0 & 0 & 0 & 1.0000 \\ 0 & 0 & 0 & 0 & 0 & 0 & 0 & 0 & 0 & 0 & 0 & 0 \end{bmatrix}$$

$$\Delta\bar{F}_{\vartheta} = \begin{bmatrix} 0 & 0 & 0 & 0 & 0 & 0 & 0 & 0 & 0 & 0 \\ 0.2747 & -0.4121 & 0.1374 & 0 & 0 & 7.1429 & 3.8462 & 0 & 0 & 0 \\ -0.2747 & 0.2747 & 0.0192 & -0.0192 & 0 & 0 & -7.6923 & 0 & 0 & 0 \\ 0 & 0.0192 & -0.0385 & 0.0192 & 0 & 0 & 3.8462 & 1.0000 & 0 & 0 \\ 0 & -0.0192 & 0.0192 & -0.0169 & 0.0169 & 0 & 0 & -2.0000 & 0 & 0 \\ 0 & 0 & -0.0169 & 0.0339 & -0.0169 & 0 & 0 & 1.0000 & 3.3898 & 0 \\ 0 & 0 & 0.0169 & -0.0169 & -0.2421 & 0.2421 & 0 & 0 & -6.7797 & 0 \\ 0 & 0 & 0 & -0.1211 & 0.3632 & -0.2421 & 0 & 0 & 3.3898 & 7.1429 \\ 0 & 0 & 0 & 0 & 0 & 0 & 0 & 0 & 0 & 0 \end{bmatrix} \cdot 10^{-2}$$

$$\bar{F}_{\vartheta} = \begin{bmatrix} 0 & 0.0014 & -0.0014 & 0 & 0 & -0.0714 & 0 & 0 & 0 & 0 \\ 0.0027 & -0.0027 & 0 & 0 & 0 & 0 & 0.0385 & 0 & 0 & 0 \\ 0 & 0 & 0.0002 & -0.0002 & 0 & 0 & -0.0385 & 0 & 0 & 0 \\ 0 & 0.0002 & -0.0002 & 0 & 0 & 0 & 0 & 0.0100 & 0 & 0 \\ 0 & 0 & 0 & -0.0002 & 0.0002 & 0 & 0 & -0.0100 & 0 & 0 \\ 0 & 0 & -0.0002 & 0.0002 & 0 & 0 & 0 & 0 & 0.0339 & 0 \\ 0 & 0 & 0 & 0 & -0.0024 & 0.0024 & 0 & 0 & -0.0339 & 0 \\ 0 & 0 & 0 & -0.0012 & 0.0012 & 0 & 0 & 0 & 0 & 0.0714 \end{bmatrix}$$

$$\bar{F}_{w} = \begin{bmatrix} 0 & 0.0096 & -0.0096 & 0 & 0 & 0.5000 & 0 & 0 & 0 & 0 \\ -0.0357 & 0.0357 & 0 & 0 & 0 & 0 & 0.5000 & 0 & 0 & 0 \\ 0 & 0 & 0.0025 & -0.0025 & 0 & 0 & 0.5000 & 0 & 0 & 0 \\ 0 & -0.0096 & 0.0096 & 0 & 0 & 0 & 0 & 0.5000 & 0 & 0 \\ 0 & 0 & 0 & -0.0085 & 0.0085 & 0 & 0 & 0.5000 & 0 & 0 \\ 0 & 0 & 0.0025 & -0.0025 & 0 & 0 & 0 & 0 & 0.5000 & 0 \\ 0 & 0 & 0 & 0 & -0.0357 & 0.0357 & 0 & 0 & 0.5000 & 0 \\ 0 & 0 & 0 & 0.0085 & -0.0085 & 0 & 0 & 0 & 0 & 0.5000 \end{bmatrix}$$

$$
\bar{\boldsymbol{M}} = \begin{bmatrix}
0 & 0 & 0 & 0 & 0 & 0 & 0 & 0 & 0 & 0 & 0 & 0 \\
-8.7088 & 12.1532 & -3.3033 & -0.1451 & -0.0034 & 0.0074 & -180.0687 & -149.7819 & -1.2538 & -0.4626 & -0.0551 & 0 \\
7.2696 & -8.1043 & 0.4005 & 0.4465 & 0.0103 & -0.0227 & 46.3611 & 187.4924 & 3.8578 & 1.4235 & 0.1695 & 0 \\
-0.8429 & 0.7372 & 0.3342 & -0.2740 & -0.0379 & 0.0834 & -5.3756 & -53.4378 & -14.1774 & -5.2313 & -0.6230 & 0 \\
0.2340 & -0.1060 & -0.2356 & 0.2189 & 0.0929 & -0.2043 & 1.4926 & 14.8376 & 16.2438 & 12.8128 & 1.5258 & 0 \\
-0.0933 & 0.0422 & 0.2528 & -0.2884 & -0.6470 & 0.7336 & -0.5948 & -5.9128 & -13.8374 & -46.0198 & -5.4801 & 0 \\
0.0255 & -0.0115 & -0.3591 & -0.3336 & 6.4274 & -5.7486 & 0.1625 & 1.6151 & 3.7798 & 148.2508 & 42.9415 & 0 \\
-0.0086 & 0.0039 & 0.1218 & 2.6848 & -9.8942 & 7.0925 & -0.0551 & -0.5477 & -1.2816 & -122.2742 & -166.2860 & 0 \\
0 & 0 & 0 & 0 & 0 & 0 & 0 & 0 & 0 & 0 & 0 & 0
\end{bmatrix}
$$

$$
\boldsymbol{\Delta}_{jk}^{-1} = \begin{bmatrix}
0 & 0 & 0 & 0 & 0 & 0 & 0 & 0 & 0 & 0 & 0 & 0 \\
0 & 2520.9616 & -649.0549 & 75.2582 & -20.8963 & 8.3272 & -2.2746 & 0.7713 & 0 & 0 & 0 & 0 \\
0 & -649.0549 & 1997.0921 & -231.5636 & 64.2964 & -25.6220 & 6.9988 & -2.3732 & 0 & 0 & 0 & 0 \\
0 & 75.2582 & -231.5636 & 850.9964 & -236.2893 & 94.1610 & -25.7206 & 8.7213 & 0 & 0 & 0 & 0 \\
0 & -20.8963 & 64.2964 & -236.2893 & 578.7321 & -230.6239 & 62.9962 & -21.3608 & 0 & 0 & 0 & 0 \\
0 & 8.3272 & -25.6220 & 94.1610 & -230.6239 & 828.3347 & -226.2641 & 76.7217 & 0 & 0 & 0 & 0 \\
0 & -2.2746 & 6.9988 & -25.7206 & 62.9962 & -226.2641 & 1772.9758 & -601.1814 & 0 & 0 & 0 & 0 \\
0 & 0.7713 & -2.3732 & 8.7213 & -21.3608 & 76.7217 & -601.1814 & 2328.0041 & 0 & 0 & 0 & 0 \\
0 & 0 & 0 & 0 & 0 & 0 & 0 & 0 & 0 & 0 & 0 & 0
\end{bmatrix}
$$

$$
\boldsymbol{\Delta}_{jk} = \begin{bmatrix}
1.0000 & 0 & 0 & 0 & 0 & 0 & 0 & 0 & 0 & 0 & 0 & 0 \\
0 & 0.0004 & 0.0001 & 0 & 0 & 0 & 0 & 0 & 0 & 0 & 0 & 0 \\
0 & 0.0001 & 0.0006 & 0.0001 & 0 & 0 & 0 & 0 & 0 & 0 & 0 & 0 \\
0 & 0 & 0.0001 & 0.0014 & 0.0005 & 0 & 0 & 0 & 0 & 0 & 0 & 0 \\
0 & 0 & 0 & 0.0005 & 0.0022 & 0.0005 & 0 & 0 & 0 & 0 & 0 & 0 \\
0 & 0 & 0 & 0 & 0.0005 & 0.0014 & 0.0002 & 0 & 0 & 0 & 0 & 0 \\
0 & 0 & 0 & 0 & 0 & 0.0002 & 0.0006 & 0.0002 & 0 & 0 & 0 & 0 \\
0 & 0 & 0 & 0 & 0 & 0 & 0.0002 & 0.0005 & 0 & 0 & 0 & 0 \\
0 & 0 & 0 & 0 & 0 & 0 & 0 & 0 & 1.0000 & 0 & 0 & 0 \\
0 & 0 & 0 & 0 & 0 & 0 & 0 & 0 & 0 & 1.0000 & 0 & 0 \\
0 & 0 & 0 & 0 & 0 & 0 & 0 & 0 & 0 & 0 & 1.0000 & 0 \\
0 & 0 & 0 & 0 & 0 & 0 & 0 & 0 & 0 & 0 & 0 & 1.0000
\end{bmatrix}
$$

$$\bar{C} = \begin{bmatrix} 5.4686 & 2.7222 & -0.0010 & -0.0002 & -0.0001 & 0.0005 & 0.0270 & 0.0518 & -0.0385 & -0.0283 & -0.0034 \\ 2.7222 & 25.7491 & 10.1386 & 0.0002 & 0 & -0.0001 & -0.0139 & 0.0321 & 0.0054 & 0.0091 & 0.0011 \\ -0.0010 & 10.1386 & 98.2828 & 38.9996 & 0.0002 & -0.0003 & -0.0141 & -0.0948 & 0.0504 & 0.0142 & 0.0019 \\ -0.0002 & 0.0002 & 38.9996 & 101.0122 & 11.5037 & -0.0005 & -0.0010 & -0.0085 & -0.0469 & 0.0689 & 0.0112 \\ -0.0001 & 0 & 0.0002 & 11.5037 & 28.4801 & 2.7211 & -0.0009 & -0.0092 & -0.0051 & -0.0375 & 0.0229 \\ 0.0005 & -0.0001 & -0.0003 & -0.0005 & 2.7211 & 5.4694 & 0.0029 & 0.0287 & 0.0346 & -0.0265 & -0.0337 \\ 0.0270 & -0.0139 & -0.0141 & -0.0010 & -0.0009 & 0.0029 & 0.7306 & 0.3793 & -0.2450 & -0.1803 & -0.0216 \\ 0.0518 & 0.0321 & -0.0948 & -0.0085 & -0.0092 & 0.0287 & 0.3793 & 8.6804 & -2.4198 & -1.7867 & -0.2138 \\ -0.0385 & 0.0054 & 0.0504 & -0.0469 & -0.0051 & 0.0346 & -0.2450 & -2.4198 & 11.5929 & -2.1437 & -0.2577 \\ -0.0283 & 0.0091 & 0.0142 & 0.0689 & 0.0112 & -0.0265 & -0.1803 & -1.7867 & -2.1437 & 7.7213 & 0.2776 \\ -0.0034 & 0.0011 & 0.0019 & 0.0112 & 0.0229 & -0.0337 & -0.0216 & -0.2138 & -0.2577 & 0.2776 & 0.7854 \end{bmatrix}$$

$$\bar{C}_2 = \begin{bmatrix} 0.0086 & -0.0078 & -0.0010 & -0.0002 & -0.0001 & 0.0005 & 0.0270 & 0.0518 & -0.0385 & -0.0283 & -0.0034 \\ -0.0078 & 0.0091 & -0.0014 & 0.0002 & 0 & -0.0001 & -0.0139 & 0.0321 & 0.0054 & 0.0091 & 0.0011 \\ -0.0010 & -0.0014 & 0.0028 & -0.0004 & 0.0002 & -0.0003 & -0.0141 & -0.0948 & 0.0504 & 0.0142 & 0.0019 \\ -0.0002 & 0.0002 & -0.0004 & 0.0022 & -0.0013 & -0.0005 & -0.0010 & -0.0085 & -0.0469 & 0.0689 & 0.0112 \\ -0.0001 & 0 & 0.0002 & -0.0013 & 0.0101 & -0.0089 & -0.0009 & -0.0092 & -0.0051 & -0.0375 & 0.0229 \\ 0.0005 & -0.0001 & -0.0003 & -0.0005 & -0.0089 & 0.0094 & 0.0029 & 0.0287 & 0.0346 & -0.0265 & -0.0337 \\ 0.0270 & -0.0139 & -0.0141 & -0.0010 & -0.0009 & 0.0029 & 0.7306 & 0.3793 & -0.2450 & -0.1803 & -0.0216 \\ 0.0518 & 0.0321 & -0.0948 & -0.0085 & -0.0092 & 0.0287 & 0.3793 & 8.6804 & -2.4198 & -1.7867 & -0.2138 \\ -0.0385 & 0.0054 & 0.0504 & -0.0469 & -0.0051 & 0.0346 & -0.2450 & -2.4198 & 11.5929 & -2.1437 & -0.2577 \\ -0.0283 & 0.0091 & 0.0142 & 0.0689 & 0.0112 & -0.0265 & -0.1803 & -1.7867 & -2.1437 & 7.7213 & 0.2776 \\ -0.0034 & 0.0011 & 0.0019 & 0.0112 & 0.0229 & -0.0337 & -0.0216 & -0.2138 & -0.2577 & 0.2776 & 0.7854 \end{bmatrix}$$

$$\bar{C}_1 = \begin{bmatrix} 5.4600 & 2.7300 & 0 & 0 & 0 & 0 & 0 & 0 & 0 & 0 & 0 \\ 2.7300 & 25.7400 & 10.1400 & 0 & 0 & 0 & 0 & 0 & 0 & 0 & 0 \\ 0 & 10.1400 & 98.2800 & 39.0000 & 0 & 0 & 0 & 0 & 0 & 0 & 0 \\ 0 & 0 & 39.0000 & 101.0100 & 11.5050 & 0 & 0 & 0 & 0 & 0 & 0 \\ 0 & 0 & 0 & 11.5050 & 28.4700 & 2.7300 & 0 & 0 & 0 & 0 & 0 \\ 0 & 0 & 0 & 0 & 2.7300 & 5.4600 & 0 & 0 & 0 & 0 & 0 \\ 0 & 0 & 0 & 0 & 0 & 0 & 0 & 0 & 0 & 0 & 0 \\ 0 & 0 & 0 & 0 & 0 & 0 & 0 & 0 & 0 & 0 & 0 \\ 0 & 0 & 0 & 0 & 0 & 0 & 0 & 0 & 0 & 0 & 0 \\ 0 & 0 & 0 & 0 & 0 & 0 & 0 & 0 & 0 & 0 & 0 \\ 0 & 0 & 0 & 0 & 0 & 0 & 0 & 0 & 0 & 0 & 0 \end{bmatrix}$$

$$
\bar{D}_3 = \begin{bmatrix}
-0.0163 & 0.0241 & -0.0076 & 0 & 0 & -0.4119 & -0.2714 & 0 & 0.0186 & 0.0024 \\
0.0183 & -0.0278 & 0.0098 & 0 & 0 & 0.4852 & 0.2186 & -0.0163 & -0.0122 & -0.0015 \\
-0.0021 & 0.0040 & -0.0024 & 0 & 0 & -0.0753 & 0.0646 & 0.0235 & 0.0012 & -0.0034 \\
0 & 0 & 0 & -0.0018 & 0.0031 & -0.0017 & 0.0027 & -0.0054 & -0.0208 & -0.0479 & 0.0667 \\
0 & 0 & 0 & 0.0087 & -0.0250 & 0.0164 & 0.0013 & 0.0126 & 0.0152 & -0.1995 & -0.4931 \\
0 & 0 & 0 & -0.0071 & 0.0221 & -0.0149 & -0.0020 & -0.0191 & 0 & 0.2397 & 0.4289 \\
0.0243 & -0.0298 & 0.0051 & 0 & 0.0016 & -0.0020 & 0.2512 & 0.3357 & 0.0060 & 0.1230 & 0.0159 \\
-0.4568 & 0.4637 & 0.0325 & -0.0363 & 0.0152 & -0.0184 & -0.9624 & -15.1250 & -0.2721 & 1.1001 & 0.1436 \\
-0.0025 & -0.0228 & 0.0274 & -0.0244 & 0.0214 & 0.0010 & -0.0049 & -0.2721 & -2.6343 & -0.1888 & 0.0071 \\
0.0180 & -0.0145 & 0.0280 & -0.0245 & -0.3981 & 0.3911 & 0.1190 & 1.1001 & -0.1888 & -12.6104 & -0.8964 \\
0.0024 & -0.0019 & -0.0012 & 0.0016 & 0.0094 & -0.0103 & 0.0159 & 0.1484 & 0.0182 & 0.1633 & -0.0826
\end{bmatrix} \cdot 10^{-3}
$$

$$
\bar{D}_2 = \begin{bmatrix}
-0.0163 & 0.0183 & -0.0021 & 0 & 0 & 0 & 0.0243 & -0.4568 & -0.0025 & 0.0180 & 0.0024 \\
0.0241 & -0.0278 & 0.0040 & 0 & 0 & 0 & -0.0298 & 0.4637 & -0.0228 & -0.0145 & -0.0019 \\
-0.0076 & 0.0098 & -0.0024 & 0 & 0 & 0 & 0.0051 & 0.0325 & 0.0274 & 0.0280 & -0.0012 \\
0 & 0 & 0 & -0.0018 & 0.0087 & -0.0071 & 0 & -0.0363 & -0.0244 & -0.0245 & 0.0016 \\
0 & 0 & 0 & 0.0031 & -0.0250 & 0.0221 & 0.0016 & 0.0152 & 0.0214 & -0.3981 & 0.0094 \\
0 & 0 & 0 & -0.0017 & 0.0164 & -0.0149 & -0.0020 & -0.0184 & 0.0010 & 0.3911 & -0.0103 \\
-0.4119 & 0.4852 & -0.0753 & 0.0027 & 0.0013 & -0.0020 & 0.2512 & -0.9624 & -0.0049 & 0.1190 & 0.0159 \\
-0.2714 & 0.2186 & 0.0646 & -0.0054 & 0.0126 & -0.0191 & 0.3357 & -15.1250 & -0.2721 & 1.1001 & 0.1484 \\
0 & -0.0163 & 0.0235 & -0.0208 & 0.0152 & 0 & 0.0060 & -0.2721 & -2.6343 & -0.1888 & 0.0182 \\
0.0186 & -0.0122 & 0.0012 & -0.0479 & -0.1995 & 0.2397 & 0.1230 & 1.1001 & -0.1888 & -12.6104 & 0.1633 \\
0.0024 & -0.0015 & -0.0034 & 0.0667 & -0.4931 & 0.4289 & 0.0159 & 0.1436 & 0.0071 & -0.8964 & -0.0826
\end{bmatrix} \cdot 10^{-3}
$$

$$
\bar{D}_1 = \begin{bmatrix}
0.1263 & -0.1301 & 0.0024 & 0.0012 & -0.0011 & 0.0014 & 0.2387 & 2.1319 & 0.0119 & -0.0840 & -0.0109 \\
-0.1301 & 0.1525 & -0.0209 & -0.0011 & 0 & -0.0011 & -1.0857 & -2.1641 & 0.1062 & 0.0679 & 0.0085 \\
0.0024 & -0.0209 & 0.0200 & -0.0017 & 0 & 0 & 0.8433 & -0.1518 & -0.1277 & -0.1305 & 0 \\
0.0012 & -0.0011 & -0.0017 & 0.0162 & -0.0172 & 0.0025 & 0.0018 & 0.1692 & 0.1141 & 0.1143 & -0.7624 \\
-0.0011 & 0 & 0 & -0.0172 & 0.1323 & -0.1141 & -0.0074 & -0.0710 & -0.0997 & 1.8576 & 1.0026 \\
0.0014 & -0.0011 & 0 & 0.0025 & -0.1141 & 0.1105 & 0.0092 & 0.0858 & -0.0048 & -1.8253 & -0.2386 \\
0.2387 & -1.0857 & 0.8433 & 0.0018 & -0.0074 & 0.0092 & 44.2442 & 4.4914 & 0.0229 & -0.5551 & -0.0720 \\
2.1319 & -2.1641 & -0.1518 & 0.1692 & -0.0710 & 0.0858 & 4.4914 & 70.5832 & 1.2696 & -5.1337 & -0.6703 \\
0.0119 & 0.1062 & -0.1277 & 0.1141 & -0.0997 & -0.0048 & 0.0229 & 1.2696 & 12.2933 & 0.8811 & -0.0331 \\
-0.0840 & 0.0679 & 0.1062 & -0.1277 & 0.1141 & 0.1143 & 1.8576 & -1.8253 & -0.5551 & -5.1337 & 0.8811 & 58.8484 & 4.1833 \\
-0.0109 & 0.0085 & 0 & -0.1305 & 0.1143 & 1.0026 & -0.7624 & -0.2386 & -0.0720 & -0.6703 & -0.0331 & 4.1833 & 45.2445
\end{bmatrix} \cdot 10^{-3}
$$

$$
\tilde{\boldsymbol{X}}^{l} = \begin{bmatrix}
1.0000 & 0.0394 & -0.0153 & -0.0344 & -0.6897 & 1.0000 & -0.0940 & -0.0357 & 0.0397 & -0.0003 & 0.0032 \\
0.9170 & -0.0793 & 0.0312 & 0.0694 & 0.2101 & -0.3199 & 0.0358 & 0.0128 & -0.0131 & 0.0006 & -0.0022 \\
-0.1354 & -0.4260 & 0.6954 & 0.6657 & -0.0488 & 0.0343 & -0.0092 & -0.0013 & 0.0019 & -0.0001 & 0.0007 \\
0.0548 & 0.4117 & -0.5588 & 1.0000 & 0.0583 & 0.0139 & 0.0086 & -0.0017 & -0.0013 & -0.0004 & -0.0005 \\
-0.0092 & 0.9906 & 0.8653 & -0.3843 & -0.2878 & -0.2021 & -0.0284 & 0.0155 & 0.0070 & 0.0012 & 0.0008 \\
0.0566 & 1.0000 & 1.0000 & -0.5519 & 1.0000 & 0.6880 & 0.0794 & -0.0505 & -0.0255 & -0.0006 & -0.0013 \\
0.0189 & 0.0055 & -0.0136 & -0.0090 & 0.0235 & -0.0361 & 0.0527 & 0.4555 & -0.9210 & -0.4700 & 1.0000 \\
-0.0034 & -0.0063 & 0.0048 & 0.0029 & 0.0304 & -0.0416 & -0.0638 & -0.5545 & 1.0000 & 0.0312 & 0.0760 \\
-0.0107 & 0.0016 & 0.0185 & -0.0060 & -0.0649 & 0.0188 & 1.0000 & 0.0853 & 0.3772 & 0.0284 & 0.0622 \\
0.0019 & -0.0018 & 0.0079 & -0.0068 & 0.0425 & 0.0263 & -0.0811 & 1.0000 & 0.7483 & 0.0477 & 0.0774 \\
0.0024 & -0.0087 & -0.0233 & 0.0210 & 0.0298 & 0.0222 & 0.0565 & -0.7587 & -0.6638 & 1.0000 & 0.4297
\end{bmatrix}
$$

$$
\bar{\boldsymbol{B}} = \begin{bmatrix}
0.0439 & -0.0557 & 0.0102 & 0.0016 & 0 & -0.0001 & 0.6221 & 0.9266 & 0.0140 & 0.0052 & 0.0006 \\
-0.0557 & 0.0722 & -0.0148 & -0.0017 & -0 & 0 & -0.8681 & -1.1192 & -0.0099 & -0.0023 & -0.0003 \\
0.0102 & -0.0148 & 0.0047 & -0 & -0.0012 & 0.0012 & 0.2359 & 0.1450 & -0.0106 & -0.0370 & -0.0087 \\
0.0016 & -0.0017 & -0 & 0.0035 & -0.0106 & 0.0073 & 0.0104 & 0.0505 & 0.0100 & -0.1039 & -0.1918 \\
0 & -0 & -0.0012 & -0.0106 & 0.0514 & -0.0395 & 0.0002 & 0.0024 & 0.0087 & 0.7931 & 0.7067 \\
-0.0001 & 0 & 0.0012 & 0.0073 & -0.0395 & 0.0311 & -0.0005 & -0.0052 & -0.0123 & -0.6550 & -0.5066 \\
0.6221 & -0.8681 & 0.2359 & 0.0104 & 0.0002 & -0.0005 & 12.8620 & 10.6987 & 0.0896 & 0.0330 & 0.0039 \\
0.9266 & -1.1192 & 0.1450 & 0.0505 & 0.0024 & -0.0052 & 10.6987 & 22.2386 & 0.8903 & 0.3285 & 0.0391 \\
0.0140 & -0.0099 & -0.0106 & 0.0100 & 0.0087 & -0.0123 & 0.0896 & 0.8903 & 0.6050 & 0.7688 & 0.0915 \\
0.0052 & -0.0023 & -0.0370 & -0.1039 & 0.7931 & -0.6550 & 0.0330 & 0.3285 & 0.7688 & 15.7558 & 8.7339 \\
0.0006 & -0.0003 & -0.0087 & -0.1918 & 0.7067 & -0.5066 & 0.0039 & 0.0391 & 0.0915 & 8.7339 & 11.8776
\end{bmatrix}
$$

$$
\bar{\boldsymbol{D}} = \begin{bmatrix}
0.1588 & -0.1725 & 0.0121 & 0.0011 & -0.0016 & 0.0020 & 0.6263 & 2.8601 & 0.0154 & -0.1206 & -0.0158 \\
-0.1725 & 0.2081 & -0.0346 & 0 & 0.0010 & -0.0016 & -1.5411 & -2.8465 & 0.1453 & 0.0946 & 0.0119 \\
0.0121 & -0.0346 & 0.0248 & -0.0028 & 0 & 0 & 0.9136 & -0.2489 & -0.1785 & -0.1597 & 0.0054 \\
0.0011 & 0 & -0.0028 & 0.0199 & -0.0290 & 0.0113 & -0.0018 & 0.2108 & 0.1593 & 0.1868 & -0.8307 \\
-0.0016 & 0.0010 & 0 & -0.0290 & 0.1822 & -0.1526 & -0.0104 & -0.0988 & -0.1363 & 2.4552 & 1.4863 \\
0.0020 & -0.0016 & 0 & 0.0113 & -0.1526 & 0.1403 & 0.0133 & 0.1233 & -0.0052 & -2.4562 & -0.6571 \\
0.6263 & -1.5411 & 0.9136 & -0.0018 & -0.0104 & 0.0133 & 43.7418 & 5.1182 & 0.0218 & -0.7970 & -0.1039 \\
2.8601 & -2.8465 & -0.2489 & 0.2108 & -0.0988 & 0.1233 & 5.1182 & 100.8331 & 1.8138 & -7.3339 & -0.9623 \\
0.0154 & 0.1453 & -0.1785 & 0.1593 & -0.1363 & -0.0052 & 0.0218 & 1.8138 & 17.5619 & 1.2588 & -0.0584 \\
-0.1206 & 0.0946 & -0.1597 & 0.1868 & 2.4552 & -2.4562 & -0.7970 & -7.3339 & 1.2588 & 84.0692 & 4.9164 \\
-0.0158 & 0.0119 & 0.0054 & -0.8307 & 1.4863 & -0.6571 & -0.1039 & -0.9623 & -0.0584 & 4.9164 & 45.4097
\end{bmatrix} \cdot 10^{-3}
$$

$$\begin{bmatrix} -1.0000 & -97.9665 & 31.8323 \\ -1.0000 & -111.5940 & 28.6241 \\ -1.0000 & -99.6777 & -21.9921 \\ -1.0000 & 95.0001 & 23.8396 \\ -1.0000 & 108.5204 & -33.5904 \\ -1.0000 & 94.8930 & -36.7986 \\ 0 & -0.2292 & 0.9734 \\ 0 & -0.9734 & -0.2292 \\ 0 & 0.2292 & -0.9734 \\ 0 & -0.9734 & -0.2292 \\ 0 & -0.2292 & 0.9734 \end{bmatrix}$$

$$\widetilde{\boldsymbol{X}}^{III} =$$

$$\overline{\boldsymbol{K}} = \begin{bmatrix} -0.4266 & -0.1581 & 0.2832 \\ -0.1581 & -0.0969 & 0.1275 \\ 0.2832 & 0.1275 & -0.2013 \end{bmatrix} \cdot 10^{-3}$$

$$\widetilde{\boldsymbol{X}}^{II} = \begin{bmatrix} 0.9842 & -0.0250 & 0.2093 & 1.0209 \\ 0.9486 & -0.1242 & 0.2836 & 0.8749 \\ -0.1172 & -0.4795 & 0.9678 & -0.3063 \\ 0.3927 & 0.9382 & -0.0934 & -0.2266 \\ -0.8165 & 0.5352 & 0.6829 & 0.7092 \\ -0.8522 & 0.4359 & 0.7572 & 0.8629 \\ 0.0205 & 0.0068 & -0.0132 & 0.0200 \\ -0.0025 & -0.0071 & 0.0053 & -0.0054 \\ -0.0205 & -0.0068 & 0.0132 & -0.0034 \\ -0.0025 & -0.0071 & 0.0053 & 0.0053 \\ 0.0205 & 0.0068 & -0.0132 & -0.0132 \end{bmatrix}$$

$$
\tilde{\boldsymbol{U}} = \begin{bmatrix}
-1.0000 & -97.9665 & 31.8323 & 5292.7866 & -0.6897 & 1.0000 & -0.0940 & -0.0357 & 0.0397 & -0.0003 & 0.0032 \\
-1.0000 & -111.5940 & 28.6241 & 4535.8682 & 0.2101 & -0.3199 & 0.0358 & 0.0128 & -0.0131 & 0.0006 & -0.0022 \\
-1.0000 & -105.6358 & 3.3160 & 1473.9019 & 0.0807 & -0.1428 & 0.0133 & 0.0057 & -0.0056 & 0.0003 & -0.0007 \\
-1.0000 & -99.6777 & -21.9921 & -1588.0643 & -0.0488 & 0.0343 & -0.0092 & -0.0013 & 0.0019 & -0.0001 & 0.0007 \\
-1.0000 & -2.3388 & 0.9237 & -1381.5039 & 0.0047 & 0.0241 & -0.0003 & -0.0015 & 0.0003 & -0.0002 & 0.0001 \\
-1.0000 & 95.0001 & 23.8396 & -1174.9435 & 0.0583 & 0.0139 & 0.0086 & -0.0017 & -0.0013 & -0.0004 & -0.0005 \\
-1.0000 & 101.7603 & -4.8754 & 1250.9025 & -0.1148 & -0.0941 & -0.0099 & 0.0069 & 0.0029 & 0.0004 & 0.0002 \\
-1.0000 & 108.5204 & -33.5904 & 3676.7485 & -0.2878 & -0.2021 & -0.0284 & 0.0155 & 0.0070 & 0.0012 & 0.0008 \\
-1.0000 & 94.8930 & -36.7986 & 4473.8301 & 1.0000 & 0.6880 & 0.0794 & -0.0505 & -0.0255 & -0.0006 & -0.0013
\end{bmatrix}
$$

$$
\bar{\boldsymbol{U}} = \begin{bmatrix}
1.0000 & 0 & 0 & 0 & 0 & 0 & 0 & 0 & 0 & 0 & 0 \\
0 & 1.0000 & 0 & 0 & 0 & 0 & 0 & 0 & 0 & 0 & 0 \\
0 & 0.5000 & 0.5000 & 0 & 0 & 0 & 0 & 0 & 0 & 0 & 0 \\
0 & 0 & 1.0000 & 0 & 0 & 0 & 0 & 0 & 0 & 0 & 0 \\
0 & 0 & 0 & 0.5000 & 0.5000 & 0 & 0 & 0 & 0 & 0 & 0 \\
0 & 0 & 0 & 0 & 1.0000 & 0 & 0 & 0 & 0 & 0 & 0 \\
0 & 0 & 0 & 0 & 0.5000 & 0.5000 & 0 & 0 & 0 & 0 & 0 \\
0 & 0 & 0 & 0 & 0 & 1.0000 & 0 & 0 & 0 & 0 & 0 \\
0 & 0 & 0 & 0 & 0 & 0 & 1.0000 & 0 & 0 & 0 & 0
\end{bmatrix}
$$

$$
\tilde{\boldsymbol{X}} = \begin{bmatrix}
-1.0000 & -97.9665 & 31.8323 & 5292.7866 & -0.6897 & 1.0000 & -0.0940 & -0.0357 & 0.0397 & -0.0003 & 0.0032 \\
-1.0000 & -111.5940 & 28.6241 & 4535.8682 & 0.2101 & -0.3199 & 0.0358 & 0.0128 & -0.0131 & 0.0006 & -0.0022 \\
-1.0000 & -99.6777 & -21.9921 & -1588.0643 & -0.0488 & 0.0343 & -0.0092 & -0.0013 & 0.0019 & -0.0001 & 0.0007 \\
-1.0000 & 95.0001 & 23.8396 & -1174.9435 & 0.0583 & 0.0139 & 0.0086 & -0.0017 & -0.0013 & -0.0004 & -0.0005 \\
-1.0000 & 108.5204 & -33.5904 & 3676.7485 & -0.2878 & -0.2021 & -0.0284 & 0.0155 & 0.0070 & 0.0012 & 0.0008 \\
-1.0000 & 94.8930 & -36.7986 & 4473.8301 & 1.0000 & 0.6880 & 0.0794 & -0.0505 & -0.0255 & -0.0006 & -0.0013 \\
0 & -0.2292 & 0.9734 & 103.7679 & 0.0235 & -0.0361 & 0.0527 & 0.4555 & -0.9210 & -0.4700 & 1.0000 \\
0 & -0.9734 & -0.2292 & -28.0656 & 0.0304 & -0.0416 & -0.0638 & -0.5545 & 1.0000 & 0.0312 & 0.0760 \\
0 & 0.2292 & -0.9734 & -17.7679 & -0.0649 & 0.0188 & 1.0000 & 0.0853 & 0.3772 & 0.0284 & 0.0622 \\
0 & -0.9734 & -0.2292 & 27.4344 & 0.0425 & 0.0263 & -0.0811 & 1.0000 & 0.7483 & 0.0477 & 0.0774 \\
0 & -0.2292 & 0.9734 & -68.2321 & 0.0298 & 0.0222 & 0.0565 & -0.7587 & -0.6638 & 1.0000 & 0.4297
\end{bmatrix}
$$

$$
\tilde{\boldsymbol{D}} = \begin{bmatrix}
0 & 0 & 0 & 0 & 0 & 0 & 0 & 0 & 0 & 0 \\
0 & 0 & 0 & 0 & 0 & 0 & 0 & 0 & 0 & 0 \\
0 & 0 & 0 & 0 & 0 & 0 & 0 & 0 & 0 & 0 \\
0 & 0 & 0 & 0 & 0 & 0 & 0 & 0 & 0 & 0 \\
0 & 0.0116 & 0.2816 & 180982.269 & 0.0116 & 0.0085 & 2.6955 & -4.1128 & -21.7236 & 2.3882 & 6.5509 \\
0 & 0.0085 & -0.0783 & 77.3881 & -0.0783 & -0.0320 & -0.9270 & 0.6479 & 3.8465 & -1.2029 & -4.1673 \\
0 & 2.6955 & -0.9270 & -18.6659 & -0.9552 & 0.2747 & 18.2951 & -2.0018 & -4.6009 & 1.2740 & 3.1920 \\
0 & -4.1128 & 0.6479 & -842.2076 & -0.0600 & 0.1371 & -2.0018 & 147.4565 & 7.8013 & -34.4672 & 5.9313 \\
0 & -21.7236 & 3.8465 & 365.8318 & -0.3765 & 0.0019 & -4.6009 & 7.8013 & 186.8489 & -4.8724 & -35.6418 \\
0 & 2.3882 & -1.2029 & 855.7133 & 0.2466 & 0.7084 & 1.2740 & -34.4672 & -4.8724 & 55.7573 & -0.2216 \\
0 & 6.5509 & -4.1673 & -498.6348 & 0.5323 & -0.4928 & 3.1920 & 5.9313 & -35.6418 & -0.2216 & 54.0684
\end{bmatrix} \cdot 10^{-3}
$$

$$
\tilde{\boldsymbol{B}} = \begin{bmatrix}
0 & 0 & 0 & 0 & 0 & 0 & 0 & 0 & 0 & 0 & 0 \\
0 & 0 & 0 & 0 & 0 & 0 & 0 & 0 & 0 & 0 & 0 \\
0 & 0 & 0 & 0 & 0 & 0 & 0 & 0 & 0 & 0 & 0 \\
0 & 0 & 0 & 0 & 0 & 0 & 0 & 0 & 0 & 0 & 0 \\
0 & 0 & 0 & 0 & 0 & 0 & 0 & 0 & 0 & 0 & 0 \\
0 & 0 & 0 & 0 & 0 & 0 & 0 & 0 & 0 & 0 & 0 \\
0 & 0 & 0 & -0 & -0 & 0 & 0 & 0 & 0 & 0 & 0 \\
0 & 0 & 0 & -0 & -0 & 0.5131 & 0 & 0 & 0 & 0 & 0 \\
0 & 0 & 0 & 0 & -0 & 0 & 13.2413 & 0 & 0 & 0 & 0 \\
0 & 0 & 0 & 0 & 0 & 0 & 0 & 20.3504 & 0 & 0 & 0 \\
0 & 0 & 0 & -0 & 0 & 0 & 0 & 0 & 15.3050 & 0 & 0 \\
0 & 0 & 0 & 0 & 0 & 0 & 0 & 0 & 0 & 17.5438 & 0
\end{bmatrix}
$$

$$
\tilde{\boldsymbol{C}} = \begin{bmatrix}
396.6300 & 0 & 0 & 0 & 0 & 0 & 0 & 0 & 0 & 0 & 0 \\
0 & 2485614.0056 & 0 & 0 & 0 & 0 & 0 & 0 & 0 & 0 & 0 \\
0 & 0 & 110749.2464 & 0 & 0 & 0 & 0 & 0 & 0 & 0 & 0 \\
0 & 0 & 0 & 1685093945.1559 & 0 & 0 & 0 & 0 & 0 & 0 & 0 \\
0 & 0 & 0 & 0 & 9.0532 & 0 & 0 & 0 & 0 & 0 & 0 \\
0 & 0 & 0 & 0 & 0 & 9.2657 & 0 & 0 & 0 & 0 & 0 \\
0 & 0 & 0 & 0 & 0 & 0 & 12.3803 & 0 & 0 & 0 & 0 \\
0 & 0 & 0 & 0 & 0 & 0 & 0 & 12.0222 & 0 & 0 & 0 \\
0 & 0 & 0 & 0 & 0 & 0 & 0 & 0 & 9.7490 & 0 & 0 \\
0 & 0 & 0 & 0 & 0 & 0 & 0 & 0 & 0 & 0.9892 & 0 \\
0 & 0 & 0 & 0 & 0 & 0 & 0 & 0 & 0 & 0 & 0.9241
\end{bmatrix}
$$

Appendix H **ABAQUS reference model**

This appendix presents all input data of the reference model and the numerical results obtained in ABAQUS (ver. 6.11-1) for the chosen Z-profile.

Input data

The same input data were used as for the GBT model analysed in Section6.3. See Figure 6.1 and Figure 6.8 for further details about the Z-profiles boundary conditions and loads.

The geometry of the FE-model is defined in [mm] and the value for the Young's modulus of elasticity is defined as $E = 210000$ [N/mm^2] and Poisson's ratio $\nu = 0.3$. The elements used in the analysis are the S4R shell elements. These are a four node conventional stress-displacement shell element, with reduced integration in order to avoid shear and membrane locking.

Boundary conditions

The boundary conditions for the Z-profile are that both ends are fully fixed, i.e. all displacements and rotations are prevented at the ends. The boundary conditions in the FE-model will then be of essential type and all displacements and rotations are locked (predefined as zero) for all nodes along both boundaries.

Applied loads

The gravity load was assigned as a gravity force in ABAQUS where the density was assigned as $7.8 \cdot 10^{-9}$ [kg/mm^3] and the gravity constant as $9.82 \cdot 10^3$ [mm/s^2].

The line-load was more troublesome to assign since there was no possibility to assign the load to the intersection between the upper flange and the web. Therefore a small partitioned surface was assigned on the upper flange, closest to the web, with a width of 0.5 [mm], see Figure H.1. The equivalent imposed surface load was then calculated and applied as 10 [N/mm^2].

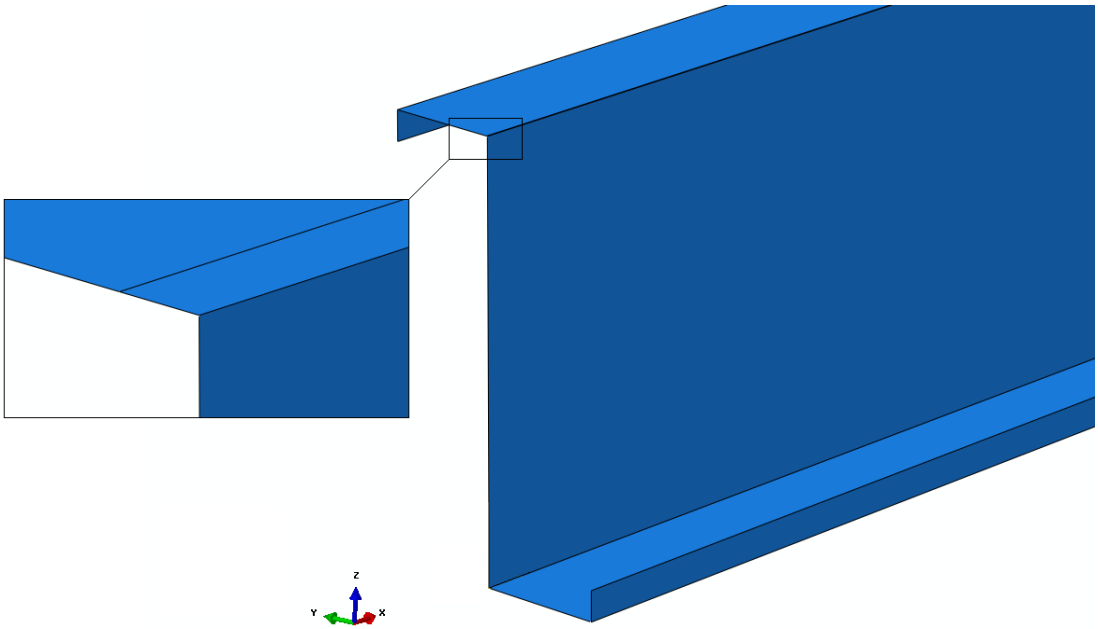

Figure H.1: Illustration from ABAQUS on the partition used to apply the load on the member.

Mesh density

In order to have a sufficient mesh density a convergence study was performed for five different shell-element sizes, namely with the element sides of 50, 25, 10, 5 and 3 [mm]. The estimated error was calculated according to:

$$Error = 1 - \frac{\sqrt{U_{4.app}^2 + V_{4.app}^2 + W_{4.app}^2}}{\sqrt{U_{4.3mm}^2 + V_{4.3mm}^2 + W_{4.3mm}^2}}$$

The mesh with element side of 3 [mm] was considered as a reference and the total displacement magnitudes at node four in the midsection were related to each other in order to have the error estimation. Figure H.2 shows the error estimation for each element size.

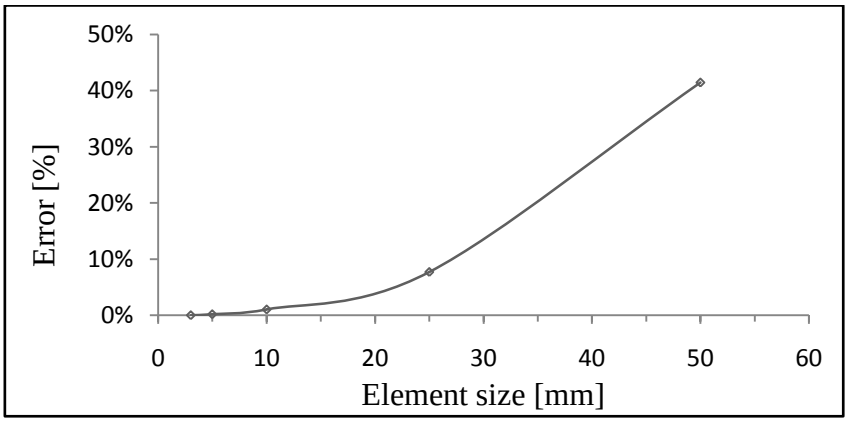

Figure H.2: The estimated error for the five different element sizes of 50, 25, 10, 5and 3 mm.

An element size of 5 [mm] resulted in an error estimation of 0.18% which were satisfactory and used as the mesh density for the model. With this mesh the model consist of 33120 elements and 33670 nodes and in total 202020 number degrees of freedom (6 degrees of freedom per node), see Figure H.3.

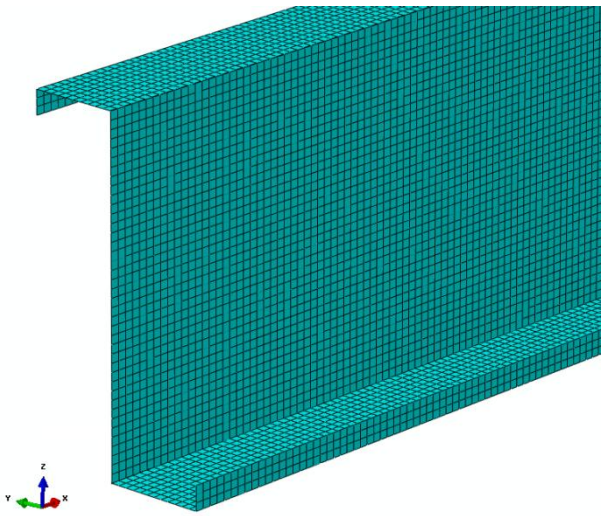

Figure H.3: The Z-Profile was modelled using S4R shell-elements with an element size of 5 [mm].

The ABAQUS results

The ABAQUS results are tabulated in Table H.1 and Table H.2 below in terms of nodal displacements $U_r(X)$, $V_r(X)$ and $W_r(X)$ and nodal normal stresses $\sigma_{x.r}(X)$ at the quarter sections $X = 0$, $0.25L$, $0.5L$ and $0.75L$. Note that the node numbering refers to the same node numbers used in the GBT analysis of the Z-profile discretized with three imposed intermediate nodes.

Table H.1: The nodal $U_r(X)$ and $V_r(X)$ displacements at the quarter sections $X = 0$, $0.25L$, $0.5L$ and $0.75L$ obtained in ABAQUS expressed in [mm].

Node r	$U_r(X)$				$V_r(X)$			
	$X = 0$	$0.25L$	$0.5L$	$0.75L$	$X = 0$	$0.25L$	$0.5L$	$0.75L$
1	3.53E-34	9.39E-02	7.23E-04	-9.35E-02	-2.88E-37	-2.41E00	-4.32E00	-2.45E00
2	3.77E-34	5.70E-02	4.43E-04	-5.68E-02	4.59E-36	-2.43E00	-4.36E00	-2.47E00
3	-7.37E-34	-8.31E-02	-6.44E-04	8.28E-02	8.40E-35	-2.43E00	-4.36E00	-2.47E00
4	-1.48E-33	-2.27E-01	-1.76E-03	2.26E-01	-1.17E-34	-2.43E00	-4.36E00	-2.47E00
5	-6.76E-36	-2.24E-03	-1.76E-05	2.23E-03	-3.38E-38	-2.29E00	-4.07E00	-2.32E00
6	2.38E-33	2.22E-01	1.72E-03	-2.21E-01	-1.98E-34	-2.11E00	-3.78E00	-2.14E00
7	5.94E-34	8.18E-02	6.34E-04	-8.15E-02	7.04E-35	-2.11E00	-3.79E00	-2.14E00
8	-3.75E-34	-5.75E-02	-4.46E-04	5.73E-02	-4.88E-36	-2.11E00	-3.79E00	-2.14E00
9	-3.16E-34	-8.85E-02	-6.85E-04	8.81E-02	-7.65E-38	-2.16E00	-3.85E00	-2.19E00

Table H.2: The nodal $W_r(X)$ displacements and normal stresses $\sigma_{x.r}(X)$ at the quarter sections $X = 0,\ 0.25L,\ 0.5L$ and $0.75L$ obtained in ABAQUS expressed in [mm] and [MPa] respectively.

Node r	$W_r(X)$				$\sigma_{x.r}(X)$			
	$X = 0$	$0.25L$	$0.5L$	$0.75L$	$X = 0$	$0.25L$	$0.5L$	$0.75L$
1	-5.01E-35	-1.22E00	-2.14E00	-1.24E00	-7.72E01	9.41E00	3.77E01	1.01E01
2	4.04E-35	-1.22E00	-2.14E00	-1.24E00	-3.10E01	3.87E00	1.65E01	4.16E00
3	-2.47E-36	-1.18E00	-2.07E00	-1.20E00	6.71E01	-8.54E00	-3.75E01	-9.21E00
4	-4.03E-34	-1.14E00	-1.98E00	-1.16E00	2.71E02	-2.47E01	-1.04E02	-2.65E01
5	-1.56E-34	-1.14E00	-1.99E00	-1.16E00	-3.18E00	-3.36E-01	-1.67E-01	-3.32E-01
6	-4.12E-34	-1.14E00	-1.98E00	-1.16E00	-2.40E02	2.47E01	1.01E02	2.64E01
7	8.72E-37	-1.05E00	-1.86E00	-1.07E00	-7.57E01	9.71E00	3.93E01	1.04E01
8	3.80E-35	-9.51E-01	-1.74E00	-9.66E-01	3.46E01	-4.27E00	-1.80E01	-4.59E00
9	-4.51E-35	-9.50E-01	-1.74E00	-9.66E-01	7.76E01	-9.10E00	-3.88E01	-9.79E00

Appendix I **Parametric study**

This appendix presents complementary results from the parametric study.

Fixed – Free conditions

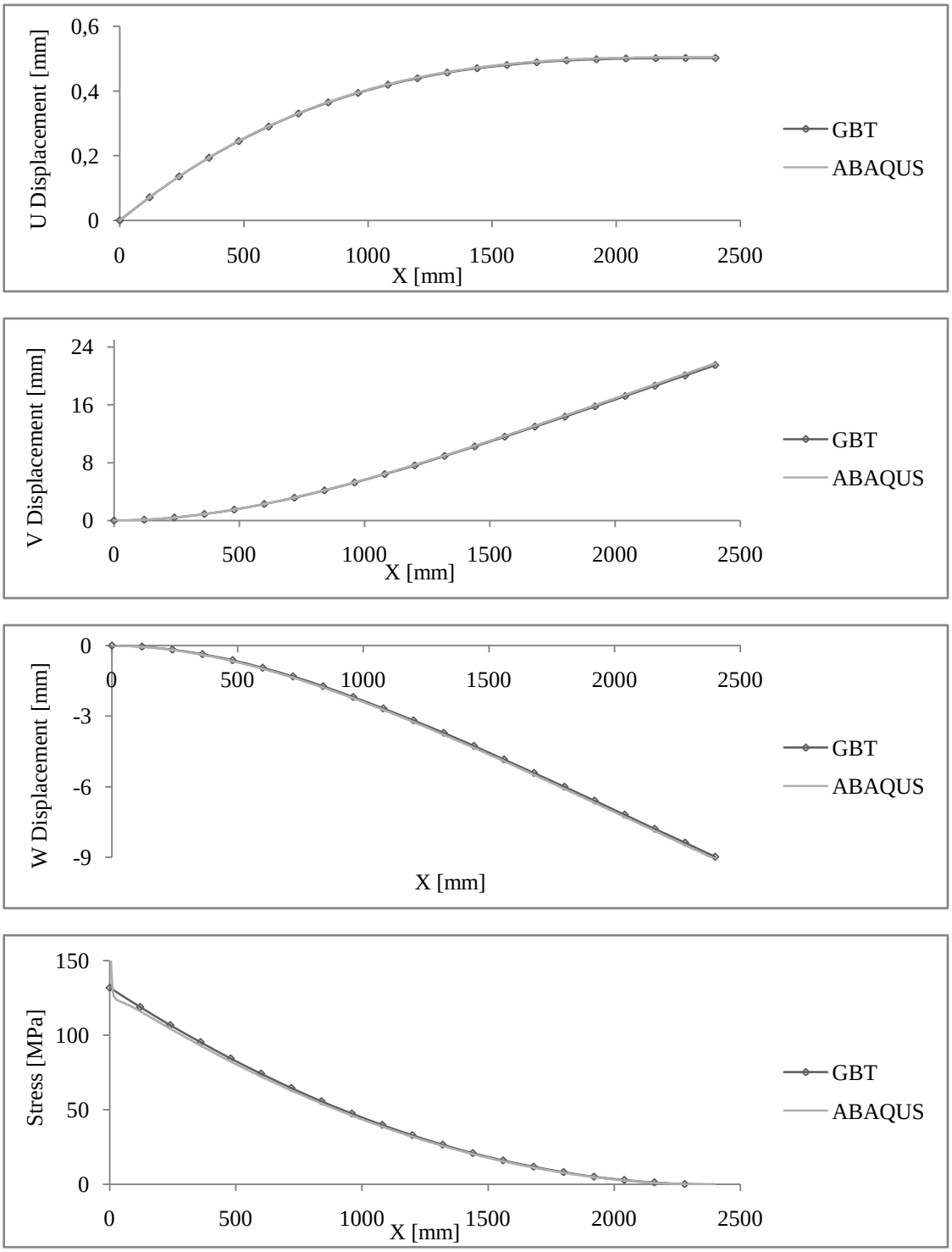

Figure I.1: The U, V and W displacements and the normal stress σ_x variations are here plotted for node four along the Z-profile modelled as a cantilever, both for the GBT and ABAQUS analysis

Fixed – Guided conditions

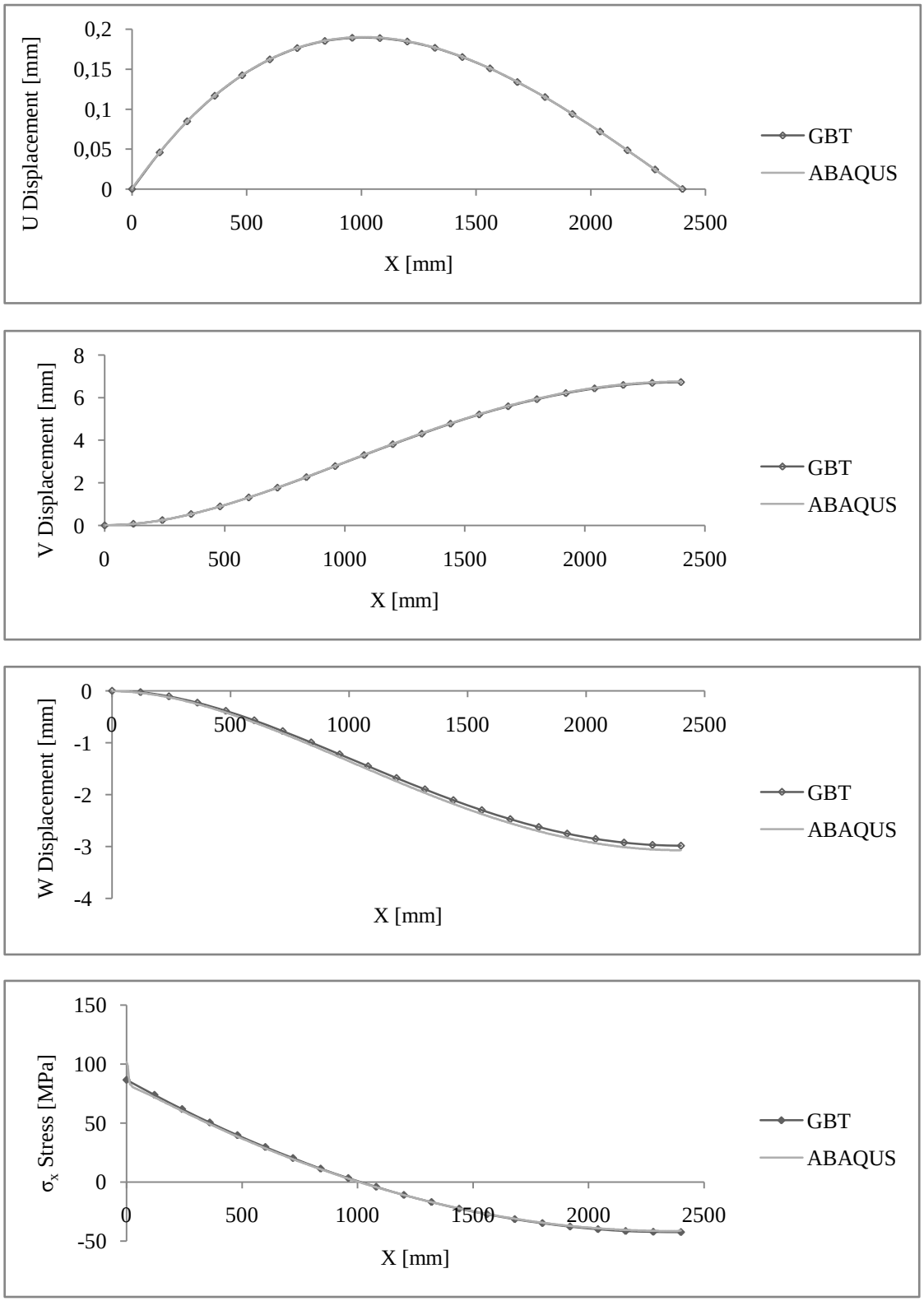

Figure I.2: The U, V and W displacements and the normal stress σ_x variations plotted for node four along the Z-profile modelled as a with a fixed and a guided end, both for the GBT and ABAQUS analysis.

Fixed – Free conditions subjected to point-load

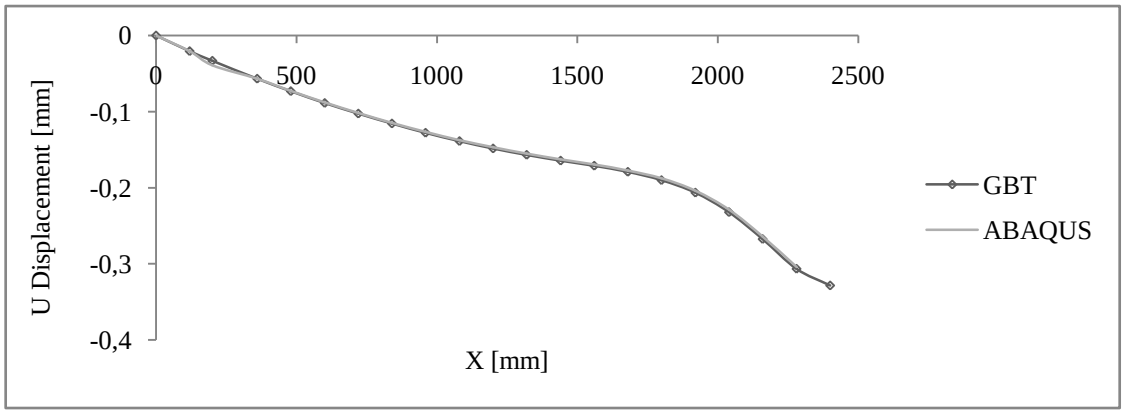

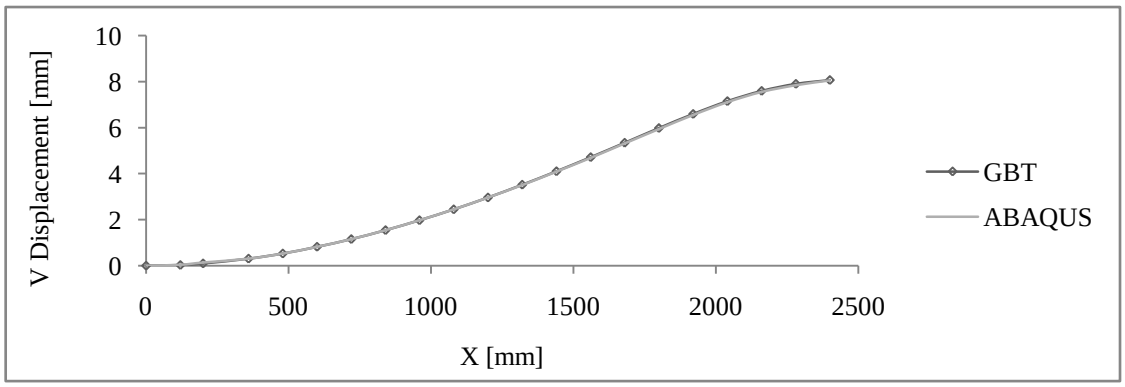

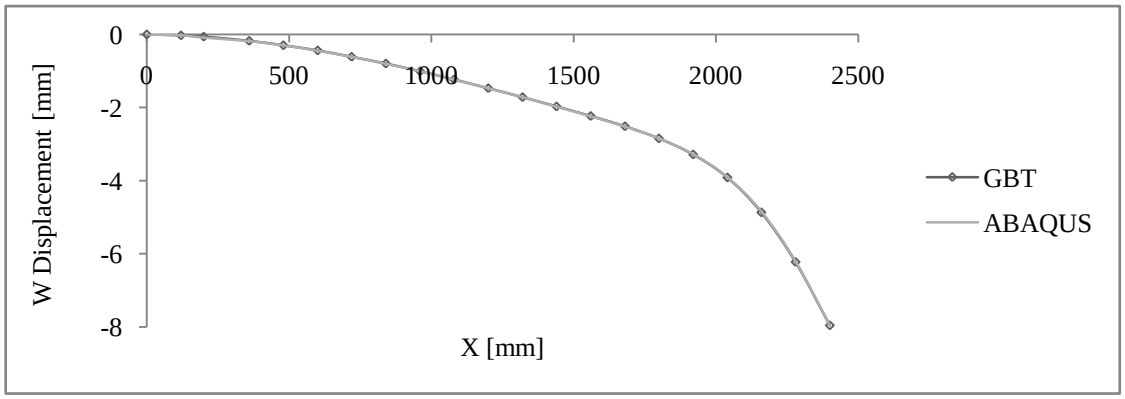

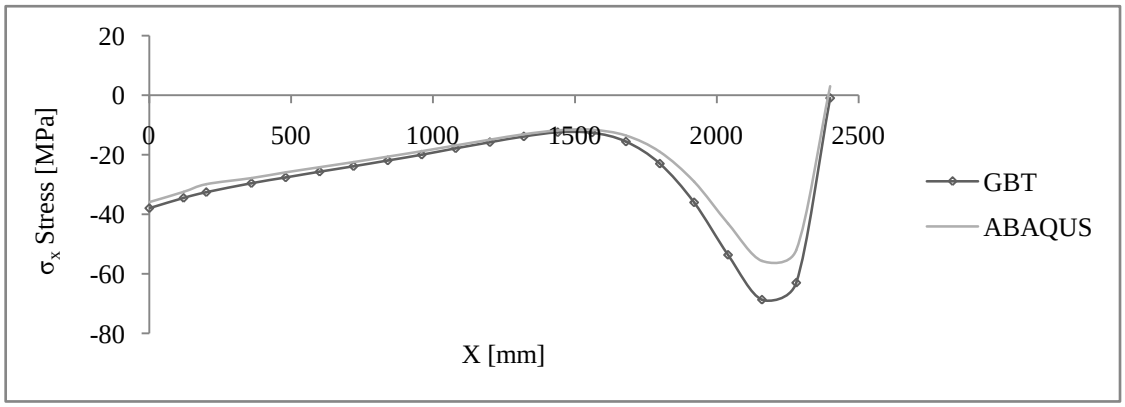

Figure I.3: The U, V and W displacements and the normal stress σ_x variations plotted for node one along the Z-profile modelled as a with a fixed and a guided end, both for the GBT and ABAQUS analysis.